WARWICK
THE UNIVERSITY OF WARWICK

A Thesis Submitted for the Degree of PhD at the University of Warwick

Permanent WRAP URL:

http://wrap.warwick.ac.uk/161375

Copyright and reuse:
This thesis is made available online and is protected by original copyright.
Please scroll down to view the document itself.
Please refer to the repository record for this item for information to help you to cite it.
Our policy information is available from the repository home page.

For more information, please contact the WRAP Team at: wrap@warwick.ac.uk

warwick.ac.uk/lib-publications

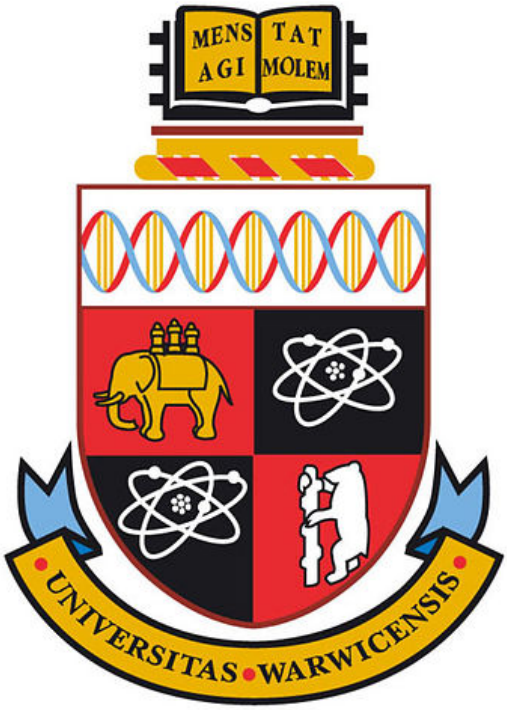

Nano-pollutants – Big Impact?

Investigating the Ecotoxicological Effects of Nanomaterials in our Oceans

Craig J. Dedman

A thesis submitted in fulfilment of the requirements for the degree of Doctor of Philosophy.

University of Warwick, School of Life Sciences.

June 2021

Contents

Chapter 3.
Investigating the impact of research-grade and commercially-available metal oxide nanomaterials upon marine microbes

List of Tables

List of Figures

Abbreviations

Nanomaterials	NMs
Silver nanoparticles	AgNPs
Titanium dioxide nanoparticles	$nTiO_2$
Metal oxide nanomaterials	MO NMs
Wastewater treatment plants	WWTPs
Predicted environmental concentration	PEC
Zinc oxide nanoparticles	nZnO
Scanning electron microscopy	SEM
Transmission electron microscopy	TEM
Gold nanoparticles	AuNPs
Dynamic light scattering	DLS
Ultraviolet–visible spectroscopy	UV-vis
Nanoparticle Tracking Analysis	NTA
Inductively coupled plasma mass spectrometry	ICP-MS
Inductively coupled atomic emission spectroscopy	ICP-AES
Nanoparticle separation and single particle inductive coupled plasma mass spectrometry	spICP-MS
Derjaguin–Landau–Verwey–Overbeek	DVLO
Natural organic matter	NOM
Polyvinylpyrrolidone-	PVP-
Poly-(acrylic acid)-stabilised	PAA-
Copper oxide nanoparticles	nCuO
Copper nanoparticles	CuNPs
Cerium oxide nanoparticles	$nCeO_2$
Aluminium oxide nanoparticles	nAl_2O_3
Cobalt nanoparticles	CoNPs
Cadmium-selenium nanoparticles	nCdSe
Dissolved organic carbon	DOC
Total organic carbon	TOC
Total nitrogen	TN

Reactive oxygen species	ROS
Hydrogen peroxide	H_2O_2
Superoxide	SOx
Superoxide dismutase	SOD
Extracellular polymeric substances	EPS
Natural seawater	NSW
Particles-per-cell	NPs $cell^{-1}$

Appendices

*Available online

Acknowledgements

First, I would like to thank my PhD supervisors, Dr Joseph Christie-Oleza and Dr Gemma-Louise Davies, for their continued support and guidance throughout the entire project. Their advice and mentorship has been invaluable and has allowed me to develop as a researcher and begin to establish my academic career. I also give my appreciation to Professor Elizabeth Wellington for taking on the role of my supervisor during my final year at Warwick. I also give thanks to the NERC CENTA DTP for funding my PhD research and giving me the opportunity to pursue this doctoral degree.

Second, I would like to pay thanks to members of the Christie-Oleza group for their support and friendship during this PhD, as well as members of the wider CENTA DTP cohort. In addition, I thank members of the Davies Group, University College London, who provided assistance with nanomaterial characterisation and always made me feel welcome when I visited the department. I would also like to give thanks to the research platform and technical support teams at the University of Warwick, for their assistance with laboratory work. In particular, I thank Dr Sarah Bennett for her assistance with flow cytometry and imaging.

I extend my gratitude to Energenics Europe Ltd. for their collaboration and provision of materials, providing a valuable addition to my thesis. Here, I pay particular thanks to Dr Riaz Choudhery for his advice and support during this work.

I send my appreciation to the handling Editors and anonymous reviewers who have worked on the publications submitted during this PhD. Their constructive feedback has undoubtedly enhanced the quality of my work and the findings presented in this thesis.

Finally, my appreciation goes to my family, for which this PhD has been a team effort. I thank my partner, Megan, for her ever-present support, without which this PhD would not have been possible, and my parents for their constant encouragement throughout my education and support of the goal that will be achieved though the submission of this thesis.

Declaration

This thesis is submitted to the University of Warwick in support of my application for the degree of Doctor of Philosophy. It has been composed by myself and has not been submitted in any previous application for any degree.

The work presented (including data generated and data analysis) was carried out by the author except in the cases outlined below:

- *Silver nanoparticles used in natural community experiments, as well as flow cytometry data (sections 2.2.2; 2.2.3) were generated by Gaby Newson and is presented in her Masters thesis.*
- *ICP-AES analysis of AgNPs in NSW (section 2.2.6b) was carried out by Connor Wells (Davies Group, University College London).*
- *EDS elemental analysis data of $nTiO_2$ extracted from consumer products (section 3.1.2.3) was generated by Dr Gemma-Louise Davies (PhD co-supervisor, University College London).*
- *P-XRD analysis of $nTiO_2$ extracted from consumer products (section 3.1.2.3) was carried out by Aaron M. King (Davies Group, University College London).*
- *UV-vis spectroscopy and DLS measurements of $nCeO_2$ in Milli-Q water (section 3.2.2.2) were carried out by Marwa M. I. Rizk (Davies Group, University College London).*

Parts of this thesis have been published by the author:

*Craig J. Dedman, Gabrielle C. Newson, Gemma-Louise Davies, Joseph A. Christie-Oleza. Mechanisms of silver nanoparticle toxicity on the marine cyanobacterium Prochlorococcus under environmentally-relevant conditions, Science of The Total Environment, **747**, 2020, 141229.*

*Craig J. Dedman, Aaron M. King, Joseph A. Christie-Oleza, Gemma-Louise Davies. Environmentally relevant concentrations of titanium dioxide nanoparticles pose negligible risk to marine microbes. Environmental Science: Nano. 2021, **8**, 1236 - 1255.*

*Craig J. Dedman, Marwa M. I. Rizk, Joseph A. Christie-Oleza, Gemma-Louise Davies. Investigating the impact of cerium oxide nanoparticles upon the ecologically significant marine cyanobacterium Prochlorococcus. Frontiers in Marine Science. 2021, **8**, 571.*

Abstract

Engineered nanomaterials (NMs) used for industrial and commercial applications, represent an emerging contaminant of environmental concern. Due to their widespread use, their entry into the environment is believed inevitable, where the ocean represents the sink for contaminants entered into the aquatic environment. In this thesis new insight is provided on the likely environment risk of engineered NMs towards marine microbial organisms which represent the base of the marine food web and play major roles in global climatic and biogeochemical processes.

Three commonly used NMs with clear pathways into the aquatic environment were selected for study; silver nanoparticles (AgNPs), titanium dioxide ($nTiO_2$) and cerium oxide ($nCeO_2$). Preliminary investigation exposing a natural phytoplankton community to AgNPs identified the marine cyanobacterium *Prochlorococcus* as particularly sensitive to NMs, and hence the model *Prochlorococcus sp. MED4* was selected for use in ecotoxicity assessments. Toxicity testing and subsequent investigation of toxic mechanisms revealed varying impacts of metal-based NMs such as AgNPs, and metal oxide NMs upon *Prochlorococcus*, largely determined by their respective fate and behaviour upon entry into saline media.

In chapter 2, AgNPs were observed to exert significant cell declines upon *Prochlorococcus via* the release of toxic silver ions and superoxide. This perturbation was associated with a significant alteration to the cellular proteome and was irreversible in the longer-term. However, cell declines were mitigated by increasing cell density likely due to an increase in production of superoxide dismutase at higher cell numbers. Significant cell declines were observed at concentrations ≥10 μg L^{-1} under natural conditions, representing the upper limit of AgNPs predicted in the environment. Hence, it is believed that negative impacts of AgNPs upon marine microbial species is only likely in hotspots of contamination.

In chapter 3, the potential impacts of metal oxide NMs ($nTiO_2$ and $nCeO_2$) were investigated. Here, little impact upon *Prochlorococcus* was recorded in extended exposure (240 h) except at extremely high concentrations (100 mg L^{-1}). Temporary declines were observed in the short-term (≤72 h) and were associated with the hetero-aggregation and co-precipitation with nanoparticles which were observed to aggregate

rapidly upon entry into seawater, as confirmed by dynamic light scattering (DLS) and fluorescent microscopy. The key role of physical interactions in driving cell declines was further supported by shotgun proteomic analysis of *Prochlorococcus* exposed to $nTiO_2$ (100 μg L^{-1}), revealing no significant alteration to the cellular or exo- proteome. Effective protocols were established to extract and characterise $nTiO_2$ utilised in consumer products such as cosmetics and sunscreen. Use of $nTiO_2$ extracted from consumer sunscreen in exposures with natural marine microbial communities, found negligible impact upon the structure and diversity of prokaryotic or eukaryotic communities. Hence the current environmental risk of $nTiO_2$ and $nCeO_2$ towards marine microbial species is believed low.

In the final experimental chapter 4, in collaboration with an industrial partner, the effectiveness of novel $nCeO_2$ antifouling surface coatings was examined by use of amplicon sequencing, nutrient analysis and 3D microscopic imaging. Investigation revealed negligible impact of the addition of $nCeO_2$ upon biofilm community structure, however nutrient analysis suggested a slight reduction in biofouling in the presence of nanoparticles.

Chapter 1

Nanomaterials in the marine environment

Nanomaterials (NMs) refer to particles with at least one dimension <100 nm.[1] Such particles have always been present in the environment, derived from natural and in more recent times, anthropogenic sources.[2] Ecological concerns have been raised in regards to the environmental fate and behaviour of engineered NMs. These materials are observed to behave differentially to their bulk counterparts,[3] and unique physicochemical properties has led to their widespread application, for example; as antibacterial agents in the biomedical industry;[4] catalysts;[5] conductive adhesives or pastes;[6] cosmetics;[7] and as agents for biosensing and imaging (Table 1.1).[8] The production of NMs has increased exponentially and is predicted to rise.[2, 9] Ever-increasingly, NMs are being incorporated into commercial products and >1800 are now listed as containing nano-components.[9, 10] With this in mind, it is increasingly likely that NMs will enter the natural environment, where the ocean represents the sink for the majority of contaminants entered into aquatic systems. Marine ecosystems play a fundamental role in regulating global climatic and biogeochemical cycles, as well as, significantly contributing to food security, world economics and human health. As such, the fate and effects of NMs released into marine waters requires investigation.[2] This important research will be of great use to inform on the likely environmental risk of engineered NMs, and direct future policy regarding their monitoring and release into the environment.

1.1 Entry of nanomaterials into the marine environment

There are numerous pathways by which NMs of anthropogenic origin may enter the natural environment (Fig 1.1). Due to difficulties in environmental sampling in the nano-scale,[11] the extent of NM release by each possible source has not been accurately recorded. Release of NMs into the marine environment may occur directly, or indirectly through entry *via* terrestrial or freshwater environments and subsequent

transportation by rivers, wind or surface-runoff.[12, 13] The ocean is widely recognised as the sink for pollutants entering the aquatic environment, although this is governed by the pollutant's physicochemical properties and stability in suspension, a factor known to vary between differing NMs and environmental zones.[14]

Table 1.1. Global production and uses of common engineered nanomaterials.[15-17]

Material	Annual Production (tons)	Example uses
Silicon dioxide	5,500 – 1,400,000	Paints, therapeutics, mechanical polishing agents, foods.[18]
Titanium dioxide	3,000 – 150,000	Sunscreens, plastic production, paints, foods.[7, 19, 20]
Zinc oxide	550 – 36,000	Sunscreens, pharmaceuticals, cosmetics, sensors.[21, 22]
Aluminium oxide	55 – 10,100	Drug delivery, biosensors, cancer therapy, oil recovery.[23, 24]
Carbon nanotubes	300 – 1,950	Catalyst support, electronics, nanotweezers, high performance composite production, supercapacitors.[25]
Cerium oxide	55 – 1,400	Fuel catalyst, biomedical applications, drug delivery, glass production, incorporation into electronic components.[26-29]
Silver	55 - 420	Antibacterial agents, clothing, cosmetics, biological sensing, and electronics.[6, 8, 30]
Fullerenes	0.6 - 100	Photovoltaics, antioxidants, pharmaceuticals, catalysts, polymer additives, medical imaging.[31]
Iron oxide	45 - 55	Magnetic inks and seals, catalysts, bioimaging, therapeutics.[32]
Quantum dots	0.6 - 9	Photovoltaics, bioimaging, batteries, cancer diagnosis, lasers.[33]

The widespread use of commercial products containing NMs means that particles are likely to enter the aquatic environment *via* wastewater systems. For example, silver nanoparticles (AgNPs) utilised in the antibacterial clothing industry,[34, 35] have been found to readily leach colloidal AgNPs and ionic silver into distilled water during experimentation.[34] NMs derived from cosmetic products, primarily titanium dioxide

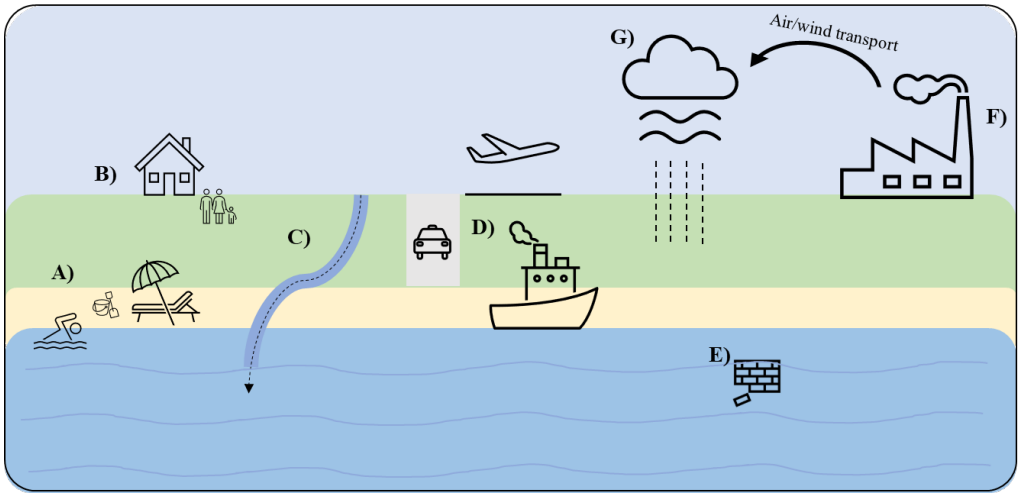

Figure 1.1. Illustrative representation of possible routes of entry of engineered nanomaterials (NMs) into the marine environment:

A – *Direct entry of nano-products* e.g., sunscreen; Sunscreens commonly use NMs for UV protection. These products are generally used by consumers at coastal locations where following coastal leisure activities *(i.e.,* swimming, water sports) NMs will likely be washed into surface waters.

B – *Domestic use of nano-products*; The use of products incorporating NMs within homes (*e.g.,* cosmetics, cleaning products, clothing) is likely to release NMs into wastewater systems. Here, a proportion of NMs will be transported to the aquatic environment as wastewater effluent.

C – *Riverine input*; NMs released within wastewater effluent, alongside any NMs that enter rivers *via* surface run-off or wind transport following terrestrial use (*e.g.,* agricultural application, surface coating leachate) will be transported by riverine systems where the ocean will be their eventual sink.

D – *Transport emissions*; NMs produced by and added to fuel used in terrestrial vehicles may enter aquatic environments following their release. NMs released by exhaust systems of shipping or leisure vessels will enter the aquatic environment directly.

E – *Break-down of larger debris*; Entry of materials of anthropogenic origin (*e.g.,* plastics) is ever-increasing. Such materials may break-down due to processes including environmental weathering into nano-scale particles.

F – *Industry*; NMs may be entered into the marine waters directly because of industrial activity such as release of production by-products or waste, or indirectly through release of materials into terrestrial wastewater systems of into the air where they may be transported to the ocean.

G – *Atmospheric deposition*; Airborne NMs will likely be transported *via* wind where they may be deposited into the marine environment.

nanoparticles ($nTiO_2$), have a clear pathway to enter the aquatic environment *via* wastewater in a similar manner to that recorded with microplastic beads derived from domestic use of facewash.[36] For example, it is predicted that 160-240 metric tonnes of TiO_2 is released into coastal waters following sunscreen use each year in tropical

countries.[37] Considering that sunscreen use in many countries displays a seasonal trend, it is likely that products such as liquid foundation, which utilise $nTiO_2$ for UV protection, or toothpastes used on a largely more regular basis may release considerably more NMs into the environment. It is therefore feasible to suggest that households may represent a considerable source of NM release into the environment.

Extraction rates for metal oxide nanomaterials (MO NMs) from wastewater treatment plants (WWTPs) have been recorded in the range of 90-95%.[38, 39] For metallic NMs such as AgNPs, WWTPs are predicted to release approximately 0.2% of particles into effluent based on influent concentrations of 5 $\mu g\ L^{-1}$.[34] However, observed extraction efficiencies for AgNPs vary (50-98%).[39] It can be argued WWTPs provide good protection to the environment from any potential deleterious effects exerted by the release of NMs into wastewater systems. However, the presence of these materials within WWTPs may alter the activity and performance of WWTP communities.[40-44] Following treatment, NMs are collected into sewage sludge, believed to contain NMs in their highest environmental concentrations.[19] Following the 1991 EU directive 91/271/EEC[45] and US Ocean Dumping Ban Act of 1988,[46] oceanic dumping of sewage sludge was prohibited, resulting in the frequent use of sludge as an agricultural fertiliser.[47] Here, approximately 250 mg/m^2 of TiO_2 is predicted to be released onto soil surfaces per year.[47] Subsequently, these particles may enter the aquatic environment *via* surface runoff.[12] Alternatively, sewage sludge may be added to landfill, where it is thought that NMs such as AgNPs may leach into the aquatic environment.[48]

In a similar fashion, NMs that are used terrestrially may pollute soils and be transported into surface water and groundwater systems.[2] For example, amphiphilic polyurethane nanoparticles are found to effectively remediate soils contaminated with polynuclear aromatic hydrocarbons.[49] Such NMs are specifically designed to not adhere to the soil surface.[49] Therefore, it is likely that such particles will be transported *via* surface run-off or wind into aquatic environments. Recently, NMs have also been utilised to remediate eutrophic waters.[50] For example, $nTiO_2$ is recorded to control the internal loading of nutrients, primarily phosphorous, in aquatic environments, due to their high adsorption capacity.[50] Any NMs entered into the aquatic environment in

order to remediate eutrophication are likely to end up in estuarine or oceanic environments.

Given their widespread use, it is clear that numerous pathways for entry of NMs into the marine environment exist. As we gather more detailed data on the production, use and fate of NMs and related products, we will be better placed to identify key sources and hence environments of concern where the accumulation of particles is likely. Whilst these aspects remain uncertain, it is important a wide lens approach is selected to examine the impact of commonly used NMs upon marine biota.

1.2 Environmental concentrations of nanomaterials

Environmental risk is dependent on toxicity and exposure, hence, the importance to evaluate both effects and sinks. As described by Johnson *et al.* (2012), risk assessment is traditionally based upon the comparison of a measured environmental concentration, with a known effect concentration determined through laboratory testing.[47] However, the exact concentration of engineered NMs in the natural environment remains unknown.[39] The lack of clarity regarding environmental levels of engineered NMs is not surprising, given their relatively recent increase in use. Additionally, difficulties in sampling techniques and varying effectiveness of methods for characterising nano-pollutants has led to a lack of environmental data.[11, 51] For example, the presence of natural and any manufactured bulk material that have previously been entered into the environment, makes the ability to distinguish between these and engineered NMs particularly challenging.[47] Typically, our understanding is based upon 'Environmental Fate Models', identified as a key tool to estimate the likely levels of NM contamination in various environmental zones.[52]

Gottschalk *et al.* (2009) simulated the predicted environmental concentrations (PECs) of five common engineered NMs across a range of environmental zones in three geographic regions: Europe, USA, and Switzerland. Here, highest environmental concentrations were predicted to occur in Europe.[19] $nTiO_2$ was predicted to be the most abundant NM released into the environment, followed by; AgNPs, zinc oxide nanoparticles (nZnO), and carbon-based materials, consisting of carbon-nanotubes and fullerenes.[19] Concentrations were predicted to be highest in WWTP sludge,

ranging from 1.68 mg kg^{-1} (AgNPs) to 136 mg kg^{-1} ($nTiO_2$) for non- carbon-based materials.[19] In surface waters, the PEC of NMs was predicted to be much lower, with $nTiO_2$ representing the most abundant material at 0.015 μg L^{-1}.[19]

The research reported by Gottschalk *et al.* (2009), described above, was one of eight studies utilised by Maurer-Jones *et al.* (2013) to provide further information on the PEC of engineered NMs. Here, as expected, WWTP sludge was found to accumulate NMs in the highest concentrations.[53] Of the materials examined, $nTiO_2$ appeared to have the highest PEC in sludge, with concentrations ranging from 100-2000 mg L^{-1}, followed by nZnO and AgNPs with predicted concentrations of 13.6-64.7 mg L^{-1} and 1.29-39 mg L^{-1} respectively.[53] WWTP effluent was similarly dominated by $nTiO_2$, predicted to be present up to 100 ng L^{-1}.[53] In surface waters the range of $nTiO_2$, AgNP and nZnO was predicted to be approximately 0.01-10,000 ng L^{-1}.[53] It was the opinion of the researchers that extensive characterisation of NMs in the environment, in terms of any alteration of oxidation state and/or species transformation would greatly benefit future research, both of which are believed to influence the ecotoxicological effects of NMs.[53]

More recently, field concentrations of NMs are beginning to emerge in the literature.[39] Bauerlein *et al.* (2017) reported data upon the presence of organic and inorganic NMs in the Dutch environment. Here, once again titanium-based materials were most abundant, with concentrations of Ti in WWTP effluent recorded in the range of 1-4 μg L^{-1},[39] lower than the value predicted in modelling studies. However, in surface waters Ti was detected in 12 of 14 sites examined, recording concentrations within the range estimated by modelling (1.3-5.7 μg L^{-1}).[39, 53] A maximum concentration of 33 μg L^{-1} was recorded in waters close to Eindhoven airport.[39] Presence of $nTiO_2$ particles was confirmed using scanning electron microscopy (SEM), revealing primary particle sizes of 60-300 nm.[39] Within the study, removal of $nTiO_2$ through WWTPs was recorded >90% at all sampling points.[39] Extraction of AgNPs was recorded in the range of 50-98%, resulting in effluent concentrations approximately 1 μg L^{-1}.[39] Gold nanoparticles (AuNPs) were also detected in WWTP effluent, where extraction efficiencies were lower than expected (<50%) and surface water concentrations were measured up to 0.25 μg L^{-1}.[39] Carbon-based C_{60} nanoparticles were identified at all

WWTP sites sampled, however here release into effluent was minimal.[39] As expected, those areas most susceptible to pollution (*e.g.* airports) are recorded to display relatively higher contamination by NMs.[39] Whilst increased efforts have been made to monitor the concentrations of engineered NMs in the environment, little work has been carried out to uncover the baseline levels of NMs that may be of natural or anthropogenic origin.[54] Such work will allow for improved analysis of data concerning engineered NMs and their presence in the environment. Graca *et al.* (2018) set out to address this problem by conducting analyses on environmental NMs obtained from the Baltic Sea to establish their atmospheric, biogenic or geogenic, or anthropogenic origin. Using a combination of Variable Pressure SEM and Energy-Dispersive X-ray spectroscopy, NMs were found to occur in the ranges of undetectable to $3.8x10^4$ particles cm^{-3}.[54] However of the NMs sampled, only a small fraction were believed to be of anthropogenic origin, identified as asbestos nanofibers.[54]

By using data generated by modelling studies and the limited environmental sampling data available, we are able to consider key trends that emerge regarding the release of engineered NMs into the environment. Firstly, we can be confident that $nTiO_2$ represents the most abundant engineered NM in the natural environment, as can be expected given that it is one of the highest produced NMs used in commercial products globally.[9] Secondly, NMs appear to accumulate in WWTP sludge in the mg kg^{-1} range, where they may be transferred to the environment through their use as fertiliser or addition to landfill. Extraction rates for NMs appear in the range 50-98%, thus in comparison, the concentration of NMs entering effluent and surface waters is estimated to be considerably lower, in the ng -µg L^{-1}range. Researchers must consider these predicted values in experimental design and conduct both short- and long-term exposures at environmentally relevant concentrations to identify any sub-lethal or chronic effects that may be exerted upon biota.

1.3 Behaviour of nanomaterials in the aquatic environment

A key theme that runs throughout the discussion surrounding nano-ecotoxicology is the influence of NM fate and behaviour upon ecotoxicity. However, given the great variation that exists in the physical and chemical properties of both NMs and aquatic

environments our knowledge of NM fate remains limited. Currently, our understanding of the behaviour of NMs within natural waters is limited and often dependent on modelling. Analysis of NMs in environmental matrices which are complex and vary greatly is challenging and a lack of effective methods exist.[55] However, such knowledge is crucial to accurately predict risk of NMs within natural systems, as well as allowing us to predict the likely form of NMs that wildlife is likely to come into contact with in varying environmental zones.

A number of techniques have been utilised by researchers to gain insight into the fate and behaviour of NMs in aquatic media under experimental conditions. However, given the challenges that exist in working with NMs, limitations to current capabilities exist.[56, 57] Given these challenges, the development of novel techniques is required.[56] Current analytical techniques are not limited to but include:

- Dynamic light scattering (DLS); DLS is commonly used to examine changes in z-average size, zeta-potential, and polydispersity of NMs.[58]
- Ultraviolet–visible spectroscopy (UV-vis); assessment of the sedimentation of metallic NMs through loss of UV-vis signal over time.[59]
- Nanoparticle Tracking Analysis (NTA); video microscopy is used to examine Brownian motion of particles in the range of nm to 1 μm. Particle size is determined using the Stokes-Einstein relation and concentration calculated is regard to the number of particles detected.[60]
- Inductively coupled plasma mass spectrometry (ICP-MS); ICP-MS and related techniques can be utilised to assess the stability of NMs in experimental media.[61] Monikh *et al.* (2018) propose the use of ICP-MS to determine the percentage of NMs remaining in suspension in relation to that added at the start of the experiment at defined timepoints. Here, particle size is not reported, nor aggregation rate or attachment efficiency.[61]
- Nanoparticle separation and single particle inductive coupled plasma mass spectrometry (spICP-MS); Nanoparticle separation techniques such as asymmetric flow field flow fractionation (AF4), spICP-MS is believed to be highly effective to examine changes in the size of particles.[62]

- On-line light scattering analysis: combining both dynamic and static light scattering to assess aggregation behaviour and the structure of NM aggregates.[56]

Alongside practical laboratory techniques, computational modelling of NM behaviour appears a useful tool.[58, 63-66] Such models can predict the likely fate of NMs entering various media, as well as the likelihood of interaction with naturally occurring particulate or dissolved matter.[58] Models make use of the experimental data currently available and are likely to be enhanced as increasing amounts of data becomes available. Therefore, to maximise effectiveness of predictive model, efforts must be made to optimise experimental procedures to best simulate natural conditions.[66]

Evidence is readily available for the behaviour of NMs under laboratory conditions in a range of aquatic environments, including seawater.[14, 57, 67, 68] In Figure 1.2, examples of important processes impacting on the fate of NMs within aquatic environments are displayed. NM mobility and fate in the aquatic environment is governed by a number of factors, including; particle size, shape, surface characteristics, and surface charge.[69] Local water chemistry is also influential, with ionic strength, pH, and the presence of natural organic and particulate matter all playing important roles.[70, 71]

Generally, NMs are observed to aggregate upon entry into aquatic media.[14, 57, 67] Aggregation is typically recorded to be enhanced when entered into media of high ionic strength such as seawater.[3, 14, 58, 72, 73] Here, based on the Derjaguin–Landau–Verwey–Overbeek (DLVO) theory, as ionic strength increases, the thickness of the diffuse layer of NMs is decreased, allowing particles to come into close enough contact to aggregate.[72] Additionally, under such conditions the ability of surface charge to stabilise nanoparticles is reduced.[3] Indeed, both metallic and MO NMs have been recorded to aggregate upon entry into saline waters.[14, 62, 74] In contrast, NMs appear more stable in freshwater with lower ionic strength.[14] However, specific surface characteristics of NMs influence this process and can enhance or mitigate the aggregation process.[71, 75] As NMs aggregate to larger sizes, their density also increases, thus increasing their likelihood to precipitate out of the water column.[63] The pH of aquatic media can also impact upon NM stability,[76] for example $nTiO_2$ has been observed to aggregate when pH reaches zero charge, thus altering the surface charge

of NMs.[3] In addition, NMs may undergo dissolution in aquatic media, as recorded in AgNPs and nZnO,[77, 78] although this is largely dependent on particle type and surface characteristics.[79] NMs may be transformed in the environment, for example losing their surface coating, or obtaining an eco-corona made up of organic material,[71, 80, 81] subsequently likely to alter their fate. These processes will largely determine the behaviour of NMs within the aquatic environment and dictate their transportation between environmental zones such as rivers, estuaries, and coastal waters. Here, sedimentation may facilitate the deposition and accumulation of NMs in sediments, where they may persist.[63]

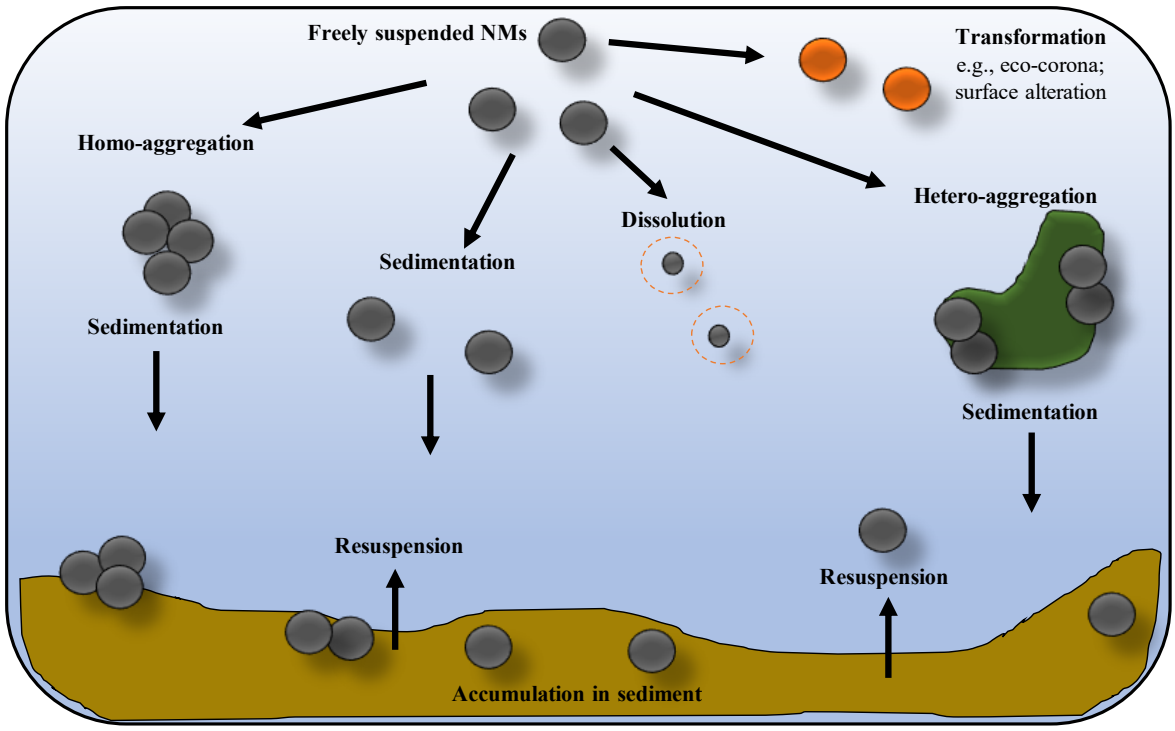

Figure 1.2. Schematic representation of NM fate and behaviour within the aquatic environment. Adapted from Markus *et al.* (2015).

Whilst insights into general behaviours of NMs in the environment have been obtained, in some cases conditions often do not accurately represent the natural environment. For example, experiments are often carried out concentrations far exceeding those predicted in the environment. However, this is commonly unavoidable due to the limitations of current analytical techniques.[56, 57] Typically, limits of detection fall in the ppb (μg L^{-1}) to ppm (mg L^{-1}) range,[82, 83] surface water concentrations of NMs are predicted in the ng-μg L^{-1} range,[53] meaning that is difficult

or at times impossible to effectively analyse environmental samples. For example, for reliable DLS analysis a concentration of 0.1-1 mg mL^{-1} is recommended.[84] Additionally, experiments may be carried out under static conditions, overlooking the effects of turbulence and other perturbations that may act to increase collision rate between particles of natural colloidal matter.[85] It is also important that the presence of such colloids and natural organic matter (NOM) is considered during investigation. The organic complexity and presence of ligating agents in natural waters is likely to influence the fate and behaviour of NMs.

The concentration of particulate matter and NOM within aquatic environments appears influential in determining NM aggregation. Here, hetero-aggregation between natural compounds and NMs is believed to primarily determine environmental fate.[58] Quik *et al.* (2014) identified that hetero-aggregation between NMs and natural colloids is highest in marine waters, where presence of particulate matter was associated with enhanced sedimentation. The rate of sedimentation is observed to vary between different particle types, recorded to be relatively low in polyvinylpyrrolidone-coated AgNPs (PVP-AgNPs) and comparatively high in carbon-based C_{60} NPs,[67] likely a result of the varied surface characteristics of the two particle types. In accordance with the findings of Quik *et al.* (2014), modelling *via* a two-component Monte Carlo model system consisting of NMs and NOM fulvic acid monomers within a range of water models representing fresh and marine waters revealed that both homo- and hetero-aggregation will be enhanced in marine waters due to increased availability of effective particle contact points.[58] In contrast, the processes of homo- and hetero-aggregation were found to compete against each other in ultrapure or fresh- waters, dependent upon the initial attachment efficiency between individual particles or naturally occurring particulate matter.[58]

Despite the evidence of varied sedimentation rate of different NMs reported by Quik *et al.* (2014) described above, when experiments are extended to a period of months with regular redispersion of water and associated sediments, sedimentation is not recorded to vary by particle type.[85] Here, sedimentation is extensive and characterised by the entrapment of NMs in 'sediment flocks'.[85] The consideration of turbulence and action of resuspension is believed to improve environmental relevance as turbulent conditions commonly found in nature are likely to increase rate of encounter between

NMs and natural colloids.[85] As a result, rates of hetero-aggregation were recorded up to 29 times higher in turbulent conditions when compared to studies carried out with natural colloids under static conditions.[85]

Whilst the presence of particulate matter has been observed to enhance aggregation and subsequent sedimentation, stabilising effects of NOM upon NM suspensions in natural waters have been recorded.[14, 62, 86, 87] In marine waters, dissoved organic carbon (DOC) in the form of alginate has been observed to form coatings upon AgNPs and enhance their stability in suspension.[62] However, significant aggregation was still recorded.[62] Stabilising effects of DOC (>2 mg L^{-1}) is also observed in riverine and WWTP waters.[86] Here, aggregation of AgNPs and $nTiO_2$ is recorded to be positively associated with Ca^{+} concentration, affecting $nTiO_2$ in a greater manner than AgNPs.[86] During this study high molecular weight biopolymers were also recorded to enhance AgNP stability.[86] The presence of microbial species is also likely to influence NM behaviour in natural aquatic environments; for example, the adsorption of algal exopolymeric substances, *via* electrostatic attraction and complexation at the particle surface has been observed during experimental work, and is recorded to enhance stability of nZnO in freshwater.[88] However, despite the growing evidence base surrounding NM fate in natural environments, results still vary. Addition of NOM extract had negligible effects upon aggregation or sedimentation of nZnO in marine media, where particles were observed to precipitate freely.[89] The interaction of NMs with naturally occurring substances requires greater attention, in particular at NM concentrations relevant to the natural environment.

In summary, it appears that NMs are likely to aggregate upon entry into the aquatic environment, the extent of which will be enhanced in saline waters due to increased ionic strength. The aggregation of NMs will alter their fate as increased density facilitates their transport to deeper zones. However, these processes will be largely dependent upon environmental variables such as the concentration of natural particulates and NOM, as well as specific water chemistry. It remains to be seen whether the processes recorded under experimental conditions are likely to occur at the concentrations of NMs predicted in the environment, where rate of particle contact is likely to be decreased. Nevertheless, research carried out to date has great use to guide our consideration of the likely impact of NM fate and behaviour during

ecotoxicity assessment, and efforts must be placed upon developing novel approaches to examine NM behaviour *in situ* or under representative environmental conditions.

1.4 Ecotoxicological effects of engineered nanomaterials

The increased ecological concern arising from release of engineered NMs into the environment has led to a rise in research output regarding their fate, behaviour, and effects upon biota. As a result, evidence for the ecotoxicity of nano-sized particles is becoming increasingly available. The research output within the field of nano-ecotoxicology was assessed by carrying out a simple Web of Science® literature database search using the terms; 'Nano* AND Ecotox*' for articles published between 2000-2019. After initial screening of article titles to remove any irrelevant manuscripts, a total of 1400 articles were identified. Figure 1.3A displays the number of articles published each year within the examined timescale. As can be seen, in the last decade the number of articles investigating the ecotoxicological effects of NMs has increased considerably from 0 in 2000 to 183 in 2019. Indeed, it appears little nano-ecotoxicological studies were published prior to 2006. Whilst the relatively simple search string utilised may not capture the entire evidence base, it is likely that the displayed results represent the general trend. By classifying studies in regard to

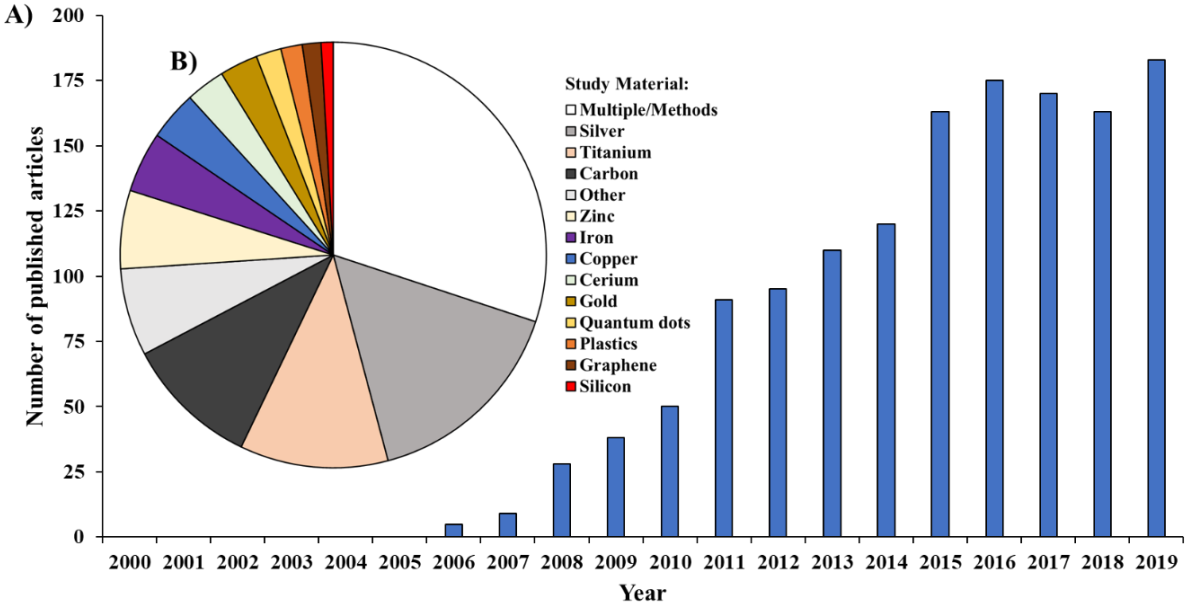

Figure 1.3. Number of articles published annually (2000-2019) within the field of nano-ecotoxicology (n=1400) (A); and proportion of studies belonging to major material groups (B), as identified by Web of Science database search (Topic: 'Nano* AND Ecotox*'). Data correct as of 27/03/20.

the NM group studied (*e.g.,* titanium based- /silver based-) we are able to gain insight into those materials that have been prioritised by researchers. As can be seen in Figure 1.3B, the majority of studies examined multiple NM types or discussed methodological approaches; representing approximately one third (30%) of articles identified. Silver, titanium and carbon-based NMs appear the most studied to date, representing 16%, 11% and 10% of articles, respectively. Upon further observation of manuscript titles and abstracts, only 78 articles appeared to focus solely upon the fate or effects of NMs within saline waters, representing approximately 6% of the dataset. It appears that marine species have been little studied in the field of nano-ecotoxicology when compared to species occupying other environmental zones *e.g.,* soil or freshwater. In this section, a brief overview will be provided upon the ecotoxic effects of NMs upon marine biota, where focus will be placed upon metal- and MO NMs.

Toxicity of engineered NMs is largely determined by the physicochemical characteristics of individual particles and the aquatic environment that they enter. In several studies NMs are observed to exert higher toxicity than their bulk counterparts.[90, 91] This is likely due to the higher surface-to-volume ratio of NMs compared to bulk materials, or as a result of unique physicochemical properties of materials in the nano-form. Size-dependent effects appear a feature of NM toxicity, with increased toxicity observed with decreasing particle size.[92, 93] Particle shape or form, on the other hand, has previously not been observed to influence toxicity of NMs, such was the case in exposures of copper oxide nanoparticles (nCuO) to a sediment-dwelling annelid.[94] Specific physico-chemical characteristics of NMs are also likely to play a key role in determining their interaction with biota. For example, crystalline structure of $nTiO_2$ has been recorded to influence toxicity, with anatase $nTiO_2$ significantly more toxic than the rutile $nTiO_2$,[95] attributed to the lower lipophilic properties of anatase $nTiO_2$ in aquatic media, thus enhancing their bioavailability to organisms.[95] Surface coating is also recorded to determine toxic effects; for example, uncoated cerium oxide nanoparticles ($nCeO_2$) induced a toxic response in the freshwater alga, *P. subcapitata.*[92] Whereas, the toxicity of dextran-coated $nCeO_2$ upon *E. coli* was negligible, rather inducing a mild antibacterial effect.[96] It has been suggested that surface characteristics influence such differences in toxicity by altering NM bioavailability.[97] For example, Poly-(acrylic acid)-stabilised (PAA-) $nCeO_2$

appear well-dispersed in saline media, therefore remaining biologically available to species occupying the water column, and hence enhancing toxicity towards these organisms.[97] Functionalisation of NMs can also increase or decrease their toxicity towards microbial species. Studies have also shown that antimicrobial agents, such as vancomycin, can be incorporated into NMs such as AgNPs and utilised to have effective antimicrobial effects upon a range of multi-drug resistant microorganisms.[4] In contrast, $nCeO_2$ nanoparticles stabilised by addition of a dextran coating $nCeO_2$ are recorded to exert negligible toxicity upon *E. coli*,[96] believed to result from the stabilisation of nanoparticle oxidative state and reduced contact between particles and cells.[96] Transformation of NMs within the environment will also alter their interaction with biota. For example, $nCeO_2$ utilised in fuels undergo significant physicochemical transformation following combustion.[69]

Similarly, characteristics of aquatic environments will also determine NM toxicity. As displayed in Figure 1.2, upon entry into the aquatic environment, NMs may aggregate with naturally occurring particulate matter or biota (hetero-aggregation), or with other individual particles (homo-aggregation).[67] This aggregation appears enhanced in marine waters and gives rise to the process of sedimentation, transporting NMs from the water column towards sediment layers.[67] As a result of these processes, the bioavailability of NMs is altered,[98] varying the extent of exposure to planktonic and benthic, or sediment-dwelling species respectively (Fig 1.4). However, such processes appear dynamic in nature and general trends appear to vary between studies. NOM has been recorded to both enhance and mitigate toxic effects of NMs, whilst aggregation of NMs can both be beneficial by reducing exposure within the water column,[99] as well as driving increased population decline in phytoplankton species.[50] As well as NOM and other particulate matter, the biological complexity of media will alter the interaction of NMs and biota by influencing NM fate and behaviour. Availability of proteins in media is observed to increase the stability of AgNPs and maghemite nanoparticles in biological cell culture medium regardless of chemical characteristics and surface charge.[100] Whilst a negative surface charge has been shown to increase stability in media with high electrolyte concentration.[100] It is likely that the biological composition of media where NMs may potentially interact with biota will influence their bioavailability and associated toxicity.

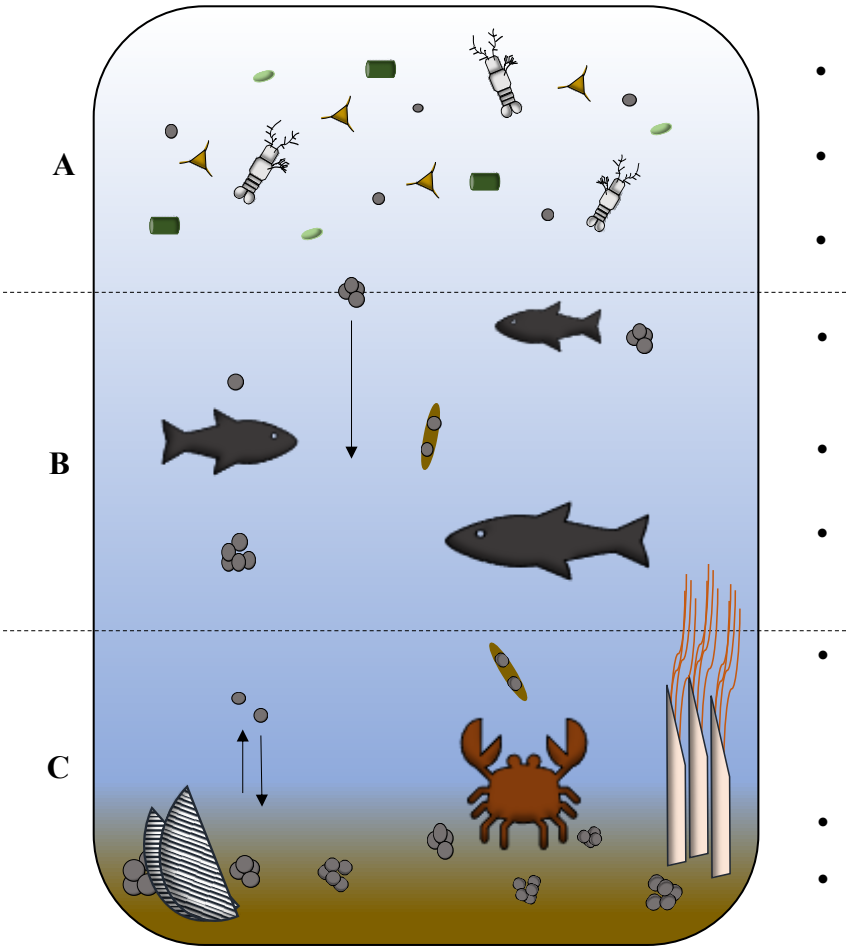

Figure 1.4. Nanomaterial fate and interaction with biota in the marine environment; A) sea surface; B) pelagic/benthic regions; C) marine sediments.

Due to their small size, NMs are bioavailable to a great range of biota and adverse effects of exposure have been recorded in a number of marine species, including; fish,[101-104] zooplankton,[105] marine bivalves,[106-108] and phytoplankton.[78, 109, 110] In zooplankton and macrofauna NM uptake may occur indirectly through feeding or respiration, and bioaccumulation may occur as a result. Marine microbes may internalise particles, if they are able to pass through the cell wall or membrane. The uptake and accumulation of NMs has been recorded in the literature.[111, 112] For example, bioaccumulation of silver derived from AgNPs (75 mg kg^{-1}) by marine invertebrates was recorded during exposure *via* sediments, although no toxic effects were observed.[111] Here, bioaccumulation and transformation of AgNPs was shown to differ with varying particle surface characteristics; where citrate-stabilised AgNPs

were accumulated to a higher extent than PVP-stabilised AgNPs.[111] Similarly, copper accumulation by the marine mussel, *Mytilus galloprovincialis* was increased 60-fold when exposed to nCuO (3 mg L^{-1}) compared to control organisms.[106] Likewise, evidence of $nTiO_2$ uptake by aquatic organisms is also available.[112] The solubility of NMs is likely to influence their uptake and accumulation within biota. For example, $nCeO_2$ which displays low solubility, is not accumulated in the same manner observed with other MO NMs following ingestion.[113] The interaction of NMs with biota, provides a platform for biotransformation which may alter NM fate in the environment. Aggregates of $nCeO_2$ (~500 nm) were observed in pseudofaeces produced by marine mussels after exposure to 65 nm rod-shaped $nCeO_2$.[113] The packaging of NMs into pseudofaeces, is likely to reduce mobility of particles and cause sedimentation.[113] Although, these particles may become increasingly bioavailable to species that feed upon faecal matter, enhancing their transport, as observed with microplastics.[114] Following sedimentation, entrapped NMs are likely to remain bioavailable to a number of sediment-dwelling or benthic species, accumulating to higher concentrations.[113]

The trophic transfer of NMs has been recorded in experimental studies within aquatic media.[102, 104, 115] Juvenile turbot, *Scophthalmus maximus,* were able to uptake and accumulate $nTiO_2$ that had previously been bioaccumulated by the clamworm, *Perinereis aibuhitensis*.[104] Following 20 d exposure, individuals were recorded to display reduced growth and abnormal symptoms in the liver and spleen.[104] In contrast, AgNPs ingested by brine shrimp were not significantly transferred to marine *Medaka*, indicating low dietary bioavailability of AgNPs,[102] highlighting the variability of this process. Although, here it is believed that extensive aggregation of AgNPs during exposure was likely to have influenced their uptake.[102] The process of trophic transfer has the potential to negatively impact upon ecosystem functioning in highly polluted areas and reduce the quality of aquaculture production.[104] The ingestion and accumulation of pollutants by marine species, particularly those at lower trophic levels is particularly concerning, given the potential for biomagnification that could threaten ecosystem functioning, aquaculture and human health. This is especially concerning in terms of NMs where biological impacts remain unclear.

Under laboratory conditions, a number of physiological effects of NM exposure have been observed using a range of model organisms. $nTiO_2$ have been found to be genotoxic to fish,[116, 117] exerting chromosomal damage in co-exposure with cadmium chloride.[117] Similar effects were recorded in the bivalve, *M. galloprovincialis* exposed to the same stressors.[118] The occurrence of NM uptake into cells is likely to be a key driver of toxicity, with NMs entering close proximity to molecular targets.[119] AgNPs are believed to exert toxicity upon phytoplankton in this manner.[119] Although NMs such as $nCeO_2$ display relatively high insolubility, nanoceria particles have been found to be internalised by immune cells of marine invertebrates,[120] albeit at relatively high concentrations. Morphological damage to the endoplasmic reticulum and lysosomes of immune cells have also been recorded in response to NMs, observed in the sea urchin, *Paracentrotus libidos* exposed to high concentrations of $nCeO_2$.[120] Similarly, sub-lethal damage to the lysosomal system has been recorded in the freshwater mussel, *Dreissena polymorpha*, alongside reductions in overall fitness, associated with the antioxidant activity of $nCeO_2$.[121] In the same study no negative effect upon the fitness of the freshwater amphipod, *Gammarus roeseli*, was observed.[121] Given that *G. roeseli* occupies the water column, whereas *D. polymorpha* is sediment dwelling, this result highlights the variation in toxicity arising from altered exposure following aggregation and sedimentation of particles,[121] described above. NM exposure has also been recorded to alter protein expression; In *Daphnia*, proteomic analysis revealed that uptake of Ti during $nTiO_2$ exposure led to altered regulation of proteins associated with vitellogenesis, likely impairing normal reproductive function.[122] Whilst this result was observed in freshwater, it can be predicted that this may occur in marine zooplankton given similarities in physiology and similar findings recorded in marine zooplankton exposed to dissolved silver.[123]

As well as exerting a detrimental physiological response, it appears that NMs also have the potential to adversely affect the behaviour of individual organisms.[124] Individuals of the bivalve *Scrobicularia plana* experienced impairments to burrowing behaviour as a response to nCuO (10-100 nm).[124] Such responses, are likely to negatively affect the fitness of the individual in terms of feeding and predator avoidance. These behavioural responses, however, appear species-specific as under the same conditions no adverse effects were observed in the polychaete, *H. diversicolor*.[124] Similarly, negative effects of nCuO exposure upon bivalve feeding

behaviour has also been recorded, reducing clearance rates of *M. galloprovincialis* by up to 50%, impairing growth.[106]

The toxicity of NMs appears to be species-specific, varying greatly between species types and position occupied in the water column. Gambardella *et al.* (2015) investigated the relative toxicity of AgNPs towards various taxonomic groups of marine species. Here, after exposure to AgNPs it was found that the jellyfish, *Aurelia aurita*, was most sensitive; followed by species representing bivalves, benthic invertebrates, algae, diatoms and zooplankton respectively.[125] In addition to taxonomic variations, adverse effects of NM exposure have been recorded to alter with varying organismal life stage.[126] Early life stages experience higher toxicity than juveniles and adults,[126] which is likely to adversely affect development to later life stages and may incur a negative effect on local ecosystem functioning in higher polluted habitats. For example, humic-acid capped AgNPs were found to induce abnormal development in the benthic annelid, *Platynereis dumerilii*.[126] Similarly, oleic acid coated- and PVP- AgNPs reduced the growth and settlement of benthic invertebrate larvae, with settlement rate significantly lower when exposed to these AgNPs rather than dissolved silver nitrate.[127] Embryotoxic effects of nZnO have also been recorded in marine fish species, *Medaka*.[101]

Although a range of toxic effects of NMs upon biota have been observed, the exact mechanisms by which particles exert toxicity are not fully understood under environmental conditions. The majority of ecotoxicological studies carried out to date, investigate concentrations considerably higher than those predicted in the environment (*i.e.,* mg L^{-1}). Few studies exist that utilise environmentally relevant concentrations in their work, however, data suggests that an environmental concentration can cause oxidative stress in marine biota.[128] An integrated biomarker assay carried out upon the bivalve, *Chlamys farreri,* revealed that environmentally-relevant concentrations of $nTiO_2$ exerted toxicity characterised by neurotoxic damage, and alterations to the gills and digestive system.[128] Although here the environmental-relevance of test concentration (1 mg L^{-1}) can be argued, given that PEC are estimated up to 10 µg L^{-1}.[53, 128] Advances in the use of molecular techniques such as metabolomics and proteomics provides great scope for investigation in this area. For example, following untargeted metabolomic analysis of human lung epithelial cells exposed to nCuO, the

occurrence of oxidative stress and apoptosis could be identified through the altered regulation of associated metabolites.[129] Similarly, proteomics has revealed alterations in protein synthesis following NM exposure in invertebrates[122] and marine phytoplankton.[130]

Evidence of NM toxicity towards marine biota is concerning, particularly declines in fitness of key species that play key roles in ecosystem functioning and are important to aquaculture industries, such as marine mussels. The potential for bioaccumulation and possible biomagnification of contaminants is also of concern. Severity of toxicity varies greatly between studies and adverse responses are recorded largely at concentrations much higher than those predicted in the environment. Commonly, research has been carried out upon model marine invertebrate species. However, to understand ecosystem level effects comprehensively, we must first examine the effects of NMs upon those species occupying the base of the marine food chain, particularly photosynthetic organisms. Such species play a vital role in ecosystem functioning, global biogeochemical cycling and climate regulation.[131]

1.5 The effects of nanomaterials upon marine microbes

The marine microbial community is often the first group of organisms to interact with anthropogenic pollutants present in the aquatic environment.[132] This dynamic community plays a fundamental role in the functioning of the entire marine ecosystem and therefore understanding the potential effects of contaminants upon marine microbes is key. Approximately 50% of global primary productivity is attributed to marine microbes, influencing climate and major biogeochemical cycles.[131, 133] As mentioned previously, the small size of NMs means that they are bioavailable to all marine biota including marine microorganisms. Figure 1.5 displays the relative sizes of NMs and major planktonic classes found in the marine environment; NMs (<100 nm) appear in the size range of viruses (~22-150 nm),[134] highlighting this bioavailability. In a number of laboratory investigations, exposure to NMs is reported to exert negative effects upon the fitness of aquatic microorganisms, including; green algae,[135-138] diatoms,[74, 77] raphidophytes,[139] dinoflagellates,[137, 140] and cyanobacteria.[141] Here, toxicity is recorded to differ in severity between freshwater and marine species, as expected given differences in chemical characteristics of both

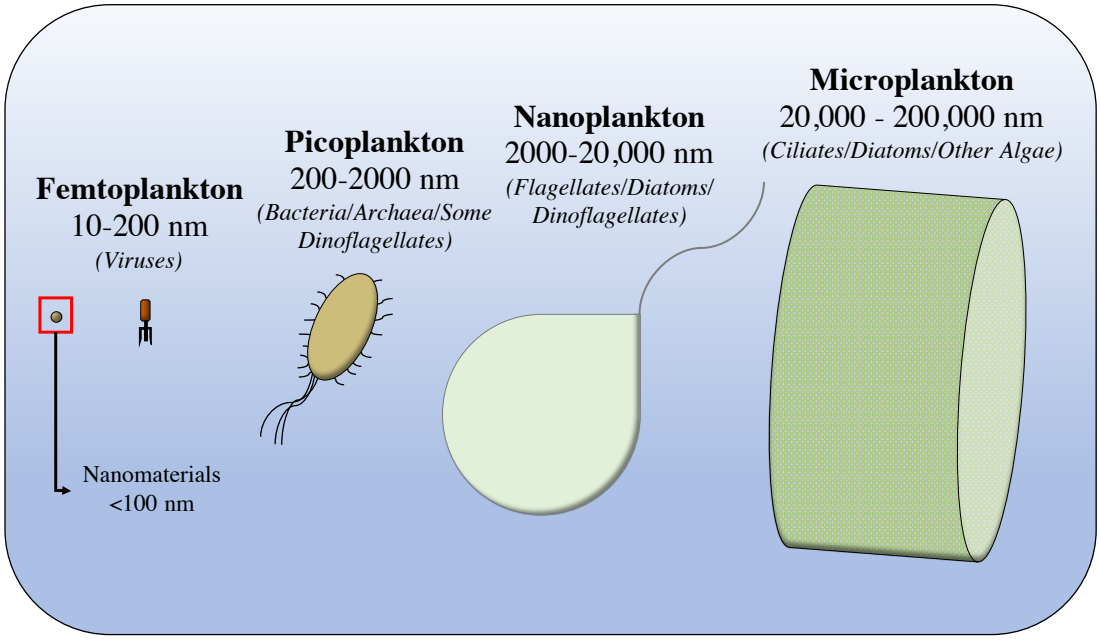

Figure 1.5. Illustrative representation of the relative size of nanomaterials compared to the major planktonic groups present in aquatic environments. Note not to scale.

media (*i.e.,* ionic strength, hardness). However, trends vary across studies; Freshwater algal species have been recorded to be more resistant to nZnO than marine species at high concentrations, although adverse effects upon population growth were experienced by both groups.[142] In contrast, reduced toxicity to $nCeO_2$ in saline media has been observed in the filamentous cyanobacterium, *Anabaena* CPB4337.[98] AgNPs on the other hand, appear to exert highest toxicity to phytoplankton in freshwaters.[77] It appears, upon an overview of the literature available, that toxicity of NMs towards microbial species is case-specific, dependent on the NM studied, experimental approach and model organism.

Research has revealed a variety of responses displayed by marine microbial organisms following NM exposure. Commonly, toxicity is characterised by a reduction in growth rate or a decline in cell density. For example, ~60% growth inhibition was recorded in *T. pseudonana* in response to AgNPs at a concentration of 10 µM.[141] Phytoplankton have also been observed to reduce cell size in response to NMs; green microalgae reduced average cell size by approximately 50% after incubation with iron oxide nanoparticles.[138] In phototrophic organisms, NMs have been found to interfere with photosynthetic processes, reducing photosynthetic output as well as chlorophyll content.[109, 136] Such effects are recorded to be influenced by varying temperature, with

phototoxicity increasing when temperature was increased from 25°C to 31°C.[136] Evidence of oxidative stress appears a common response, characterised by induction of antioxidant pathways and increased intracellular reactive oxygen species (ROS) content, recorded in the presence of a number of NMs including metallic NMs such as AgNPs,[109, 135] and MO NMs such as $nTiO_2$.[143] Additional responses include; inhibited cell motility and sporulation in marine *Bacillus* when exposure to alumina nanoparticles (nAl_2O_3),[144] and physical damage to cell morphology.[98, 145] Responses appear to vary between species, with differential sensitivity observed between phyla. For example, the dinoflagellate *Amphidinium carterae* appeared more resilient than the green alga, *Nannochloropsis gaditana*, when exposed to $nTiO_2$.[140] However, whilst exposure to NMs has resulted in toxic responses in a range of marine microbial species, albeit often at concentrations far exceeding those predicted in the environment, examples where NMs exert no adverse effect exist, highlighting the need for further investigation to accurately evaluate their environmental risk.[132, 146]

Whilst the exact mechanisms driving NM toxicity under environmental conditions remain unknown, a number have been proposed by researchers (Fig 1.6). In experimental work, NMs (primarily MO NMs) have been observed to attach to the cell wall or membrane of marine phytoplankton. Here, it is proposed that 'shading effects' may cause declines in photosynthetic output by reducing light intensity, however results suggest this effect may be minimal.[147] The attachment of NMs to the cell wall is also believed to cause physical damage to cell morphology in some cases, such as observed in phytoplankton exposed to $nCeO_2$[48] and $nTiO_2$.[87] The hetero-aggregation of NMs and microbial cells is likely to increase density, thus resulting in transport of the aggregate through the water column towards sediments. Upon entry into aquatic media, metallic and MO NMs have been observed to undergo dissolution, releasing ionic species and in a number of cases where oxidative dissolution occurs generating ROS. Where this release of toxic species occurs, metal ions and ROS may be transported by diffusion, inducing a toxic effect upon interaction with microbial cells. Toxicity recorded in exposure of cobalt nanoparticles (CoNPs) and nZnO towards marine phytoplankton have both been attributed to the release of toxic Co and Zn ionic species respectively.[137, 148] The ROS hydrogen peroxide (H_2O_2) and superoxide (SOx) have also both been associated with NM toxicity in microbial species.[149, 150] Where NMs interact directly with the cell wall or membrane, the

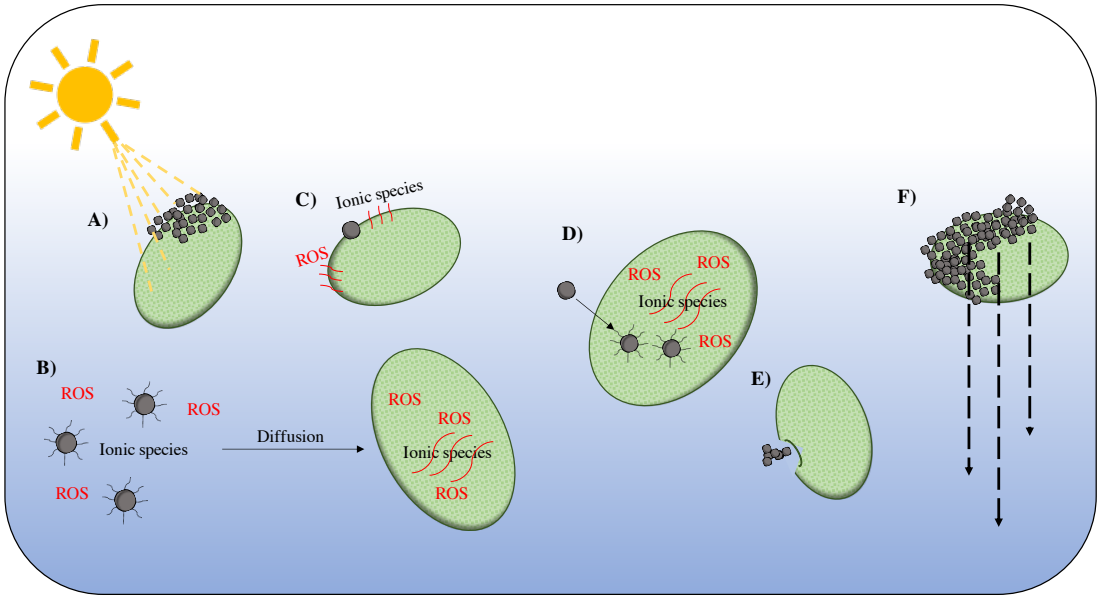

Figure 1.6. Proposed mechanisms of NM toxicity towards microbial species:
A – *Shading effects*; Attachment of NMs to the cell wall/membrane may reduce photosynthetic output by blocking sunlight, thus compromising photosynthetic activity.
B – *Dissolution of toxic ionic species and associated ROS generation*; metal and metal oxide NMs are recorded to release ionic species by processes of dissolution. Oxidative dissolution may release toxic ROS in addition. Such toxic species may be transported by diffusion to microbial species where they may interact and exert adverse effects.
C – *NM-cell membrane/wall interaction*; attachment of NMs to the cell wall/membrane may release toxic ROS and ionic species in close proximity to the cell wall/membrane.
D – *Internalisation*; NMs may be internalised where toxic species may be released in close proximity to molecular targets.
E – *Physical damage*; Aggregates of NMs may come into contact with microbial species where they may cause physical damage to cell morphology.
F – *Hetero-aggregation*; NMs and microbial cells may undergo hetero-aggregation, causing the negative effects observed in A, C and D, as well as potentially removing cells from the water column due to sinking.

delivery of toxic ionic species and ROS occur at a more local scale, likely disrupting enzymatic process, membrane permeability and eventually resulting in lysis of the cell. In a number of cases, NMs have been recorded to be internalised by microbial species.[119, 141] This process is likely to enhance toxicity by facilitating the delivery of toxic species closer to molecular targets.[119] Researchers have developed techniques to visualise the internalisation of NMs into cells,[119] and such techniques will be highly useful in determining the exact mechanisms by which particles induce toxicity in microbial species. By exploiting electron microscopy AgNPs in the range of 5-120 nm

have been observed to be internalised and enter the cytoplasm of *T. pseudonana*.[119] Similarly, internalisation of AgNPs was observed in the diatom, *P. tricornutum*, exerting toxicity by increasing cell complexity.[77] Cell morphology as well as solubility of NMs is likely to affect the uptake of particles by cells. For example, internalisation of $nCeO_2$ is believed to generally not occur in microbes and algal species with thick cell walls.[151] The internalisation and uptake of NMs by organisms raises questions regarding the possible transfer of pollutants to higher trophic levels *via* ingestion, and subsequent bioaccumulation of contaminants, as described in the previous section. It has been observed that primary consumers receive much of their dietary metals from those metals accumulated in algal species.[152] The pathways by which metals are transferred between phytoplankton and primary consumers is not well understood.[153] Such processes should be considered when evaluating the likely trophic-level effects resulting from NM-microbe interactions, particularly as phytoplankton have been recorded to accumulate metals derived from NMs in their cell wall.[153]

Research pertaining to the adaptation and defence mechanisms utilised by marine microbes towards NM exposure is also starting to emerge in the literature.[144] Following treatment with aluminium oxide nanoparticles (nAl_2O_3), marine *Bacillus sp.* elevated surfactin production and biofilm formation, as well as altering cell morphogenesis, motility and sporulation.[144] It is believed that direct contact between the cell membrane and nAl_2O_3 induced a defensive response to counteract damage to the cell membrane, oxidative stress and damage to the flagellum, optimising conditions for growth.[144] Whether such a response is unique to nAl_2O_3 is not known and requires investigation. Secretion of extracellular polymeric substances (EPS) by algae is also believed a defensive mechanism in response to NMs.[154, 155] The function of these high-molecular polymers is to protect the algal cells from external compounds.[154] The presence of EPS has been found to mitigate the toxic effects of AgNPs to *Chlorella pyrenoidosa.*[154] It is believed that the EPS is able to bind AgNPs, as well as ionic Ag^+, which effectively reduces internalisation of silver into algal cells and mitigates toxicity.[154] The production of EPS, therefore, could serve as an effective defensive strategy for algal species exposed to NMs. However, the binding of NMs and metal ions to EPS may act as a pathway for transportation to higher trophic levels *via* feeding and possible bioaccumulation of pollutants.[154] The emergence and advance in methods such as proteomics provide great scope to investigate the mechanisms of

NM toxicity in more detail. Proteomic analysis was carried out to investigate the response of *P. tricornutum* to cadmium selenide nanoparticles (nCdSe).[130] Here, it was observed that diatom cells regulated the synthesis of proteins associated with oxidative stress protection, cellular redox homeostasis, S-nitrosylation and S-glutathionylation, as well as the regulation and signalling of Ca^{2+}.[130] As a result, *P. tricornutum* was able to regulate intracellular ROS and ionic Cd^{2+} levels as to maintain growth.[130] Molecular methods such as proteomics provide great scope for further investigation into the manners by which microbial cells are able to deal with NM-associated stress and reveal new information regarding mechanisms of toxicity.

The majority of studies have examined antibacterial or antimicrobial action upon single species. However, it is important work is extended to study their effect upon communities of microbial species. A review of the effects of NMs upon microbial communities is provided by Mohanty *et al.* 2014.[156] Exposure to NMs has been found to affect microbial communities that inhabit soils,[157-163] sediments,[164, 165] freshwater environments[166-168] and sludge from wastewater treatment plants;[40-44] exerting a number of varying effects that are both material- and community- dependent, but include alteration to community composition and functioning.[41, 159, 167] Although this evidence exists, in a number of studies little or no impact of NMs upon the microbial community structure or functioning is recorded.[164, 169-172] Limited research is available upon for the impact of engineered NMs upon natural marine communities; in the above mentioned review only 1 of 40 studies was carried out upon marine microorganisms.[156]

Since 2014, the number of studies examining the impacts of NM exposure upon marine microbial communities has increased, much of this work has focussed upon the effects of AgNPs.[9, 30, 173-177] In contrast, relatively little data is available for the impact of MO NMs upon marine microbial communities, despite these NMs being the highest produced worldwide.[9] However, evidence for effects of MO NMs on terrestrial and freshwater communities is more readily available.[162, 163, 168, 178, 179] In the evidence currently available, NMs have been recorded to drive a number of effects upon marine microbial communities, including; decline in cell number,[173] a reduction in photosynthetic output,[173] decreases in the biomass and volume of biofilms,[30] declines

in bacterial diversity,[174] and an alteration of community structure and dynamics.[30, 175, 176, 180]

Experimental work has been carried out upon planktonic, as well as biofilm communities.[30, 173-176, 181] Here, planktonic cell growth has been recorded to decline relative to control populations in free-living communities,[174] whilst in biofilms both density and biovolume have been recorded to decrease.[30] Studies upon sediment-dwelling microbes also exist.[164] However, here no impact of AgNPs upon the bacterial community inhabiting estuarine sediments was identified, believed due to the formation of AgCl complexes, which display lower toxicity than Ag^+ due to decreased bioavailability.[77, 164] Likewise, no impact upon abundance of prokaryotic organisms inhabiting waters above the sediment was recorded during the incubation.[164]

Through community analysis, it is possible to identify specific taxa that appear particularly sensitive to NM exposure. In coastal seawater, photosynthetic cyanobacteria have been recorded to display high sensitivity to AgNPs at concentrations close to those predicted in the environment.[175, 176] Likewise, when exposed to $nTiO_2$, the relative abundance of Bacteroidetes within marine biofilms was observed to decrease, whilst abundant Proteobacteria on the other hand displayed a relative increase.[180] The increased sensitivity of particular members may affect community functioning due alterations in abundance of community members which possess specific roles in community functioning. Such effects have been observed in other environments, for example alteration of activated WWTP sludge communities following the addition of $nTiO_2$ reduced the efficiency of nitrogen removal by 24-80%.[179] Community analysis provides the opportunity to gather a comprehensive understanding of the response of various taxa to NM exposure, thus enabling the identification of sensitive or resistant taxonomic groups, allowing for more effective inference of likely environmental impacts. Increased research output in this area will be of great use to evaluate the environmental risk of nano-sized pollutants.

The small size of NMs means that unlike some pollutants they are bioavailable to the majority of marine biota and their potential to interact at a cellular level must be assessed. Evidence suggests that these contaminants have the potential to exert adverse effects upon marine microbial species, which given their key ecological role

may have negative knock-on effects for entire marine ecosystems. It is clear that due to the great variation in particle-specific properties, there is unlikely to be a 'one-size-fits-all' mechanism by which engineered NMs exert stress on marine organisms. However, key drivers of toxicity can be identified through experimental work, such as the dissolution of toxic species, production of ROS and associated oxidative stress, internalisation of NMs, which appears to be size-specific, and the direct physical interaction between particles and cells. A limitation of previous experimental work is that in most studies experimental conditions do not accurately represent the natural environment. Similarly, any differences in toxicity of research-grade *versus* commercial NMs remains unclear and requires addressing. Modern molecular methods allow us to examine the interaction between NMs and microbial species in greater detail, and such work will be of great importance in accurately assessing the safety of pollutants entering the environment. Laboratory work must be carried out using environmentally relevant concentrations and conducted over a range of timeframes in order to gain a strong understanding of the likely short and long-term effects that NMs may have upon the microbial community, allowing for the comprehensive evaluation of their likely risk.

1.6 Summary and aims

In this PhD thesis, novel insights are provided upon the ecotoxicological effects of engineered NMs within the marine environment, allowing for an improved perception of their likely environmental risk and impact upon biota. Owing to their ecological significance and key role in regulating major biogeochemical and climatic cycles, focus is placed upon marine microbial species which often are the first group of organisms to interact with anthropogenic pollutants. These species represent the base of the marine food web and thus any negative effect experienced may incur adverse outcomes upon the local ecosystem, potentially affecting aquatic industries and human health. Given the vast array of NMs that are currently produced worldwide and that may enter the natural environment, a selection of commonly used NMs are utilised for research based on their prevalent use and likely entry into aquatic environments.

The first two experimental chapters focus upon two groups of NMs: AgNPs and MO NMs. First, their effect upon the ecologically significant marine cyanobacterium

Prochlorococcus is assessed under environmentally relevant conditions. Subsequently, additional experimentation utilising advanced imaging and molecular techniques provides insight into toxic mechanisms. In the third experimental chapter, to provide a commercially relevant case study, and explore any effect of NM exposure upon biofilm communities, the impact of novel NM-based antifouling surface coatings upon marine biofilm formation is examined in collaboration with an industrial partner.

Experimental techniques have been developed to enhance the environmental relevance of work, thus improving their function in accurately recording effects representative of those in that may occur in nature. Natural seawater is used as experimental medium throughout, examining impacts of NMs upon microbial species at ambient cell densities representative of those found in the natural marine environment. Additionally, NMs are extracted from consumer products to allow for the characterisation of materials likely to enter the environment following domestic use and allowing for their toxicity relative to research-grade NMs to be assessed. Molecular methods including shotgun proteomics and amplicon sequencing of the 16S and 18S rRNA genes, provide new insight into the effects of NMs upon marine microbial species at both the organism- and community- level. Whilst a combination of light scattering, flow cytometric and microscopic methods is utilised to infer likely NM fate and behaviour under natural conditions.

As a result of this comprehensive investigation, findings provide scope to evaluate the likely environmental risk of NMs in the ocean and provide recommendations for future research in the field of nano-ecotoxicology. Ultimately, providing evidence to direct regulation of monitoring and release of engineered NMs into the environment.

Chapter 2

Investigating the toxicity of silver nanoparticles upon the ecologically significant marine cyanobacterium *Prochlorococcus*

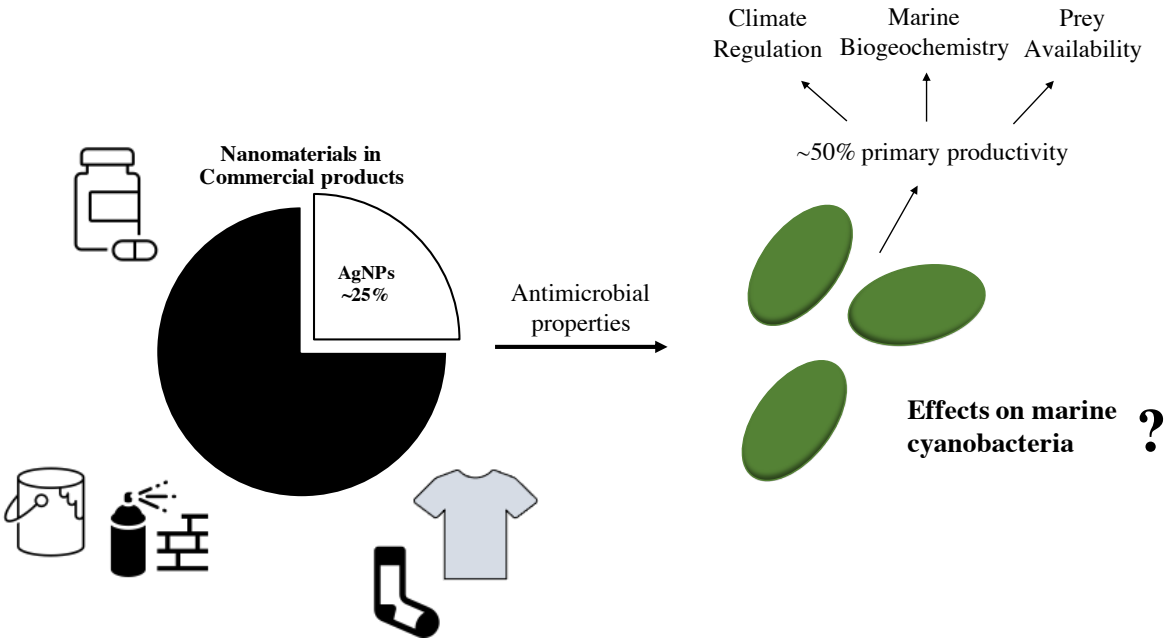

*Much of the data presented in this chapter is published in the article, "Mechanisms of silver nanoparticle toxicity on the marine cyanobacterium Prochlorococcus under environmentally-relevant conditions", Sci Total Environ, 2020, **747**, 141229. C. J. Dedman, G. C. Newson, G.-L. Davies, and J. A. Christie-Oleza.*

2.1 Introduction

The fate and effects of engineered NMs within the aquatic environment has become a subject of concern and focus of research in recent years.[66, 182-184] Silver nanoparticles (AgNPs) are present in approximately one quarter of commercially marketed nano-products (24%), primarily because of their antibacterial properties.[9, 185] This represents the fastest growing class of engineered NMs used for commercial purposes.[186] Global production of AgNPs is currently >800 metric tonnes per annum[187] and is predicted to rise.[188] The surfaces of AgNPs can be altered to control the release of ionic Ag^{+}, believed to be primarily responsible for their antibacterial properties.[189] Citrate-stabilised AgNPs represent the most widely used silver colloids for research and commercial purposes.[190-193]

The widespread use of AgNPs and the significant increase in the production of consumer goods utilising nanosized Ag, has increased the likelihood of these particles entering the aquatic environment, either through accidental release, leaching of AgNP-treated surfaces or in wastewater discharge.[34, 194] Antibacterial fabrics utilised in the antibacterial clothing industry are recorded to contain AgNPs in concentrations up to 1360 μg-Ag g^{-1}.[34] Such fabrics have been found to readily leach colloidal and dissolved silver.[34, 35] For example, up to 650 μg of silver (AgNPs, 10-500 nm) was recorded to leach when representative fabrics were entered into 500 mL distilled water,[34] a process enhanced under conditions representative of domestic washing due to addition of cleaning agents containing bleach.[35] It is feasible to suggest that domestic or industrial scale washing of fabrics incorporating AgNPs, is likely to release nanoparticles and ionic silver into wastewater systems. Leaching of AgNPs from outdoor paints has also been recorded; concentrations up to 145 μg L^{-1} are released during runoff events, with 30% total loss of AgNPs over the course of one year.[194] Environmental sampling of NMs remains challenging[11] and uncertainties exist in the concentrations of engineered NMs predicted in the environment.[195] Therefore, little evidence exists for the exact concentration of AgNPs within aquatic ecosystems.[53] Current values for surface waters vary according to their proximity to polluting sources and, hence, predicted AgNP concentrations range from those in the

ng L^{-1} range, up to 10 μg L^{-1}.[53] Due to water fluxes, oceans represent the ultimate sink for these materials.

Approximately 50% of global primary production is carried out by marine phototrophic microorganisms[131, 133] and, hence, the effect of AgNPs on these organisms is of uttermost relevance. However, relatively little evidence exists for the effects of AgNPs upon marine microbial species compared to those from freshwater.[196] Growth inhibition following AgNP exposure has been previously recorded in a number of marine photosynthetic species (*e.g.* diatoms,[74, 77, 109, 125, 141, 197, 198] green microalgae,[125, 135, 136, 199, 200] marine raphidophytes,[139] and cyanobacteria[141]). A summary of recorded effects of AgNPs upon marine microbial species is displayed below in Table 2.1. Here, AgNPs appear to exert adverse effects upon microorganisms in a species- and material-specific manner.[109, 125, 199] Typically, ecotoxicological endpoints (*i.e.,* EC_{50} and IC_{50} values) are recorded in the concentration range of 24.3 μg L^{-1} to 25.77 mg L^{-1}, dependent on the model species and specific AgNPs used.[74, 77, 109, 125, 198, 199] Often toxic effects are attributed to oxidative stress and damage to cell walls or membranes due to the generation of ROS or release of toxic silver ions.[150, 189] Disruption to photosynthetic processes have also been recorded, such as a decrease in chlorophyll-α content,[198, 200] and interference of photosystem-II electron transport.[109, 136] However, it appears that in most studies, high cell-dense, rich-nutrient cultures are used for experimentation with a potential loss of environmental significance. As a result, the exact antimicrobial action of AgNPs under environmentally-relevant conditions remains unclear.[201]

In this chapter, new evidence is provided upon the toxicity of citrate-stabilised AgNPs towards marine microbial microorganisms. Experimentation utilising natural phytoplankton communities shows how the marine cyanobacterium *Prochlorococcus*, numerically the most abundant phototrophic organism on Earth and major contributor of primary production in oligotrophic oceans,[202, 203] experiences the strongest detrimental effect recorded during community exposure to AgNPs. Owing to its ecological significance, this species is identified as an appropriate and relevant model organism for further ecotoxicological study.

Table 2.1. Effects of silver nanoparticles upon marine microbial species

Species	Taxonomic Group	AgNPs	Exposure conditions	IC_{50}/EC_{50} Reported?	Effects/Additional findings	Ref.
Thalassiosira pseudonana	Diatom	Laboratory-synthesised maltose-coated AgNPs 20, 40, 100 nm	72 h exposure 0, 10 µ M Artificial seawater/natural seawater (Harbour) Cell density at T_0: 0.75 x 10^6 cells mL^{-1} 20 mL culture	NA	- 20 and 40 nm AgNPs exerted relatively higher toxicity than 100 nm AgNPs (50, 60 and 40% growth inhibition respectively). - Toxicity results from synergistic effect of AgNPs and released silver ions.	141
Chattonellla marina	Raphidophyte	Laboratory-synthesized Citate-stabilised AgNPs 56 nm	1 h exposure 0, 0.02, 0.2, 2, 10, 20 µ M GSe medium 1 mL culture	NA	- Dissolved silver displayed considerably higher toxicity than AgNPs. - 25% uptake in silver from AgNPs by *C. marina* - Toxicity attributed to the release of ionic silver.	139
Dunaliella tertiolecta	Green microalgae	Silver nanopowder (MTI Corporation, USA) 50 nm	24 h exposure 0, 0.01, 0.1, 1, 10 mg L^{-1} Seawater growth medium Cell density at T_0: 1 x 10^6 cells mL^{-1} 100 mL culture	NA	- AgNP exposure resulted in; decreased chlorophyll, decrease in cell viability, increased lipid peroxidation and increased ROS generation.	135

Species	Taxonomic Group	AgNPs	Exposure conditions	IC_{50}/EC_{50} Reported?	Effects/Additional findings	Ref.
Phaeodactylum tricornutum	Diatom	- Citrate-stabilised (ABC Nanotech, South Korea) 14 nm - PVP-coated (Mercator Gmbh, Germany) 15 nm	72 h exposure F/2 growth medium (half strength) 6 mL culture Cell density at T_0: 3×10^4 cells mL^{-1}	Cit-stabilised AgNPs: IC_{50} 2380± 1880 µ g L^{-1} PVP-coated AgNPs: IC_{50} 3690± 2380 µ g L^{-1}	- Growth inhibition recorded - Ionic silver relatively higher toxicity than NPs - Toxicity to silver in both forms was >two orders of magnitude higher than with freshwater species *P. subcapitata.*	74
Dunaliella tertiolecta *Skeletonema costatum*	Green microalgae Diatom	AgNP suspension in deionized water (Polytech Inc., Germany) 1-10 nm	72 h exposure 0, 0.4, 0.8, 1.6, 3.2, 6.4 mg L^{-1} f/2 culture medium 12:12-h light:dark	*D. tertiolecta:* IC_{50} 0.9 mg L^{-1} *S. costatum:* IC_{50} 3.1 mg L^{-1}	- Growth of the green alga was inhibited at the lowest concentration. - The diatom showed a significant decline in growth in relation to the control at concentrations >1.6 mg L^{-1}.	125
Skeletonema costatum	Diatom	Oleylamine-coated AgNPs (Suzhou Cold Stones Technology Co., Ltd., China) 10 nm	24 h exposure 0, 0.05, 0.5, 5, 50 mg L^{-1} f/2 culture medium Cell density at T_0: 1×10^6 cells mL^{-1}	EC_{50} 25.77 mg L^{-1}	- Dissolved silver displayed higher toxicity by one order of magnitude. - Intracellular ROS was significantly induced by AgNPs. - Chlorophyll-α content was reduced and disrupts photosynthetic processes in a different manner to ionic silver.	109

Species	Taxonomic Group	AgNPs	Exposure conditions	IC_{50}/EC_{50} Reported?	Effects/Additional findings	Ref.
Phaeodactylum tricornutum	Diatom	Silver Nanopowder (US Research Nanomaterials Inc., USA) <2, <15, 30-50 nm	72 h exposure 0, 10, 40, 75, 150, 300 μ g L^{-1} f/2 medium without EDTA Cell density at T_0: 1 x 10^4 cells mL^{-1}	<2 nm AgNPs: EC_{50} not reached. <15 nm AgNPs: EC_{50} 143-184 μ g L^{-1} 30-50 nm AgNPs: EC_{50} not reached	- Toxicity to *P. tricornutum* was attributed to direct AgNP effects: cell surface attachment and internalization. - Oxidative stress, disruption to photosynthetic processes, and cell morphology were affected by AgNP exposure.	77
Chaetoceros gracilis	Diatom	PVA-stabilised AgNPs (laboratory-synthesised) ~10 nm	96 h exposure 0, 1, 10, 20, 50, 100 μ g L^{-1} f/2 media 12:12 h light:dark Cell density at T_0: 5 x 10^4 cells mL^{-1}	EC_{50} 24.3 μ g L^{-1}	- Growth inhibition recorded at a higher extent than freshwater green algae *Scenedesmus acuminatus.*	197
Chlorella autotrophica *Dunaliella salina*	Green microalgae	AgNPs (US Research Nanomaterials, USA) <15 nm	72 h exposure 0, 0.01, 0.05, 0.1, 1, 5 mg L^{-1} Substitute Ocean Water Cell density at T_0: 1x10^4 cells mL^{-1}	*C. autotrophica:* EC_{50} 0.57 mg L^{-1} *D. salina:* EC_{50} 0.64 mg L^{-1}	- Ionic silver exerted higher toxicity than AgNPs. - Cell density was observed to decline in presence of AgNPs. - Toxicity was associated with ROS production, decreased chlorophyll and decreased effective quantum yield of PSII.	199

Species	Taxonomic Group	AgNPs	Exposure conditions	IC_{50}/EC_{50} Reported?	Effects/Additional findings	Ref.
Thalassiosira sp.	Diatom	PVA-stabilised AgNPs (Laboratory-synthesised) ~6-10 nm	72 h exposure 0, 5, 20, 50, 100, 200 μ g L^{-1} f/2 media 12:12 h light:dark Cell density at T_0: 5 x 10^4 cells mL^{-1}	EC_{50} 107.21± 7.43 μ g L^{-1}	- EC_{50} higher than that recorded in freshwater green algae *Scenedesmus acuminatus.* - 100 and 200 μ g L^{-1} AgNPs caused a significant increase in cell diameter in *Thalassiosira sp.* - AgNP concentrations >20 μ g L^{-1} caused a significant decrease in chlorophyll-α - Lipid production was significantly increased in the presence of AgNPs.	198
Chlorella vulgaris	Green microalgae	AgNPs (American Elements, USA) 50 and 100 nm	96 h exposure 0, 10, 50, 100, 200 mg L^{-1} f/2 media 12:12 h light:dark Cell density at T_0: 3.3 x 10^5 cells mL^{-1}	NA	- AgNPs entered into and formed aggregates inside microalgal cells - ROS formation was increased in the presence of AgNPs. - Cell viability was negatively affected. - Larger particles (100 nm) exerted higher levels of toxicity.	200
Dunaliella tertiolecta	Green microalgae	Silver nanopowder (MTI Corporation, USA) 50 nm	24 h exposure 0, 0.1, 1, 10 mg L^{-1} Seawater growth medium 25° C and 31° C Cell density at T_0: 1 x 10^6 cells mL^{-1} 50 mL culture	NA	- AgNPs exert a stronger adverse effect upon marine *D. tertiolecta* than freshwater *Chlorella vulgaris.* - AgNPs disrupt photosynthetic processes, namely PSII electron transport. This effect is enhanced at higher temperature.	136

Using the model *Prochlorococcus sp.* MED4 grown under environmentally relevant conditions (*i.e.,* at environmentally-relevant cell densities in natural oligotrophic seawater) it is shown for the first time that the toxicity and ability of populations to recover from short-term stress caused by AgNP exposure is largely dependent on cell density, a feature often overlooked in ecotoxicological studies upon microbial organisms. A simplistic approach is used, utilising natural seawater without added nutrients to enhance our understanding of the effects of AgNPs in natural waters, hence minimising any effect of other experimental parameters observed to alter outcomes of research.[72] The calculation of the particles-to-cell (NPs $cell^{-1}$) ratio at the beginning of exposures (T_0) is presented as an effective tool to account for any variation in cell density, and correctly assess AgNP toxicity. Where appropriate, the consideration of this particles-to-cell value in future research within the field of nano-ecotoxicology is promoted. Novel insight into the mechanisms of AgNP toxicity towards marine microbial organisms under natural conditions is provided through a series of experimental approaches, exploring the respective influence of ROS and ionic silver in driving toxicity; and any alterations to the *Prochlorococcus sp.* MED4 proteome in response to sub-lethal to- toxic concentrations of AgNPs.

2.2 Materials and methods

2.2.1 Materials

Research-grade materials were purchased from Sigma Aldrich (for material-specific information please see specific sections). Glassware used for experimentation was acid-washed and rinsed in Milli-Q ultrapure water (0.22 μm filter operated at 18.2 MΩ at 298 K) prior to their use. Synthesised nanoparticles and those purchased from Sigma Aldrich were stored at 4°C and stocks used for experimentation were freshly prepared prior to use. Natural seawater (NSW) used in experimental work was obtained from Station L4, Plymouth (50°15.0'N; 4°13.0'W), and was prepared by autoclave (20 mins, 120°C), and subsequently filtered through a 0.22 μm polyethersulfone membrane (Corning®). Transmission electron microscopy (TEM) was used to determine the size of nanoparticles used during experimental work. Here, a JEOL 2000FX or 2100 TEM,

200 kV, LaB_6 instrument was used, operated with a beam current of ~115 mA. Images were captured using a Gatan Orius 11-megapixel camera. Samples were prepared by deposition and drying of nanoparticle samples (10 μL aqueous suspension) onto formvar-coated 300 mesh copper TEM grids (EM Resolutions). Diameters were measured using ImageJ version 3.2; average values were calculated by counting a minimum of 100 particles.

2.2.2 Synthesis of citrate-stabilised AgNPs for use in community exposure and preliminary tests with cyanobacteria

Citrate-stabilised AgNPs were synthesised by the stepwise reduction of silver nitrate by sodium borohydride and trisodium citrate, using a protocol adapted from Dong *et al*. (2010).[204]

Synthesis 1: AgNPs utilised in community exposure (section 2.2.3).
Trisodium citrate (0.83 g, 3.23 mmol) and sodium hydroxide (30 μg, 0.0038 mmol) were dissolved in 160 mL Milli-Q ultrapure water. The resulting solution was heated to 60 °C in the dark for 30 mins whilst stirring. Separately, $AgNO_3$ (14 mg, 0.08 mmol) was dissolved in 40 mL Milli-Q ultrapure water and added to the citrate solution dropwise. The temperature was increased to 90 °C and sodium hydroxide (0.1 M) was added to adjust the pH to 10.5. After 20 mins stirring, the solution was removed from the heat and allowed to cool to room temperature.

Synthesis 2: AgNPs utilised in preliminary experiments section 2.2.5).
Reactions were set-up as follows: $AgNO_3$ (0.00255 g, 1 mmol) and trisodium citrate (0.103 g, 3.5 mmol) were added to 90 mL Milli-Q ultrapure water in a 250 mL round-bottomed flask and put on ice whilst stirred. $NaBH_4$ (0.01g) was added to 10 mL ultrapure H_2O to produce a stock solution. Subsequently, 19 μL $NaBH_4$ stock solution was added to 10 mL Milli-Q ultrapure water, producing a final concentration of 1.9 x 10^{-5} g (0.005 mmol). This was then added dropwise to the 90 mL aqueous solution under vigorous stirring, resulting in a colour change of the solution from pale yellow to gold. The 100 mL aqueous solution was stirred on ice for 30 mins in the dark. After

30 mins, the temperature was raised to 70°C and the solution stirred for 2 h. Final solutions were subsequently allowed to cool to room temperature.

Following synthesis, nanoparticles were washed with Milli-Q ultrapure water using dialysis and stored at 4°C. AgNP size and morphology was assessed using TEM as described above (section 2.1.1). Synthesis yielded two stocks of AgNPs; the first used in community exposures (section 2.2.3) represented a mixed population of spherical (22.0±3.3. nm, diameter) and rod-shaped (51.2±14.9 nm, length) AgNPs. The second stock utilised in preliminary experiments with *Prochlorococcus* (section 2.2.5) comprised of spherical AgNPs (10.5±3.3 nm) only.

2.2.3 Natural marine community exposure to AgNPs

Surface seawater (SW) containing its full natural microbial community was obtained from Mallorca, Spain (39°29'37.9"N 2°44'23.4"E, 6th January 2017). 10 mL of SW was incubated in 50 mL tissue culture flasks and exposed in triplicate to a mixed population of laboratory-synthesised citrate-stabilised AgNPs (22.0±3.3 nm (spheres), 51.2±14.9 nm (rods, length)) at 0, 1 and 500 μg L^{-1}. Flasks were incubated at ambient seawater temperature (18 °C) at a light intensity of 10 μmol photons m^{-2} s^{-1} and light:dark cycles of 14:10 h. Phytoplankton communities were monitored by flow cytometry at days 1, 5 and 8, using their distinctive autofluorescence and size to gate the different phototrophic populations (section 2.2.8 below for details).

2.2.4 *Prochlorococcus* culture

Axenic *Prochlorococcus sp.* MED4 cultures were routinely prepared in nutrient rich Pro99 media throughout experimental work. Pro99 media[205] was prepared in autoclaved and filtered natural oligotrophic seawater; to 500 mL NSW, 0.8 mL NH_4Cl (final concentration, 0.5 M), 1 mL $NaH_2PO_4 \bullet H_20$ (final concentration, 0.025 M) and 50 μL trace metal stock was added and mixed by inversion three times. To make-up trace metals stocks; a)1.5 g $ZnSO_4 \bullet 7H_20$; b) 0.595 g $CoCl_2 \bullet 6H_20$; c) 8.905 g $MnCl_2 \bullet 4H_20$; d) 0.363 g $Na_2MoO_4 \bullet 2H_20$; e) 0.865 g Na_2SeO_3; f) 1.19 g $NiCl_2 \bullet 6H_20$; was added to 50 mL Milli-Q ultrapure water and mixed by inversion before storage at

4ºC. Subsequently, to make up the working stock, 50 µL of each primary trace metal stock was added to a falcon tube containing 50 mL Milli-Q ultrapure water to which 0.2175 g $Na_2EDTA•2H_20$ and 0.16 g $FeCl_3•6H_20$ had been added.

Each component of media was filter sterilized using a 0.22 µm filter prior to addition to NSW. Ionic strength of the NSW used during experiments was measured using an Eutech Instruments COND610 handheld meter and was recorded as 44.2 and 50.5 mS, before and after autoclaving respectively, within the range of natural seawater in relevant regions (~40-60 mS).[206]

2.2.5 Observational study of *Prochlorococcus sp.* MED4 when exposed to AgNPs in rich culture.

Axenic *Prochlorococcus sp.* MED4 culture was prepared as described in section 2.2.4. To establish exposures, 30 mL of cell-dense *Prochlorococcus* culture (~10^7 cells mL^{-1}) was added to 50 mL filter-capped tissue culture flasks in triplicate. Flasks were spiked with a defined volume of laboratory-synthesised AgNP stock (citrate-stabilised spheres, 10.5±3.3 nm (TEM)) made up in Milli-Q ultrapure water to a final concentration of 0, 0.66, 6.61, 65.93 and 639.53 µg L^{-1}. Following spiking, samples were placed onto an orbital shaker (100 rpm) inside a 23.5°C incubator at constant 10 µmol photons m^{-2} s^{-1} light intensity for a period of 144 h. At regular intervals (T_0, T_{24}, T_{48}, T_{72}, T_{144}) photographs of the culture were taken to determine the health of the cyanobacterial culture by visual observation. Here, populations were assessed to have crashed when cultures were no longer green in colour, indicating a loss of the living cyanobacterial population.

2.2.6 Behaviour and dissolution of AgNPs within natural seawater

a) AgNP behaviour

To examine behaviour of AgNPs in NSW, as prepared above, AgNPs (citrate-stabilised spheres, Sigma Aldrich, 20.4±3.9 nm (TEM)) were added to 20 mL NSW at a test concentration of 1 mg L^{-1} and maintained at room temperature for a period of 72 h under shaking (100 rpm) (n=3). At defined timepoints (0, 0.5, 2, 4, 24, 48 and 72

h) a 200 µL subsample was collected from the mid-point of flasks and analysed using Dynamic Light Scattering (DLS) using a Malvern Zetasizer Nano instrument. For each sample, data was collected as the average of 3 measurements made up of 11 readings, each lasting 10 seconds. To assess aggregation of AgNPs, the alteration in z-average size (d.nm) was recorded at each timepoint. An observation of the mean count rate (kcps) provided insight into the extent of AgNP precipitation out of the water column. The test concentration of 1 mg L^{-1} was selected based on preliminary investigation, which revealed this to be the lowest detectable AgNP concentration for reliable data acquisition.

b) AgNP dissolution

For monitoring of the dissolution of ionic Ag^{+} from AgNPs during the timescale of toxicity testing, AgNP (citrate-stabilised spheres, Sigma Aldrich, 20.4±3.9 nm (TEM)) suspensions were made up in 100 mL NSW, as prepared above, in tissue culture flasks to produce concentrations of 0, 10, 50 and 250 µg L^{-1} (n=3). Flasks were maintained under the experimental conditions described in section 2.2.7. At defined timepoints (0, 0.5, 1, 2, 24, 48, 72, 168 and 240 h), a 5 mL sub-sample was collected from each flask. To ensure AgNPs were effectively removed, ultrafiltration *via* centrifugation using a Macrosep Advance Centrifugal Device with 10K Omega Membrane (Pall Laboratory, approximate pore size 2.9 nm) was carried out, as done previously.[74] Subsequently, filtered NSW samples were transferred to a new 15 mL falcon tube and stored at -20°C. Prior to analysis, samples, including controls, were thawed at room temperature and acid-digested by nitric acid (70% HNO_3, Sigma Aldrich) under heating, to remove particulate material and ensure all AgNPs were converted to their ionic form. To remove excess salt, samples were diluted 100x in Milli-Q ultrapure water. Following this, ionic silver content was measured against an internal metal ion standard (100 mg L^{-1} in 5% HNO_3) by inductively coupled atomic emission spectroscopy (ICP-AES) using a Varian 720-ES ICP-AES.

2.2.7 *Prochlorococcus sp.* MED4 culture exposure to AgNPs

Axenic *Prochlorococcus sp.* MED4 was routinely grown using Pro99 media[205] (see section 2.2.4). Prior to AgNP exposure (citrate-stabilised spheres, Sigma Aldrich,

20.4±3.9 nm (TEM)), *Prochlorococcus* was preadapted to environmentally relevant conditions by inoculating cells in NSW (obtained from station L4, Plymouth, 50°15.0'N; 4°13.0'W; filtered through a 0.22 µm polyethersulfone membrane (Corning®) to eliminate particulate organic carbon and further autoclaved for sterility). *Prochlorococcus* was added at close-to-ambient cell densities (*i.e.,* 10^4-10^5 cells mL^{-1})[207] and incubated for 72 h under optimal conditions (*i.e.* 23 °C at constant 10 µmol photons m^{-2} s^{-1} light intensity using a Lifelite™ full spectrum bulb, with 100 rpm shaking). The light intensity used is optimal for cultured *Prochlorococcus sp.* MED4 and ensured cyanobacteria were not affected by light stress during experiments. After 72 h, 30 mL of preadapted *Prochlorococcus* cultures were transferred to 50 mL filter-capped tissue culture flasks (n=3) and spiked with AgNPs (citrate-stabilised spheres, Sigma Aldrich, 20.4±3.9 nm) at final concentrations of 0, 5, 10, 25 and 50 µg L^{-1} as determined by preliminary screening tests carried out under identical conditions in the concentration range 0-500 µg L^{-1}. Cultures were incubated under optimal conditions and monitored by flow cytometry after 0, 6, 24, 48 and 72 h of incubation.

Table 2.2. Summary of experiments included in the NPs $cell^{-1}$ investigation (Fig 2.2); [a] T_0 refers to the cell density at the start of the experiment, at which point treated samples were spiked with AgNPs.

T_0 Cell Density[a] (cells mL^{-1})	**Test volume (mL)**	**Test concentration (µg L^{-1})**
2.5 x 10^4	30	0, 5, 10, 25, 50
3.1 x 10^4	30	0, 1, 10, 25, 50, 250
1.3 x 10^5	30	0, 5, 10, 25, 50
1.4 x 10^5	40	0, 1, 5, 10, 50, 100, 500
8.7 x 10^5	30	0, 5, 10, 25, 50
1.8 X 10^6 (Pro99 media)	30	0, 1, 10, 25, 50, 250

To aid our interpretation of experimental data, the number of particles-per-cell (NPs $cell^{-1}$) added to cultures at T_0 was calculated by estimating the number of NPs mL^{-1} based on the mass and density of nanoparticles at each concentration (equation 2.1).[208, 209]

$$NPs\ mL^{-1} = \frac{(Ag\ concentration\ \div Ag\ density)}{NP\ volume} \quad \{2.1\}$$

Subsequently, this value was divided by the cell density at timepoint zero (T_0) to provide the NPs cell^{-1} (equation 2.2) for each individual treatment (see Table 2.2).

$$NPs\ cell^{-1} = \frac{NPs\ mL^{-1}}{cells\ mL^{-1}} \quad \{2.2\}$$

Longer incubations (*i.e.,* 240 h) were set up in both NSW (~3 x 10^4 *Prochlorococcus* cells mL^{-1}) and nutrient-rich Pro99 medium (~1.8 x 10^6 *Prochlorococcus* cells mL^{-1}) to evaluate the ability of cultures to recover after initial stress. AgNPs were spiked at final concentrations of 0, 1, 10, 25, 50, 250 μg L^{-1} and cultures were monitored over time by flow cytometry (*i.e.,* 0, 24, 48, 72, 96 and 240 h). For details of flow cytometric analyses see section 2.2.8, below.

2.2.8 Flow cytometric analysis

Flow cytometry was carried out using a Becton Dickinson Fortessa Flow Cytometer. Data was collected three times per replicate to ensure accuracy of the flow cytometric output. For the natural community experiment (outlined in section 2.2.3) data was collected at days 1, 5 and 8. Here, a 2 mL subsample was collected from each sample and fixed using 0.5% glutaraldehyde. This sample was stored at 5°C prior to sampling by flow cytometry. Samples were stained prior to data collection by adding 1 μL SYTOX green nucleic acid stain (ThermoFisher). Gates were established using BD FACSDiva software and used to count distinct populations of cells (Eukaryotes, *Synechococcus* (type I), *Synechococcus* (type II), and *Prochlorococcus*). Cell densities of each group were calculated in reference to AccuCheck counting beads (ThermoFisher).

For experimental work with *Prochlorococcus sp.* MED4 (outlined in section 2.2.7), when examining cultures grown to ambient cell densities in oligotrophic NSW, a 1 mL sub-sample of each replicate was analysed at each time-point. For analysis of samples grown in Pro99 media, a 10-fold dilution in autoclaved and filtered NSW was used for data collection. 10 μL of 2.2 μm high Intensity fluorescent Nile Red particles,

Spherotech FH-2056-2 (10^6 particles mL^{-1}) was added to each sub-sample to act as a reference for cell count quantification. Gates were set-up using BD FACSDiva software in order to quantify the number of reference beads and cyanobacteria cells (Fig 2.1). Here, chlorophyll fluorescence and side scatter (SSC) were routinely used to monitor *Prochlorococcus* populations. Samples were run at a medium flowrate until 100 reference beads were counted by the software. Subsequently, cell counts were calculated using Microsoft Excel.

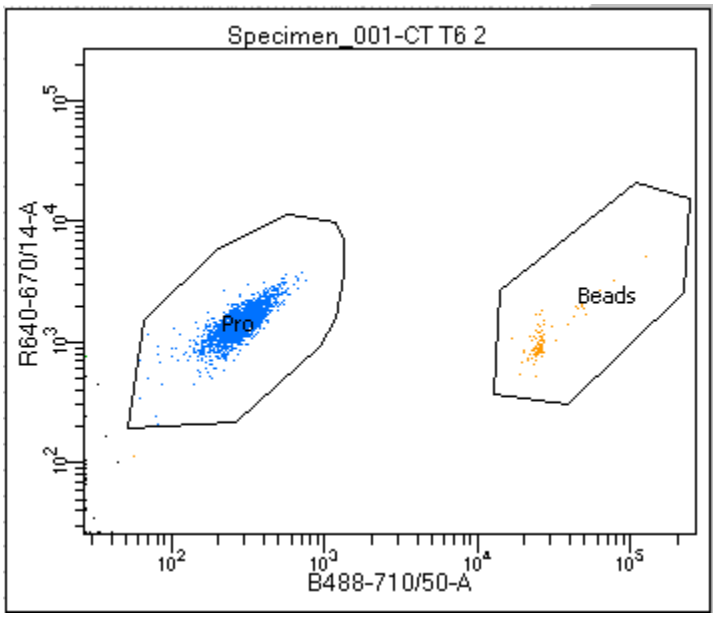

Figure 2.1. Gates used for enumeration of *Prochlorococcus sp.* MED4 (blue) in relation to fluorescent reference beads (Orange).

2.2.9 Role of reactive oxygen species in the toxicity of AgNPs on *Prochlorococcus*

Prochlorococcus sp. MED4 was exposed to AgNPs (citrate-stabilised spheres, Sigma Aldrich, 20.4±3.9 nm (TEM)) at a concentration of 50 µg L^{-1} under environmentally-relevant conditions (*i.e.,* ~10^4-10^5 cells mL^{-1} in NSW) and supplemented with sodium pyruvate, a quencher of hydrogen peroxide (H_2O_2);[210] added at 0, 40 and 60 mM (>99% purity, Sigma Aldrich) or superoxide dismutase (SOD, Sigma Aldrich); a quencher for superoxide (SOx); added at 250 U mL^{-1} during two individual experiments. Cultures were incubated under optimal conditions (section 2.2.7) for 24 h and cell density was monitored by flow cytometry, as previously described (section 2.2.8).

2.2.10 *Prochlorococcus* culture exposed to dissolved silver.

Cultures of axenic *Prochlorococcus* sp. MED4 were prepared as described in section 2.2.4 and exposed to Ag_2SO_4 (>99% purity, Sigma Aldrich) under identical experimental conditions following 72 h pre-adaptation (see section 2.2.7). Test concentrations of 0, 0.5, 1, 2.5, 5, 10, 25 and 50 μg L^{-1} total Ag (n=3) were established, and cyanobacterial populations monitored by flow cytometry, as previously described at defined timepoints (0, 6, 24, 48 and 72 h).

2.2.11 Shotgun proteomic analysis of *Prochlorococcus sp.* MED4 exposed to AgNPs.

To investigate changes to the *Prochlorococcus sp.* MED4 proteome under AgNP-stress, cell-dense cultures of were routinely grown in Pro99 media (section 2.2.4). Cell-dense cultures were used to ensure sufficient biological material for proteomic analysis. At T_{-72} cultures were subbed and supplemented with additional Pro99 media to a final volume of 20-30 mL, allowing for growth to rich cell densities and adaptation to experimental conditions, as above (n=3). At T_0 treated samples were spiked with AgNPs (citrate-stabilised spheres, Sigma Aldrich, 20.4±3.9 nm (TEM)) at five sub-lethal to toxic concentrations, as determined by previous toxicity testing (section 2.2.7), over three experimental runs (outlined in Table 2.3). Following the addition of AgNPs, treated samples and untreated controls were maintained under experimental conditions (section 2.2.7) for 24 h. Proteomic analysis was carried out upon cellular and exoproteomes of AgNP-treated cultures and compared to that of an untreated control.

Table 2.3. Experimental conditions during sample collection for proteomic analysis of sub-lethal AgNP exposure.

Experimental run	Initial cell density (cells mL^{-1})	Concentration AgNPs (μg L^{-1})	Estimated number of NPs $cell^{-1}$
1	~1 x 10^7	0, 100	0, 250
2	~1 x 10^6	0, 25, 50	0, 750, 1500
3	~1 x 10^5	0, 30, 60	0, 5000

a) Sample collection

After 24 h incubation, samples were immediately placed on ice and centrifuged for 10 mins at 4 °C at 4000 xg. The resultant cell pellet was kept on ice and transferred to a 1.5 mL Eppendorf. Following this the cell pellet was further centrifuged for 1 min at 13,000 rpm at 4 °C. Supernatant was then discarded and the pellet snap-frozen on dry ice and stored at -20 °C before further processing. The culture supernatants containing the exoproteomes were subsequently collected and filter-sterilised using a 0.22 μm filter before being stored at -20 °C.

b) TCA protein precipitation for exoproteomes

Supernatants were thawed at room temperature and underwent trichloroacetic acid (TCA) protein precipitation as previously described.[211] For 30 mL extracellular proteome samples that had previously been filtered, 750 μL 0.6 % (w/v) sodium deoxycholate (DOC) was added and vortexed to mix. Samples were incubated at room temperature for 10 mins before adding 1.8 mL 50% trichloroacetic acid (TCA) and incubating on ice for a further 30 mins. Subsequently, samples were then centrifuged for 15 mins at 4 °C at 4000 rpm and the supernatant was discarded. The resultant pellet containing exoproteome proteins was resuspended in 750 μL Milli-Q ultrapure water and transferred to a 1.5 mL Eppendorf. 28 μL 0.6 % DOC was added, and the solution was incubated for 10 mins at room temperature, followed by the addition of 67.5 μL 50 % TCA and incubation on ice for 30 mins as previous. Eppendorfs were then centrifuged for 10 mins at 4 °C at 8000 rpm and the supernatant was discarded. Finally, pellets were resuspended in 750 μL ethanol/ether (1:1 v/v) and centrifuged for a further 15 mins at 4 °C at 13,000 rpm. The supernatant was carefully removed by pipette and the pellet left to dry completely. Once dried, extracellular proteome pellets were stored at -20 °C.

c) Preparation and processing of protein gels

Cell and extracellular proteome pellets were resuspended in 1x LDS buffer (ThermoFisher) containing 1% beta-marcaptoethanol and run on a NuPage 4-12% Bis-Tris precast polyacrylamide gels as previously done.[212] Firstly, cell and extracellular proteome pellets were resuspended in 300 μL and 70 μL LDS beta-mercaptoethanol respectively and vortexed to mix. To ensure samples were well-

suspended samples were first placed on a 95 °C hot plate for 5 mins and subsequently vortexed, this process was repeated three times. Following this samples were sonicated for 5 mins and heated once again for 5 mins at 95 °C, this process was also repeated three times. Prior to loading, samples were maintained at 95°C. Samples (30 μL) were subsequently loaded into 10-well NuPage 4-12% Bis-Tris Novex Gels,[212] using separate gels for cellular and extracellular samples. Two wells were left blank between control and treated samples to ensure no cross-contamination occurred. SDS-PAGE was performed at constant voltage (200 V) and gels run for 5 mins. Following this, gels were washed with Milli-Q ultrapure water and stained using SafeStain for 30 mins. Gels were washed following staining three times using Milli-Q ultrapure water and left overnight. Subsequently, gel bands for proteomic analysis were cut into small cubes (approx. 2-4 mm) using a sterile blade and placed in 50% ethanol- 50 mM ammonium bicarbonate (ABC) overnight and maintained at 5 °C to aid the de-staining process.

d) In-gel protein digestion and mass spectrometry

In-gel trypsin digestion and peptide recovery was performed.[213] To remove the stain, gels were washed three times in 50% ethanol 50 mM ABC for 20 mins whilst heated to 55 °C under shaking (650 rpm). Following washing 100% ethanol was added to dehydrate the gel for 5 mins whilst shaken (650 rpm) at room temperature. Subsequently, 10 mM tris(2-carboxyethyl)phosphine hydrochloride (TCEP) 40 mM chloroacetamide (CAA) was added and shaken gently for 5 mins at 70 °C. The 50% ethanol 50 mM ABC washing procedure was repeated at room temperature and gel samples dehydrated using 100% ethanol, as previous. Following this, gels were hydrated with 2.5 ng L^{-1} Trypsin solution (Promega) for 10 mins at room temperature, after which sufficient 50 mM ABC was added to cover gels and samples were left overnight at 37 °C for digestion. The following day peptides were extracted by sonication (5-10 minutes) with the addition of 25% acetonitrile 5% formic acid. Following sonication, all liquid extractions were transferred to a clean 1.5 mL Eppendorf. This process was repeated three times. Extracted peptides were concentrated using a Speed-vac set at 45 °C and resuspended in 50 μL 2% acetonitrile (CAN), 0.1% trifluoroacetic acid (TFA). To ensure no gel passed through to the final sample for analysis, all resuspended samples were filtered using a 0.22 μm Costar®

Spin-X® centrifuge tube before being stored at -20 °C. Following this, a nano liquid chromatography tandem mass spectrometry (nanoLC-ESI-MS/MS) analysis was carried out using an UltiMate 3000 RSLCnano System coupled to an Orbitrap Fusion (Thermo Scientific) using conditions and settings as previously described.[214]

e) Data processing and analysis

The RAW mass spectrometry data files have been deposited to the ProteomeXchange Consortium (http://proteomecentral.proteomexchange.org) *via* the PRIDE partner repository[215] under the dataset identifier, PXD025932. RAW mass spectral files were processed using MaxQuant version 1.5.5.1[216] for peptide identification and protein label-free quantification using the *Prochlorococcus* UniProt coding domain sequences (downloaded on 16/01/2018) using default parameters with the exception of "Match between runs" for "Identification". Downstream statistical analysis was carried out using Perseus version 1.5.5.3[217] following the pipeline described previously.[218] Briefly, two-way multi-variate analysis was carried out between untreated and treated samples at each concentration, and any significantly up- or down-regulated proteins identified for further analysis. To aid our understanding of the overall impact of AgNPs upon the proteome of *Prochlorococcus sp.* MED4, proteins were classified into key groups, Basic cellular processes, Photosynthesis, Metabolism, Carbon fixation, Membrane transport, Oxidative stress, Energy production and storage, and Inorganic nutrient processing. The relative abundance of each protein group compared between control samples and treatments by means of two-way T-tests.

2.3 Results and discussion

2.3.1 Natural marine phytoplankton community response to AgNPs

Previous studies have revealed an ability of AgNPs to alter marine microbial communities, reducing bacterial growth and diversity.[173, 174] In particular, photosynthetic microorganisms such as cyanobacteria and diatoms have been recorded to display enhanced sensitivity to AgNPs at concentrations as low as 0.2-2 μg L^{-1}.[175, 176] To examine the effects of AgNP exposure upon marine phototrophs, NSW was

incubated for a period of 8 days with citrate-stabilized AgNPs (laboratory-synthesised spheres and rods, 22.0±3.3 and 51.2±14.9 nm, see Fig 2.2 and section 2.2.2) at 1 and 500 μg L^{-1}. These concentrations were selected to represent predicted environmental and supra-environmental concentrations, respectively. A clear reduction of the photosynthetic community due to AgNP exposure was observed even at the lowest concentration (*i.e.,* 1 μg L^{-1}; ~50% cell number decline; Fig 2.3). This decline was primarily driven by the decrease in abundance of the cyanobacterial community in accordance with previous studies carried out with natural seawater.[175, 176] Here, cyanobacterial decline was mainly of *Prochlorococcus*, displaying 67% and 91% decline in cell numbers at the end of the 8 day incubation in presence of 1 and 500 μg L^{-1} of AgNPs, respectively (Fig 2.3). In contrast, little or no effect was observed in other phototrophic groups (*i.e.,* pico-eukaryotic or *Synechococcus*) when exposed to the lowest concentration of AgNPs (1 μg L^{-1}). However, at higher AgNP concentrations (500 μg L^{-1}), cell declines of 57%, 73% and 33% compared to the untreated control were recorded in the pico-eukaryotes, and *Synechococcus* subgroups SYN-I and SYN-II, respectively (Fig 2.3).

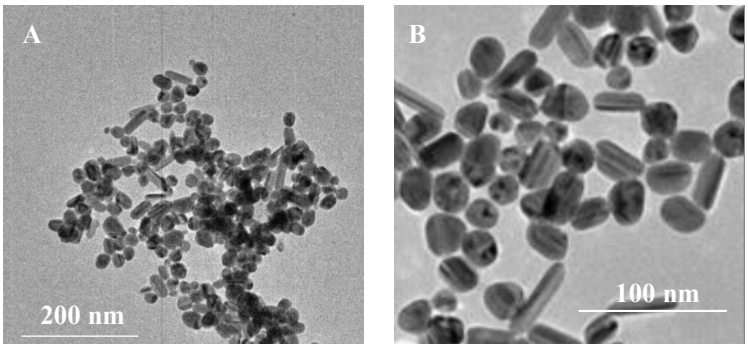

Figure 2.2. TEM images of laboratory-synthesized citrate-stabilised AgNPs used in experimental work with Natural seawater. Two populations of AgNPs were observable in the images grouped by shape: spherical and rod-shaped. These two groups were measured separately and had average sizes of 22.0 ± 3.3 nm (diameter) and 51.2 ± 14.9 nm (length) respectively.

AgNPs are believed to exert toxicity primarily *via* the release of toxic silver ions into media and that other modes of AgNP toxicity are neglible.[219] Dissolution of ionic silver from AgNPs within saline media has been reported, and occurs at an increased rate compared to freshwater.[74, 77, 135] Silver ions may be released by AgNPs *via* processes of desorption or oxidation, where the latter produce reactive oxygen species (ROS) as a result.[220, 221] Tsiola *et al*. suggest that the greater sensitivity displayed by

marine cyanobacteria is attributed to the increased affinity of AgNPs to sulfur groups present in the cell wall of cyanobacterial cells,[176] thus driving increased interaction between cells and particles by generating silver ions and ROS in close proximity of these organisms. This causes disruption to membrane permeability and deactivation of enzymes, resulting in lysis and cell death.[222] The higher toxicity on *Prochlorococcus* observed here may also be caused by the particularly higher susceptibility of this genus to oxidative stress due to the lack of mechanisms for quenching ROS.[223]

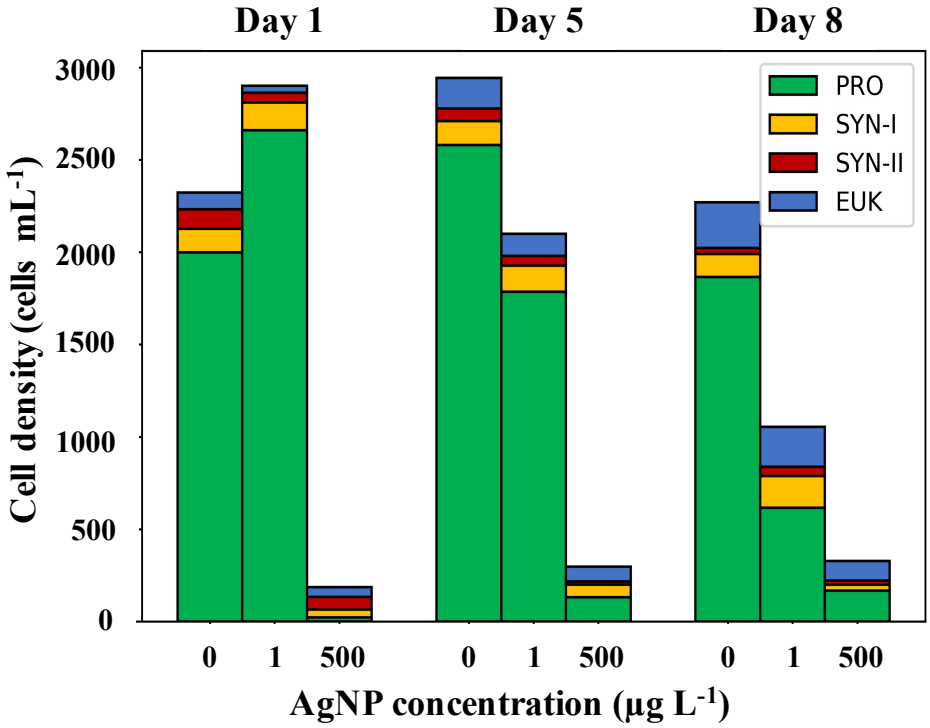

Figure 2.3. Effect of AgNPs (1 and 500 µg L^{-1}) upon natural communities of marine phytoplankton. Phytoplanktonic groups are: Green - *Prochlorococcus* (PRO), Yellow – *Synechococcus-I* (SYN-I), Red – *Synechococcus-II* (SYN-II), Blue – *Pico-eukaryotes* (EUK). Data is presented as the mean of three biological replicates (n=3).

2.3.2 Preliminary investigation of AgNP toxicity towards *Prochlorococcus*: Establishing experimental conditions.

Based on the high susceptibility of *Prochlorococcus* to AgNPs observed in the natural community analysis (section 2.3.1) and in the literature,[175, 176] the strain *Prochlorococcus sp*. MED4 was selected as a model for further laboratory investigation on the ecotoxicity of AgNPs towards marine microbial organisms.

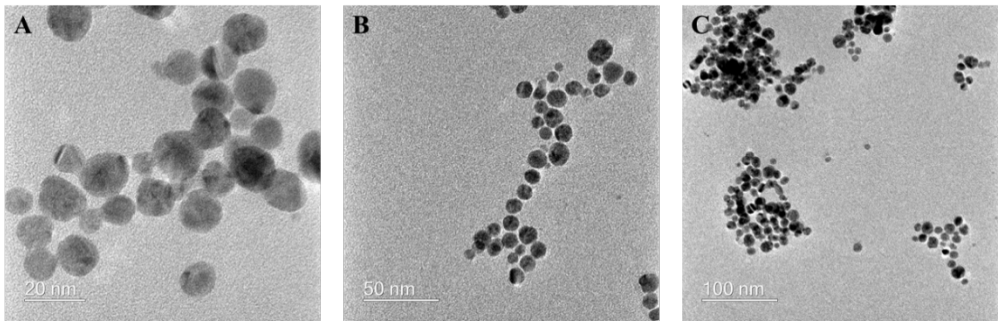

Figure 2.4. TEM images of laboratory-synthesised citrate-stabilised AgNPs used in preliminary observational study. Average diameter of particles was calculated as 10.5±3.3 nm.

To establish effective experimental conditions two preliminary experiments were completed (see sections 2.2.5 and 2.2.7). First, cell-dense cultures of *Prochlorococcus* (~10^7 cells mL^{-1}) were exposed to laboratory-synthesised AgNPs (citrate-stabilised spheres, 10.5±3.3 nm) (Fig 2.4) under optimal growth conditions for a period of 144 h (0-639.53 µg L^{-1}). Here, a wide range of concentrations were used, spanning the predicted environmental, to supra-environmental range in order to facilitate the identification of a suitable concentration range for further study. A single population of spherical AgNPs were used to minimise any variation in outcome caused by a mixed particle size and morphology. A clear negative response of exposure could be seen at the highest concentration (639.53 µg L^{-1}) after 24 h, which continued throughout the experiment (Fig 2.5), evident by the clear

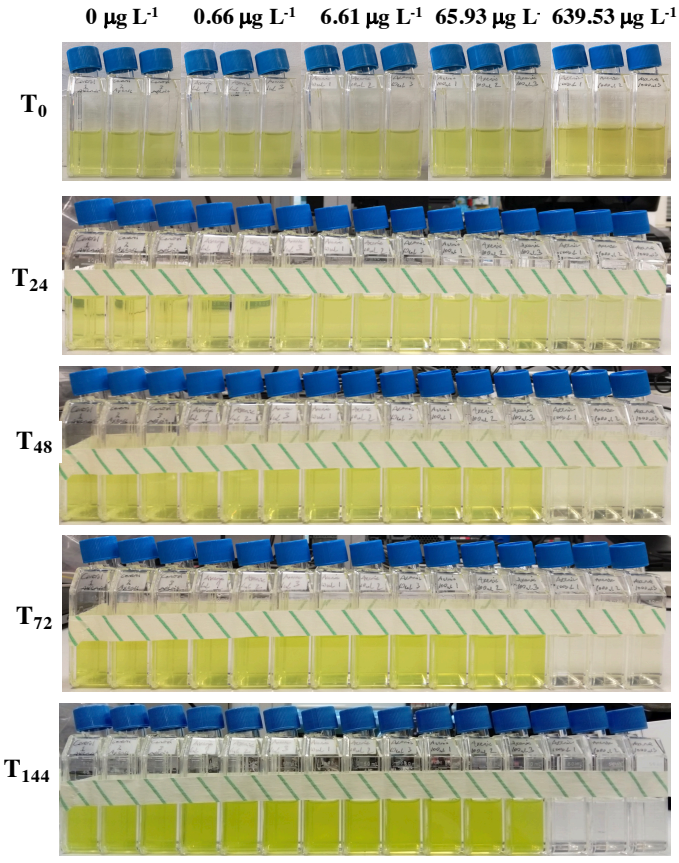

Figure 2.5. Photographic observations of *Prochlorococcus* culture in nutrient-rich Pro99 media when exposed to a range of AgNP concentrations (0-639.53 µg L^{-1}) for a period of 6 days.

discolouration of the cyanobacterial culture indicating the loss of living cells. For treated groups <639.53 µg L^{-1}, no visual difference was observed between treated and control groups (Fig 2.5). This preliminary screening allowed for the identification of a toxic concentration range of AgNPs to *Prochlorococcus sp.* MED4 under optimal growth conditions between ~65-650 µg L^{-1}, providing scope for further experimentation with quantitative methods.

Further testing of *Prochlorococcus* cultures grown in NSW to ambient cell densities[207, 224] exposed to purchased AgNPs (citrate-stabilised, 20.4±3.9 nm, Sigma Aldrich), revealed a negative response of exposure at concentrations ≥50 µg L^{-1} (Fig 2.6), resulting in significant declines in cell density of up to 90% in comparison to the untreated control after 72 h (two-way T-test, p≤0.05). As a result of this preliminary investigation, a concentration range of 0-50 µg L^{-1} was selected for evaluation of AgNP ecotoxicity under environmentally relevant concentrations. For the remaining work presented in this chapter, purchased AgNPs (citrate-stabilised spheres, Sigma Aldrich, 20.4±3.9 nm) continued to be used based on their uniformity facilitating more effective comparison between experiments and the elucidation of toxic mechanisms, which may be complicated by any variability in morphology and size of particles

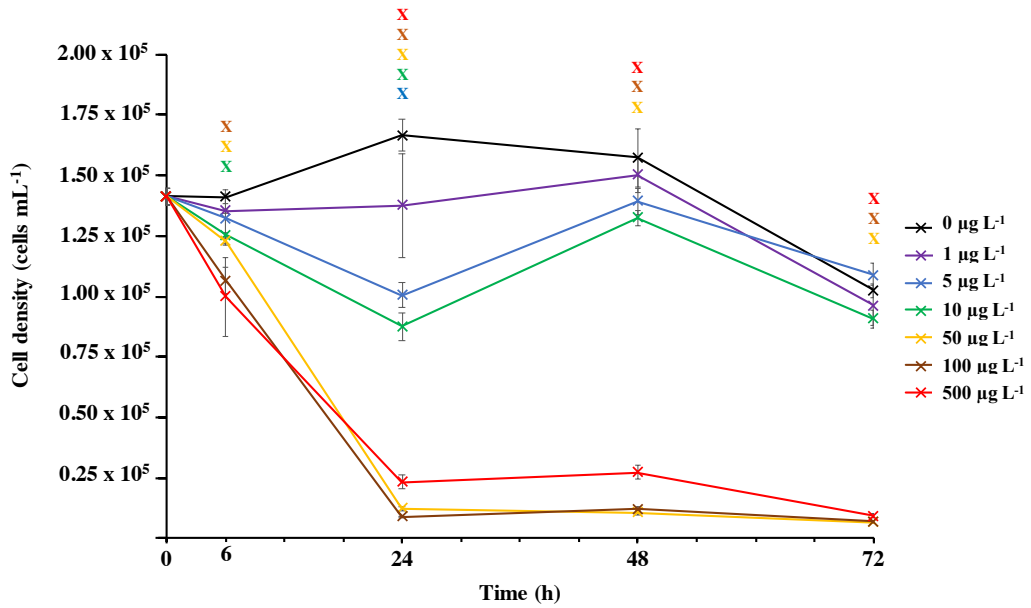

Figure 2.6. Preliminary screening of *Prochlorococcus sp.* MED4 to 20.4±3.9 nm AgNPs (0-500 µg L^{-1}). Data points are provided as the mean ± standard error (n=3). Crosses indicate where two-way T-tests identified the cell density of treated groups to be significantly lower than the control group at each timepoint (p≤0.05).

obtained though synthetic approaches. The particle size of ~20 nm examined falls within the size range of spherical AgNPs used in commercially available antimicrobial products.[225]

2.3.3 Behaviour and dissolution of AgNPs in natural seawater

Prior to establishment of experiments with *Prochlorococcus*, the behaviour of AgNPs (citrate-stabilised spheres, Sigma Aldrich, 20.4±3.9 nm (TEM)) (Fig 2.7) to be used during ecotoxicity assessments upon entry into NSW was investigated, to aid understanding of how these materials may interact with marine microorganisms and exert their potential toxic effects. It was found that currently available techniques do not provide reliable measurements at the concentrations assayed in this study and hence we discuss these results in the context of higher AgNP concentrations and available literature.

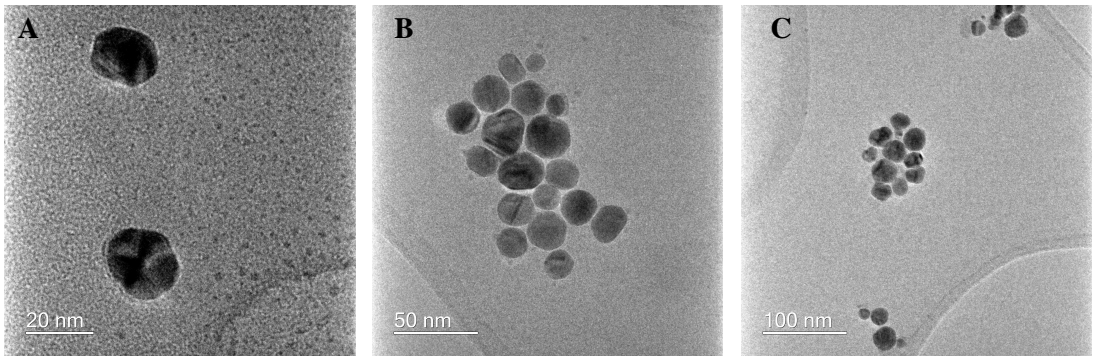

Figure 2.7 TEM images of purchased citrate-stabilised AgNPs. Average diameter of particles was calculated as 20.4±3.9 nm.

a) Aggregation behaviour of AgNPs

The fate and behaviour of NMs within the environment is believed to greatly influence their bioavailability and interaction with biota.[98, 226] DLS was utilised to observe the behaviour of AgNPs upon their entry into NSW (Fig 2.8). Previously, the aggregation of AgNPs within saline media has been recorded but is often altered by use of nutrient-rich media.[74, 109, 135, 136] To address this, NSW was utilised in this study to maximise environmental relevance. Here, the aggregation of AgNPs was observed to occur immediately upon entry into NSW (*i.e.,* DLS z-average size of 122.2±55.2 d.nm), increasing to 271.2±121.6 d.nm after 30 mins (Table 2.4 and Fig 2.8), as compared to

the initial 36.9 d.nm of the AgNP stock measured in Milli-Q ultrapure water. This confirms that AgNPs aggregate following their addition to NSW, a finding consistent with previous research.[74, 77, 109, 227, 228] The enhanced aggregation of AgNPs in NSW is likely explained by DLVO theory due to the enhanced ionic strength of saline water acting to promote particle aggregation as repulsion between charged particles is hindered by the increased presence of ions in the solution.[228]

Table 2.4. Z-average size (d.nm) of AgNPs (1 mg L^{-1}) suspended in natural seawater for a period of 72 h as measured by Dynamic Light Scattering (DLS).

Time (h)	z-average size (d.nm)
0	122.2 ± 55.2
0.5	271.2 ± 121.6
2	379.6 ± 159.4
4	532.3 ± 170.5
24	826.4 ± 106.5
48	964.0 ± 105.0
72	819.0 ± 125.5

Over the subsequent 48 h, z-average size continued to increase, reaching a maximum value of 964.0±105.0 d.nm. The high variability recorded in z-average size throughout the experiment highlights the large range in AgNP aggregate sizes that are generated once introduced into NSW. However due to limitations of analytical techniques,[226] particularly DLS, only concentrations far exceeding those predicted in the environment could be effectively analysed. Typically, studies utilising DLS examine AgNP behaviour using concentrations in the range 1-100 mg L^{-1}.[74, 109, 135, 136]

A concentration of 1 mg L^{-1} was identified as the minimum concentration that allowed effective data acquisition throughout the 72 h test period which represents 100-fold those predicted in the environment[53] and that were used in experiments with cyanobacteria (section 2.3.4). Therefore, whilst the potential for AgNPs to aggregate in the marine environment exists, the decreased encounter rate between individual AgNPs caused by dilution in the environment (*i.e.,* <10 μg L^{-1}) is likely to cause a considerably reduced aggregation rate under environmentally-relevant concentrations.[229, 230] As such, the true fate and behaviour of AgNPs at environmental

concentrations remains uncertain. Interestingly, despite observed AgNP aggregation, examination of the mean count rate revealed that AgNPs and aggregates remained suspended in the water throughout the experiment (Fig 2.8B) with negligible sedimentation of AgNPs as previously recorded.[227] Therefore, AgNPs under environmentally relevant concentrations will remain bioavailable to planktonic species and other marine biota.

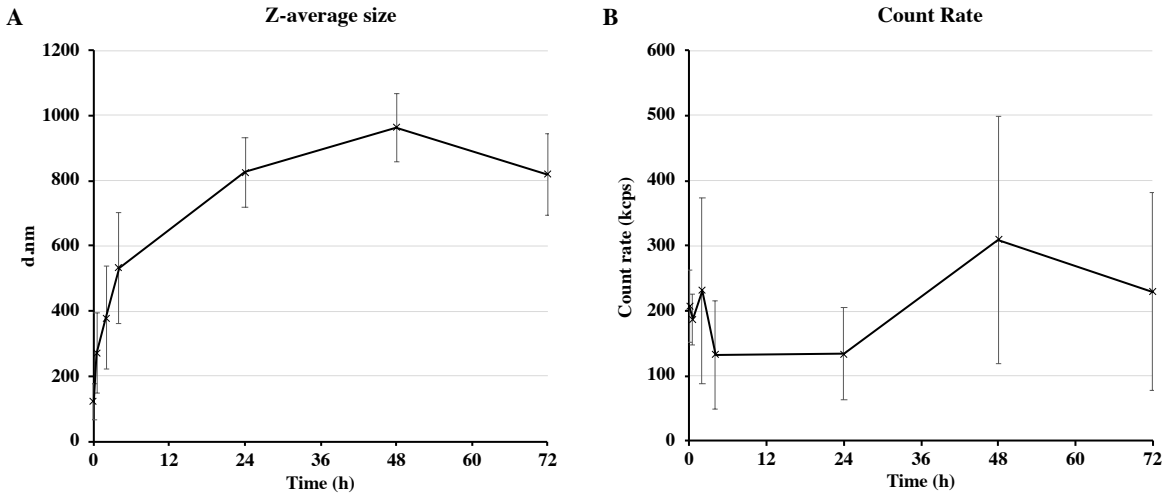

Figure 2.8. (A) Z-average size (d.nm) and (B) mean count rate (kcps) of AgNPs (1 mg L^{-1}) suspended in natural seawater for a period of 72 h. Data is presented as the mean ± standard deviation (n=5 - 0, 0.5, 2, 4, 24 h; n=4 - 48 and 72 h).

b) Dissolution of ionic silver from AgNPs in natural seawater

The release of ionic silver from AgNPs within saline media *via* dissolution has been widely reported, although largely only at high concentrations.[74, 77, 135] Despite ICP-AES analyses having been utilised for trace metal analyses in seawater in the ppb to ppm range,[82, 83] the release of ionic silver from AgNPs at the concentration range utilised in this study (*i.e.,* 0-250 µg L^{-1}) was below the technique's limit of detection. Previous work examining citrate-stabilised AgNP dissolution (10 mg L^{-1}) revealed the process to be slow.[231] Hence, the slow dissolution rate of ionic silver together with the requirement to dilute seawater samples to remove salts prior to analysis, explain why investigation of NM behaviour is typically carried out at relatively high concentrations, exceeding those found in the environment. Such limitations highlight the uncertainty surrounding the mechanisms of AgNP toxicity under environmental conditions.

The rate of silver ion dissolution is described by Jin *et al.* (2010) as a 'continuous state of flux', dependent on particle size, surface characterisation, as well as chemical and biological characteristics of experimental media.[201, 232] Typically, AgNP dissolution has been characterised by two major pathways; oxidation and desorption (Fig 2.9).[220] The latter is proposed to be the primary mechanism of Ag^+ release into natural environments, with oxidative dissolution playing a slower and less significant role.[220] However, in laboratory work the relative importance of oxidation in dissolution is argued, as under anaerobic conditions the release of silver ions is not recorded.[221] The oxidation of AgNPs is likely to involve a number of redox reactions that produce peroxide intermediates.[221] For example, Liu *et al.* (2010) detected release of H_2O_2 from AgNPs following 3 h suspension in aerated water. The presence of oxidizing species, such as H_2O_2 and SOx are thought to enhance the release of silver ions,[233] and therefore are likely to play a synergistic role in toxicity alongside dissolved silver. Surface interactions can halt dissolution, for example compounds containing thiol or selenide, or the formation of sulfidic coatings can block the particle surface preventing release of Ag^+.[189, 233] Modifying the surface of AgNPs allows for control of release of biologically active silver.[189] Surface coating greatly influences the extent of ionic silver release from AgNPs.[74, 189, 220, 232] Generally, the most widely used coating in commercial AgNPs is citrate.[190-193] Citrate-stabilised particles release less dissolved silver than other coatings, *e.g.* PVP and tannic acid,[220, 232] although results are variable and dependent on the persistence of the coating upon entry into the environment.[74]

Generally, dissolution of AgNPs has been recorded to be higher in saline water versus freshwater by 20-fold.[74, 77, 135, 234] The increased rate of dissolution in marine water has been attributed to the higher concentration of NaCl providing chloride to catalyse the release of silver ions from the particle surface.[77] However, despite this increase in dissolution, the specific Ag species formed vary in abundance within freshwater and seawater.[77] Sendra *et al.* (2017) recorded that in freshwater, release of free Ag^+ can be up to four orders of magnitude above marine.[77] In contrast, colloidal AgCl species dominate ionic silver release into seawater, making up to 99% of dissolved silver content.[74, 77, 221] Therefore, the larger amounts of free Ag^+ in freshwater in comparison to marine water is thought to account for the increased toxicity of AgNPs recorded in freshwater, leading researchers to conclude that AgNP release into seawater results in increased dissolution of less toxic Ag species.[74, 77]

Particle size appears to influence the dissolution rate of AgNPs, with increased rate of dissolution observed with reduced particle size, likely due to increased surface-area-to-volume for oxidation.[193, 220, 235] Dissolution of AgNPs has been recorded up to 90% of the initial weight of the particle,[232] but this is determined greatly by properties of the media. The rate of dissolution of Ag species from AgNPs is highest during the first 8-12 h of entry into media.[193] Following this, the rate of release slows towards an equilibrium point, determined by AgNP size, with smaller particles taking longer to reach this point.[193] Studies suggest AgNPs are unlikely to fully dissolve during experimentation.[193, 220, 221, 232] Rather, AgNPs release ions slowly for a period of hours to several days,[221, 232] resulting in the build-up of ionic silver in media. Large particles are therefore predicted to persist in the natural environment and may act as a long-term source of Ag^{+} release,[220] possibly causing accumulation of these toxic ions. Smaller particles, on the other hand may persist for the medium term, a timeframe believed to be long enough to allow for interaction with biota.[221] The complete dissolution of AgNPs is only thought to occur over longer timeframes where sufficient dissolved oxygen persists in the environment.[193, 221] New methods to accurately examine AgNP behaviour under environmental conditions are required.

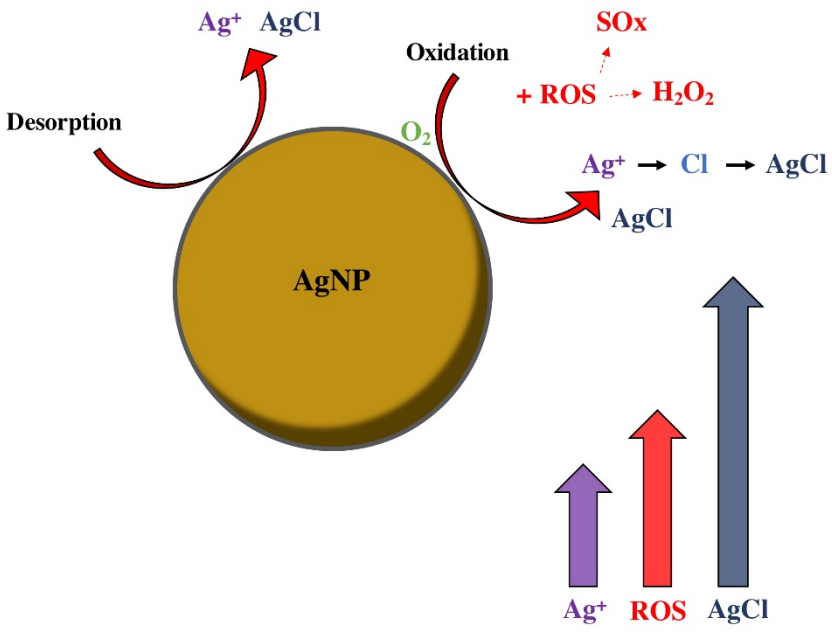

Figure 2.9. Schematic representation of AgNP dissolution in seawater by processes of desorption and oxidation, and associated release of reactive oxygen species. High concentrations of chloride ions present in seawater, promote the formation of AgCl complexes, which represent the majority of silver species derived from AgNPs in saline media.

2.3.4 Toxicity of AgNPs on *Prochlorococcus*: particles-to-cell ratio matters

Following the establishment of effective experimental conditions (section 2.3.2) and characterisation of AgNPs (citrate-stabilised spheres, Sigma Aldrich, 20.4±3.9 nm) upon entry into NSW (section 2.3.3), experiments with *Prochlorococcus* were performed mimicking natural environmental conditions (*i.e.,* 10^4-10^5 cells mL^{-1} in NSW)[21] to reduce misleading results caused by high cell density or particle alteration when exposed to enriched media.[72] Flow cytometric analysis was utilised to monitor cyanobacterial population density following AgNP exposure. Here, given that dead *Prochlorococcus* cells rapidly lose fluorescence,[236, 237] any observed reduction in cell counts by flow cytometry would indicate a loss of the living population. A detrimental effect on *Prochlorococcus sp.* MED4 was recorded at AgNP concentrations ≥10 μg L^{-1} (Fig 2.10 A-B), observing a significant population decrease by up to 96% following 72 h exposure (two-way T-test, $p \leq 0.05$). Cell decline was rapid and clear after only 24 h of exposure to AgNP. Cultured cyanobacteria appeared more resilient than *Prochlorococcus'* natural populations, which suffered a considerable decline at lower AgNP concentrations (*i.e.,* 1 μg L^{-1}; Fig 2.3). Typically, marine phototrophs experience toxic effects in the concentration range of 24.3 μg L^{-1} to 25.77 mg L^{-1} AgNPs,[74, 77, 109, 125, 198, 199] hence in accordance with previous work, *Prochlorococcus* appears particularly susceptible to AgNP exposure.[175, 176] The value of 10 μg L^{-1} represents the upper value of AgNPs predicted in the environment, hence such adverse effects are only likely to occur only in hotspots of AgNP pollution areas where concentrations of these materials reach toxic levels. However, the decline in the phototrophic community in these areas may result in a reduction in primary productivity, with adverse effects upon the surrounding local ecosystem.

Noteworthy, toxicity appeared to differ with varying cell densities, with negative effects of AgNP exposure mitigated by higher cell numbers (Fig 2.10 A-C). Indeed, no negative effect of AgNP exposure was observed in the most cell-dense culture even at concentrations of 50 μg L^{-1} (Fig 2.10C). The effect of varying cell density upon NM toxicity is a feature that is yet to be investigated in detail but is one that is likely to vary between studies and experimental runs. As such, variations in the response observed by organisms due to differing cell density are likely to affect the generation

of key ecotoxicological endpoints. Whilst a concentration gradient is typically utilised to investigate the toxicity of a particular substance (*i.e.,* EC_{50}); in the case of NMs this concentration can be considered as the number of particles per volume or per cell, as previously suggested by Metzler *et al.* and Unciti-Broceta *et al.*[209, 238] However, the use of this parameter is not enforced, resulting in the impossibility to compare studies that use cultures with different cell densities. To aid understanding of the relationship between AgNP toxicity and cell density, the estimated number of particles-per-cell (NPs cell^{-1}) added at the start of each experiment (including those performed with

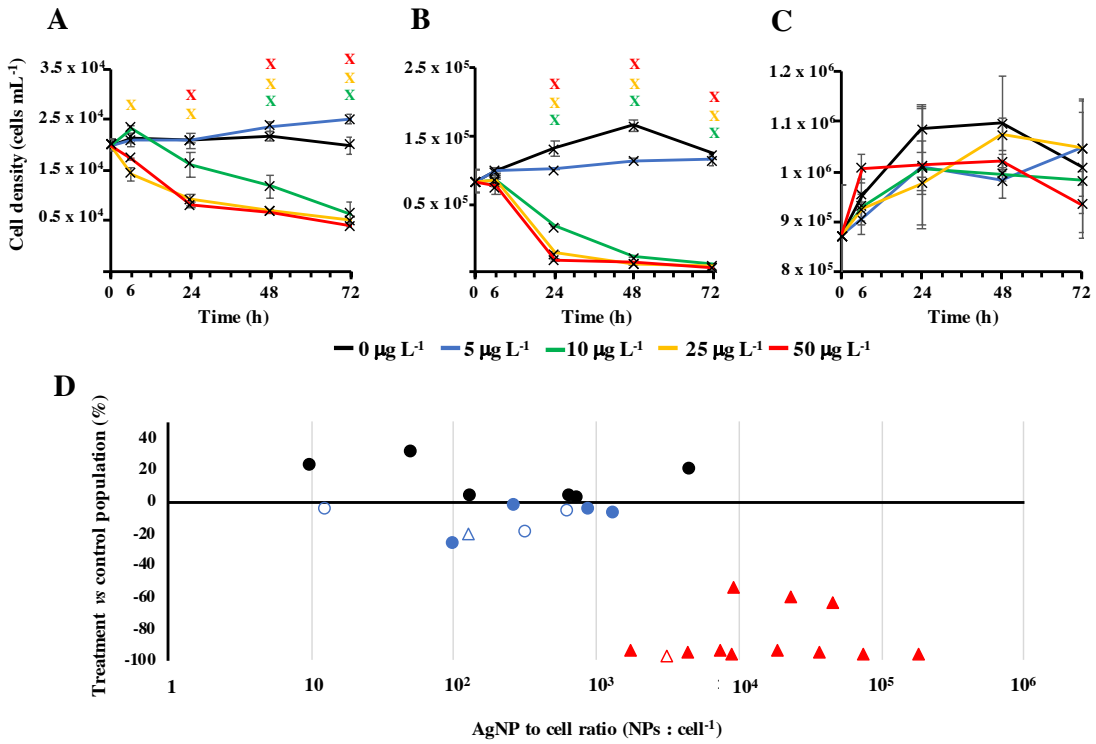

Figure 2.10. AgNP toxicity on *Prochlorococcus*. Panels A-C display three independent incubation experiments of *Prochlorococcus* grown at varying cell densities when exposed to AgNPs (0, 5, 10, 25, 50 µg L^{-1}): A – 2.5 x 10^4 cells mL^{-1}, B – 1.3 x 10^5 cells mL^{-1}, C – 8.7 x 10^5 cells mL^{-1}. Data points represent the mean ± standard error of three biological replicates (n=3). Significant decreases in cell density due to AgNPs are indicated with crosses (two-way T-tests; $p \leq 0.05$). Panel D represents the toxic effect of AgNPs on *Prochlorococcus* cultures after 72 h as a function of the nanoparticle-to-cell (NPs cell^{-1}) ratio at T_0. Red markers indicate where cell numbers had decreased >50% *versus* the control. Triangles indicate cultures with a significant reduction in cells (two-way T-tests; $p \leq 0.05$). Circles indicate where the percentage change in cell density between treated and control cultures was <50%. Full and empty markers represent experiments carried out in natural marine seawater and nutrient-rich media (*i.e.,* Pro99), respectively.

higher cell densities in enriched seawater, *i.e.,* Pro99 medium) was plotted against the percentage change in cell density after 72 h exposure (Fig 2.10D and Table 2.2). Interestingly, a strong decline in population was only observed when >1,000 NPs cell^{-1} was applied, regardless of media type or initial cell concentration (Fig 2.10D). This explains the variability in response observed in Figure 2.10 A-C. It is proposed here that the build-up of ionic silver and associated release of ROS by AgNPs, can be mitigated by denser cell cultures but may become unbearable at a certain threshold. This is particularly damaging to *Prochlorococcus* which lacks appropriate defence mechanisms. Upon consideration of the ambient cell density of microbes in the marine environment (~10^6 cells mL^{-1})[239] and upper limit of AgNPs predicted (10 μg L^{-1}),[53] we are able to estimate a likely maximum environmental NPs cell^{-1} ratio of 230 NPs cell^{-1}. While this value is well below the 1000 NPs cell^{-1} threshold reported for *Prochlorococcus sp.* MED4, it may be toxic for natural populations. Nevertheless, in-line with comments above, the current environmental risk of AgNPs appears low and limited to hotspots of AgNP pollution.

It can be argued that altered nanoparticle behaviour within experimental media is likely to reduce accuracy of the NPs cell^{-1} ratio calculation. Above, it has been shown that there is a potential for AgNPs to aggregate in NSW (see section 2.3.3), thus lowering the effective particle number in suspension during exposure. However, aggregation of AgNPs has only been recorded at concentrations far exceeding those predicted in the environment. It is believed that such aggregation will be considerably reduced at the concentrations utilised in this study and predicted in the environment, due to lowered rate of encounter between nanoparticles. Additionally, given that AgNP aggregates were observed to remain in suspension, it is likely that at the low concentration of AgNPs will remain bioavailable in the water column exerting a detrimental effect on marine plankton, as recorded in this study. However, it must be noted that due to the non-defined nature of natural seawater, specific water chemistry, dissolved organic matter,[62] and particulate content of seawater will vary and influence differently the fate and behaviour of AgNPs.[85] Hence, despite accounting for this by using natural oligotrophic seawater, the impact of such environmental variables must be assessed in future work.

Whilst the NP cell^{-1} ratio is likely to vary throughout experimental exposure due to alterations in AgNP behaviour and microbial cell decline, through its application during experimental design, any alteration in cell density shown to cause variation in organismal response is accounted for. Standardisation and direct comparison between studies and experimental replicates is possible as a result. As such, utilisation of this parameter during experimental design proves an effective tool for nano-ecotoxicological investigation upon microbial species.

2.3.5 Ability of *Prochlorococcus* to overcome AgNP stress in extended exposures.

It is expected that upon entry into the aquatic environment, AgNPs are likely to persist for the medium term (*i.e.,* months), with the rate of dissolution dependent on the size and physicochemical properties of particles.[220, 232] Hence, the ability of *Prochlorococcus* to overcome the early stress observed within the 72 h exposure over longer incubation periods (*i.e.,* 240 h) in both natural oligotrophic and enriched seawater was assessed. As expected, AgNPs (≥1,000 NPs cell^{-1}) produced a strong decrease in the cyanobacterial population in NSW from which it did not recover (Fig 2.11A). This response was also observed in higher cell-dense cultures in enriched medium, in which populations did not recover following exposure to concentrations >1000 NPs cell^{-1} (Fig 2.11B) resulting in a 94% decline in cell density at the end of the experiment ($p \leq 0.05$). This demonstrates the inability of *Prochlorococcus* to recover from AgNP-stress and highlights the long-term consequences of such a population decline in areas where AgNP contamination remains high. As a consequence, natural endemic populations are likely to be replaced by other more-resistant species changing community dynamics in polluted areas.

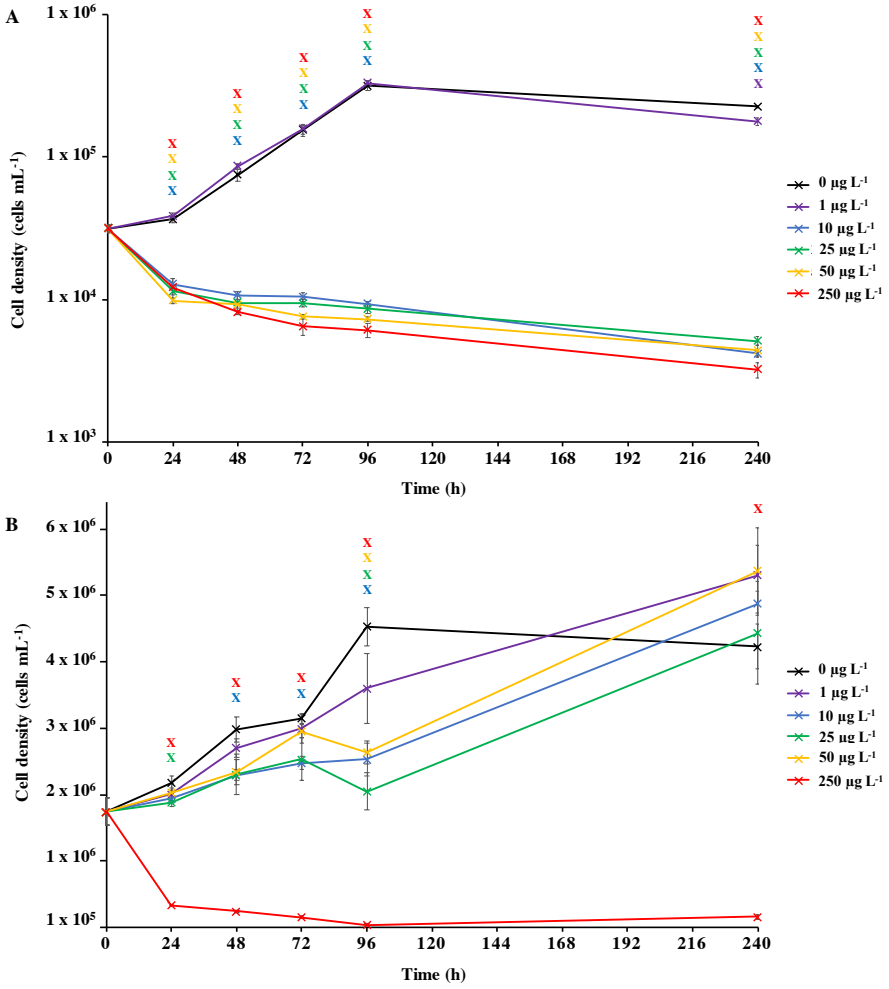

Figure 2.11. Long-term exposure (240 h) of *Prochlorococcus* to AgNPs (20.4±3.9 nm) in natural seawater (A) or nutrient-enriched seawater (B). Data points are provided as the mean ± standard error (n=3). Crosses indicate where two-way T-tests confirmed treated groups are significantly lower than the control group at each timepoint ($p \leq 0.05$). Given the extent of cell decline recorded in natural seawater, cell density is presented in the log scale.

2.3.6 Mechanisms of AgNP toxicity: Superoxide, but not hydrogen peroxide, drives AgNP toxicity on marine cyanobacteria.

As mentioned, despite being an oxygenic photosynthetic organism, *Prochlorococcus* surprisingly lacks mechanisms to effectively quench ROS and is particularly susceptible to oxidative stress.[223, 240, 241] While it lacks catalase to deal with H_2O_2, it does possess a nickel-dependent SOD essential for the detoxification of SOx.[202, 242] AgNPs are known to release ROS into the media as a result of oxidation, and exacerbate cell stress.[221, 233] In order to provide insight into the role that ROS plays in toxicity, *Prochlorococcus sp.* MED4 was incubated with AgNPs (citrate-stabilised

spheres, Sigma Aldrich, 20.4±3.9 nm) in the presence of the H_2O_2- or SOx-quenching agents pyruvate[210] and SOD,[149] respectively. The test concentration of 50 μg L^{-1} (~3000 NPs $cell^{-1}$) was selected based on evidence of significant cell decline being recorded in previous experimentation (section 2.3.4). Given that H_2O_2 is particularly damaging to *Prochlorococcus*,[243] experiments were first carried out with pyruvate. However, no impact of H_2O_2-quenching was recorded, and cell density represented approximately 20-23% of those present in control cultures after 24 h (Fig 2.12A). Following this, focus was placed upon SOx. Interestingly, the addition of SOD mitigated the toxicity of AgNPs up to >50% on this relevant marine cyanobacterium (Fig 2.12B), suggesting that SOx species is a key driver of toxicity in this system. Other ROS such as hydroxyl radical and singlet oxygen may also play a role, but their high reactivity, extremely short half-life in seawater,[210] and results shown here, suggest these may not be as important. Although, SOx too has a relatively short half-life,[60] the dissolution of AgNPs in the environment is believed to continue for as long as oxygen is available[189, 193, 244] providing a continued SOx production in the local environment through the process of oxidation. SOx is believed to be unable to pass

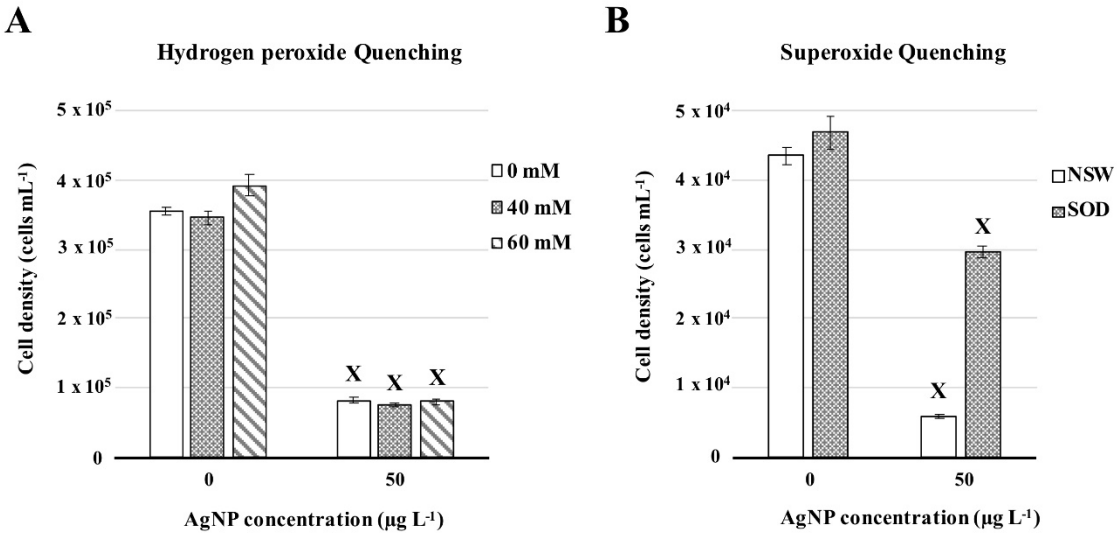

Figure 2.12. Cell density of *Prochlorococcus* following 24 h growth when exposed to AgNPs (50 μg L^{-1}) in the presence of A – Pyruvate or B – Superoxide dismutase (SOD) as respective quenchers of hydrogen peroxide and SOx. Data represents the mean ± standard error of three biological replicates (n=3). Cultures with a significant decrease in cell number due to AgNP toxicity are indicated with crosses (two-way T-tests; $p \leq 0.05$). Concentrations of pyruvate used are indicated in panel A. Natural Sea Water (NSW) and SOD (250 U mL^{-1}) is indicated in panel B.

through the cell membrane, therefore SOx produced by AgNP oxidation are likely to interact with the membrane or cell surface.[210] Previous research has also shown that SOx is the most abundant ROS generated intracellularly when bacteria are exposed to AgNPs[139, 149] and, hence, experiments confirm that this ROS species plays a critical role in driving the antimicrobial action of AgNPs under environmental conditions. This finding also explains the reduced toxicity of AgNPs in cell-dense cultures. The collective production of SOD at a specific cell-to-nanoparticle threshold may counteract the rate at which SOx is produced allowing the culture to overcome ROS toxicity.

2.3.7 The role of dissolved silver in the AgNP toxic response towards marine cyanobacteria.

The antimicrobial action of dissolved silver is widely acknowledged.[219] Whilst we were unable to detect ionic silver during ICP-AES analyses (section 2.3.3b), silver ions are likely to be released by citrate-stabilised AgNPs as recorded when using higher concentrations (1-100 mg L^{-1}).[74] *Prochlorococcus sp.* MED4 cultures were

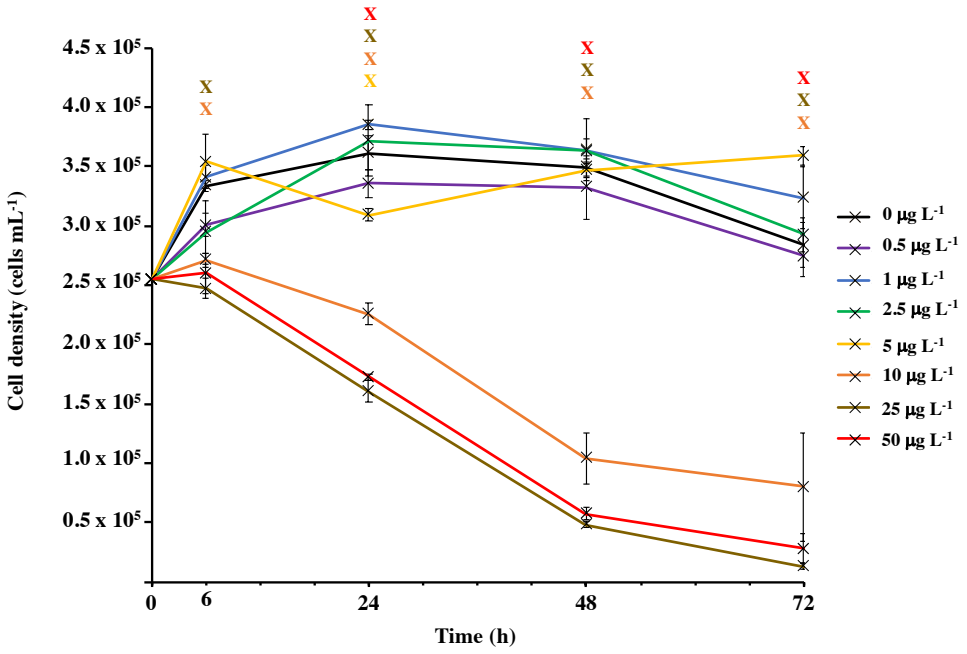

Figure 2.13. 72 h exposure of *Prochlorococcus* to dissolved silver (Ag_2SO_4) in natural oligotrophic seawater (0-50 µg L^{-1}). Data points are provided as the mean ± standard error (n=3). Crosses indicate where two-way T-tests confirmed treated groups are significantly lower than the control group at each timepoint ($p \leq 0.05$).

exposed to dissolved silver (Ag_2SO_4) to determine the toxicity of trace Ag^+ leached from AgNPs, hence becoming bioavailable to *Prochlorococcus* during exposure (Fig 2.13). The impact of dissolved silver upon *Prochlorococcus* was remarkably similar to that recorded in earlier experimentation with AgNPs (section 2.3.4). Following 72 h incubation, *Prochlorococcus* experienced significant cell decline in response to Ag^+ concentrations $\geq$10 μg L^{-1}, resulting in declines of 71.7-95.3% in response to 10-50 μg L^{-1} (two-way T-test, $p \leq 0.05$). Dissolved silver produced slower cell declines, requiring 48 h for population depletion as opposed to 24 h needed when exposed to AgNPs. Interestingly, no adverse effect of exposure was recorded at lower concentrations (0.5-5 μg L^{-1}), indicating little effect of trace Ag^+ levels on this cyanobacterium. Given that similar extents of toxicity are recorded in dissolved silver treatments – where all bioavailable silver is in a dissolved form– and in AgNP treatments – where it is not, alongside data recorded during ROS-quenching experiments described above (section 2.3.6), it appears that both SOx generation and leached silver from nanoparticles drives AgNP toxicity. This result confirms that the remaining decline of *Prochlorococcus* recorded in cultures where SOD was present (Fig 2.12B) may be attributed to the synergistic adverse effect of any remaining SOx species and toxic silver species released from AgNPs. This interaction is likely to occur in close proximity to cyanobacterial cells due to high affinity between AgNPs and the cyanobacterial cell membrane,[176] resulting in localised release of SOx and ionic silver through oxidative processes. Here, SOx and toxic silver species are likely to disrupt enzymatic processes and induce membrane instability, resulting in cell lysis and death.

2.3.8 Impact of AgNP exposure upon the *Prochlorococcus* proteome

Molecular methods such as shotgun proteomic analysis provide great scope to investigate the response of organisms towards environmental stressors and pollutants in greater detail and reveal new insight into mechanisms that drive any toxic effects.[245] During environmental stress, the synthesis of specific proteins can be regulated to allow for acclimatisation to specific stress conditions.[246] To date, such approaches have been used to a limited extent in nano-ecotoxicity investigation, but are believed

to provide a more comprehensive understanding of the molecular features of NM exposure.[247]

In order to investigate protein-level effects of AgNP exposure, *Prochlorococcus sp.* MED4 was first exposed to a series of sub-lethal to near-toxic concentrations (*i.e.,* 250, 750 and 1500 NPs cell^{-1}) for a period of 24 h. Here, cell-dense cultures were exposed to AgNPs in nutrient-rich Pro99 media, allowing for the collection of sufficient biological material for analysis. It is possible that results may be altered at higher cell densities, as discussed in the previous chapter, however this was accounted for by use of number-based concentrations in this work.

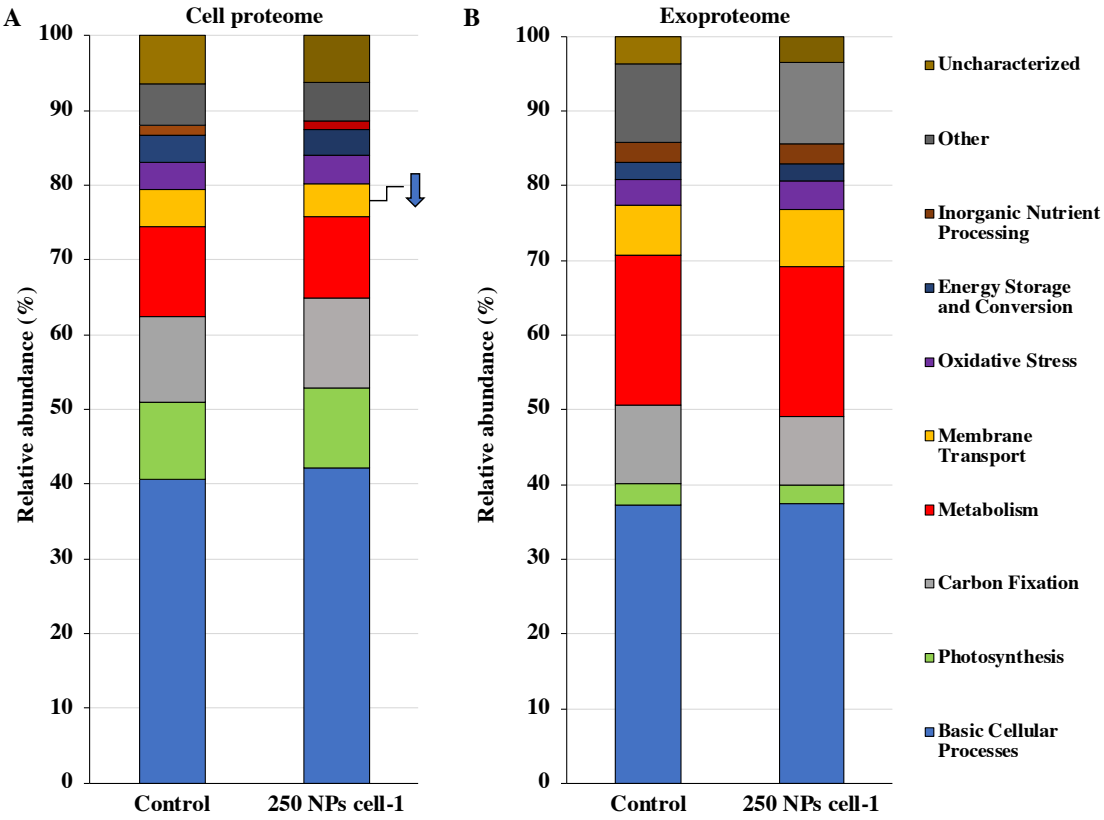

Figure 2.14. Relative abundance of protein groups identified in cellular- (A) and exo- (B) proteome samples of *Prochlorococcus sp.* MED4 exposed to AgNPs (~250 NPs cell^{-1}) for a period of 24 h (n=3). Blue arrow indicates where two-way T-tests revealed the relative abundance of respective protein groups to significantly vary between AgNP-treated and control samples ($p \leq 0.05$).

At the lowest tested concentration (250 NPs cell^{-1}), little effect was observed in either the cell or exoproteome (Fig 2.14). Only two proteins were identified to significantly

vary between treated and control cultures, both identified within the cell proteome (two-way T-test, $p \leq 0.05$), see Table A1.1, Appendix 1. These two proteins were identified as, the putative glycosyl transferase and tyrosine binding protein, both with central metabolic functions and down-regulated in the presence of AgNPs (250 NPs cell^{-1}). The 20 proteins in both the cellular- and exoproteome which corresponded to the lowest q-values as a result of a two-way T-tests were further investigated (Table A1.1 and A1.2). However, no clear trend could be identified in either dataset. Of the 20 proteins identified in the cellular proteome, 15 were down-regulated in the presence of AgNPs. Interestingly, two proteins related to Photosystem I were up-regulated in the AgNP treatment. In the exoproteome, 12 out of 20 proteins were down-regulated. Proteins involved in magnesium and sulfur transport were reduced in relative abundance from 0.017 and 0.009% to 0.007 and 0.004% respectively. However, this difference was not statistically significant.

For all analyses of proteomics data, proteins were grouped according to their biological function and subsequently the respective relative abundance of each functional group was compared between treated and control samples. Only one group significantly differed in the 250 NPs cell^{-1} treatment (two-way T-test, $p \leq 0.05$), identified in the cell proteome (Fig 2.14). Here, relative abundance of proteins associated with membrane transport were down-regulated 4.82% to 4.29% in the presence of AgNPs. Such reductions in membrane transport proteins have been reported in previous work investigating AgNP toxicity, where production of ABC transporters was altered in *Staphylococcus aureus*, compromising the transport of nutrients into cells.[248] To assess the extent of cell lysis in exoproteome samples, the relative abundance of total ribosomal proteins was calculated for both control and AgNP-treated samples. This value equated to 5.44% in the control group and 5.76% in the presence of AgNPs, a difference which was statistically insignificant and indicates little cell lysis as expected by the sub-inhibitory concentrations of AgNPs used in this work.

Upon increasing AgNP concentrations to 750 and 1500 NPs cell^{-1}, representing the near-toxic range (*i.e.,* >1000 NPs cell^{-1}, see section 2.3.4), little significant features of AgNP exposure were revealed by proteomic analysis in cellular or exoproteome

samples (Fig 2.15). No individual proteins were recorded to vary significantly between treated and control samples in response to 750 NPs cell^{-1}, and only 5 were identified to significantly differ in the 1500 NPs cell^{-1} treatment (two-way T-test, $p \leq 0.05$), all found in the exoproteome (see Table A1.6, Appendix 1). These proteins were identified as four ribosomal proteins and the S1 RNA binding domain, all less abundant in AgNP-treated cultures apart from one ribosomal protein. As previous, the 20 proteins in each dataset which corresponded the lowest q-value during two-way T-tests against the untreated control were identified for further analysis, see Tables A1.3-A1.6. It appears the majority of these proteins were down-regulated in the cellular proteome in the presence of AgNPs; 16/20 and 19/20 in the cellular proteome of the 750 NPs cell^{-1} and 1500 NPs cell^{-1} treatments respectively. No key trend in protein function can be identified in either cellular or exoproteome dataset at the 750 NPs cell^{-1} concentration, or cellular proteome of the 1500 NPs cell^{-1} treatment. In addition to the five significant proteins identified in the exoproteome of the 1500 NPs cell^{-1} treatment, a further five were identified with a $p \leq 0.1$. Included here were a further two ribosomal proteins that were both down-regulated in the presence of AgNPs, the Protein GrpE and Transketolase that were both also down-regulated, and one

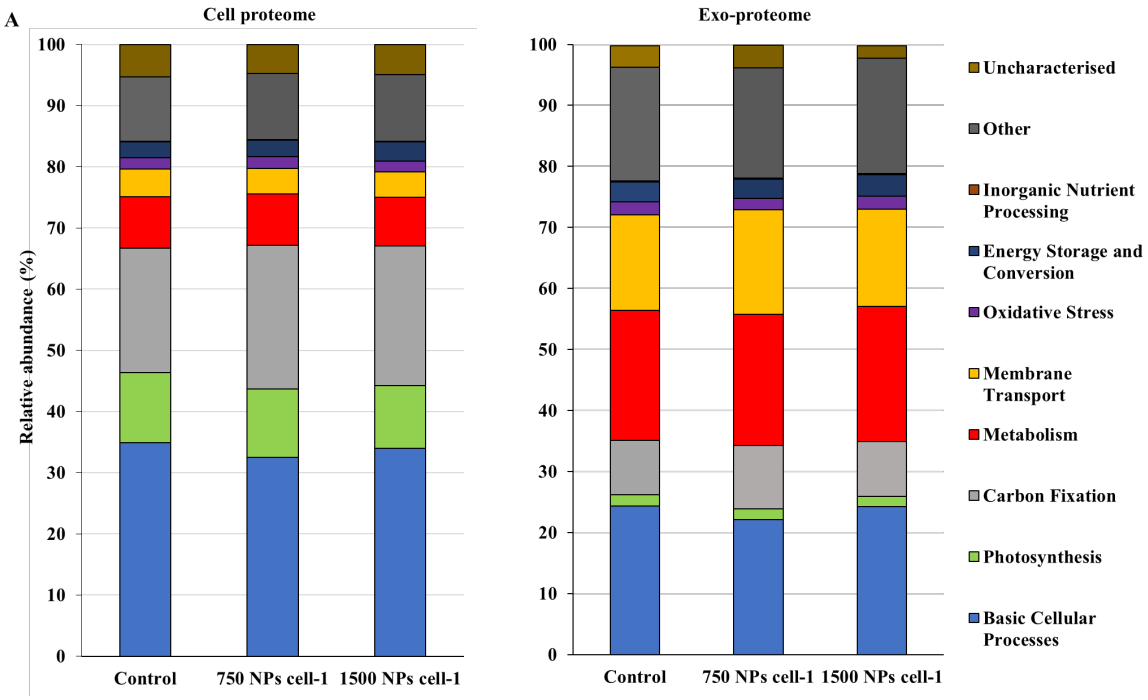

Figure 2.15. Relative abundance of protein groups identified in cellular- (A) and exo- (B) proteome samples of *Prochlorococcus sp.* MED4 exposed to AgNPs (~750 and 1500 NPs cell^{-1}) for a period of 24 h (n=3).

uncharacterised protein that was up-regulated in the 1500 NPs cell^{-1} treatment. Unexpectedly, the relative abundance of ribosomal proteins in exo-proteome samples was significantly lowered in the 1500 NPs cell^{-1} treatment. Here, the relative abundance of ribosomal proteins was recorded as 5.27%, compared to 6.62% and 6.76% in control and 750 NPs cell^{-1} treatments respectively. Although, it is possible that in the short term, cell death at high concentrations could occur without immediate cell lysis. No alteration in abundance of any functional protein group was identified in either cell or exoproteome datasets (Fig 2.16). It must be noted that the quality of proteomics data obtained from this second experiment is uncertain given that for this dataset approximately 300 proteins were successfully annotated, compared to >700 in the other two experimental runs. The reason for this lack of data is uncertain but is likely to have hindered the outcome of analysis in some manner. For full details of proteins identified throughout analysis see electronic supplementary data tables 1-8.

Due to the lack of mechanistic insight revealed at lower concentrations, exposures were repeated at a higher concentration of 5000 NPs cell^{-1}, well-within the toxic range identified in previous works (section 2.3.4). Indeed, at this concentration 19.8% of the cell proteome was observed to differ significantly compared to the untreated control (two-way T-test, p≤0.05) (Fig 2.16A), representing a total of 275 individual proteins,

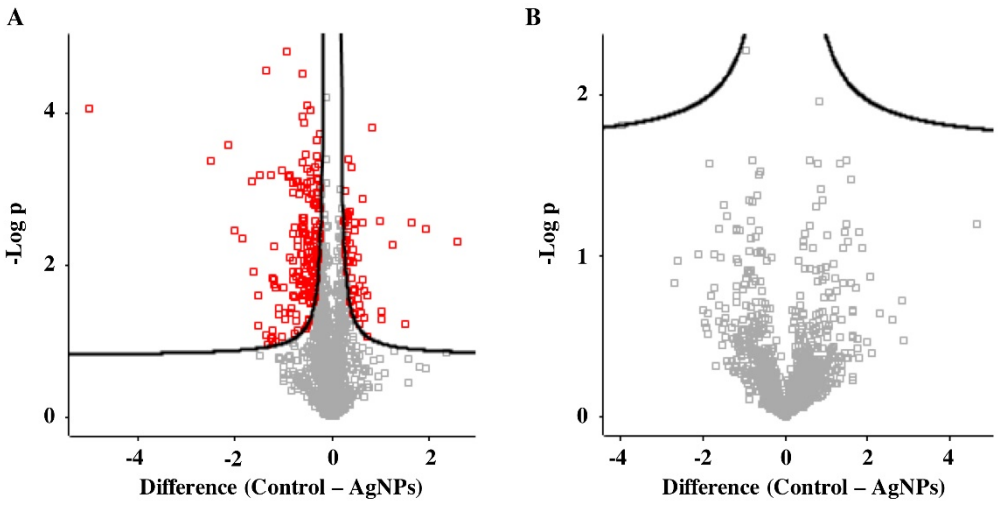

Figure 2.16. Volcano plots (T-test; FDR=0.05, S0=0.1) of A) Cellular proteome and B) Exoproteome of *Prochlorococcus sp.* MED4 exposed to AgNPs (5000 NPs cell^{-1}) for a period of 24 h (n=3). Red markers indicate proteins identified as significantly altering in abundance between control and treated samples (two-way T-test, p≤0.05)

see Table A1.7, Appendix 1. Unexpectedly, no such changes were identified in the exoproteome, where no individual proteins significantly varied in the presence of AgNPs (Fig 2.16B). Here, only those proteins associated with inorganic nutrient processing were significantly down-regulated in the exoproteome (two-way T-test, $p \leq 0.05$) (Fig 2.17). This alteration was largely caused by a decreased detection of phosphate-binding protein in AgNP-treated cultures, reducing in average relative abundance from 14.2% to 9.9% in control and treated cultures, respectively. Also of note, in the exoproteome the most abundant protein in both control and treated cultures was the putative iron ABC transporter, substrate binding protein. This protein was on average considerably more abundant in AgNP-treated cultures (40.3±11.7% *versus* 28.0±4.6% in the control). However, due to the large variation between replicates in the AgNP treatment this variation was not statistically significant. Interestingly, this iron transporter was also the most abundant protein in the cell proteome and relative abundance was significantly higher in the presence of AgNPs (7.5% *versus* 6.8%). On average, relative abundance of ribosomal proteins in the exoproteome, a marker for cell lysis, was higher in AgNP-treated cultures compared to the control (2.98% *versus* 2.58%). However, as a result of variation between replicates this result was not significant. In contrast to the exoproteome, a number of significant alterations in relative abundance of functional protein groups were identified in the cell proteome (see Fig 2.17A). Here, proteins associated with basic cellular processes and carbon fixation were significantly up-regulated; whilst, those involved with central metabolism, inorganic nutrient processing, and surprisingly, oxidative stress were significantly down-regulated (two-way T-test, $p \leq 0.05$). Uncharacterised proteins were also on average more abundant in the AgNP treatment. Where possible significant uncharacterised proteins were identified using BLAST search (Table A1.8, Appendix 1), however little insight was gained. The observed significant changes in the cell-proteome in response to AgNPs at toxic concentrations (*i.e.,* 5000 NPs cell^{-1}) will be discussed in greater depth below.

On average, proteins associated with basic cellular processes were significantly up-regulated in the AgNPs treatment (5000 NPs cell^{-1}) within the cell proteome. A total of 81 proteins involved in basic cellular processes were differentially expressed in the presence and absence of AgNPs, 67 of which were significantly more abundant in

treated cultures. Of the 14 down-regulated proteins, little trend can be observed in their function, however, of those up-regulated over 50% played a role in translation processes. Here, 34 ribosomal proteins displayed a significant increase in the presence of AgNPs. Previous work with *Pseudomonas* also observed an increase of ribosomal proteins upon the addition of AgNPs.[249] Also of note, the DNA repair protein RadA was also significantly up-regulated. Seven proteins involved with protein biosynthesis and folding were also significantly more abundant in the AgNP treatment. The up-regulation of genes encoding for the synthesis of chaperones and enzymes that are involved with the re-folding or proteolysis of polypeptides that have been denatured has previously been recorded in response to AgNP exposure in *E. coli*.[250]

Proteins involved in central metabolic processes displayed an overall significant decrease in abundance as a functional group upon the addition of AgNPs, decreasing in relative abundance from 22.2-20.3%. However, upon examining this variation at the individual protein level, little pattern could be identified to ascertain which

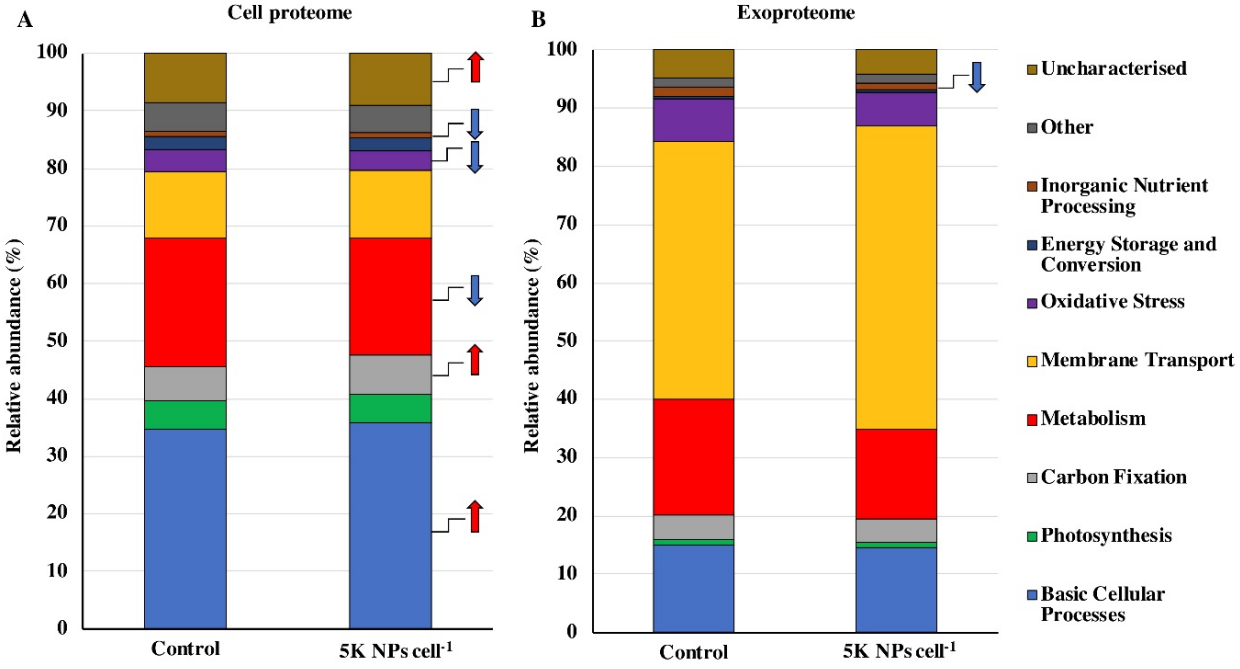

Figure 2.17. Relative abundance of protein groups identified in cellular- (A) and exo- (B) proteome samples of *Prochlorococcus sp.* MED4 exposed to AgNPs (5000 NPs cell^{-1}) for a period of 24 h (n=3). Arrows indicate where relative abundance of individual protein groups varies significantly from the untreated control, as identified by two-way T-tests ($p \leq 0.05$). Red arrows indicate where protein groups are significantly up-regulated; blue arrows indicate where protein groups are significantly down-regulated.

metabolic processes were most affected by AgNP exposure. A total of 43 and 37 proteins associated with central metabolic processes were up- or down-regulated respectively in the presence of AgNPs. A key feature of many of the proteins significantly more or less abundant in the AgNPs treatment was the ability to bind metal ions, often for catalytic functions. It has been recorded that ionic silver may displace the binding of metal co-factors to such proteins, and hence cases of up-regulation may be attributed to increases in the number of sites available for the binding of correct co-factors.[250] This process may explain a number of the proteins observed to increase in abundance in the AgNP treatment, however, does not explain why a number of these proteins were significantly down-regulated. Although, it is possible that displacement of iron by ionic silver may account for the considerable increase in the iron ABC transporter, substrate binding protein observed in both the cellular and extracellular proteomes in the presence of AgNPs, described above.

As mentioned above (section 2.3.4), a common feature of AgNP toxicity described in the literature is oxidative stress. This has previously been associated with release of H_2O_2 and SOx species, the latter believed to be the key driver of stress in experiments with *Prochlorococcus* described above (section 2.3.6). In the cellular proteome, abundance of oxidative stress proteins was observed to alter significantly in the presence of AgNPs, however, no such effect was seen in exoproteome samples. As expected, *Prochlorococcus*' sole superoxide dismutase protein, the putative nickel-containing superoxide dismutase, was significantly up-regulated in the presence of AgNPs in the cellular proteome from 0.15-0.25%. Although, no effect upon this protein was seen during exposures at lower sub-lethal concentrations, suggesting that this is only a feature when concentrations reach a certain threshold.

Whilst in ROS quenching experiments hydrogen peroxide was not shown to play a key role in toxicity (section 2.3.6), proteins associated with protection from hydrogen peroxide were differentially regulated upon addition of AgNPs. Thioredoxin represents a widely conserved redox protein, acting to maintain the cellular reducing environment and thus correct functioning of enzymatic activities.[251] This protein has been recorded to have roles in DNA synthesis and repair, transcriptional regulation and antioxidant activity against oxidative stress, namely from hydrogen peroxide.[251] Herein, thioredoxin was observed to significantly increase in relative abundance from

0.32% to 0.41% upon the addition of AgNPs. Induction of thioredoxin has previously been recorded during exposure with heavy metals in green algae.[252] Unexpectedly, the related protein thioredoxin peroxidase was significantly down-regulated in the presence of AgNPs. This antioxidant protein also acts against hydrogen peroxide and associated peroxide intermediates, and in recent work using budding yeast is believed essential for the induction of the entire thioredoxin pathway.[253] As such it is unclear as to why we would observe a down-regulation of thioredoxin peroxide, whilst thioredoxin increases.

The toxic stress response proteins glutathione-S-transferase and methionine sulphoxide reductase were also recorded to increase in the presence of AgNPs, 0.005-0.006% and 0.007-0.008% respectively. Glutathione-S-transferase is a widely recognised component of toxic stress response in organisms, and contributes to protection from oxidative stress.[254, 255] Additionally, glutathione-S-transferase has been recorded to contribute to correct synthesis, folding and degradation of enzymes.[254] Methionine sulphoxide reductase catalyses the reduction of methionine sulphoxide, a toxic agent disrupting biological processes, to methionine, thus restoring cell function.[256] This protein has previously been recorded to be co-induced with glutathione-S-transferase during chemical stress in the bacterium *Ochrobactrum anthropi*, but not during oxidative stress by hydrogen peroxide.[255] As such, it is possible that given both of these proteins were significantly upregulated, these were co-induced due to presence of toxic ionic silver species, although this requires additional testing.

Despite the significant up-regulation of a number of key proteins involved in oxidative stress response, it was observed that in the cellular proteome the collative oxidative stress functional group decreased in the presence of AgNPs compared to the untreated control. The cause of this overall decline in oxidative stress proteins is unclear. However, it remains that the presence of free silver or dissolved metals may affect the correct functioning of antioxidant systems.[257] Hansen *et al.* (2006) found that a variety of ionic metal species exerted a number of varying oxidative effects upon thiol-antioxidant systems, potentially altering apoptosis and toxic signalling pathways. It may be possible that any ionic silver present in treated cultures may interact with antioxidant proteins in this manner, so disrupting their activity and induction of related

proteins within antioxidant pathways, thus accounting for their significant down-regulation recorded.

AgNPs have been previously observed to disrupt photosynthetic processes of marine phytoplankton. As a result of exposure, disruption of electron transport in Photosystem II has been recorded in algal species.[135] In the marine diatom, *S. costatum*, significant down-regulation of photosystem II reaction centre proteins was recorded following exposure to AgNPs (5 mg L^{-1}).[109] Specifically, the *D1* protein involved in electron transport, was down-regulated. Here, it was believed that during AgNP exposure a photo-protective response was induced in the diatoms, up-regulating the expression of two genes encoding for the synthesis of light harvesting proteins.[109] Exposures to 500 μg L^{-1} in the same study found a significant increase in intracellular ROS and reduced cell viability, suggesting that in photosynthetic microbial species, a combined photo-oxidative stress is exerted by Ag NPs.[109] In the study presented here a total of 14 proteins associated with photosynthesis were significantly altered by exposure to AgNPs (5000 NPs $cell^{-1}$). Unlike the previous work described all but one were significantly upregulated in the AgNPs treatment. The down-regulated protein was identified as glutamyl-tRNA reductase, involved in the biosynthesis of chlorophyll. However, whilst this effect would be expected to induce an adverse effect upon *Prochlorococcus* a further two proteins involved in chlorophyll biosynthesis were significantly upregulated. The Photosystem I assembly proteins Ycf3 and Ycf4 were also significantly upregulated under the AgNP treatment. Five proteins associated with electron transport within the photosynthetic pathway were significantly upregulated. The functioning of the photosynthetic electron transport chain is dependent upon a fine balance between oxidised and reduced cofactors.[203] It is likely that AgNPs and associated silver ions interfere with this process, perhaps in a similar fashion to that proposed to disruption of central metabolism proteins described above. A common feature of the significantly up-regulated photosynthesis-related proteins identified in the 5000 NPs $cell^{-1}$ AgNP treatment was the presence of 2-Fe, 2-sulfur cluster binding units. Disruption of iron-sulfur cluster units has previously been recorded in response to AgNP exposure in *E. coli*, hence AgNPs are believed to possibly alter iron and sulphate homeostasis.[250] Interestingly, despite these alterations in photosynthetic processes, abundance of proteins involved in carbon fixation appeared to be up-

regulated in the AgNP treatment, increasing in relative abundance from 5.9% to 6.9%. As such, phototoxicity does not appear to be significant. Largely, this increase was attributed to an increase in the relatively abundant carbon dioxide-concentrating mechanism protein CcmK, which was observed to significantly increase in relative abundance from 2.2-3.0% in the presence of AgNPs.

Proteomic analysis proved effective in revealing mechanistic insight into AgNP toxicity towards marine microbial species and its use in future experimentation is highly recommended. Exposure to AgNPs at lower concentrations revealed limited effect upon the *Prochlorococcus* proteome, whilst toxic concentrations caused a significant cellular response, characterised by ~20% alteration in the cell proteome. These results suggest that as a threshold AgNP concentration is reached, *Prochlorococcus* is no longer able to withstand stress, likely arising due to the release of ionic silver and SOx. However, it must be noted that microorganisms such as *Prochlorococcus* that possess streamlined genomes have limited capacity to regulate gene activity,[202] therefore, observing only small alterations between cultures under varying conditions can be expected.[236, 258] Hence, subtle sub-lethal effects of exposure are likely to be difficult to identify in such species. Surprisingly, exposure to toxic AgNPs concentrations resulted in no significant effects upon the exoproteome. However, significant alterations in the cellular proteome reveal key trends in *Prochlorococcus'* response to AgNPs; the cellular response towards oxidative stress appears unclear, but the significant increase in superoxide dismutase supports the belief that SOx plays a key role in driving AgNP toxicity (see section 2.3.6); translation processes appear to be altered by AgNP exposure, characterised by an increase in ribosomal protein production; central metabolic proteins, particularly those with metal ion binding capabilities appear affected by presence of AgNPs; similarly, proteins with electron transport properties are particularly affected. Further investigation is required to fully understand these proteomic changes under laboratory conditions. Going forward, the use of metaproteomic techniques may play an important role in determining the whole community response towards contaminants such as engineered NMs.

2.3 Chapter Summary

Under environmentally relevant conditions citrate-stabilised AgNPs exert a toxic response upon the ecologically significant marine cyanobacteria *Prochlorococcus*. Given the substantial contribution of marine cyanobacteria to global primary production, any negative effect exerted upon this relevant phytoplanktonic group is likely to affect local ecosystems as a whole due to a decrease in primary productivity or replacement by other more-resistant photosynthetic organisms, disrupting natural marine food chains. However, given current predictions of environmental AgNP concentrations, such adverse effects are likely only to occur at a local level in highly polluted areas. Further investigation into determining accurate field concentrations of AgNPs will aid in effectively evaluating their risk in natural environments.

Our findings also revealed that the extent of toxicity was highly dependent on cell density and, hence, future ecotoxicological research with microbial species may need to consider assaying nanoparticles at environmentally relevant concentrations to achieve useful and informative conclusions. Here, the use of the particle-to-cell ratio (NPs cell^{-1}) is presented as an effective parameter to standardize nano-

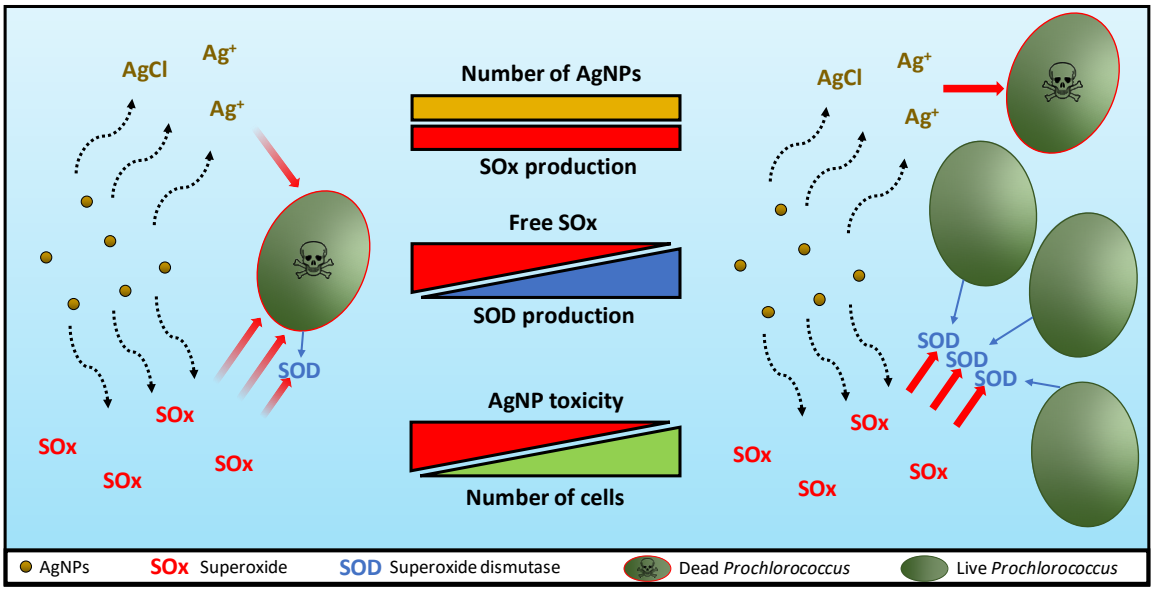

Figure 2.18. Graphical representation of AgNP toxicity towards *Prochlorococcus*. Toxicity results from the synergistic adverse effect of leached ionic silver and released superoxide. At higher cell densities, cyanobacteria are able to withstand toxicity due to increased production of superoxide dismutase (Image used as Table of Contents figure in Dedman *et al,* 2020).

ecotoxicological studies and experimental replicates where cell densities may vary and is recommended for future work with research-grade NMs (Fig 2.10).

Subsequent investigation into the mechanisms of AgNP toxicity provided an explanation of this particle-to-cell dependency. We showed that ionic silver was not solely responsible for the cell decline recorded in *Prochlorococcus* and, rather, SOx is a key driver of AgNP toxicity. Thus, above a particular particle-to-cell ratio (*i.e.,* >1,000 AgNPs cell^{-1}) the population of *Prochlorococcus* is unable to collectively mitigate the build-up of toxic SOx species though the production of SOD, at which point a clear crash in the population is observed (Fig 2.18). Proteomic analysis supported our belief that AgNP toxicity occurs at a threshold concentration where toxic species accumulate such that cyanobacteria are unable to overcome stress. Exposure to relatively low AgNPs concentrations resulted in negligible effect upon the *Prochlorococcus* proteome, whilst exposure to AgNPs in the toxic range resulted in substantial changes to normal cellular function, significantly altering 20% of proteins in the cellular proteome. Of note, proteins involved in translation and central metabolism were particularly affected, specifically proteins associated with metal ion binding or electron transport. In support of the key role of SOx in AgNP toxicity, the putative nickel-dependent superoxide dismutase was significantly more abundant.

In future, it will be important to place greater emphasis upon the impact of AgNPs upon the entire marine microbial community and assess whether the community-wide response is sufficient to overcome any negative impact of AgNP exposure. It has been shown herein that by exposing a natural community to AgNPs, specific taxa can be identified as particularly sensitive or resistant to exposure for further investigation. Expanding this work to examine the response of non-photosynthetic organisms, as well as utilising molecular approaches such as amplicon sequencing provide great scope for this work.

Chapter 3

Investigating the impact of research-grade and commercially available metal oxide nanomaterials upon marine microbes

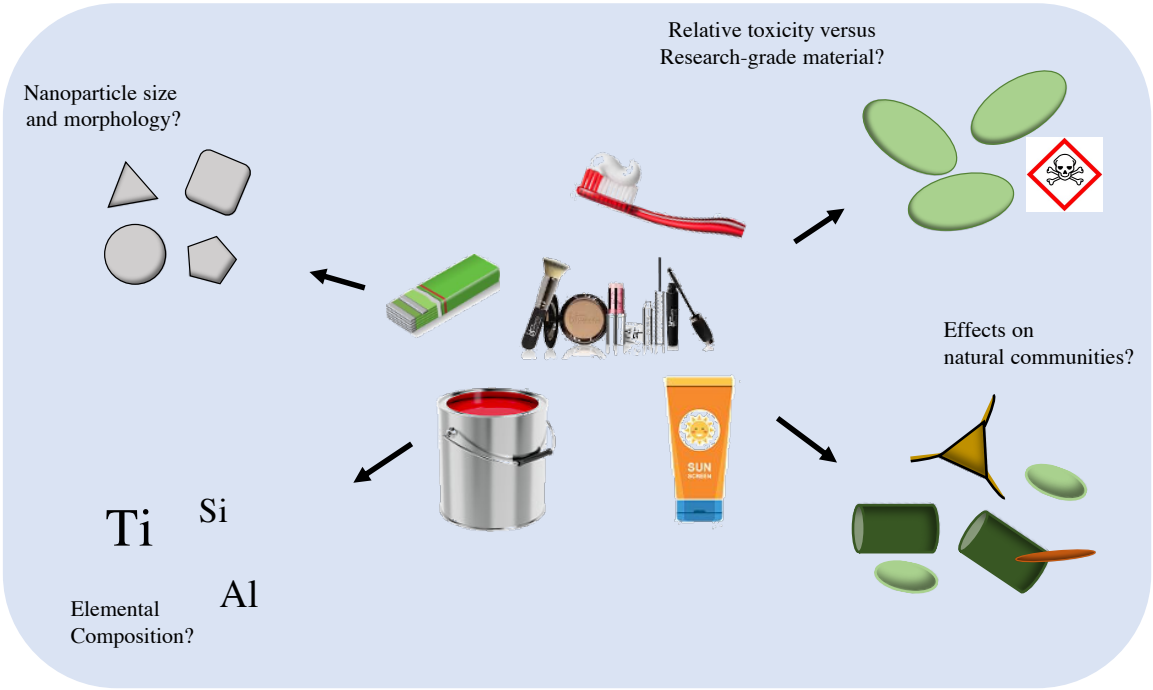

Much of the data presented in this chapter is published in the following articles:

i. *"Environmentally relevant concentrations of titanium dioxide nanoparticles pose negligible risk to marine microbes", Environ. Sci. Nano., 2021,* ***8****, 1236 - 1255. C. J. Dedman, A. M. King, J. A. Christie-Oleza, and G.-L. Davies*

ii. *"Investigating the impact of cerium oxide nanoparticles upon the ecologically significant marine cyanobacterium Prochlorococcus", Front. Mar. Sci., 2021,* ***8****, 571. C. J. Dedman, M. M. I. Rizk, J. A. Christie-Oleza, and G.-L. Davies.*

In this chapter the impact of exposure to metal oxide nanomaterials (MO NMs) upon marine microbial organisms is explored by using two MO NMs, $nTiO_2$ and $nCeO_2$, detailed in sections 3.1 and 3.2, respectively.

3.1 Examining the risk of titanium dioxide nanoparticles towards marine microbes under environmentally relevant conditions.

3.1.1 Introduction

Nano-sized titanium dioxide ($nTiO_2$) represents the one of the highest produced NM worldwide, with annual production predicted to reach 2.5 million tonnes by 2025.[9, 19] Due to its prevalent use across a wide range of industries, including plastic production, paints, foods and cosmetics,[7, 19, 20] $nTiO_2$ is highly likely to enter the natural environment.[259] The utilisation of $nTiO_2$ in nano-enabled products is largely dependent upon its unique physicochemical properties,[57] which include: photocatalytic activity, high resilience to corrosion, pure crystallinity, high stability, and high surface area.[260] Three crystalline forms exist for $nTiO_2$: rutile, anatase and brookite,[57] with the former two being the most commonly used within commercially available products.[261] The cosmetics industry dominates the use of $nTiO_2$, and accounts for approximately 70-80% of $nTiO_2$ use.[7] For many years $nTiO_2$ have been used in sunscreen due to their effective ability to filter UV.[47, 262] These nanoparticles possess a high refractive index and are a small band gap semi-conductor allowing for the absorption and scattering of UV light across a broad spectrum (UVA and UVB).[263] This is advantageous over organic sunscreens which comparatively absorb UV light in a narrow band of the spectrum.[263] Additionally, $nTiO_2$ does not cause irritation and is not penetrative, has high transparency to natural light and iridescent properties leading to its use in a wide range of cosmetic products.[20, 263] Typically product formulations are made up of 2-14 wt% $nTiO_2$,[264, 265] however, the exact physicochemical properties of NMs used vary greatly. In fact, it is estimated that the chemical composition of NMs utilised for over 50% of commercial products is not widely publicised.[9]

Domestic use of consumer products such as sunscreen and toothpaste is predicted to release considerable volumes of TiO_2 into the aquatic environment *via* direct entry into the ocean, or following release into wastewaters.[7, 37] Extraction of metal oxide (MO) NMs from wastewater treatment works has been recorded at an efficiency of approximately 95%,[38] resulting in the entry of approximately 5% of MO NMs into the aquatic environment *via* wastewater effluent. Given that 4100 tonnes of TiO_2 is predicted to enter US wastewaters as a result of toothpaste use every year,[7] we can estimate that up to 205 tonnes will enter wastewater effluent and be transported to natural systems, where their ultimate fate remains unknown.

In recent years, increasing efforts have been made to uncover the environmental concentrations of engineered NMs. Difficulties in sampling techniques and varying effectiveness of methods for characterising nano-pollutants, particularly at the low concentrations predicted in the environment, has led to a lack of environmental data.[51, 266] 'Environmental Fate Models' represent a powerful tool for this purpose,[52] and surface water concentrations of $nTiO_2$ are estimated in the range of 0.021-10.000 μg L^{-1}.[53] However, more recently, environmental sampling has revealed concentrations of up to 40 μg L^{-1} close to major transport infrastructure and locations heavily impacted by tourism.[39, 267] For example, during the peak tourist season, TiO_2 derived from sunscreen use has been measured in the range of 7-40 μg L^{-1} in surface waters off the Mallorcan coast.[267] As such, it appears that the environmental risk from nano-sized pollutants is likely focused within localised areas of contamination which may vary temporally, where particle-specific properties govern their subsequent fate and transport.[13]

As highlighted in the previous chapters, the microbial community plays a fundamental role in the functioning of the marine ecosystem, contributing approximately 50% of global primary productivity and influencing major climatic and biogeochemical cycles.[131, 133] Hence, understanding the potential effects of contaminants upon marine microbes is key to evaluating their likely ecosystem-wide impact. Previous research has revealed a toxic effect of MO NMs, including $nTiO_2$, upon marine microbial species,[7, 95, 140, 143, 145, 268-273] although studies where little or no adverse effect is recorded also exist.[132, 146] A summary of results obtained from ecotoxicity studies

examining the response of marine microbial species, primarily phytoplankton, towards MO NMs is provided in Table 3.1. The primary adverse effect of $nTiO_2$ exposure appears to be growth inhibition, however EC_{50} values are typically recorded in the mg L^{-1} range, far greater than those measured in the environment (up to 40 μg L^{-1}).[145, 269, 270] In addition to growth inhibition, negative effects such as the induction of oxidative stress pathways, physical damage to cells, and entrapment of cells within aggregates of NMs have been recorded following exposure, however results vary greatly.[145, 146, 269, 270, 274] Indeed, physical interaction between phytoplankton and aggregates of $nTiO_2$ appears widespread in laboratory exposure[50, 147, 275, 276] and may represent a possible pathway for phototrophic removal from epipelagic layers[275] or transport of NMs to higher trophic levels.

Much of the toxicological work examining $nTiO_2$ and other MO NMs has so far been carried out using standardised research-grade NMs, which are not usually surface modified. More recently, studies have begun to emerge focussing upon the toxicity of surface functionalised $nTiO_2$ (*e.g.* sunscreens which often possess surfactant/polymer surface modifications) upon marine phytoplankton.[7, 140] In these studies, adverse effects were observed in phytoplankton exposed to sunscreens containing $nTiO_2$, associated with increased production of reactive oxygen species (ROS), membrane damage and possible genotoxicity.[140] However, biostimulating effects of $nTiO_2$-containing sunscreens have also been recorded, attributed to other organic components of the sunscreen formulation.[264] Interestingly, $nTiO_2$ derived from commercial products have been reported to result in greater growth inhibition than research-grade nanoparticles.[7] It should be noted, though, that much of the work investigating MO NMs are carried out using exposure concentrations in the mg L^{-1} range (*i.e.* 1-30 mg L^{-1}),[7, 95, 140, 143, 145, 268-273] far exceeding those predicted and measured in the environment (0.021-40 μg L^{-1}).[7, 53, 264, 267] Increased research is required to examine the end-products of consumer goods which may enter the aquatic environment.[264 265] Given the great variation in physicochemical properties between specific NMs, and hence varied fate in aquatic media, it is important that representative NMs derived from consumer goods are utilised alongside research-grade materials during experimentation.[265, 277] To provide a greater understanding of the environmental

Table 3.1. Summary of effects of metal oxide nanomaterials upon marine microbial species.

Species	Nanomaterial	Exposure length (h)	Result*	Ref.
Diatoms				
Nitzschia closterium	TiO_2 (21 nm)	96	EC_{50}: 88.78 mg L^{-1}	269
Nitzschia closterium	TiO_2 (60 nm)	96	EC_{50}: 118.80 mg L^{-1}	269
Phaeodactylum tricornutum	TiO_2 (15 nm)	72	EC_{50}: 10.91 mg L^{-1}	95
Phaeodactylum tricornutum	TiO_2 (25 nm)	72	EC_{50}: 11.30 mg L^{-1}	95
Phaeodactylum tricornutum	TiO_2 (32 nm)	72	EC_{50}: 14.30 mg L^{-1}	95
Phaeodactylum tricornutum	TiO_2 (15 nm)	120	EC_{50}: 167.71 mg L^{-1}	145
Skeletonema costatum	ZnO (20 nm)	96	LC_{50}: 2.36 mg L^{-1}	103
Skeletonema marinoi	TiO_2 (15-20 nm)	96	No toxicity reported	132
Thalassiosira pseudonana	ZnO (20 nm)	96	LC_{50}: 4.56 mg L^{-1}	103
Thalassiosira pseudonana	TiO_2 (15-20 nm)	96	No toxicity reported	132
Green algae				
Chlorella autotrophica	CeO_2 (<25 nm)	72	EC_{50}: >5 mg L^{-1}	199
Chlorella sp.	TiO_2 (21 nm)	72	EC_{50}: 1.6 mg L^{-1} (UV-A irradiation)	273
Chlorella sp.	TiO_2 (21 nm)	72	EC_{50}: 5.0 mg L^{-1} (Under darkness)	273
Chlorella vulgaris	TiO_2 (21 nm)	96	EC_{50}: 80 mg L^{-1} (pH 8.20)	271
Chlorella vulgaris	TiO_2 (21 nm)	96	EC_{50}: 10-20 mg L^{-1} (pH 7.77)	271
Chlorella vulgaris	TiO_2 (21 nm)	96	EC_{50}: 60-70 mg L^{-1} (pH 7.47)	271
Dunaliella salina	CeO_2 (<25 nm)	72	EC_{50}: >5 mg L^{-1}	199
Dunaliella salina	TiO_2 (21 nm)	72	EC_{50}: 1.8 mg L^{-1} (UV-A irradiation)	273
Dunaliella salina	TiO_2 (21 nm)	72	EC_{50}: 13.3 mg L^{-1} (Under darkness)	273
Dunaliella tertiolecta	TiO_2 (25 nm)	72	No toxicity reported	146
Dunaliella tertiolecta	ZnO (100 nm)	96	EC_{50}: 1.94 mg L^{-1}	278
Dunaliella tertiolecta	ZnO (<100 nm)	96	IC_{50}: 1.50 mg L^{-1} (BG-11 media)	142
Dunaliella tertiolecta	ZnO (<100 nm)	96	IC_{50}: 1.33 mg L^{-1} (F/2 media)	142
Dunaliella tertiolecta	SiO_2 (10-20 nm)	96	EC_{50}: 187.77 mg L^{-1}	270
Dunaliella tertiolecta	TiO_2 (25 nm)	96	EC_{50}: 24.10 mg L^{-1}	270
Dunaliella tertiolecta	TiO_2 (15-20 nm)	96	No toxicity reported	132
Isochrysis galbana	TiO_2 (15-20 nm)	96	No toxicity reported	132
Isochrysis galbana	TiO_2 (5 nm)	96	No toxicity reported	147
Nannochloropsis oculata	CuO (<100 nm)	72	EC_{50}: 116.98 mg L^{-1}	279
Tetraselmis suesica	ZnO (<100 nm)	96	IC_{50}: 2.10 mg L^{-1} (BG-11 media)	142
Tetraselmis suesica	ZnO (<100 nm)	96	IC_{50}: 2.57 mg L^{-1} (F/2 media)	142
Dinoflagellates				
Alexandrium tamarense	TiO_2 (35 nm)	96	EC_{50}: 85.1 mg L^{-1}	280
Alexandrium tamarense	TiO_2 (35 nm)	312	EC_{50}: 140.9 mg L^{-1}	280

*LC_{50} refers to the lethal concentration required to kill 50% of the population; EC_{50} refers to the concentration which exerts half the maximal response recorded; IC_{50} refers to the concentration required to inhibit growth by 50%; all toxicity endpoints are reported at the end of exposure.

impact of $nTiO_2$, research must also be directed to simulate environmental conditions as effectively as possible.

As with work examining AgNPs, described in Chapter 2, much of the previous research in this field has focussed upon phytoplankton species such as diatoms and green algae. Therefore, comparatively little evidence for the effects of MO NM exposure upon photosynthetic cyanobacteria exist. As mentioned in Chapter 2, marine cyanobacteria, mainly *Prochlorococcus* and *Synechococcus* species, are the most abundant photosynthetic organisms on earth and major contributors to global primary productivity.[202, 203] Among phytoplankton taxa, cyanobacteria appear particularly sensitive to nano-pollutants *e.g.* silver nanoparticles[281] (see Chapter 2). In this section, a broad-spectrum analysis of both commercially available research-grade (non-surface modified) $nTiO_2$, as well as $nTiO_2$ extracted from common consumer products, was used to examine their impact upon marine phytoplankton at both the organism- and community-level. Short-term (72 h) and medium-term (240 h) toxicity of $nTiO_2$ was examined using the ecologically significant cyanobacterium *Prochlorococcus sp*. MED4 under environmentally relevant conditions (*i.e.,* at ambient cell densities, 10^4-10^5 cells mL^{-1}),[207, 224] in oligotrophic NSW). The behaviour of $nTiO_2$ in NSW and its interaction with cyanobacteria was investigated through the use of dynamic light scattering (DLS), flow cytometry and fluorescent microscopy. Molecular features of toxicity were assessed by shotgun proteomic analysis and appeared negligible. Finally, an additional experiment was conducted using natural coastal seawater to characterise the whole community response towards consumer $nTiO_2$ exposure. Amplicon sequencing of the 16S rRNA and 18S rRNA genes revealed little impact of extracted $nTiO_2$ derived from sunscreen upon natural marine microbial community structure at environmental concentrations. This multi-OMIC study provides a comprehensive assessment of the differing effects that result from exposure to various types of $nTiO_2$, representative of materials likely to enter the marine environment, thus facilitating effective evaluation of their likely interaction with marine microbial species and overall environmental risk.

3.1.2 Materials and Methods

3.1.2.1 Materials

Research-grade $nTiO_2$ used during experimentation was purchased from Sigma Aldrich (Material number: 718467, 21 nm (19.9±6.6 nm, TEM). Three consumer products; Skinceuticals™ sunscreen (S1), Boots Soltan™ sunscreen (S2), and The Body Shop™ liquid foundation (P1) were selected based on $nTiO_2$ being listed as an ingredient and purchased from a high street retailer. Natural seawater (NSW) utilised in experimental work was prepared as outlined in section 2.2.1. 'Neat' sunscreen stocks were prepared by diluting the cream directly in NSW. For all experimental work, $nTiO_2$ stocks were prepared in NSW and sonicated for 15-30 mins (Branson 1210 Sonicator, 40 kHz) prior to addition to experimental media to avoid extensive aggregation. Glassware was acid-washed before use. Axenic *Prochlorococcus sp*. MED4 was routinely grown using Pro99 media[205] (section 2.2.4) and maintained at 23 °C before use in experimentation.

3.1.2.2 Extraction procedure

Methods adapted from those described by Galletti *et al*. (2016) were utilised to extract $nTiO_2$ from consumer goods.[7] Briefly, 1.5-2.5 g of product was soaked in 20 mL hexane for 2 h. Suspensions were then shaken manually and centrifuged at 4400 rpm for 5 mins. The supernatant was subsequently discarded, and 20 mL ethanol was added and shaken manually. The solution was then centrifuged at 4400 rpm for 5 mins and the resultant supernatant was discarded. Following this, the remaining product was washed in Milli-Q ultrapure water (0.22 μm filter operated at 18.2 MΩ at 298 K) three times using centrifugation; first centrifuging at 11,000 rpm for 5 mins, extending this to 10 mins for the final two washes. Extracted pellets were subsequently dried in a 60 °C oven to form a powder. Samples were stored in darkness prior to characterisation and use in experiments with marine phytoplankton.

3.1.2.3 Characterisation of $nTiO_2$

Transmission electron microscopy (TEM) was utilised to determine primary nanoparticle size, using the protocol outlined in section 2.2.1. Diameters were measured using Image J version 3.2; average values were calculated by measuring the diameter of >100 particles with errors represented as standard deviations. Energy-dispersive X-ray spectroscopy (EDS) was collected using an Oxford Instruments X-Max 80T detector. Additionally, samples were ground to fine powders before Powder X-ray diffraction (P-XRD) was performed using a STOE Stadi-P diffractometer with a molybdenum X-ray source (operated at 50 kV and 30 mA), λ = 0.7093 Å. The 2θ scan range was 2–40.115°at a step size of 0.495° and 5 seconds per step. Samples were prepared using STOE zero scattering foils before being inserted into the transmission sample holder.

3.1.2.4 Short-term (72 h) toxicity testing of *Prochlorococcus* towards consumer $nTiO_2$

Prochlorococcus sp. MED4 was inoculated into oligotrophic NSW at ambient cell densities (1.5-5.5 x 10^4 cells mL^{-1}) and incubated 72 h for pre-adaptation to the oligotrophic conditions prior to experimentation, as previously described (*i.e.,* 23 °C at constant 10 μmol photons m^{-2} s^{-1} light intensity, using a Lifelite™ full spectrum bulb with UV, and with shaking at 100 rpm). 30 mL of pre-adapted *Prochlorococcus* culture was aliquoted into 50 mL filter-capped tissue culture flasks and spiked with $nTiO_2$ stocks to make up test concentrations of 0, 5, 50 and 500 μg L^{-1}, all in triplicate. Four $nTiO_2$ treatments were investigated: $nTiO_2$ nanopowder (Sigma Aldrich), $nTiO_2$ derived from sunscreen S1 and S2, and $nTiO_2$ derived from liquid foundation P1. Additionally, a 'neat' sunscreen treatment was tested, where 0.1 g of sunscreen S2 was immersed in NSW and mixed *via* manual shaking and 15 mins sonication. Cultures were subsequently spiked with a defined volume of the sunscreen suspension to make up equivalent test concentrations based on $nTiO_2$ making up ~10 wt% of the sunscreen formulation.[264, 265] After the addition of each treatment, cultures were further incubated under the conditions described above and monitored by flow cytometry at time points 0, 24, 48 and 72 h, as previously described (section 2.2.8). To identify

significant alterations in cell density recorded during toxicity tests with *Prochlorococcus sp.* MED4 two-way T-tests were carried out between untreated controls and cultures exposed to various $nTiO_2$ treatments at each timepoint.

3.1.2.5 Extended (240 h) $nTiO_2$ exposure

To investigate effects of $nTiO_2$ upon *Prochlorococcus sp.* MED4 in extended exposure (240 h), research-grade $nTiO_2$ (Sigma Aldrich, 19.9±6.6 nm) was utilised for experimentation, based on results of earlier experiments described in section 3.1.2.4. Two culture conditions were tested: i) cell-dense cultures ($2x10^6$ cells mL^{-1}) in nutrient-rich Pro99 media, and ii) cultures grown to ambient cell densities ($3.5x10^4$ cells mL^{-1}) in oligotrophic NSW, representing environmental conditions. Cultures were set up as described in section 3.1.2.4. Culture flasks were subsequently spiked with a $nTiO_2$ stock achieving final concentrations in the μg L^{-1} (1, 10 and 100 μg L^{-1}) and mg L^{-1} range (1, 10 and 100 mg L^{-1}), all in triplicate; representing environmental and supra-environmental concentrations, respectively. Cell counts were monitored at 0, 24, 48, 72, 192 and 240 h by flow cytometry as previous and compared to that of an untreated control. In addition to monitoring of cell density, flow cytometric analysis was utilised to infer the behaviour of $nTiO_2$ within test media and their interaction with cyanobacterial cells. To identify significant alterations in cell density recorded during toxicity tests with *Prochlorococcus sp.* MED4 two-way T-tests were carried out between untreated controls and cultures exposed to various $nTiO_2$ treatments at each timepoint.

3.1.2.6 Imaging of $nTiO_2$-cyanobacterial aggregates by fluorescent microscopy

To investigate the hetero-aggregation between $nTiO_2$ and *Prochlorococcus*, a 200 μL sample was collected from the bottom of culture flasks from one replicate of each treated group during extended exposures (section 3.1.2.5). This sub-sample was stained with 1X SYBR Gold nuclear stain (Thermofisher) and imaging was carried out at 40x magnification using a Nikon Widefield Fluorescence Microscope under brightfield and GFP fluorescence. Images were captured from both channels and subsequently merged to assess the presence and extent of aggregation between

cyanobacterial cells and $nTiO_2$. Controls containing $nTiO_2$ only (100 mg L^{-1}) were included to prove the nanoparticles did not get stained by the dye. In addition, NSW samples and untreated *Prochlorococcus* culture in the absence of $nTiO_2$ were imaged to confirm aggregates were indeed $nTiO_2$ rather than other particulate material.

3.1.2.7 Light scattering analysis of $nTiO_2$ behaviour within natural seawater

The aggregation behaviour of $nTiO_2$ (Sigma Aldrich, 19.9±6.6 nm) within NSW was assessed by z-average size (d.nm) over a period of 336 h (14 d). Here, hydrodynamic particle size measurements were determined by dynamic light scattering (DLS) using a Malvern Zetasizer Nano ZS instrument, equipped with a 4 mW He-Ne 633 nm laser module. A stock of $nTiO_2$ was sonicated for 15-30 mins prior to addition to NSW. Concentrations of 1 mg L^{-1} and 100 mg L^{-1} were utilised due to limitations of the DLS at lower concentrations, hence hindering the ability to assess $nTiO_2$ aggregation at the environmentally relevant concentrations (*i.e.,* in the μg L^{-1} range) used in this study during toxicity testing. $nTiO_2$ suspensions were made up in 20 mL autoclaved and filtered (0.22 μm) NSW in 50 mL tissue culture flasks and placed on an orbital shaker (100 rpm) to simulate natural movement of water. DLS measurements were carried out upon a 200 μL sub-sample collected from the mid-point of flasks at set timepoints (0, 1, 2, 4, 24, 48, 72, 168, 240, 336 h). For each sample the average was taken from 3 measurements made up of 11 sampling runs lasting 10 s each.

3.1.2.8 Shotgun proteomic analysis of *Prochlorococcus* exposed to $nTiO_2$.

To examine any impact of $nTiO_2$ exposure upon the *Prochlorococcus* proteome, cell-dense cultures were prepared as described in Pro99 media, as previously described (section 2.2.11). Triplicate cultures were spiked with research-grade $nTiO_2$ stock (Sigma Aldrich, 19.9±6.6 nm) to achieve a test concentration of 100 μg L^{-1}. Untreated cultures were also prepared as controls. Following the addition of $nTiO_2$, cultures were incubated for 24 h. Following this, cellular and extracellular proteome samples were prepared and analysed as described previously (section 2.2.11). The mass spectrometry data have been deposited to the ProteomeXchange Consortium

(http://proteomecentral.proteomexchange.org) via the PRIDE partner repository[215] with the dataset identifier PXD024726.

3.1.2.9 Examining the whole community response *via* 16S rRNA/18S rRNA amplicon sequencing

A site for experimental work was selected in the Balearic Islands, Spain (39.493868, 2.739820). Field experiments were carried out during April 2018. Here, coastal seawater (NSW) containing its natural microbial community was collected at a depth of approximately 1 m, representing those microorganisms most likely to interact with $nTiO_2$ derived from sunscreen in the coastal system. Subsequently, 500 mL was transferred to pre-washed 1 L Nalgene plastic bottles, leaving sufficient volume empty for air exchange. Microbial communities were exposed to one of three treatments: 1) Untreated control, where no $nTiO_2$ was added; 2) $nTiO_2$ extracted from sunscreen S2; 3) 'Neat' sunscreen S2 dispersed in NSW. Extracted $nTiO_2$ from S2 were obtained as described above (section 3.1.2.2) and added at a final concentration of 25 μg L^{-1}. 'Neat' sunscreen stock was made up in NSW and a defined volume was added to achieve ~25 μg L^{-1} of $nTiO_2$, assuming that $nTiO_2$ typically makes up ~10 wt% of such products.[264, 265] Bottles were mixed by inversion three times and incubated over two days in an outdoor water container to provide temperature stability while being exposed to natural sunlight to best replicate natural conditions. Bottle caps were loosened to ensure sufficient gas exchange and bottles were shaken manually (15-30 s) at regular intervals throughout the experiment to ensure water was well mixed. Following exposure, microbial cells were collected by filtering the 500 mL through a 0.22 μm filter (Millipore). Filters were transferred to a 2 mL Eppendorf containing lysis buffer (Qiagen) and immediately stored at -20°C.

DNA extraction was carried out using the DNeasy Power Biofilm extraction kit (Qiagen) according to the manufacturer's instructions, including a bead beating step as previously described.[282] DNA quantification was obtained by Qubit® HS DNA kit (Life Technologies Corporation). Extracted DNA samples were stored at -20°C. Prokaryotic and eukaryotic community analysis was performed by amplicon sequencing using the 515F-Y and 926R primers to amplify the 16S rRNA v4-5

regions, and V8F and 1510R primers to amplify the 18S rRNA v8-9 regions, respectively.[283, 284] PCR products were purified, indexed, normalized and analysed by 2 x 300 bp paired-end sequencing using the MiSeq system with v3 reagent kit (Illumina) as described in Wright *et al.* 2019.[282] Raw sequencing data was analysed using the DADA2 bioinformatic pipeline based on its enhanced taxonomic resolution compared to alternative methods.[282, 285-287] Taxonomically assigned data in the form of amplicon sequencing variants (ASVs) were analysed using MicrobiomeAnalyst software.[288, 289] Briefly, following normalisation by Total Sum Scaling, principle coordinates analysis (PCA) based on Bray-Curtis dissimilarity, in conjunction with Permutational multivariate analysis of variance (PERMANOVA) was utilised to assess significant alterations in community composition between treatments at the individual ASV level. Subsequently, two-way T-tests were utilised to identify significant variations in relative abundance of various taxonomic groups between control and treated samples. Sequence files have been deposited in the NCBI Short Read Archive (SRA) database under Bioproject: PRJNA690209. For additional details of the amplicon sequencing methods, see section A1.2.1, Appendix 1.

3.1.3 Results and Discussion

3.1.3.1 Characterisation of research-grade and consumer $nTiO_2$

$nTiO_2$ was initially extracted from commercial sunscreen and cosmetics products, S1, S2, and P1, as detailed in the methods section, and characterised. The extraction method utilised to extract particles from the three product formulations was largely effective, yielding a visible powder that could be dried and stored for experimental use. Characterisation of research-grade and extracted materials was carried out using a combination of TEM and EDS mapping, revealing primary particle size, morphology and elemental composition (Table 3.2 and Figure 3.1).

Research-grade $nTiO_2$ (Sigma Aldrich) possessed an average particle size of 19.9±6.6 nm, close to the manufacturer's advertised size (21 nm), whilst materials extracted from consumer products ranged in average primary particle size 50.0 to 158.1 nm. Interestingly, all primary particles extracted from commercially available products

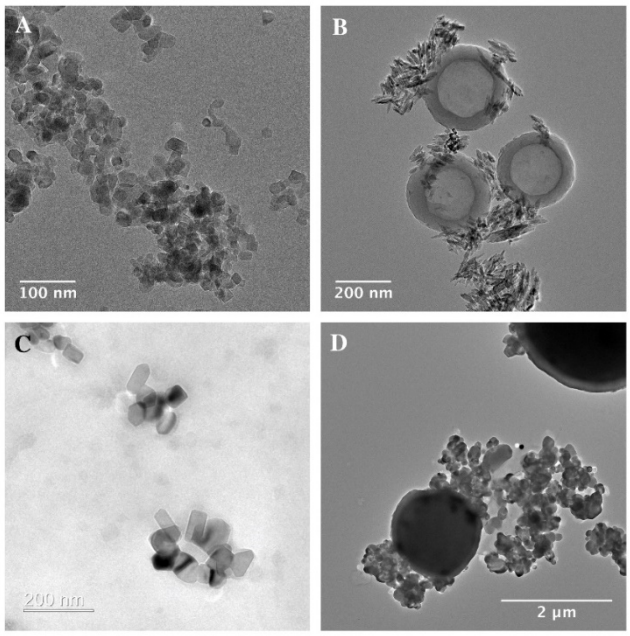

Figure 3.1. TEM images of $nTiO_2$ utilised in experimental work; A – research-grade $nTiO_2$ purchased from Sigma Aldrich; B – $nTiO_2$ extracted from Skinceuticals™ sunscreen (S1); C – $nTiO_2$ extracted from Boots Soltan™ sunscreen (S2); D – $nTiO_2$ extracted from The Body Shop™ liquid foundation (P1).

had large standard deviations in sizes, indicating a wide size range in particle populations (Table 3.2). Typically, samples appeared as small aggregates, a common feature often observed as a result of drying of the samples onto TEM grids (Fig 3.1). EDS mapping confirmed that all primary particles were entirely composed of Ti and O (Table 3.2 and Fig 3.2).

Table 3.2. Summary of material characteristics as determined by TEM, EDS mapping and P-XRD.

	Primary particle characteristics				**Secondary particle characteristics**		
$nTiO_2$ source	**Size (nm) (TEM)**	**Elemental composition**	**Phase**	**Morphology (TEM)**	**Size (nm) (TEM)**	**Elemental composition**	**Morphology (TEM)**
Sigma Aldrich	19.9±6.6	TiO_2	Anatase and Rutile	Mixed cuboid and spherical	n/a	n/a	n/a
Sunscreen S1	50.0±32.9	TiO_2	Rutile	Needle shaped	294.3±37.5	Carbon-based	Spherical
Sunscreen S2	64.6±26.4	TiO_2	Rutile	Cuboid	n/a	n/a	n/a
Product P1	158.1±68.7	TiO_2	Anatase	Cuboid	2705.8±1333.8	SiO_2	Spherical

P-XRD was carried out on all samples (Fig 3.3). This showed research-grade $nTiO_2$ to have a mixture of anatase and rutile phases, with peaks corresponding with the JCPDS patterns 21-1272[290] and 21-1276[291] for the tetragonal structure of anatase and

rutile TiO_2, respectively. The sunscreens S1 and S2 samples appeared to be present as the rutile phase only, whilst the product P1 sample presented only anatase phase. All samples showed some peak broadening, indicative of the presence of nano-sized crystallites, as previously observed by electron microscopy. Previous research has indicated that $nTiO_2$ phase has impacted upon toxicity towards biota,[95, 292] hence, such information is important to fully evaluate outcomes of toxicity testing.

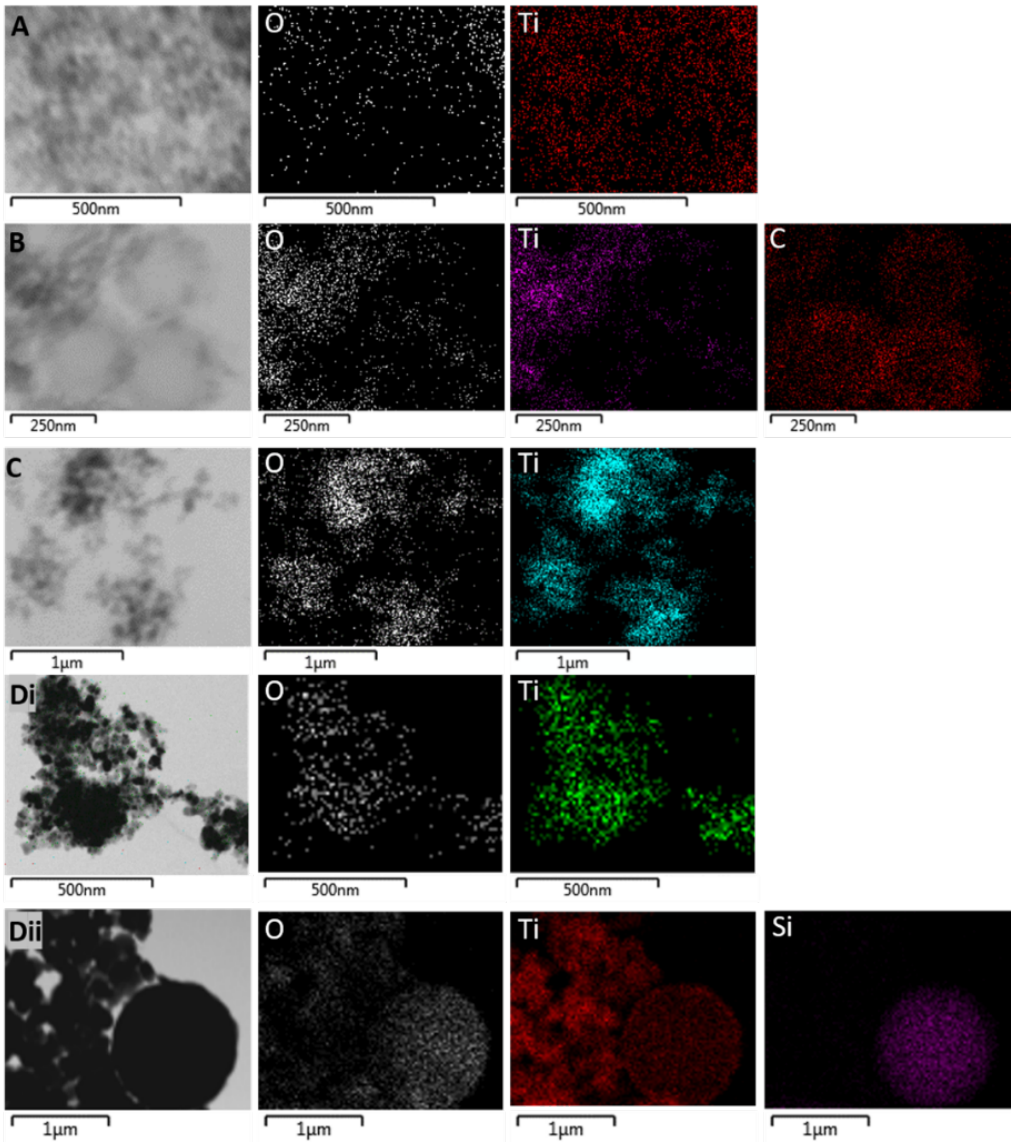

Figure 3.2. EDS analysis of $nTiO_2$**:** A – research-grade $nTiO_2$ nanopowder purchased from Sigma Aldrich; B – $nTiO_2$ extracted from Skinceuticals™ sunscreen (S1); C – $nTiO_2$ extracted from Boots Soltan™ sunscreen (S2); Di and Dii – $nTiO_2$ extracted from The Body Shop™ liquid foundation (P1). Left panel shows scanning transmission electron microscope image of samples; other panels show false coloured EDS image of element as labelled.

In accordance with previous studies, variation in physical properties of extracted particles is observed.[265, 277] For example, primary $nTiO_2$ particles extracted from consumer products S1 and S2 showed significant differences in morphology (Figs 3.1 B-C), despite both being utilised for UV protection in sunscreen formulations. Additional images of all extracted particles are provided in Figures A1.1-A1.3, Appendix 1. These results emphasize the difficulty researchers face in the field of nano-ecotoxicology in selecting appropriate NMs for investigation, where NMs belonging to the same class of material vary extensively in physicochemical properties which will inevitably alter their fate and behaviour in the environment. As a result, it is difficult, or impossible, to effectively compare between studies utilising such materials. This issue is exacerbated by the fact that for >50% of NMs used commercially, the chemical structure is unknown.[9] Additionally, other components of the product formulation may be difficult to separate from nanoparticles during the extraction process.[293] In studies carried out by Philippe *et al*. (2018), all $nTiO_2$

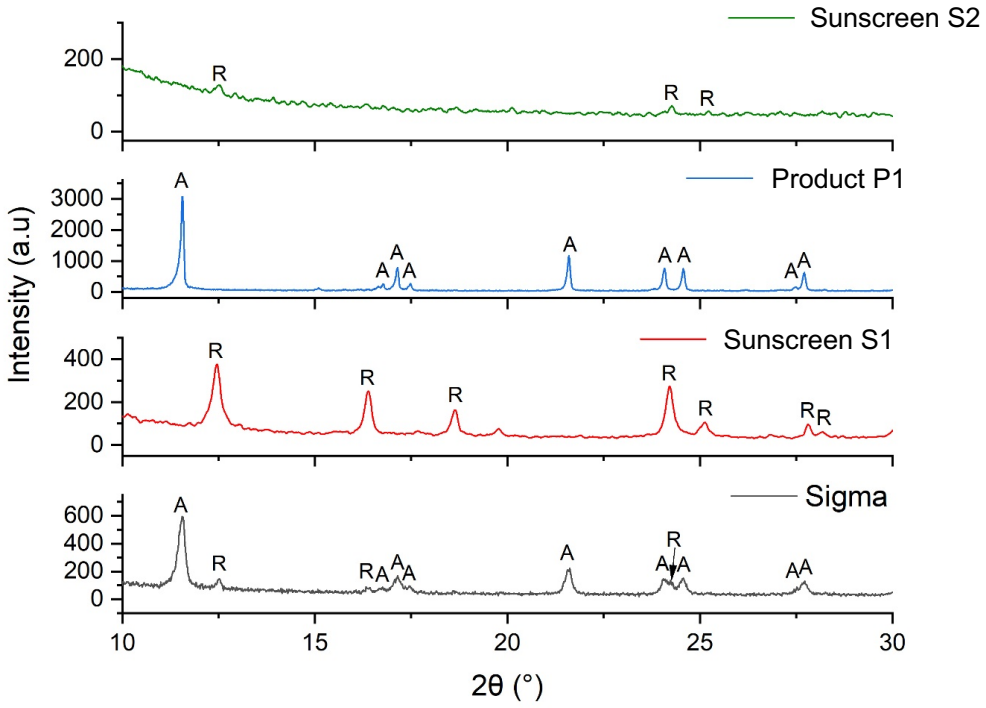

Figure 3.3. Powder X-ray diffraction patterns of $nTiO_2$ samples, with anatase (A) and rutile (R) planes indexed to JCPDS card numbers 21-1272 and 21-1276 for the tetragonal structures of anatase and rutile TiO_2, respectively, as labelled. Peaks at 11.5°, 17.2°, 21.6°, 24.1°, 24.6°, 27.8°, 30.1°, and 30.7° can be indexed to the (101), (004), (200), (105), (211), (118), (116), and (220) planes of the tetragonal anatase crystal system. Major peaks observed at 12.5°, 16.4°, 18.7°, 24.2°, 25.1°, 27.8°, 28.2°, and 30.1° can be indexed to the (110), (101), (111), (211), (220), (002), (310), and (301) planes of rutile TiO_2.

extracted from sunscreen was believed to be coated, most commonly with alumina or silica.[265] However, herein, based on EDS mapping, primary particles appeared to be present as pure TiO_2. Product P1 additionally showed the presence of secondary particles - large micron-sized spheres (Fig 3.1D) composed of SiO_2 (from EDS measurements, Fig 3.2 Di and Dii), a common filler used in cosmetics. On the other hand, S1 showed the additional presence of hollow carbon-based organic spheres (Fig 3.1B; EDS, Fig 3.2B), believed to be micellar structures from additional organic components present in the sunscreen which were not completely removed during extraction. No alumina (Al_2O_3), another common filler in cosmetics, was found during EDS measurements of all samples. Efforts must be directed at producing materials for ecotoxicological research that are representative of those that are likely to enter the natural environment, such as those displayed here from common user products.

3.1.3.2 Investigating the toxicity of research-grade and consumer $nTiO_2$ on the marine cyanobacterium *Prochlorococcus*

The numerically most abundant phototroph on Earth, the marine cyanobacterium *Prochlorococcus,* was grown in the presence of research-grade $nTiO_2$ (Sigma Aldrich) and nanoparticles extracted from common consumer products, as well as 'neat' sunscreen under environmentally relevant conditions, *i.e.,* natural oligotrophic seawater with relevant cell density (~10^4 cell mL^{-1}) and $nTiO_2$ concentrations (1, 50 and 500 μg L^{-1}). Following 72 h exposure under simulated natural conditions (Fig 3.4), significant declines in population size were experienced by *Prochlorococcus sp.* MED4 in response to three out of four $nTiO_2$ treatments when compared to the untreated control (*i.e.,* research-grade $nTiO_2$, and $nTiO_2$ extracted from S1 and P1, two-way T-test; $p \leq 0.05$). Despite previous research indicating a key role of TiO_2 phase in determining toxicity,[95, 292] no clear influence of varying $nTiO_2$ phase was observed. Toxic effects were recorded in both rutile and anatase treatments, as well as mixed phase $nTiO_2$. It must be acknowledged that due to the methods used to extract nanoparticles, materials may not accurately reflect those released into the environment within product matrixes. Here, behaviour of nanoparticles may be altered by the presence of other components of the product formulation, which require consideration. The process of nanoparticle release from consumer products upon their entry into the environment requires further investigation to comprehensively evaluate their impact.

Upon comparing the response displayed by cultures exposed to research-grade and extracted materials, recorded cell decline of *Prochlorococcus* was greatest during exposure to research-grade $nTiO_2$ at higher concentrations (*i.e.,* 50 and 500 µg L^{-1}). Here, exposure resulted in a significant reduction in cell density of up to 70% compared to the control after 72 h (two-way T-test, $p \leq 0.05$), recorded in the 500 µg

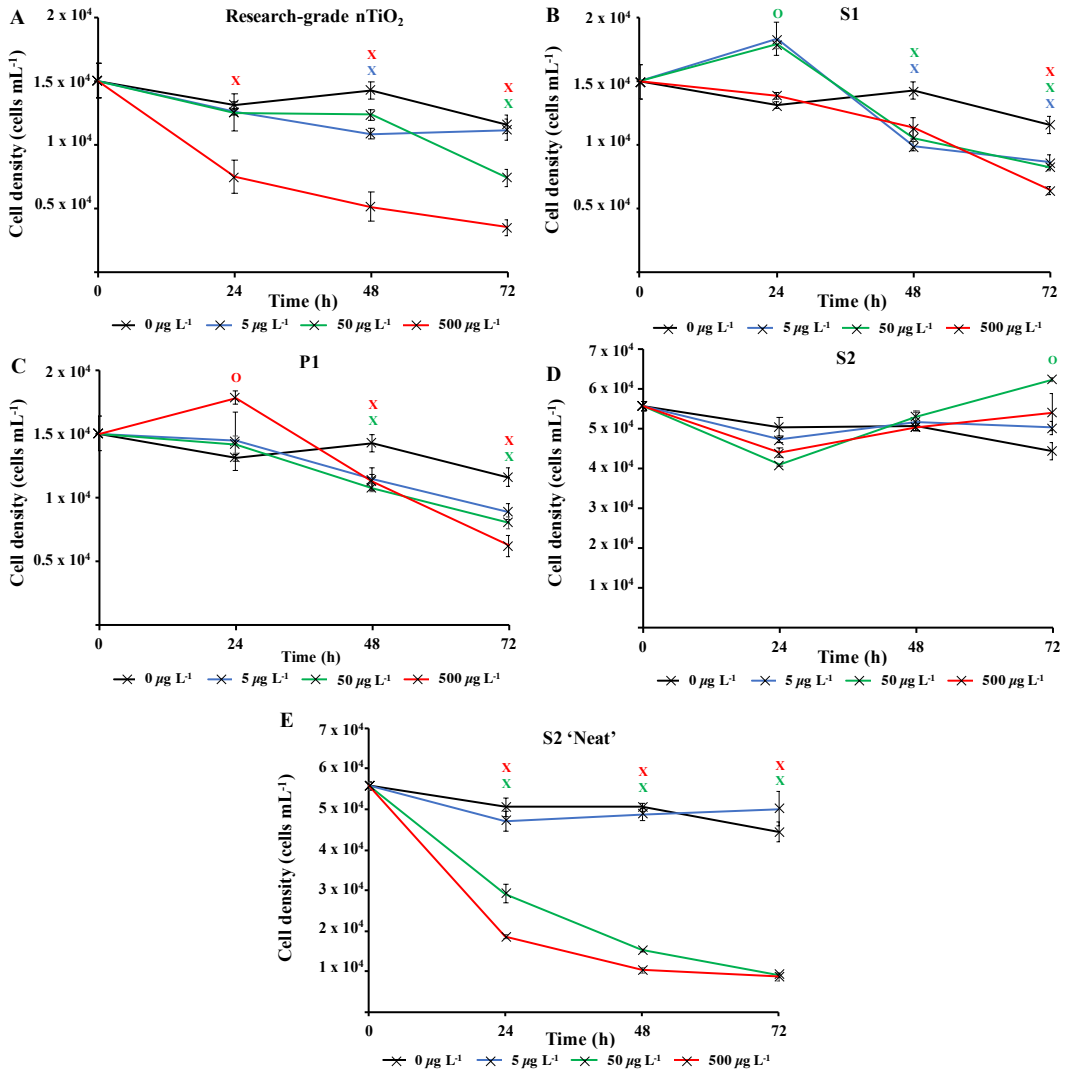

Figure 3.4. Cell density of *Prochlorococcus sp.* MED4 when exposed to $nTiO_2$ (0-500 µg L^{-1}) for a period of 72 h under simulated natural conditions as measured by flow cytometry; A – research-grade $nTiO_2$ nanopowder purchased from Sigma Aldrich; B – $nTiO_2$ extracted from Skinceuticals™ sunscreen (S1); C – $nTiO_2$ extracted from The Body Shop™ liquid foundation (P1); D – $nTiO_2$ extracted from Boots Soltan™ sunscreen (S2); E – 'Neat' Boots Soltan™ sunscreen immersed in NSW. Data points are presented as the mean ± standard error (n=3). Markers indicate where two-way T-tests revealed cell density of treated groups to be significantly lower (crosses) or higher (circles) than the untreated control at each timepoint ($p \leq 0.05$).

L^{-1} treatment (Fig 3.4A). Significant declines were also recorded in the extracted S1 and P1 treatments; however, these were less severe, resulting in decreases in cell density of up to 46%, and 56% compared to the untreated control respectively (two-way T-test, $p \leq 0.05$), at the highest concentration (500 μg L^{-1}) (Figs 3.4 B-C). This result differs from trends described in previous works in literature, where materials extracted from sunscreen and toothpaste were recorded to exert stronger adverse effects than pristine research-grade $nTiO_2$.[7] In that work, it is likely that residual components of product formulations, not fully removed during the extraction process, are toxic at the relatively high concentrations which were tested (1-5 mg L^{-1}).[7] Whilst the highest concentration (500 μg L^{-1}) tested here is greater than that predicted in the environment,[53] some evidence of *Prochlorococcus* decline was also observed at 50 μg L^{-1}. This concentration does not far exceed the concentration of TiO_2 derived from sunscreen recorded in areas of high tourism within the natural environment (7-40 μg L^{-1}).[267] Therefore, potential exists for such materials to exert an adverse effect upon marine cyanobacteria such as *Prochlorococcus* in those areas more susceptible to localised pollution.

No adverse effect of exposure was recorded in response to S2 extracted nanoparticles. In fact, after 72 h average cell density of cultures exposed to S2 nanoparticles reached slightly higher values than control cultures (Fig 3.4D). Interestingly, herein, cultures exposed to $nTiO_2$ extracted from S1 and P1 also displayed evidence of enhanced growth during early stages (24 h) of experimentation (Figs 3.4 B-C). Here, an approximate 10% increase in cell density of both the S1 and P1 treatment was observed relative to the untreated control following 24 h exposure (two-way T-test, $p \leq 0.05$). A beneficial effect of some sunscreen formulations upon phytoplankton growth has been observed in previously published research.[264] Such increases in cell density may arise from possible biostimulating effects of residual product components such as antioxidants, preservatives and moisturisers, believed able to enhance or stimulate growth of phytoplankton;[264] or essential nutrients such as N, P and Si, reportedly released by sunscreen upon entry into seawater.[267]

Whilst evidence of significant cell decline was observed in the presence of both research-grade and consumer $nTiO_2$ (after 72 h), these declines were not as severe as

those experienced by cultures exposed to 'neat' sunscreen S2 immersed in seawater (Fig 3.4E). Here, decline of the cyanobacterial population was the most rapid, and resulted in an 81% decrease of the population by the end of the 72-h incubation at the highest concentration (500 μg L^{-1}) relative to the untreated control (two-way T-test, $p \leq 0.05$). However, given 'neat' sunscreen treatments were established based on estimated $nTiO_2$ content, exact $nTiO_2$ concentrations may be higher or lower than intended. Nevertheless, sunscreens containing $nTiO_2$ have previously been recorded to exert toxicity upon phytoplankton *via* generation of ROS,[140] which are particularly toxic to *Prochlorococcus* due to its lack of catalase.[223] Given that no adverse effect was observed when exposing *Prochlorococcus* to $nTiO_2$ extracted from sunscreen S2, it is likely that toxic effects arise from the other components of the sunscreen formulation which *Prochlorococcus* is highly sensitive to, such as organic compounds or metals.[294, 295] For example, the organic UV-filter octocrylene, found in many sunscreen products, is toxic to a range of marine species.[296] These findings support the belief that whilst examining the effects of NMs utilised in consumer goods, understanding the exact chemical characteristics of materials is vital. It is important to consider any unknown components of product formulations which may too exert adverse (or stimulating) effects upon biota,[297] or alter outcomes of toxicity testing. Without such information, we are unable to attribute potential toxicity solely to NMs.

3.1.3.3 Extended exposure of *Prochlorococcus* to research-grade $nTiO_2$

Typically, ecotoxicological studies are carried out for a number of days (3-4 d),[7, 95, 132, 140, 143, 147, 268, 269, 271] thus missing the opportunity to assess chronic effects (>5 d) of a particular substance.[298] However, examples of longer-term studies do exist.[99, 153, 280] To address this and assess the ability of *Prochlorococcus sp.* MED4 populations to recover from short-term (72 h) stress, incubations with research-grade $nTiO_2$ observed to exert strongest effects during short-term exposure, were extended to 240 h. These nanoparticles were identified as mixed rutile and anatase phase by P-XRD (see section 3.1.3.1) and hence represent all TiO_2 phase types investigated. In this work, the $nTiO_2$ concentrations examined were altered to span the predicted environmental (μg L^{-1}) and supra-environmental range (mg L^{-1}); hence, results are not directly comparable to short-term (72 h) experiments. Additionally, cultures grown in nutrient rich Pro99

Figure 3.5. Evidence of $nTiO_2$ aggregation and sedimentation after 24 h during incubations with *Prochlorococcus sp.* MED4 at supra-environmental concentrations (10 and 100 mg L^{-1}). A – 10 and 100 mg L^{-1} ambient cell density (~10^4 cells mL^{-1}) in natural seawater, B – 10 and 100 mg L^{-1} 'rich' cell density (~10^6 cells mL^{-1}), in nutrient-rich Pro99 media. C – Increased magnification image of aggregates observed within 100 mg L^{-1} 'rich' cell density samples.

media were tested to assess the effect of altered experimental conditions. When monitoring cultures exposed to research-grade $nTiO_2$ in the mg L^{-1} range, deposited material was visible in the culture flasks (Fig 3.5), believed to be hetero-aggregations of $nTiO_2$ and cyanobacterial cells (NP-cell). Due to precipitation arising from increased density, any cells entrapped in NP-cell aggregates would likely be removed from the water column, thus reducing the planktonic cyanobacterial population. Given this, only freely suspended *Prochlorococcus* cells were used for the calculation of cell density, although NP-cell aggregates were also monitored.

Significant declines in the free-living *Prochlorococcus* population were observed at a range of concentrations of added $nTiO_2$ ≥10 µg L^{-1} at specific timepoints throughout the 240-h incubation in both NSW and Pro99 media (Fig 3.6). In NSW (Fig 3.6A), at the 24 h timepoint only the 10 and 100 mg L^{-1} treatments caused a significant decline in cell density compared to the untreated control (two-way T-test, $p \leq 0.05$). After 48 h the 100 mg L^{-1} continued to exert significant declines in the cyanobacterial population, additionally the cell density of the 10 µg L^{-1} treatment was also significantly lower than the untreated control (two-way T-test, $p \leq 0.05$). Following 72 h exposure, significant declines were recorded in the 10 µg L^{-1}, 100 µg L^{-1}, 10 mg L^{-1} and 100 mg L^{-1} treatments (two-way T-test, $p \leq 0.05$). However, in later stages of exposure (*i.e.,* 192 and 240 h) only 100 mg L^{-1} $nTiO_2$ caused a significant decline in the *Prochlorococcus* population in NSW compared to control cultures (two-way T-test,

p≤0.05). Cultures grown in nutrient rich Pro99 media (Fig 3.6B) experienced a decrease in cell density compared to the control in response to 100 mg L^{-1} $nTiO_2$ at each timepoint between 24-72 h (two-way T-test, p≤0.05). Additionally, at the 24 h timepoint, the 10 µg L^{-1} treatment also caused a significant decline in the cyanobacterial population (two-way T-test, p≤0.05). In later stages of exposure (*i.e.,*

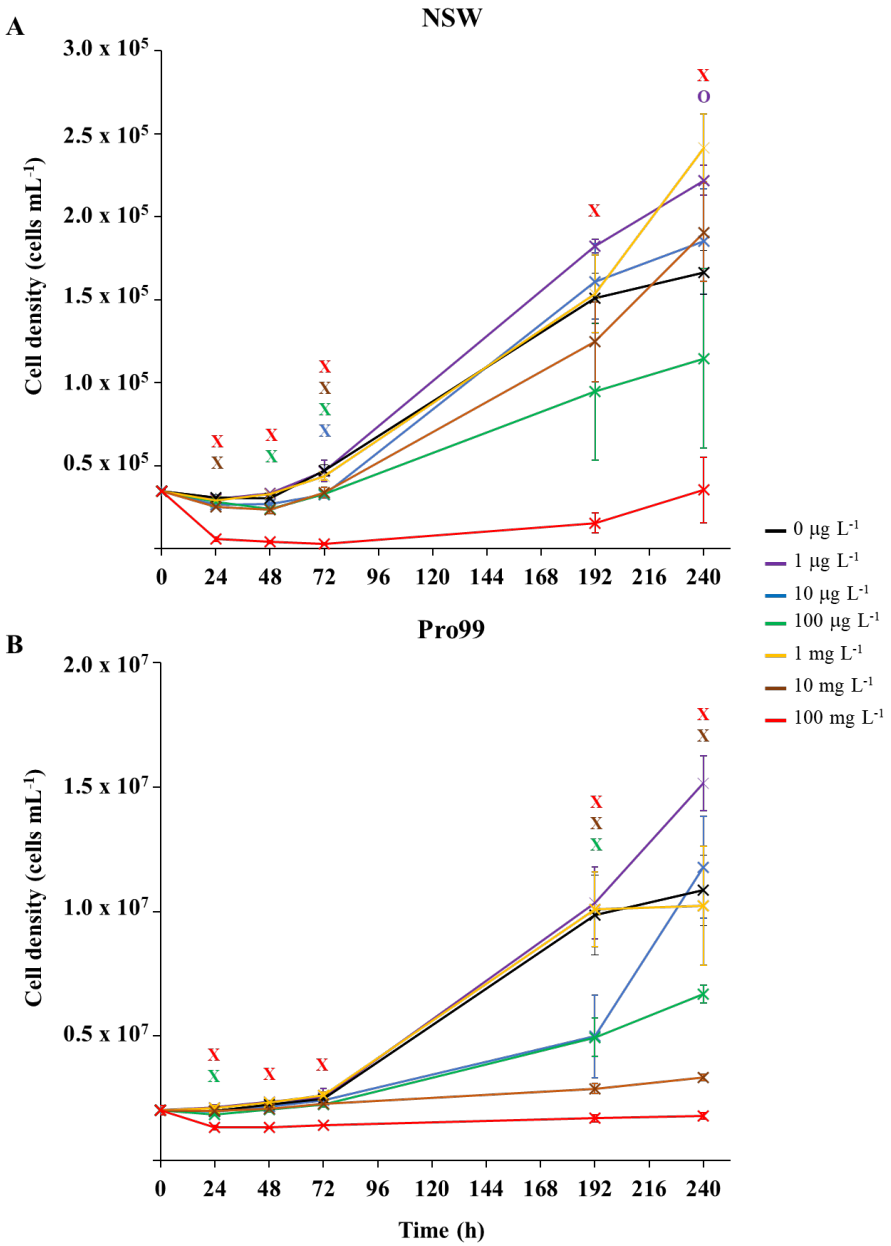

Figure 3.6. Extended exposure (240 h) of *Prochlorococcus sp.* MED4 to research-grade $nTiO_2$ (Sigma Aldrich, 19.9±6.6 nm (TEM)) in both NSW (A) and nutrient rich Pro99 media (B) at concentrations representing the environmental (0, 1, 10, 100 µg L^{-1}) to supra-environmental range (1, 10, 100 mg L^{-1}). Data points are presented as the mean ± standard error (n=3). Markers indicate where two-way T-tests revealed cell density of treated groups to be significantly lower (crosses) or higher (circles) than the untreated control at each timepoint (p≤0.05).

192-240 h) cultures grown in Pro99 media experienced significant declines in cell density in response to 10 and 100 mg L^{-1} $nTiO_2$ compared to the untreated control, where at the 192 h timepoint 10 μg L^{-1} was also observed to significantly reduce cell number (two-way T-test, $p \leq 0.05$).

Adverse effects in terms of cell decline were augmented when concentrations were increased to those in the supra-environmental range (*i.e.,* 100 mg L^{-1}, see Figs 3.6 A-B), likely due to increased rate of encounter between nanoparticles and cyanobacteria. Following 240 h, exposure to 100 mg L^{-1} $nTiO_2$ drove cell declines of 79% and 84% in NSW and Pro99 media when compared to the untreated control respectively (two-way T-test, $p \leq 0.05$). Cultures grown to higher cell densities in nutrient-rich media were observed to suffer greater adverse effects of exposure than those grown in NSW (see Fig 3.6B). This likely arises due to an increased rate of encounter between $nTiO_2$ and cyanobacteria in cell-dense cultures. Unexpectedly, no negative effect was observed at the concentration of 1 mg L^{-1} in NSW or Pro99 media, possibly representing an anomalous result. This being said, evidence of increased growth following incubations with metal oxide NMs has previously been recorded in phytoplankton exposed to $nCeO_2$ (<5 mg L^{-1}).[143, 199]

Despite evidence of early declines (<72 h) in cell number displayed by *Prochlorococcus* following exposure to research-grade $nTiO_2$ (*i.e.,* ≥10 μg L^{-1} and up to 72 h), the ability of the cyanobacterial culture to overcome initial stress in NSW was revealed in extended incubations when exposed to both environmentally relevant and supra-environmental concentrations ≤10 mg L^{-1} (Fig 3.6A). The recovery of microbial populations following MO NM exposure has recently been reported.[99, 280, 298] For example, decline of *Picochlorum sp.* during early exposure in response to $nTiO_2$ and nZnO (10 mg L^{-1}) was reversed in later stages, believed due to aggregation and sedimentation of particles, thus reducing direct exposure of phytoplankton to stable non-sedimenting particles.[99] Herein, growth of *Prochlorococcus* was positive in the majority of treatments investigated, despite being significantly lower than the untreated control at specific concentrations, particularly in early stages. This suggests that although MO NMs such as $nTiO_2$ may remove a fraction of the microbial population through processes of aggregation and sedimentation, the remaining

planktonic population continues to grow and is able to recover to ambient cell densities in extended exposure.

3.1.3.4 Physical toxicity and entrapment of cyanobacteria by $nTiO_2$

Previous research has highlighted that aggregation between MO NMs and phytoplankton is widespread during laboratory exposure.[98, 145, 146, 269, 270] The physical interaction between NMs and cells, and their entrapment by aggregates is often considered the primary driver of adverse effects experienced by marine microbial organisms.[98, 145, 269, 276] Adherence of MO NMs to the cell surface is believed to enhance oxidative stress by increasing ROS production[209, 274] and may cause physical damage to the cell wall or membrane.[98] Aggregation is also proposed to reduce light

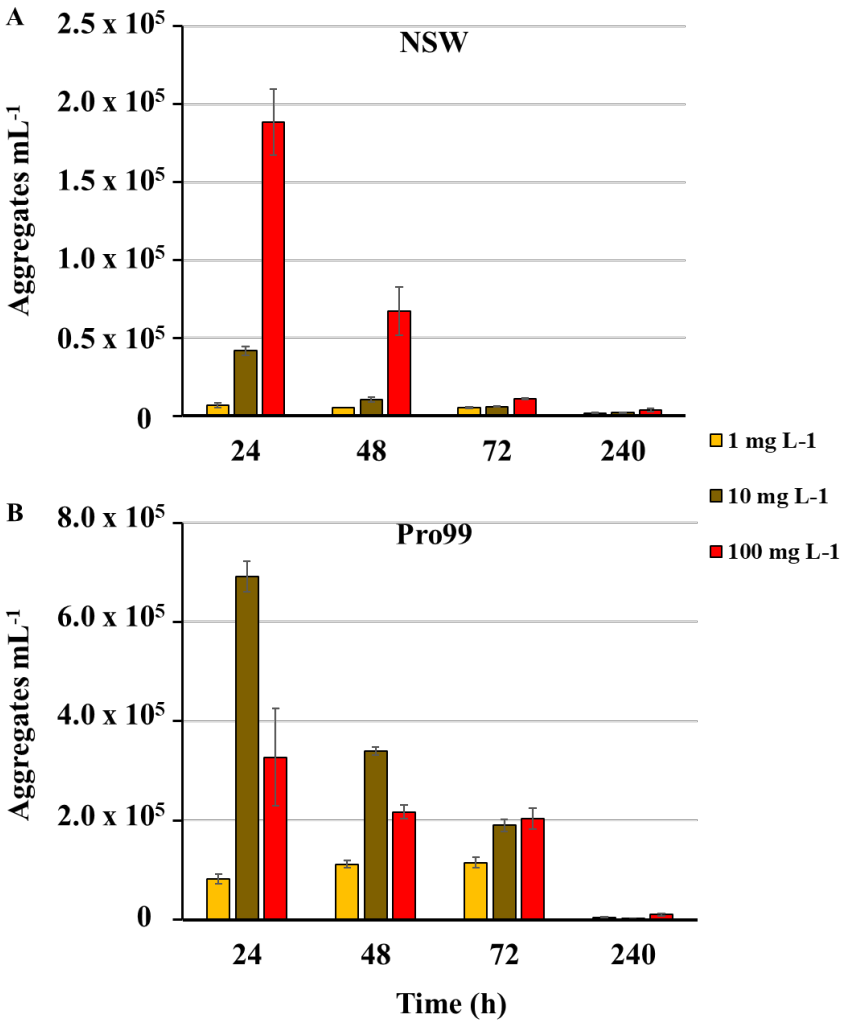

Figure 3.7. Estimated number of NP-cell Aggregates mL^{-1} comprised of $nTiO_2$ and *Prochlorococcus* MED4 observed during flow cytometric analysis of *Prochlorococcus sp.* MED4 exposed to $nTiO_2$ (Sigma Aldrich) in A) NSW, and B) Pro99 media for a period of 240 h (n=3).

availability in water, although such shading effects have not been conclusively proven.[50, 147, 299] Through the subsequent process of sedimentation, hetero-aggregation of NMs and cells effectively removes phytoplankton from the water column, and this is believed to be the primary cause of cell decline in the work presented herein. During flow cytometric analysis of cyanobacterial cultures, it was possible to estimate the number of NP-cell aggregates present within samples in mg L^{-1} treatments (Fig 3.7).

The estimated number of NP-cell aggregates was recorded to decline rapidly within the early stages of incubation, indicating their rapid settling and hence removal of cyanobacteria from the water column. As displayed in Figure 3.5, a considerable proportion of $nTiO_2$ had already undergone sedimentation during the initial 24 h following addition to saline media. Further investigation would be required to confirm the extent of loss of suspended $nTiO_2$ and cyanobacterial during the initial stages of exposure (0-24 h). In NSW (Fig 3.7A) the number of aggregates in the 100 mg L^{-1} treatment declined by 64% between 24 and 48 h. The rapid precipitation and hence decrease in estimated NP-cell aggregate number was also observed in Pro99 supplemented cultures (Fig 3.7B), and as expected the total aggregate count far exceeded those recorded in NSW, likely due to increased rate of encounter between $nTiO_2$ and cyanobacteria at higher cell densities. In previous work, this trend has also been observed, with highest rates of aggregation associated with highest cell density and maximised detrimental effect to cells.[50] Such increased rates of aggregation and interaction between $nTiO_2$ and cyanobacteria may have driven the enhanced decline in cell number observed in cell-dense cultures observed in this study. However, findings vary, and it has also previously been recorded that aggregation and subsequent sedimentation of MO NMs can reduce the negative effects associated with exposure.[147] This process may explain the patterns of *Prochlorococcus* recovery observed when exposures were extended in NSW, where following aggregation and subsequent sedimentation of the majority of $nTiO_2$, free-living cyanobacterial populations are able to recover.

The hetero-aggregation and subsequent entrapment of *Prochlorococcus* by $nTiO_2$ was confirmed using fluorescent microscopy (Fig 3.8). Here, aggregates of $nTiO_2$ and cells readily formed in both NSW and nutrient-rich media, observed by microscopy at concentrations of 10 and 100 mg L^{-1}. Control images obtained from NSW and

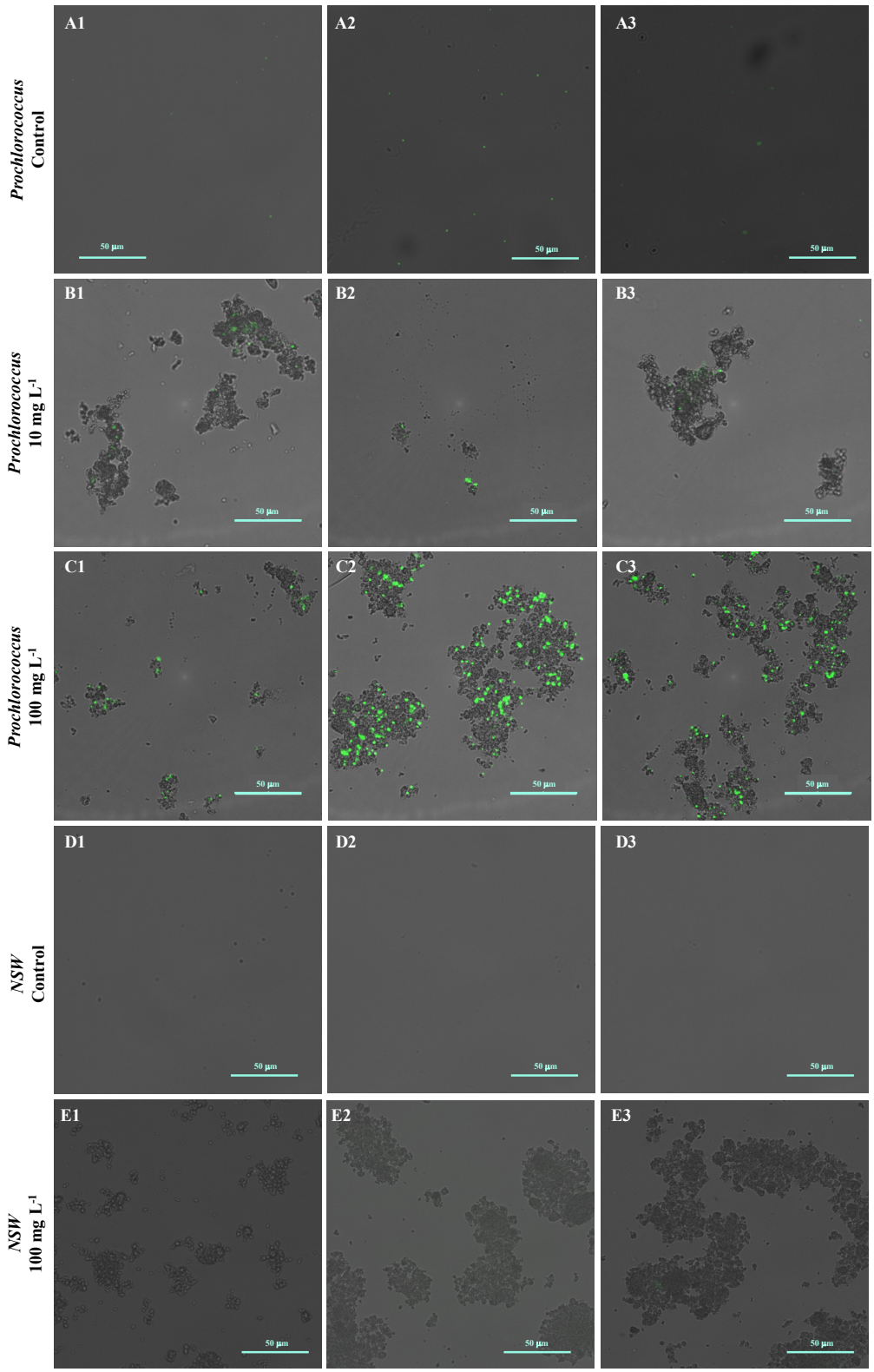

Figure 3.8. Hetero-aggregation of *Prochlorococcus sp.* MED4 (stained with SYBR Gold (green)) and research-grade $nTiO_2$ (Sigma Aldrich; non-stained particles) as observed by fluorescent microscopy; A1-3: Untreated *Prochlorococcus* culture; B1-3 *Prochlorococcus* culture exposed to 10 mg L^{-1} $nTiO_2$; C1-3 *Prochlorococcus* culture exposed to 100 mg L^{-1} $nTiO_2$; D1-3 Natural seawater control (no $nTiO_2$); E1-3 Natural seawater $nTiO_2$ suspension (100 mg L^{-1}). Images represent those merged from GFP and Brightfield channels.

Prochlorococcus samples in the absence of nanoparticles, supported the belief that precipitated material observed was indeed $nTiO_2$, rather than other particulate matter. The entrapment of phytoplankton by $nTiO_2$ previously has been observed using microscopic techniques in work carried out with *P. tricornutum* in response to concentrations similar to those used in our study (50 mg L^{-1}).[145] Hetero-aggregates were recorded to reach sizes in the micron-range when measured along their longest axis (2.4-133.5 µm, ImageJ analysis), and displayed an average size of 28.0 µm (n=100). Such aggregations of research-grade $nTiO_2$ (25 nm) have been previously recorded to form within 30 mins of addition into saline f/2 media within this concentration range.[146]

In response to NM exposure, marine phytoplankton have been observed to enhance the production of exopolymeric substances (EPS).[154, 155, 300-302] The secretion of EPS is associated with microbial stress and believed a defence mechanism against NMs.[300] For example, EPS was shown to protect the freshwater cyanobacterium *Synechocystis* PCC6803 from $nTiO_2$-mediated stress by quenching toxic ROS species and reducing direct contact of nanoparticles with the cell surface.[155] Whilst cyanobacteria are able to produce EPS, *Prochlorococcus* lacks most EPS related proteins, believed lost through the evolutionary streamlining of the *Prochlorococcus* genome due to energy costs of EPS production likely outweighing any benefits.[303] As such, any enhancement to EPS production displayed by *Prochlorococcus* during exposures is likely to be limited, and is not believed to be an influential factor in the hetero-aggregation process proposed.

However, as the presence of EPS is believed likely to enhance aggregation of $nTiO_2$ and hence reduce its bioavailability over time,[302] any increase in EPS production may act to promote the processes of entrapment and co-precipitation described. Indeed, while EPS was recorded to mitigate toxicity in *Synechocystis,* hetero-aggregation between the EPS-producing cyanobacteria and $nTiO_2$ was still observed.[155]

In the natural environment, processes of entrapment and sedimentation may reduce the availability of phytoplankton prey,[275] potentially causing an energy deficit in higher trophic levels. Additionally, through ingestion of entrapped phytoplankton, or indirect ingestion during feeding, trophic transport, and possible bioaccumulation of

metal oxide NMs such as $nTiO_2$ may occur. Evidence of trophic transfer of $nTiO_2$ from marine invertebrates to fish has been observed under laboratory conditions.[104] Once ingested, MO NMs may exert adverse effects upon higher organisms, such as disruption to immune processes and antioxidant activities, as has been recorded in marine invertebrates following exposure to $nCeO_2$.[120, 121] Given that $nTiO_2$ has been recorded to interact with other contaminants within the water column including tributyltin, phenanthrene, polycyclic aromatic hydrocarbons; enhancing their uptake and toxicity to biota,[105, 304] it is important to also consider the potential of metal oxide NM aggregates to adsorb such pollutants which may also be passed to higher trophic levels of the marine food web.

3.1.3.5 Behaviour of $nTiO_2$ in seawater

The fate and behaviour of NMs upon entry into the environment largely determines their bioavailability and mechanism of toxicity towards biota, and is therefore a key consideration during nano-ecotoxicological research.[98, 99, 302] Upon entry into saline media with high ionic strength (0.7×10^{-1} eq L^{-1}),[14] MO NMs have generally been observed to aggregate freely and undergo sedimentation, at a faster rate than bulk material.[14, 276] Herein, dynamic light scattering (DLS) methods were utilised to confirm that research-grade $nTiO_2$ (1 and 100 mg L^{-1}) displays rapid aggregation upon entry into saline media. Hence, supporting our belief that the processes of $nTiO_2$ aggregation and subsequent co-precipitation with cells is the key driver of cyanobacterial decline recorded in toxicity experiments described above (sections 3.1.3.2 and 3.1.2.3).

DLS revealed that $nTiO_2$ reached sizes far exceeding those of primary particles analysed by TEM (19.9±6.6 nm), displaying an average size of 1547-6560 nm throughout the 14-d experiment (Table 3.3). These sizes are expected to be somewhat larger than those recorded by TEM (19.9±6.6 nm), since dynamic light scattering measures the hydrodynamic size of colloidal nanoparticles, taking into account van der Waals and interparticle interactions. However, the sizes observed for particles in NSW are far larger than would be expected due to their colloidal behaviour, indicating their rapid aggregation. It should be noted that supra-environmental concentrations have been investigated here due to the poor sensitivity of the equipment to the lower,

environmentally relevant concentrations. Nanoparticles were recorded to aggregate immediately upon entry into NSW and DLS measurements displayed that variation in z-average size between replicates was large, suggesting a high variability in aggregate size and low uniformity of this process. This is reflected in the polydispersity index (PDI) values, which remained in the range of 0.58-1.00 throughout the 14-d experiment observed, indicating the presence of a largely polydisperse system. It must be noted, though, that due to biases towards larger particles through use of DLS analysis, smaller particles are likely under-represented.[305] Precipitation of $nTiO_2$ from the water column as a result of increased aggregation was recorded, and deposits of $nTiO_2$ were visible at the bottom of flasks after 24 h incubation with media and throughout the remaining timepoints of the experiment (Fig 3.9).

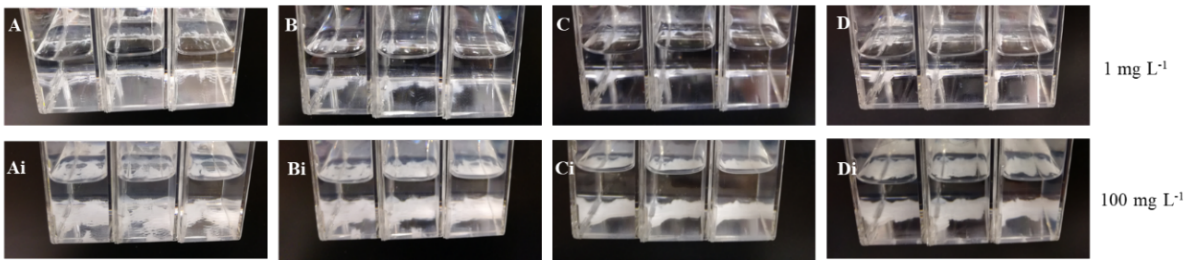

Figure 3.9. Photographic observation of sedimentation of $nTiO_2$ samples during DLS analysis; A/Ai – 24 h, B/Bi – 168 h, C/Ci – 240 h, D/Di – 336 h.

The mean z-average size (d.nm) of $nTiO_2$ at T_0 was 1580±124 and 1624±113 nm for 1 and 100 mg L^{-1} samples respectively, indicating the rapid aggregation of $nTiO_2$ upon entry into NSW. The PDI at the start of the experiment also indicated a high level of aggregation between $nTiO_2$ particles, 0.804 and 0.580 for 1 and 100 mg L^{-1} samples, respectively. Over the first hour, aggregation of $nTiO_2$ was most rapid, reaching respective peaks in z-average size of 5626 and 6560 nm in the 1 and 100 mg L^{-1} treatments, whilst PDI reached a value of 1.000. Following this, z-average size in the 1 mg L^{-1} group appeared to show a slight decrease for subsequent timepoints, although standard deviations remained high, likely indicating that particles are aggregating and sinking, with larger particles no longer within the measurement window of the DLS. PDI values remained high during this period, with a value of 1.000 observed at 24, 48 and 72 h. After 72 h, samples at the 1 mg L^{-1} concentration were undetectable and therefore unsuitable for data acquisition by DLS. The removal of $nTiO_2$ from the water column *via* precipitation, observable in flasks after 24 h (Fig 3.9), and hence reduction

in suspended $nTiO_2$ particles is believed to cause the lack of data acquisition at these timepoints following 72 h during DLS measurement at the 1 mg L^{-1} concentration.

Mean z-average size of $nTiO_2$ added to NSW at the 100 mg L^{-1} concentration varied throughout the 14-d experiment but displayed clear evidence of extensive aggregation of $nTiO_2$, also indicated by the high PDI values recorded. Overall, z-average size varied 1547-6560 nm during the experiment. Hence, the aggregation of $nTiO_2$ within NSW appears a rapid, non-uniform and highly variable process. As with lower concentration samples, a large extent of deposition of $nTiO_2$ aggregates were visible after 24 h and continued throughout the 14-d experiment (see Fig 3.9). In later stages (>72 h), mean z-average size appeared to show a slight decrease. As before, such data suggests that the size of aggregates remaining in suspension during later stages of the experiment were smaller in size as larger aggregates had likely undergone precipitation and were deposited at the bottom of flasks. Despite the clear evidence of extensive aggregation and sedimentation behaviour of nanoparticles recorded, it should be noted that these observations were made at concentrations considerably higher than those predicted in the environment (due to the low sensitivity of equipment to μg L^{-1} concentrations). As such, at lower environmental concentrations the rate of homo-aggregation is likely to be reduced, due to effects of dilution and a decreased rate of encounter between individual particles.

Table 3.3. Summary of results obtained from DLS analysis of research-grade $nTiO_2$ (Sigma Aldrich, 19.9±6.6 nm (TEM)) suspensions in NSW.

	1 mg L^{-1}		**100 mg L^{-1}**	
Time (h)	**Z-average size (d.nm)**	**Polydispersity index (PDI)**	**Z-average size (d.nm)**	**Polydispersity index (PDI)**
0	1580±124	0.804±0.170	1624±113	0.580±0.156
1	5626±586	1.000	6560±464	1.000
2	2262±129	0.890±0.191	4994±198	1.000
4	1393±284	0.907±0.081	1569±129	0.737±0.108
24	2367±665	1.000	5636±670	0.980±0.035
48	2253±519	1.000	4133±956	0.957±0.055
72	2741±670	1.000	1966±936	0.978±0.025
168	Undetectable		1994±141	1.000
240	Undetectable		1564±168	0.953±0.060
336	Undetectable		3133±215	1.000

Additional information regarding $nTiO_2$ sedimentation was obtained during flow cytometric analysis by recording the event number during sampling of $nTiO_2$ suspensions made-up in NSW in the absence of cyanobacteria. By sampling these standards as with cultures, it was possible to infer the abundance of $nTiO_2$ aggregates in suspension by recording the total event number (Fig 3.10). Here, it is assumed that events represent suspended $nTiO_2$ aggregates, as all analysed samples were obtained from the midpoint of flasks. Here, particularly in the mg L^{-1} range, $nTiO_2$ was observed to undergo rapid sedimentation following entry into seawater, correlating with previous research[14, 146, 147, 276] and the results acquired by DLS. Up to 58% loss of $nTiO_2$ *via* precipitation within 6 h has previously been observed using UV-Vis spectrophotometry.[146] Herein, $nTiO_2$ counts were recorded to decrease 57%, 81% and 89% in 1, 10 and 100 mg L^{-1} samples respectively during the initial 24 h of entry into NSW. Following 48-72 h, the number of $nTiO_2$ aggregates observed in suspension during our work was comparable between all concentrations.

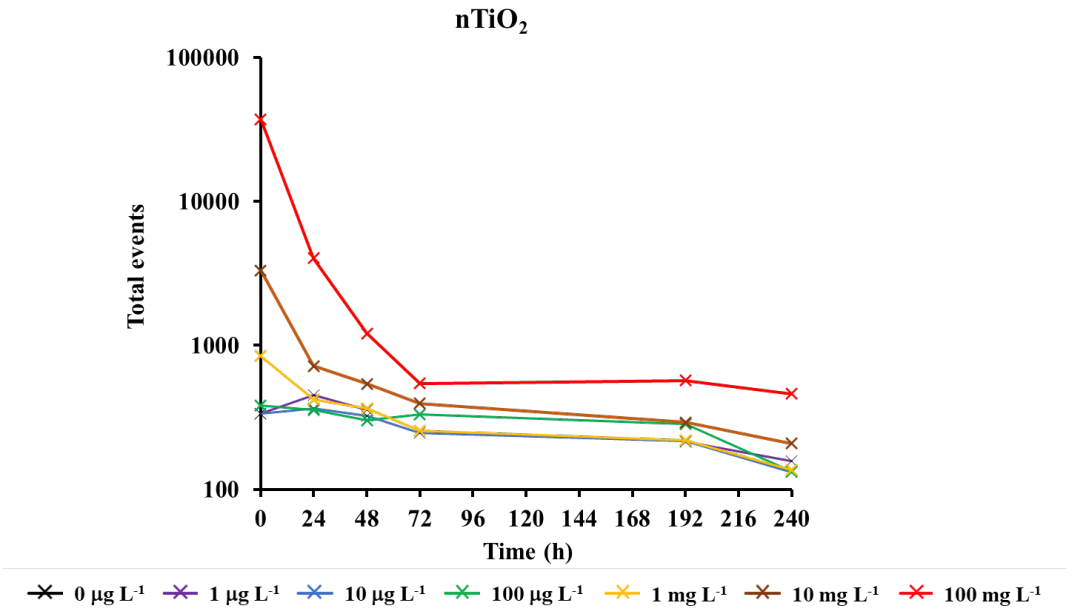

Figure 3.10. Total number of events (Total events) measured during flow cytometric analysis of cell-free $nTiO_2$ suspensions in natural seawater. Here, samples were analysed until 100 high Intensity fluorescent Nile Red particles (2.2 µm, Spherotech FH-2056-2) added at a concentration of 10^4 particles mL^{-1} were detected.

It is clear from DLS and flow cytometry experiments that rapid aggregation and sedimentation of $nTiO_2$ occurs in marine water. As a result, the bioavailability of $nTiO_2$ towards planktonic organisms displays a continual decrease, as has been

recorded previously.[302] As such, the risk of $nTiO_2$ towards marine microbial species appears lowered during extended exposure. However, at high concentrations, negative effects of exposure may be experienced for longer periods as populations take time to recover. In the natural environment the process of reduced bioavailability will likely be concentration-specific, with a lowered rate of encounter between individual $nTiO_2$ particles at lower concentrations and hence likely lowered homo-aggregation. Extent of sedimentation observed will also be influenced by other environmental variables not investigated in detail here, including pH, and the presence of natural organic and particulate matter.[70] However, despite the high levels of sedimentation recorded in this study, previous environmental assessment by Gondikas *et al.* (2018) has revealed $nTiO_2$ derived from seasonal use of sunscreen remain in suspension for a period of weeks before settling, where particles may interact with planktonic organisms.[266]

3.1.3.6 Identifying molecular features of $nTiO_2$ toxicity: Shotgun proteomic analysis

Alongside observations of cell decline, and direct physical entrapment of cyanobacteria, we performed a shotgun proteomic analysis of *Prochlorococcus* to inform on any other potential toxic effects on this phototroph other than physical entrapment in NM aggregates. Here, exposure to research-grade $nTiO_2$ did not produce metabolic alterations in *Prochlorococcus*, such as oxidative and nutrient stress or reduction in photosynthetic machinery as previously seen in Chapter 2 when exposed to AgNPs.

A number of toxic modes of action have been proposed for MO NMs against microbial species, although largely these have been performed at much higher concentrations. Oxidative stress due to the photocatalytic generation of reactive oxygen species (ROS) by $nTiO_2$ is believed a key driver of stress.[92, 146, 268, 306] Presence of UV light is therefore a key consideration in experimental design,[140] hence in our study full spectrum bulbs with environmentally-relevant levels of UV were utilised. Environmental levels of UV have been previously recorded to induce phototoxic effects of $nTiO_2$ against phytoplankton with ROS concentration increasing with increased $nTiO_2$ concentration.[268] Therefore, it can be proposed that oxidative stress due to ROS production may be a feature of toxicity observed herein during incubations

with $nTiO_2$. Photosynthetic processes have also been observed to be disrupted in response to $nTiO_2$, such as decreased oxygen generation[147] and damage to photosystems.[307] MO NMs such as nZnO have been recorded to cause toxicity due to the release of toxic Zn ions,[78, 132, 137] however the release of dissolved Ti^{4+} from $nTiO_2$ is believed to be negligible under experimental conditions.[269, 308, 309] Additionally, TiO_2 has been reported to absorb Zn and P from experimental media,[310] as well as to effectively reduce total N and P during microcosm experiments carried out in freshwater.[50]

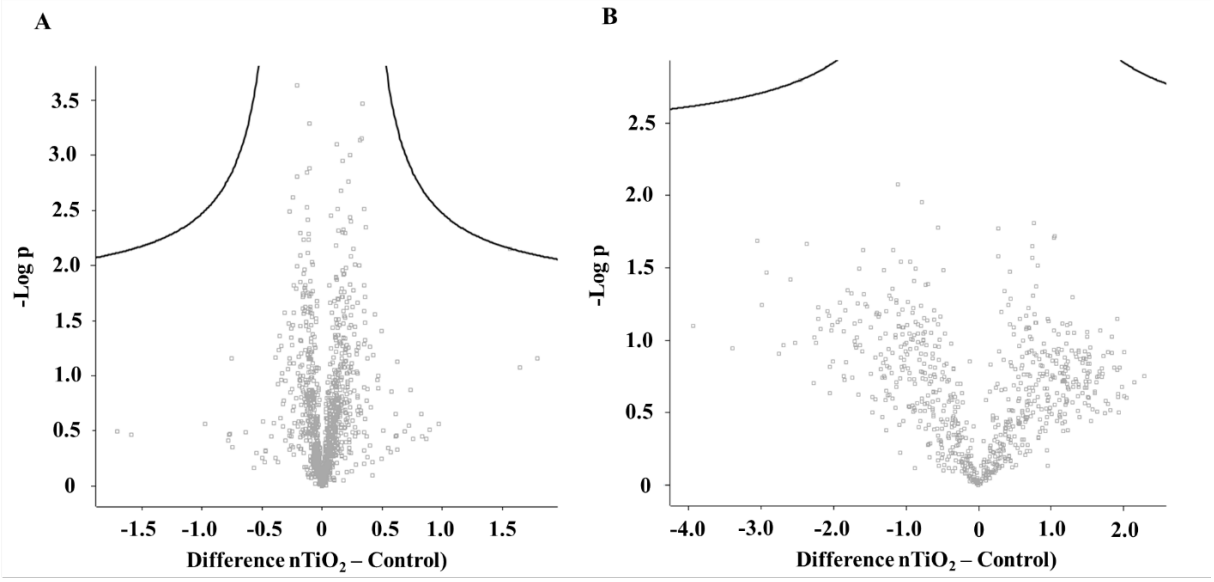

Figure 3.11. Volcano plots (T-test; FDR=0.05, S0=0.1) of cellular (A) and extracellular (B) proteomes obtained from *Prochlorococcus sp.* MED4 cultures exposed to $nTiO_2$ (100 μg L^{-1}).

Cultures were exposed to an environmentally relevant concentration (100 μg L^{-1}) of research-grade $nTiO_2$ previously recorded to induce a decline in average cell density in both cell dense and ambient cell densities, for a period of 24 h (7-8% decline (24 h), see Fig 3.6). Here, experiments were carried out using cell-dense cultures only grown in Pro99 media to ensure sufficient biological material was collected. Following analysis of both cellular and extracellular proteomes, little difference was observed between treated and control samples (Fig 3.11). Indeed, no individual proteins were significantly altered in abundance following the addition of $nTiO_2$. Protein function was classified using the Uniprot database and KEGG assignment. Here, little difference was also apparent upon classifying proteins based upon their biological function (Fig 3.12). The cellular proteome was largely comprised of proteins associated with basic cellular processes, making up ~33% of proteins

identified. Proteins involved with central metabolic processes were also relatively abundant in cellular proteome samples and made up ~20% of proteins identified in control and $nTiO_2$-treated cultures. For a full list of proteins identified during analysis see electronic supplementary data tables 9-10. Despite previous research suggesting disruption to photosynthesis and induction of oxidative stress pathways is likely associated with $nTiO_2$ exposure, evidence of such effects was not recorded. Herein, proteins associated with photosynthetic processes and oxidative stress represented approximately 6% and 3% of the cellular proteome, respectively. Similarly, any evidence of nutrient stress was not apparent. In the extracellular proteome, $nTiO_2$ exposure was associated with a slight decrease in membrane transport proteins (40% (Control) to 36% ($nTiO_2$)), and slight increase in proteins associated with basic cellular processes (20% (Control) to 22% ($nTiO_2$)) and metabolism (17% (Control) to 21% ($nTiO_2$)). The increase in cytoplasmic-associated proteins may be indicative of a slight increase in cell lysis in treated samples, which may result from hetero-aggregation and entrapment by $nTiO_2$. Based on the proteomic data reported here, it

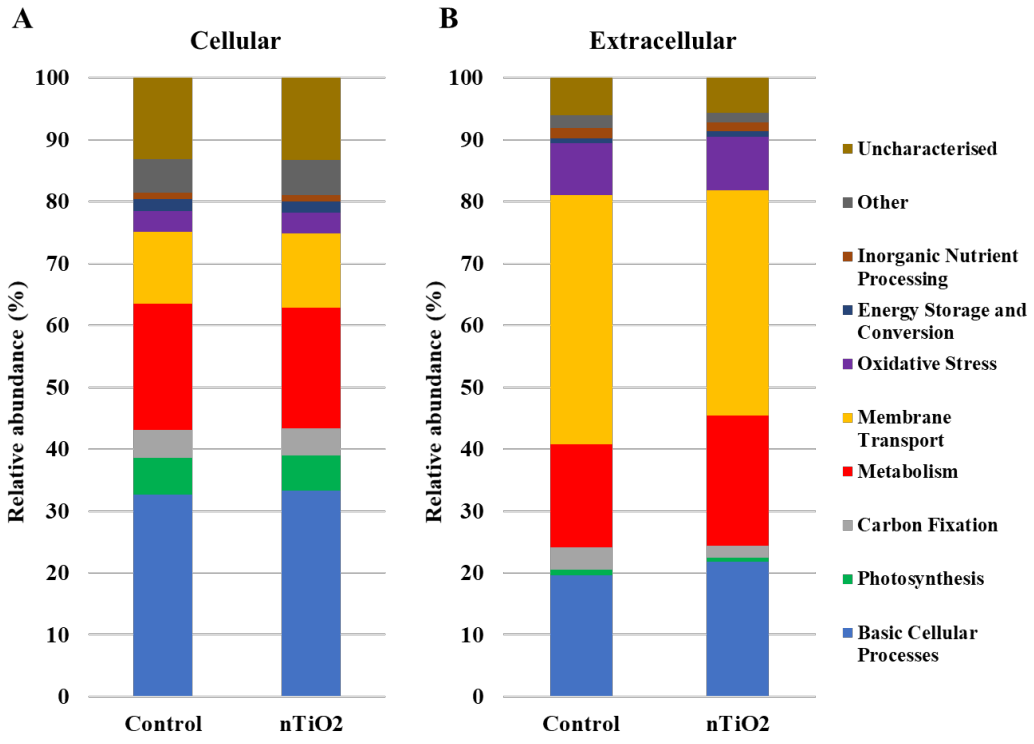

Figure 3.12. Relative abundance of protein groups, classified in terms of biological function as listed on the Uniprot database and KEGG assignment, identified by proteomic analysis of; A) cellular and B) extracellular samples of *Prochlorococcus sp.* MED4 exposed to research-grade $nTiO_2$ (100 µg L^{-1}) for a period of 24 h. Data is presented as the mean of three biological replicates.

can be suggested that molecular features of $nTiO_2$ toxicity may be negligible at the population scale when exposed to environmentally relevant concentrations. Rather, it appears planktonic cell decline is primarily driven by physical effects of exposure and removal in hetero-aggregates that sediment.

3.1.3.7 Effects of consumer $nTiO_2$ upon natural marine communities

Given the complex nature of the marine microbial community, it is important to consider the community-wide response towards environmental contaminants. A natural marine microbial community was exposed to $nTiO_2$ extracted from sunscreen (S2) and 'neat' $nTiO_2$-containing sunscreen (S2) immersed in seawater at an environmentally relevant concentration of 25 μg L^{-1},[267] to best replicate natural conditions. Amplicon sequencing of the 16S and 18S rRNA genes revealed negligible effects of $nTiO_2$ exposure upon community composition under environmental conditions. Rather, any observed alterations in community structure were primarily associated with the presence of 'neat' sunscreen, and likely attributed to the other components of the product formulation.

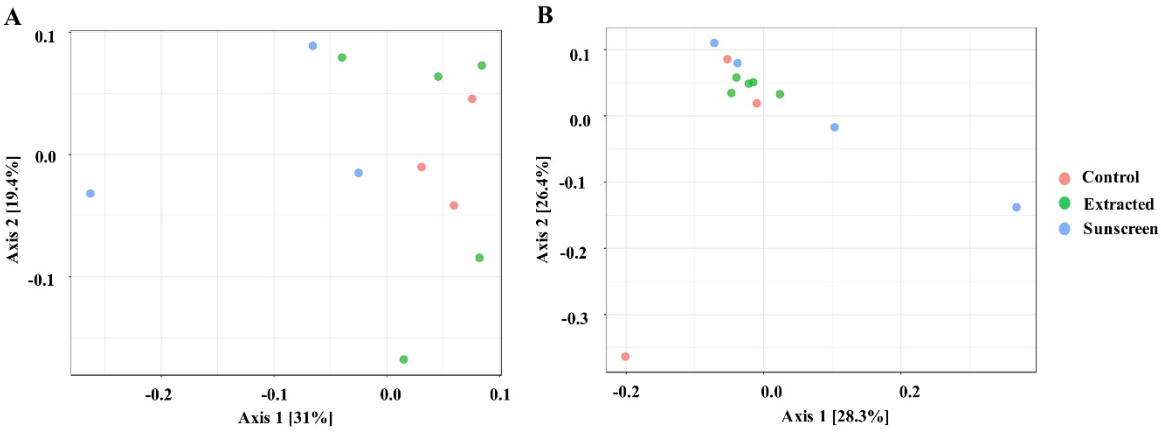

Figure 3.13. PCoA plot of 16S rRNA (A) and 18S rRNA (B) data based on Bray-Curtis dissimilarity. Coloured circles indicate samples belonging to each treatment; Red circles represent control samples, where no $nTiO_2$ was added; Green circles represent samples treated with $nTiO_2$ extracted from sunscreen (S2); Blue circles represent samples treated with 'neat' sunscreen. PERMANOVA analysis was performed on both datasets respectively; 16S rRNA: F-value = 1.4814, R-squared = 0.27025, p-value <0.06; 18S rRNA: F-value = 1.2109, R-squared = 0.21203, p-value <0.144. Panel A and B were adapted from output generated by MicrobiomeAnalyst software.

Amplicon sequencing data for bacterial and eukaryotic communities exposed to either treatment was compared to that obtained from of an untreated control where no $nTiO_2$ or sunscreen was added. Principle coordinates analysis based on Bray-Curtis dissimilarity, in conjunction with PERMANOVA analysis (Fig 3.13), revealed no significant differences in the 16S rRNA bacterial or 18S rRNA eukaryotic community composition at the ASV level between individual treatments. Similarly, measures of species richness and evenness for both 16S and 18S rRNA datasets, displayed no statistical variation between treatments (see Tables 3.4 and 3.5).

Table 3.4. Alpha diversity of prokaryotic communities

			Species Richness		Species Evenness	
Sample	**No. of replicates**	**No. of ASVs**	**Chao 1**	**ACE**	**Shannon**	**Simpson**
Control	3	751 ± 44	825.55 ± 54.32	864.11 ± 47.25	4.10 ± 0.15	0.89
Extracted $nTiO_2$ (S2)	5	758 ± 46	837.85 ± 51.89	878.12 ± 52.89	4.01 ± 0.30	0.88
Neat Sunscreen (S2)	3	586 ± 174	655.79 ± 172.37	677.21 ± 161.69	4.06 ± 0.10	0.91

To gain additional insight into the composition of bacterial and eukaryotic communities, the relative abundance of major bacterial and eukaryotic phyla present in control and treated samples (25 μg L^{-1}) was calculated (see Figs 3.14 and 3.16). Here, bacterial communities were dominated by the Bacteroidetes and Proteobacteria phyla, making up approximately 90% of the total community (Fig 3.14). In the 'neat' sunscreen treatment the proportion of Bacteroidetes to Proteobacteria appeared to differ from both the untreated control and $nTiO_2$ treatments. In control and extracted $nTiO_2$-exposed samples average relative abundance of Proteobacteria and Bacteroidetes was approximately 41±1 to 41±5%, and 52±6 to 53±2% respectively, compared to 48±8% and 44±11% in 'neat' sunscreen samples (Fig 3.15 A and B). However, due to large variation between individual samples belonging to the 'neat' sunscreen treatment this difference was not statistically significant. The increase in relative abundance of Proteobacteria in the sunscreen treatment was largely due to an increase in relative abundance of Gammaproteobacteria from 26±3% to 34±8%. Specifically, an increase in the Cellvibrionales order (19±1% to 25±7%) made up much of this change (Fig 3.15B).

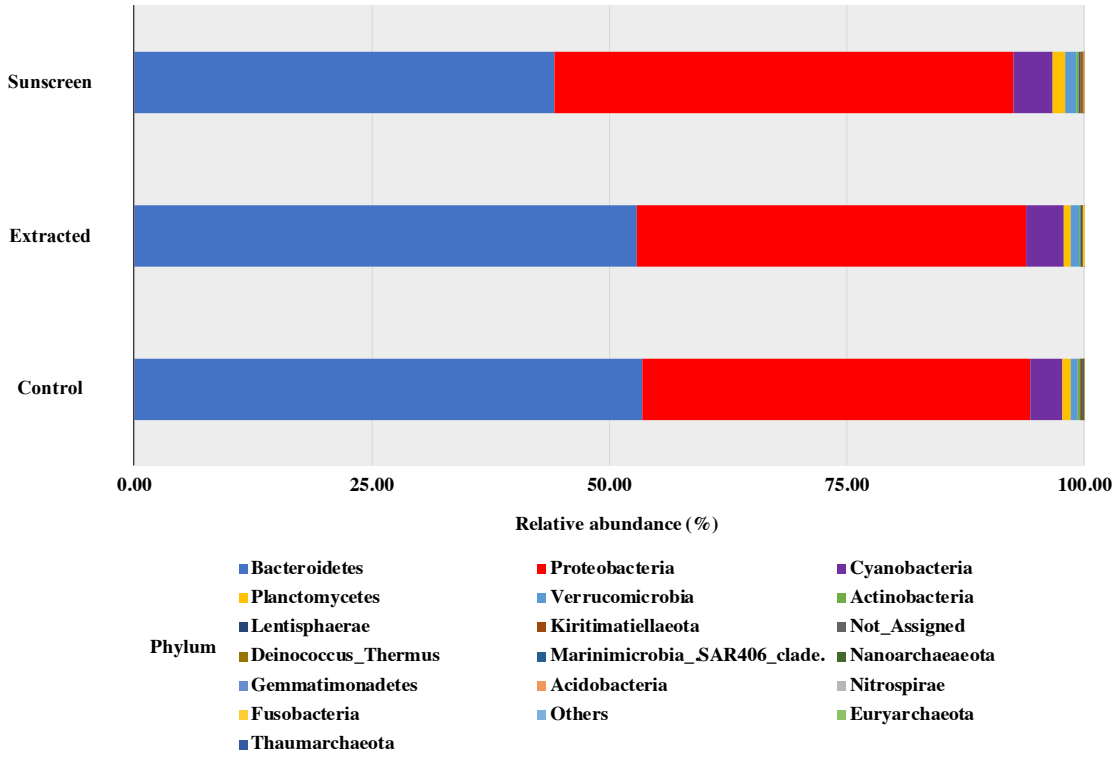

Figure 3.14. Relative abundance of major prokaryotic phyla identified by 16S rRNA amplicon sequencing of natural marine communities exposed to extracted $nTiO_2$ and neat sunscreen: Control (n=3); Extracted (n=5); Sunscreen (n=3).

The relative decrease in the Bacteroidetes phylum was largely attributed to a decline in average relative abundance of the Flavobacteria in response to neat sunscreen, reducing on average from 51±2% in the untreated control to 41±11% (Fig 3.15A). The reduction in the ratio of Bacteroidetes to Proteobacteria has previously been recorded in marine biofilm communities exposed to $nTiO_2$-treated surfaces.[180] Similarly, in riverine environments, Bacteroidetes members such as Flavobacteria have been recorded to display increased susceptibility to $nTiO_2$ during community exposure.[168] In this example, Actinobacteria also displayed a reduced relative abundance in the presence of $nTiO_2$, whereas comparatively Betaproteobacteria were observed to increase by approximately 40% under the same conditions in comparison to the untreated control.[168] These results were obtained at a test concentration of 100 mg L^{-1}, far exceeding that measured in the environment.[267] It is possible that should $nTiO_2$ concentrations have been increased in this experiment, any decline in abundance of Flavobacteria in response to $nTiO_2$-containing sunscreen would have been exacerbated and perhaps observed in the extracted $nTiO_2$ treatment. However, in our study it appears these alterations arise because of other components of the sunscreen

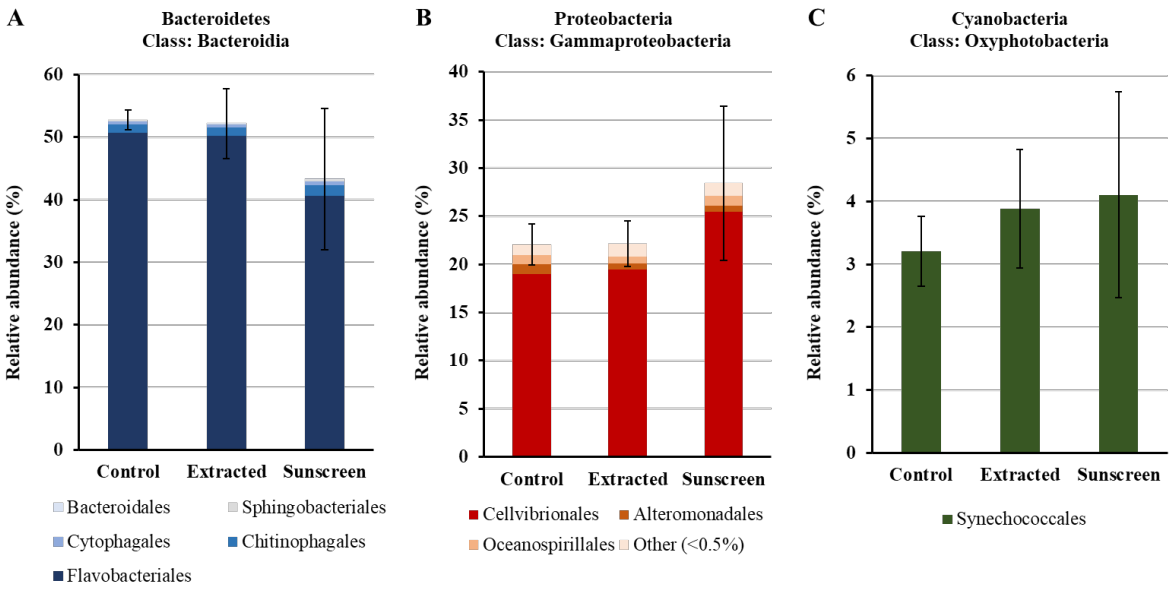

Figure 3.15. Average relative abundance (%) of the *Bacteroidia, Gammaproteobacteria* and *Oxyphotobacteria* classes in terms of individual taxonomic orders in each of the treatments respectively: Control (n=3); Extracted (n=5); Sunscreen (n=3).

formulation rather than the action of $nTiO_2$, as no such changes were observed in the extracted $nTiO_2$ treatment. Despite *Prochlorococcus* displaying declines in cell density in earlier testing (sections 3.1.3.2 and 3.1.3.3), no significant effect on relative abundance of cyanobacteria was recorded in either treatment during community exposure. In fact, on average a slight increase in cyanobacteria was observed in both extracted $nTiO_2$ and neat sunscreen treatments (Figure 3.15C). Overall, only two bacterial phyla were observed to alter significantly in relative abundance between control and extracted $nTiO_2$ or sunscreen-treated samples as a result of two-way T-tests. Both were observed in the extracted $nTiO_2$ (S2) treatment and belonged to low abundant phyla; here, Fusobacteria displayed a significant increase in relative abundance from 0.007% in the control to 0.035% in the extracted S2 $nTiO_2$ treatment ($p=0.043$); whilst Lentisphaerae, reduced in relative abundance from 0.0015% in the control to 0.0011% in S2 $nTiO_2$ samples ($p=0.024$).

Eukaryotic communities were principally made up of phototrophic organisms belonging to the Ochrophyta, Prymnesiophyceae, Chlorophyta and Protalveolata phyla, with Arthropoda also relatively abundant in control and 'neat' sunscreen treatments (Fig 3.16). Species belonging to the Ochrophyta phylum were most abundant in all treatments, representing 28±5-31±3% of ASVs identified. The

Ochrophyta largely comprises phototrophic organisms, and here diatoms made up the majority of taxa in this phylum and represented ~25% of eukaryotic species identified across all treatments. Once again, differences in relative abundance of eukaryotic phyla between control and treated samples were tested by means of two-way T-tests.

Table 3.5. Alpha diversity of eukaryotic communities

			Species Richness		Species Evenness	
Sample	**No. of replicates**	**No. of ASVs**	**Chao 1**	**ACE**	**Shannon**	**Simpson**
Control	3	990 ± 73	1052.71 ± 60.62	1062.45 ± 61.75	4.74 ± 0.93	0.93
Extracted $nTiO_2$ (S2)	5	926 ± 80	989.40 ± 74.72	1005.83 ± 67.96	5.21 ± 0.08	0.98
Neat Sunscreen (S2)	4	767 ± 180	823.66 ± 175.81	837.70 ± 169.45	4.92 ± 0.39	0.97

As can be seen in Figure 3.16, the relative abundance of the Arthropoda phylum was on average reduced in the extracted $nTiO_2$, and sunscreen treatments compared to the control. However, the relative abundance of this phylum varied greatly between individual samples, representing 15±24%, 3±2% and 11±10% in control, extracted

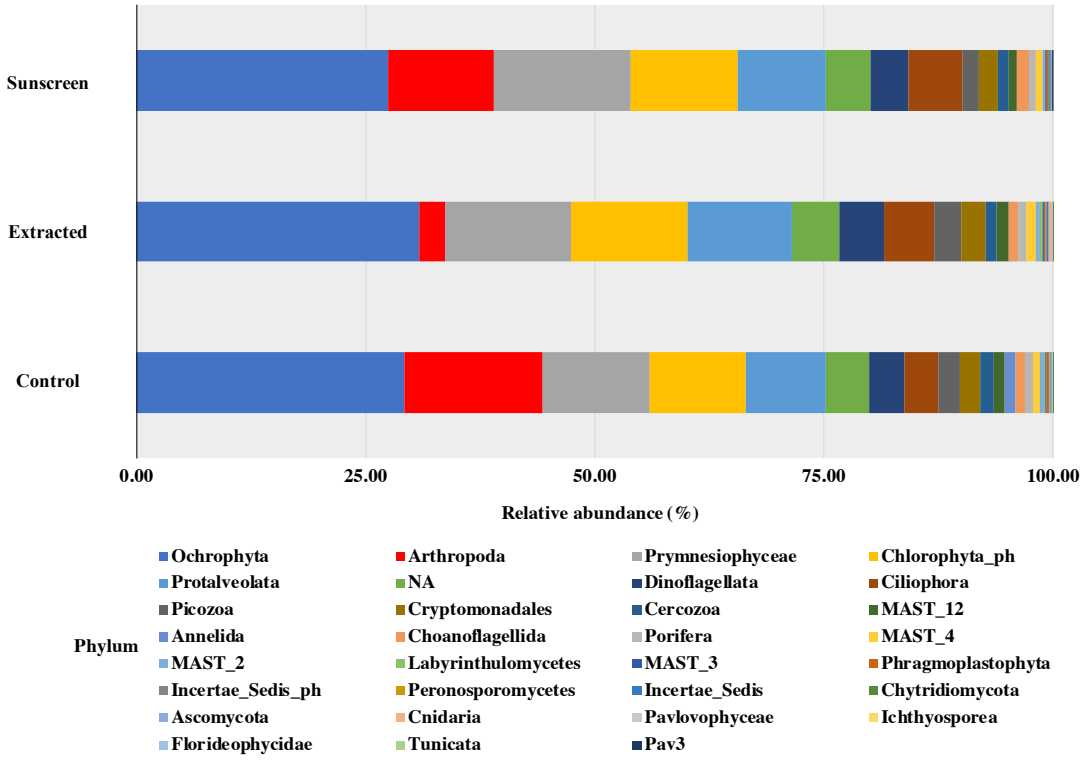

Figure 3.16. Relative abundance of major eukaryotic phyla identified by 18S rRNA amplicon sequencing of natural marine communities exposed to extracted $nTiO_2$ and neat sunscreen. Control (n=3); Extracted (n=5); Sunscreen (n=4).

$nTiO_2$ and 'neat' sunscreen treatments, respectively. As a result, statistical testing revealed no significant variation in the abundance of the Arthropoda phylum between treatments. Indeed, no significant differences were identified across all eukaryotic phyla, despite evidence being available upon the negative effect of $nTiO_2$ exposure towards phytoplankton in the literature, albeit largely recorded at greater concentrations (1-13 mg L^{-1}).[7, 95, 140, 143, 145, 268-273] Previous research has revealed that at such concentrations, varying eukaryotic taxa display differential sensitivity to $nTiO_2$ exposure.[140, 268] For example, Sendra *et al.* (2017) present that following exposure to $nTiO_2$, and $nTiO_2$-containing sunscreens the marine microalgae *Nannochloropsis gadiatana* displays highest sensitivity to all treatments compared to the diatom, *Chaetoceros gracilis*, the dinoflagellate, *Amphidinium carterae*, and coccolithophore, *Pleuroochrysis roscoffensis*.[140] Whilst such evidence exists, our results suggests that marine eukaryotic communities are little affected by exposure to environmentally-relevant concentrations of $nTiO_2$ extracted from, or in the presence of $nTiO_2$-containing sunscreen.

The findings presented suggest that current concentrations of $nTiO_2$ are unlikely to drive alterations to the structure and biodiversity of natural marine communities and is therefore unlikely to impact upon community functioning. Based on this, we can predict that the likely environmental risk of $nTiO_2$ derived from consumer products such as sunscreen towards marine microbial communities is low. However, it remains that should contamination of the marine environment by NMs continue to increase, evidence suggests that phototrophic organisms may be negatively affected within hotspots of pollution comprising higher concentrations, mainly due to hetero-aggregation and removal from the water column *via* sinking.

3.1.4 Conclusions

In this section, the interaction between marine microbial species and $nTiO_2$ has been shown to be a highly dynamic process influenced largely by the behaviour of nanoparticles in saline media. Toxic endpoints appear dependent upon the length of exposure, where risks associated with $nTiO_2$ exposure to marine microbial species appear low at currently predicted environmental concentrations. It has been shown for

the first time that the ecologically significant cyanobacterium, *Prochlorococcus,* suffers short-term (72 h) adverse effects following exposure to $nTiO_2$, mainly due to hetero-aggregation with agglomerated $nTiO_2$, and subsequent sinking out of the water column. Nevertheless, populations could recover when incubations were extended in natural oligotrophic seawater. No other sign of metabolic stress was observed by high throughput proteomics at a concentration relevant to those predicted in the environment, suggesting that physical interactions between nanoparticles and cyanobacteria are responsible for cell declines recorded. Monitoring of natural marine bacterial and eukaryotic communities exposed to $nTiO_2$ and $nTiO_2$-containing sunscreen, revealed no effect of either treatment at current environmental concentrations, suggesting that neither is likely to alter marine community structure or diversity in the natural environment.

The works presented here support the belief that the current environmental risk of $nTiO_2$ is low, however uncertainties exist in the environmental concentrations of NMs currently predicted,[195] and hotspots of contamination may serve to produce localised areas of cell decline given that severity of negative effects is enhanced with increasing $nTiO_2$ concentration. The interaction and synergistic effect of NMs and other contaminants also requires attention given the high affinity of materials such as $nTiO_2$ with other contaminants,[105, 311, 312] which may act to enhance toxicity at lower concentrations. It is important that we continue to develop analytical techniques to reveal NM concentrations within the natural environment and enhance experimental work by studying materials that represent those likely to be entered into aquatic systems. As such, the use of extracted materials as done in the above study provides great scope for future research in the field. However, there is a need to consider the whole product formulation in research on nano-enabled products, where specific components may play key roles in toxicity which are not identified when using uncoated nanoparticles. In particular, processes of NM release from product matrixes and their resultant state requires attention and is important to fully assess the environmental impact of engineered nanomaterials.

3.2 Investigating the impact of cerium oxide nanoparticles upon the ecologically significant marine cyanobacterium *Prochlorococcus*

3.2.1 Introduction

Cerium oxide nanoparticles ($nCeO_2$) represent an emerging contaminant with widespread use across a range of industries. Nano-sized cerium possesses unique properties compared to the bulk material and exhibit properties such as redox activity, scavenging of free radicals and inhibition of biofilm formation,[313] leading to their use across a variety of applications including; biomedical applications,[26, 27] drug delivery and therapeutics,[29] glass production and incorporation into electronic components.[28]

Annual production of $nCeO_2$ is estimated to reach up to 10,000 tonnes,[314] and their ever-increasing use is likely to result in greater release of engineered $nCeO_2$ into the environment.[70] The use of $nCeO_2$ as an additive for diesel fuels is a major ecological concern, and is believed to be the main source of $nCeO_2$ particles into the natural environment.[13] Overall, it is predicted up to 70 million metric tonnes of ceria could be released annually by road transport worldwide,[69] with the highest environmental levels of $nCeO_2$ predicted to be present in water draining from road surfaces,[13] where nanoparticles may then enter the aquatic environment. Additionally, aquatic transport responsible for 80% of global trade shipping[315] may represent an understudied source of $nCeO_2$ release. Boat engines have been recorded to utilise fuels containing nanosized additives including cerium oxide.[316-318] It is possible that $nCeO_2$ may enter the ocean in this manner if used in boat fuels to enhance efficiency,[317] and may represent a previously understudied source of $nCeO_2$ entry into the environment. Aside from transport, $nCeO_2$ may enter the natural environments *via* release into wastewater, use of wastewater treatment sludge as fertiliser, or as a consequence of industrial production of $nCeO_2$ or related products.[38, 319]

Research carried out to date suggests that the environmental risk of $nCeO_2$ is low,[13] however, limited evidence exists outlining the potential impact of $nCeO_2$ upon marine microorganisms. Upon entry into the environment, airborne and waterborne $nCeO_2$ may become widely dispersed.[28] In some cases, nanoparticulate matter emitted from diesel engines has been traced internationally, for example $nCeO_2$ released in the UK

has been identified in mainland Europe.[320] However, insufficient data exists to accurately predict the current levels of $nCeO_2$ in the natural environment,[13, 321] and great variation exists in such estimations. For example, Dale *et al*. (2017) predicts a global release of 70 million metric tonnes of Ce-based pollution into the environment by road transport, a value considerably higher than the estimated 15.6-114.9 kg $year^{-1}$ predicted in the UK by Johnson and Park (2012). To address this uncertainty, increased efforts must be placed into improving methods by which we are able to accurately monitor the release of engineered nanomaterials into the environment. Subsequently, experimental work can be carried out under environmentally relevant conditions, facilitating the effective assessment of the environmental risk of nanosized contaminants in natural systems.

The marine environment represents the sink for pollutants entered into aquatic systems. Here, microbial organisms which display high surface area-to-volume ratios are at significant risk from waterborne pollutants, particularly in coastal regions.[322] As mentioned in the previous section, MO NMs including; titanium dioxide, [95, 143, 269, 270] zinc oxide[78, 103] and copper oxide[279] have previously been reported to exert adverse effects upon marine phytoplankton (Table 3.1). However, limited evidence is available examining the impact of $nCeO_2$ upon marine microbial species. A significant reduction in growth of marine phytoplankton has been recorded in response to $nCeO_2$ exposure at concentrations in the range 10-40 mg L^{-1},[143, 323] although findings vary. At concentrations of up to 5 mg L^{-1} no adverse effects of $nCeO_2$ exposure upon the green algae *Chlorella autotrophica* and *Dunaliella salina* were observed.[199] Currently, the effect of $nCeO_2$ upon marine microbial species under environmental conditions remain uncertain and further research is required to reveal potential impacts.

In this section, the impact of $nCeO_2$ exposure upon *Prochlorococcus sp.* MED4 is examined using the toxicity testing protocols developed during analysis of $nTiO_2$, described in the previous section (*i.e.,* 72 h and 240 h exposure). Cultures were incubated with $nCeO_2$ at both environmentally relevant and supra-environmental concentrations under simulated natural conditions or in cell-dense cultures grown in nutrient-rich media. Alterations in cyanobacterial cell density were monitored by flow cytometry. As in work with $nTiO_2$, an assessment of $nCeO_2$ behaviour in saline media was carried out by dynamic light scattering (DLS) and microscopic methods, revealing

extensive aggregation behaviour. Such research present novel insight into the likely behaviour and impact of an emerging contaminant within the marine environment for which limited information exists, hence, facilitating the effective evaluation of their likely environmental risk and interaction with microbial species.

3.2.2 Materials and Methods

3.2.2.1 Materials

Nanomaterials utilised for research were purchased from Sigma Aldrich (cerium oxide, <25 nm (material no. 544841)). Natural oligotrophic seawater (NSW) used during experimental work was prepared as previously described (section 2.2.1). For each experiment $nCeO_2$ stocks were added directly to NSW prepared as described and sonicated for 15-30 min using a Branson 1210 Sonicator operating at 40 kHz to ensure suspensions were well-mixed and to minimise aggregation of nanoparticles. Sterile filter capped tissue culture flasks were used for all experimental work with cyanobacteria and glassware was acid-washed before use. Axenic *Prochlorococcus sp.* MED4 cultures were grown on-site using Pro99 media.[205]

3.2.2.2 Characterisation of $nCeO_2$

To determine primary particle size and examine the morphology of $nCeO_2$ utilised during study, transmission electron microscopy (TEM) was used as previously described (section 2.2.1). Following image acquisition, the average particle diameter was determined by measuring 100 nanoparticles using Image J v.3.2 software. Visual observation of particle morphology was also carried out at this time. UV-visible spectra were collected using an Agilent Cary 60 UV-vis spectrophotometer of a sample of 100 mg L^{-1} $nCeO_2$ in Milli-Q ultrapure water. Dynamic light scattering (DLS) was carried out using the procedure described previously (section 3.1.2.7), to evaluate the aggregation behaviour of $nCeO_2$ (1 and 100 mg L^{-1}) when entered into NSW for a period of 240 h.

3.2.2.3 Short-term (72 h) toxicity testing of *Prochlorococcus* towards $nCeO_2$

Prochlorococcus sp. MED4 was exposed to $nCeO_2$ (0, 1, 10 and 100 µg L^{-1}) for a period of 72 h under two test conditions: i) ambient cell density ($2.8x10^4$ cells mL^{-1}) grown in NSW and ii) cell-dense cultures grown in nutrient-rich Pro99 media ($8.9x10^5$ cells mL^{-1}). 72 h prior to experimentation, axenic culture was added to NSW or Pro99 media respectively and preadapted to experimental conditions, as previous (section 3.1.2.4). To establish exposures, triplicate 30 mL samples were added to 50 mL filter-capped tissue culture flasks under sterile conditions and spiked with a defined volume of $nCeO_2$ stock to make up test concentrations. Flasks were subsequently maintained under the experimental conditions described and the cyanobacterial population monitored at 0, 24, 48 and 72 h using a Becton Dickinson Fortessa Flow Cytometer, as previously described (section 2.2.8). To identify significant alterations in cell density recorded during toxicity tests with *Prochlorococcus sp.* MED4 two-way T-tests were carried out between untreated controls and cultures exposed to various $nCeO_2$ treatments at each timepoint.

3.2.2.4 Extended (240 h) exposure to $nCeO_2$

Following 72 h toxicity testing, incubations with $nCeO_2$ were repeated and extended to 240 h to examine longer-term impacts of exposure. Initial cell densities were $1.7x10^5$ and $6.6x10^5$ cells mL^{-1} in NSW and Pro99 media, respectively. The $nCeO_2$ test concentrations utilised were also expanded to include both environmentally relevant and supra-environmental values (0, 1, 10 and 100 µg L^{-1}; and 1, 10 and 100 mg L^{-1}), hence allowing for inference of likely impacts in hot spots of pollution or should release of $nCeO_2$ into the marine environment increase. Exposures were established as described above and the cyanobacterial population monitored by flow cytometry at 0, 24, 48, 72, 168 and 240 h, as previous. To identify significant alterations in cell density recorded during toxicity tests with *Prochlorococcus sp.* MED4 two-way T-tests were carried out between untreated controls and cultures exposed to various $nCeO_2$ treatments at each timepoint.

3.2.2.5 Imaging of $nCeO_2$-cyanobacterial aggregates by fluorescent microscopy

To investigate the occurrence of $nCeO_2$-cell hetero-aggregation during extended toxicity testing (section 3.2.2.4), the imaging protocol described in section 3.1.2.6 during earlier work with $nTiO_2$ was carried out on sub-samples of deposited material collected from the base of culture flasks.

3.2.3 Results and Discussion

3.2.3.1 Characterisation of $nCeO_2$ and aggregation behaviour upon entry into natural seawater.

Analysis of TEM images revealed the primary particle size of $nCeO_2$ to be 20.6±12.1 nm, close to that stated by the manufacturer (<25 nm). However, nanoparticles displayed a great variation in primary particle size. In terms of morphology, $nCeO_2$ were generally cuboid in shape, although a range of forms could be observed, including diamond- and triangular-shaped particles (Figs 3.17A and B). As is common in TEM analysis, $nCeO_2$ readily formed aggregates, as a result of drying onto TEM grids (Fig 3.17C). UV-vis spectroscopy demonstrated an absorption band between 250 and 400 cm^{-1} with a maximum absorbance at 317 nm (Fig 3.18), attributed to the electronic structure of ceria and defects, including oxygen vacancies, in accordance with the literature.[324, 325]

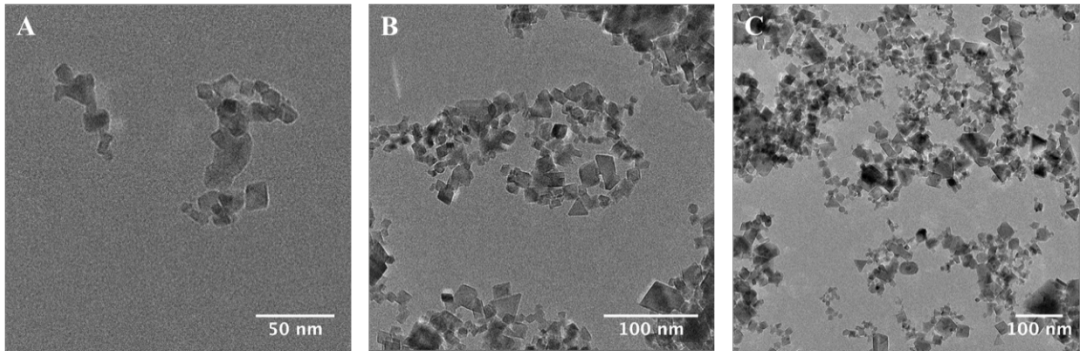

Figure 3.17. Transmission electron microscope imaging of $nCeO_2$ (Sigma Aldrich, <25 nm) used for experimental work.

As mentioned in works with $nTiO_2$, it is widely acknowledged that the fate and behaviour of NMs within the natural environment largely determines their bioavailability and hence likely effect upon biota.[98, 99, 302] To improve our understanding of $nCeO_2$ behaviour in the marine environment, the aggregation behaviour of nanoparticles in NSW was assessed using DLS over a period of 0-240 h (Table 3.6), as previously described.[58, 326, 327]

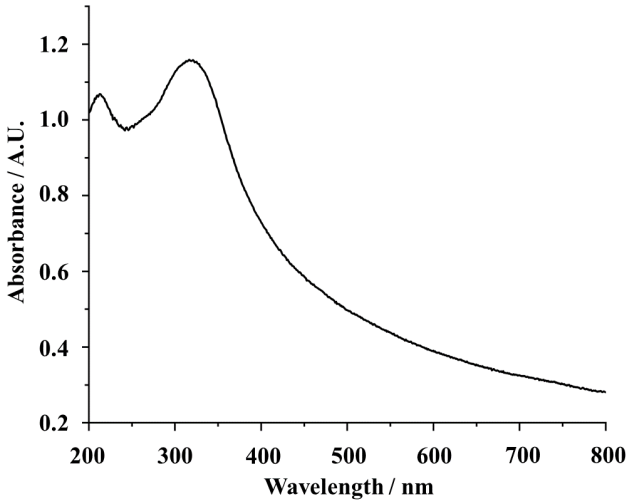

Figure 3.18. UV-vis spectra of $nCeO_2$ utilised in experimental work.

First, the z-average size of $nCeO_2$ (20.6±12.1 nm, TEM) was monitored in Milli-Q ultrapure water. As with work utilising $nTiO_2$ (section 3.1.3.5), concentrations of 1 and 100 mg L^{-1} were selected for DLS analysis, as limitations of DLS at lower concentrations meant that environmental concentrations (*i.e.* μg L^{-1}) could not be accurately measured.[328] Analysis of $nCeO_2$ suspensions made up in Milli-Q ultrapure water revealed respective z-average sizes of 136±20 nm and 125±11 nm for concentrations of 1 and 100 mg L^{-1}. Here, z-average size of $nCeO_2$ exceeded that measured using TEM, likely a result of Van der Waals forces and interparticle interactions which are common in uncoated MO NMs. Upon entry into NSW (0 h), z-average size was recorded as 1293±141 nm and 1196±140 nm for 1 mg L^{-1} and 100 mg L^{-1} samples respectively, considerably higher than the average size recorded in Milli-Q ultrapure water, indicating the immediate aggregation of $nCeO_2$. The aggregation of $nCeO_2$ within saline media with high ionic strength is expected and in accordance with previous research.[14, 67, 323, 329]

Table 3.6. Summary of data obtained during DLS analysis of $nCeO_2$ (20.6±12.1 nm) added to natural seawater for a period of 240 h at a concentration 1 and 100 mg L^{-1} (n=3).

	1 mg L^{-1}		100 mg L^{-1}	
Time (h)	**Z-average size (nm)**	**Polydispersity Index**	**Z-average size (nm)**	**Polydispersity Index**
0	1293 ± 141	0.525 ± 0.097	1196 ± 140	0.336 ± 0.177
1	2576 ± 1933	0.683 ± 0.368	3601 ± 1794	0.716 ± 0.492
2	2382 ± 1924	0.760 ± 0.208	3097 ± 2784	0.638 ± 0.362
4	1862 ± 489	0.772 ± 0.203	2875 ± 1757	0.655 ± 0.396
24	1767 ± 187	0.893 ± 0.113	3122 ± 2622	0.794 ± 0.281
48	2338 ± 1428	0.845 ± 0.138	3414 ± 2027	0.910 ± 0.156
72	1016 ± 298	0.607 ± 0.079	1549 ± 449	0.729 ± 0.096
168	1390 ± 971	0.812 ± 0.180	1724 ± 992	0.816 ± 0.242
240	1218 ± 914	0.799 ± 0.071	1638 ± 359	0.909 ± 0.041

During the next 2 h, $nCeO_2$ displayed an increase in z-average size at both concentrations, indicating a continuation of the aggregation process. Alongside increases in z-average size, the average polydispersity index (PDI) also increased, rising from 0.525 to 0.760 in 1 mg L^{-1} samples, and 0.336 to 0.638 in 100 mg L^{-1} during the initial 2 h, further indicating the presence of aggregation. For both concentrations, a slight decrease in z-average size was recorded at the 4 h timepoint, however in this case average PDI continued to increase, implying continued aggregation (slight reductions in size observed may be due to precipitation of the largest aggregates, leaving smaller particle species in suspension). The highest z-average sizes of $nCeO_2$ were reached after 48 h entry into NSW at both concentrations, reaching average values of 2338±1428 nm and 3414±2027 nm for 1 and 100 mg L^{-1}, respectively. Generally, following this the average particle size at both concentrations displayed a gradual decrease for the rest of the 240-h experiment, ultimately reaching sizes similar to those recorded at 0 h, although with large standard deviations

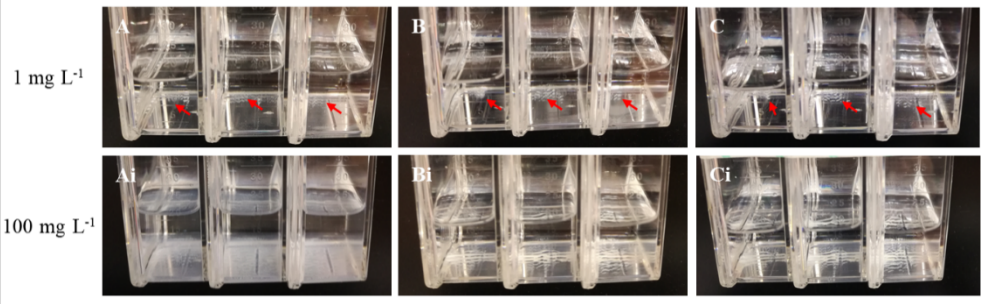

Figure 3.19. Photographic observation of $nCeO_2$ (1 and 100 mg L^{-1}) sedimentation during DLS analysis; A – 24 h, B – 168 h, C – 240 h. Red arrows indicate where deposited material is not immediately obvious in 1 mg L^{-1} samples.

indicating the presence of aggregates. This gradual decrease likely represents the reduction in abundance of larger particles which precipitated out of the water column at a faster rate. PDI values displayed a less generalised trend and remained considerably higher than those recorded at 0 h, indicating the consistent presence of multiple populations of particles, indicative of continuing aggregation. Throughout the experiment, the deposition of $nCeO_2$ at the bottom of flasks was observed, clearly evident from 24 h onwards, indicating the precipitation of aggregated particles (Fig 3.19).

In accordance with previous research, it is clear that $nCeO_2$ is likely to aggregate upon entry into saline media with high ionic strength such as seawater.[14, 67, 323, 329] The aggregation of particles causes a reduction in the surface-area-to-volume ratio of nanomaterials and is likely to influence the toxicity and reactivity of particles.[330] As previously mentioned in this thesis, in the natural environment a number of additional factors will also govern the fate and behaviour of engineered NMs, including; particle specific physicochemical properties[69] and local water chemistry with pH, natural organic matter (NOM) and particulate matter all playing influential roles.[70 73, 85, 331] For example, in the presence of NOM, Quik *et al.* (2010) observed up to 88% of $nCeO_2$ added to deionised water to remain stable in suspension. The presence of NOM in natural waters is likely to influence particle stability,[331] although this will also largely depend on specific surface characteristics of nanoparticles. Hence, in our work we utilised NSW to simulate natural waters that $nCeO_2$ may enter. Given $nCeO_2$ nanoparticles' propensity to aggregate and undergo sedimentation in saline media, they have the potential to interact with marine biota throughout the water column as they are transported towards deeper zones.

3.2.3.2 Short-term (72 h) exposure of $nCeO_2$ towards *Prochlorococcus*

Flow cytometry was used to monitor alterations in populations of the marine cyanobacterium *Prochlorococcus sp.* MED4 in response to $nCeO_2$ (20.6±12.1 nm) added at environmentally relevant concentrations (*i.e.,* $\mu g\ L^{-1}$). As mentioned in earlier work with AgNPs (section 2.3.4), it is known that dead cells of *Prochlorococcus* lose fluorescence rapidly,[236, 237] therefore flow cytometry can be used to monitor changes

in the viable cyanobacterial population during exposure to NMs. Exposures were carried out under natural conditions (oligotrophic NSW at ambient cell densities), as well as under optimal growth conditions in nutrient-rich Pro99 media allowing for the impact of varying experimental conditions on ecotoxicity.

Figure 3.20 displays the effects of $nCeO_2$ (0-100 µg L^{-1}) upon 72 h growth of *Prochlorococcus sp.* MED4. At ambient cell densities grown in NSW (Figure 3.20A) only exposure to the highest concentration (100 µg L^{-1}) had a significant negative effect upon growth of *Prochlorococcus,* visible at every timepoint (two-way T-tests, $p \leq 0.05$). After 24 h and 48 h incubation, cell density was decreased on average 46.6% and 55.5% respectively in this treatment compared to the untreated control (two-way T-tests, $p \leq 0.05$). By the end of the 72-h incubation, this significant decrease reached 68.8% (two-way T-test, $p \leq 0.05$). At the final 72 h timepoint the average cell density of the 10 µg L^{-1} treatment was also lower than that of the control, however, this result was not significant. In contrast, when grown in nutrient rich Pro99 media (Figure 3.20B), no negative effect upon *Prochlorococcus* following 72 h incubation with $nCeO_2$ was recorded at any concentration, indicating an impact of varying experimental condition. However, significantly reduced growth was observed at the 48 h timepoint in both the 10 and 100 µg L^{-1} treatments as cell density was lowered by approximately 17.8% and 25.2% respectively compared to the untreated control (two-way T-test, $p \leq 0.05$).

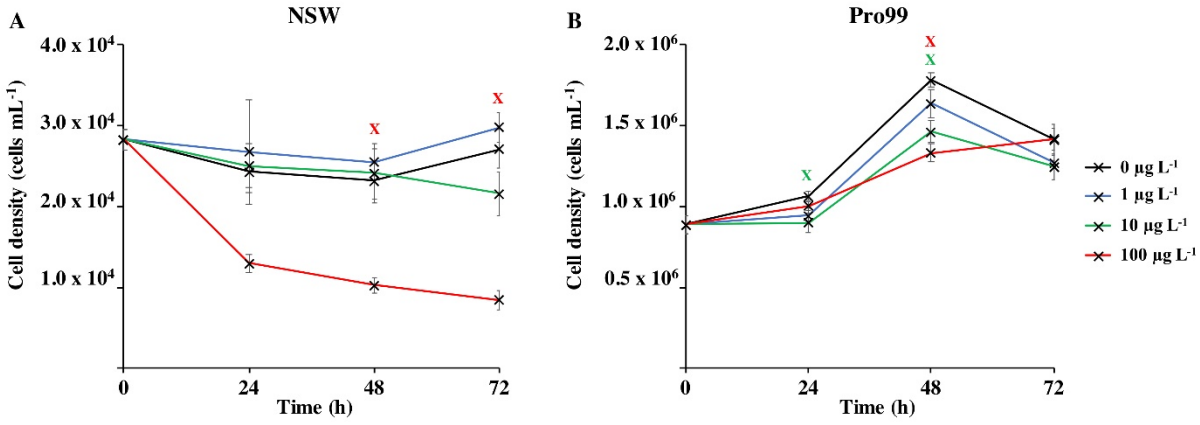

Figure 3.20. 72 h exposure of *Prochlorococcus sp.* MED4 to $nCeO_2$ (0-100 µg L^{-1}) in; A) – natural oligotrophic seawater, and B) nutrient-rich Pro99 media. Data points represent the mean of three culture replicates ± standard error (n=3). Crosses indicate where two-way T-tests revealed cell density to significantly vary from the untreated control ($p<0.05$).

3.2.3.3 Extended exposure of *Prochlorococcus* to $nCeO_2$

a) μg L^{-1} concentrations

During short-term (>72 h) exposure, presence of μg L^{-1} $nCeO_2$ was recorded to significantly reduce the cell density of marine cyanobacterium *Prochlorococcus*, when grown under environmentally relevant conditions in NSW, causing up to a 68.8% decrease in cell density. However, no such effect was observed in cultures grown to higher cell densities in nutrient rich Pro99 media (section 3.2.3.2), highlighting the influence of specific exposure conditions. Upon extending incubations to 240 h (Fig 3.21 A) the trends observed in early stages of exposure (<72 h) continued. The lowest tested concentration of 1 μg L^{-1} had no effect on *Prochlorococcus* grown in NSW (Fig 3.21 A1) throughout the 240-h experiment, whilst the 10 μg L^{-1} treatment caused a significant decline in cell density (17.7%) at the 48 h timepoint only (two-way T-test, $p \leq 0.05$), an effect not observed in earlier 72 h toxicity testing. Such a result highlights the variability in outcomes of toxicity testing that can occur between experimental runs. As recorded in 72 h toxicity testing (section 3.2.3.2), exposure to 100 μg L^{-1} $nCeO_2$ within NSW caused a significant decline in cell density at each timepoint during the initial 72 h of exposure, resulting in a decline in cell density of up to 45.7% compared to the untreated control (two-way T-test, $p \leq 0.05$). The extent of population decline in this treatment appears less severe as recorded in 72 h toxicity testing presented above (68.8%), likely due to the initial cell density of *Prochlorococcus* being relatively lower upon the establishment of the first experiment, indicating a possible impact of varying cell:nanoparticle ratios as recorded in previous research examining AgNP toxicity (section 2.3.4).[281] However, despite this early decline, the cyanobacterial population was observed to reach to cell densities comparable to that of the untreated control between 72-192 h in all the μg L^{-1} range treatments. Although, it must be noted that between 192 and 240 h, all cultures grown in NSW declined in cell density, likely due to nutrient depletion.

In contrast, *Prochlorococcus* grown in the nutrient-enriched Pro99 media did not suffer any adverse effect of exposure to $nCeO_2$ concentrations in the μg L^{-1} range during early stages of exposure (Fig 3.21 A2), similarly to data described in the previous section (3.2.3.2). In the long-term, however, the apparent enhanced resilience

of cell-dense cultures was reversed as cyanobacteria grown in Pro99 media experienced declines in response to both 10 and 100 µg L^{-1} $nCeO_2$. Unexpectedly, the 10 µg L^{-1} treatment had the greatest effect, significantly reducing the cell density by 27.3% compared to the untreated control (two-way T-test, $p \leq 0.05$). The lowest concentration of 1 µg L^{-1} exerted no negative impact on *Prochlorococcus* throughout the 240-h exposure in Pro99 media but resulted in an increase in cell density (38.8%) than the control after 240 h. However, this increase was not statistically significant (two-way T-test, p=0.07).

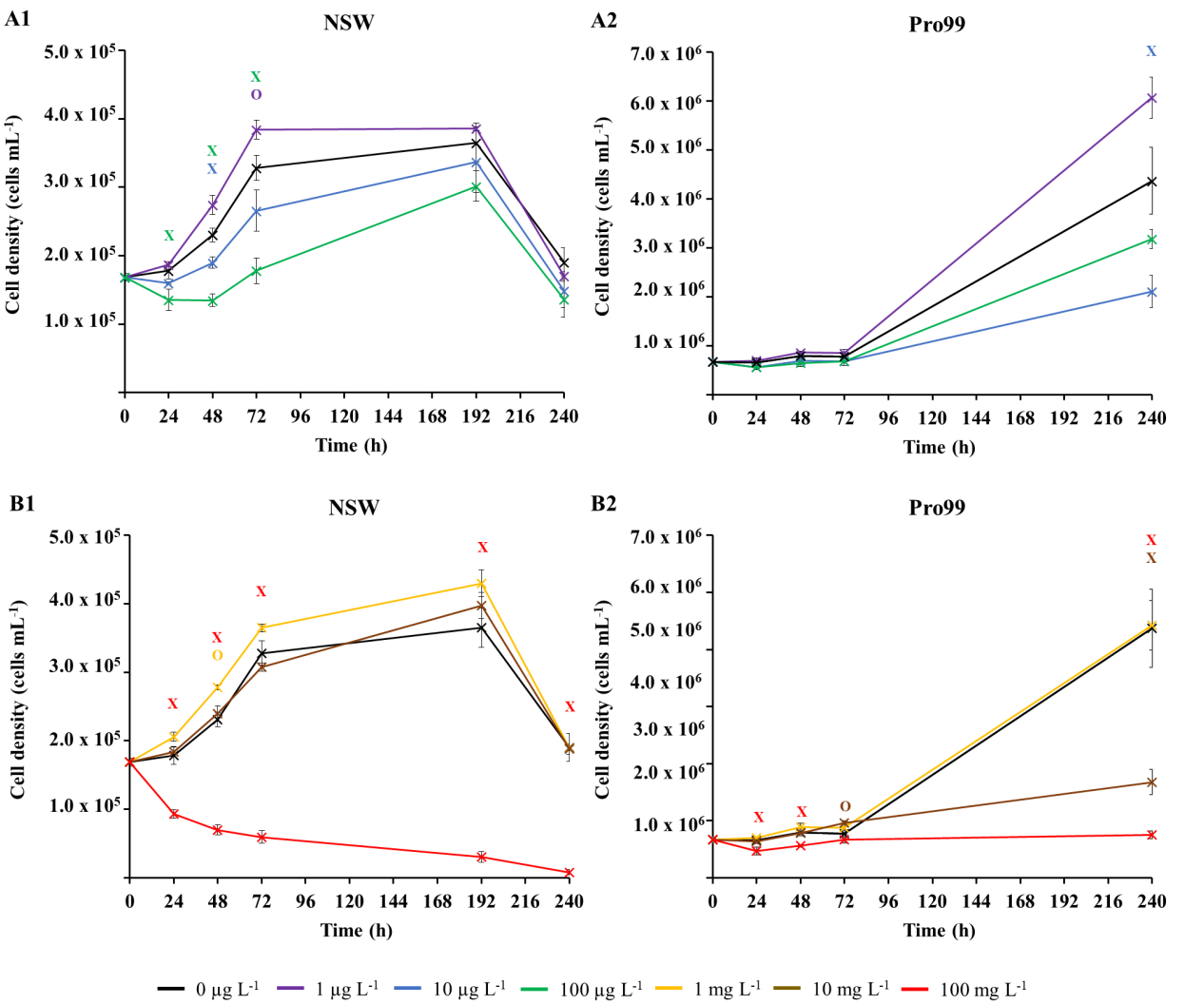

Figure 3.21. Long-term exposure of *Prochlorococcus sp.* MED4 to $nCeO_2$ in the µg L^{-1} (A) and mg L^{-1} (B) concentration range, when exposed in natural oligotrophic seawater (Panels A1 and B1) or Pro99 media (Panels A2 and B2). Data is presented as the mean of three culture replicates ± standard error (n=3). Two-way T-tests were used to identify significant variations in cell density between $nCeO_2$-treated cultures and the untreated control at each timepoint ($p \leq 0.05$); Crosses indicate where cell density was significantly lowered in the $nCeO_2$ treatment; Circles represent where a significant increase in cell density was recorded.

b) mg L^{-1} concentrations

To further evaluate the impact of $nCeO_2$ should emissions into the environment rise or hotspots of pollution occur due to accumulation of nanoparticles, the response of *Prochlorococcus* towards supra-environmental concentrations (*i.e.,* mg L^{-1}) was also assessed (Fig 3.21 B). In both NSW and Pro99 exposure to the highest concentration (100 mg L^{-1}) exerted a negative impact upon *Prochlorococcus* throughout the 240-h exposure, causing a maximum decline in cell density of 95.7% (two-way T-test, $p \leq 0.05$). As with lower concentrations, differences in response between the two culture conditions could also be observed in mg L^{-1} treatments. Whilst 10 mg L^{-1} $nCeO_2$ exerted no effect on *Prochlorococcus* grown in NSW (Fig 3.21 B1), cell-dense cultures experienced a 61.6% decrease in cell density (Fig 3.21 B2) by the end of the experiment (two-way T-test, $p \leq 0.05$). The enhanced cell decline observed in cell-dense cultures, may arise due to increased likelihood of encounter between nanoparticles and cyanobacteria. Previous research has also shown that cultures grown to higher cell densities suffer greater adverse effect of MO nanomaterial exposure,[50] also observed during extended $nTiO_2$ exposures presented in section 3.1.3.3.

Interestingly, following 240 h exposure no effect was recorded in 1 and 10 mg L^{-1} $nCeO_2$ treatments in NSW, or the 1 mg L^{-1} treatment in Pro99 media. However, declines were observed at lower concentration at specific timepoints (10 and 100 μg L^{-1}). It is proposed that the difference in effect caused by these treatments is likely due to the extensive aggregation of $nCeO_2$ upon entering saline media. It is possible that in μg L^{-1} treatments, stability of $nCeO_2$ in suspension is increased following lowered homo-aggregation due to reduced rate of encounter between individual $nCeO_2$ particles, hence facilitating their interaction with planktonic cells. In contrast, at higher concentrations (1-10 mg L^{-1}) homo-aggregation occurs at a higher rate causing $nCeO_2$ to aggregate and sink before interacting with cyanobacteria. At the highest concentration (100 mg L^{-1}) where effects are most severe, and in the 10 mg L^{-1} in cell-dense cultures where particle-cell contact is more likely, the aggregation process is extensive enough to significantly reduce *Prochlorococcus* numbers. Throughout supra-environmental concentration treatments, small aggregates were observed by flow cytometry and large aggregates were visible at the bottom of the culture flasks

(Fig 3.22) confirming nanoparticle aggregation and possible cyanobacteria-nanoparticle aggregation which deserved further investigation.

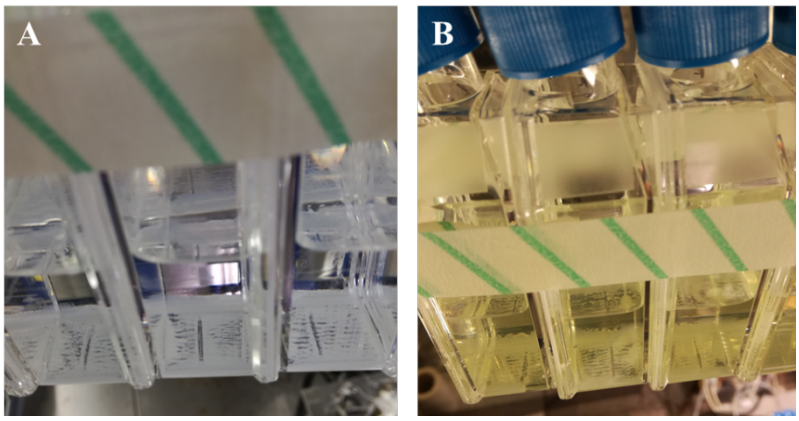

Figure 3.22. Visual observation of deposited material, believed to be hetero-aggregates of cyanobacteria and $nCeO_2$, observed during extended exposure: A-NSW; B-Pro99 media.

3.2.3.4 Mechanisms of cyanobacterial cell decline in response to $nCeO_2$.

Adverse effects associated with $nCeO_2$ exposure have previously been recorded in studies with marine phytoplankton.[143] The diatom *P. tricornutum* suffered adverse effects following exposure to $nCeO_2$ at concentrations (10-30 nm) >10 mg L^{-1}, resulting in significant reductions in growth.[143] However, interestingly, lower concentrations <5 mg L^{-1} were recorded to stimulate growth of this diatom.[143] Such enhanced growth following exposure to $nCeO_2$ has also been recorded in marine algal species.[199]

Due to the limited evidence available, the exact mechanisms by which $nCeO_2$ drives significant declines in phytoplankton abundance remain unclear. Based on work in freshwater, $nCeO_2$ is thought to exert oxidative stress upon microbial species *via* photocatalytic ROS production.[92] This suggests that the presence of natural light may be a key factor in determining toxicity of $nCeO_2$, hence in our study full-spectrum bulbs were used to best simulate natural conditions. Oxidative stress and associated lipid peroxidation have been recorded in the marine diatom *P. tricornutum* in response to $nCeO_2$.[143] Although, whether such effects arise due to the nanoparticles' presence, or as a consequence of physical interactions with cells is not clear. In that work, concentrations of 10-40 mg L^{-1} led to considerable increases in activity of superoxide

dismutase, peroxidase and malondialdehyde, associated with oxidative stress and lipid peroxidation respectively.[143] It is possible ROS production and associated oxidative stress may have played a role in the significant declines of *Prochlorococcus* recorded during our study. However, it has also been suggested that due to $nCeO_2$ being a redox catalyst, nanoparticles display the potential to both mitigate, as well as exert, oxidative stress.[91, 151] For example, $nCeO_2$ has been recorded to display antioxidant activities towards secondary oxidative stress exerted upon phagocytic and human bronchial epithelial cell lines,[306] and during incubation with phytoplankton.[323] It is possible any antioxidant properties may account for the enhancement of phytoplankton growth recorded in previous research in response to $nCeO_2$, and lack of decline observed at concentrations of 1 and 10 mg L^{-1} observed in the study presented herein. However, such enhanced growth can also be attributed to hormetic effects.[332] The exact mechanisms by which $nCeO_2$ exerts and mitigates oxidative stress requires attention, particularly in seawater. Additionally, $nCeO_2$ exposure has been linked to a decrease in photosynthetic activity,[143, 333] as well as reducing carbon fixation in freshwater phytoplankton,[333] suggesting phototoxic properties of $nCeO_2$. Deng *et al.* (2017) recorded a decline in quantum yield of PSII by approximately 29% following 96 h exposure to $nCeO_2$ in the diatom *P. tricornutum*. However, such effects are only observed at relatively high concentrations (2.5-40 mg L^{-1}).[143, 333] As such, it is unlikely photosynthetic processes will be adversely affected by $nCeO_2$ in the natural marine environment at current levels.

During exposures of *Prochlorococcus* to $nCeO_2$ the formation and precipitation of aggregates of cyanobacteria and $nCeO_2$ (which aggregate readily in the high ionic strength of seawater, as demonstrated, and described by DLS analysis) were visible in culture flasks (Fig 3.22). Whilst monitoring cyanobacterial populations by flow cytometry, it was possible to estimate the number of these hetero-aggregates within suspension (Fig 3.23). $nCeO_2$ aggregates alone do not fluoresce and, hence, would not be picked up during flow cytometric analysis. Nevertheless, the occurrence of large fluorescent particles were observed only at mg L^{-1} treatments. By gating these aggregates using FACSDiva software, it was possible to estimate their abundance relative to free *Prochlorococcus* cells (described above, section 3.2.3.3) and reference beads. Only freely suspended *Prochlorococcus* were used to calculate cell density

presented in the work above as those entrapped within hetero-aggregates would likely be removed from the water column by co-precipitation with $nCeO_2$.

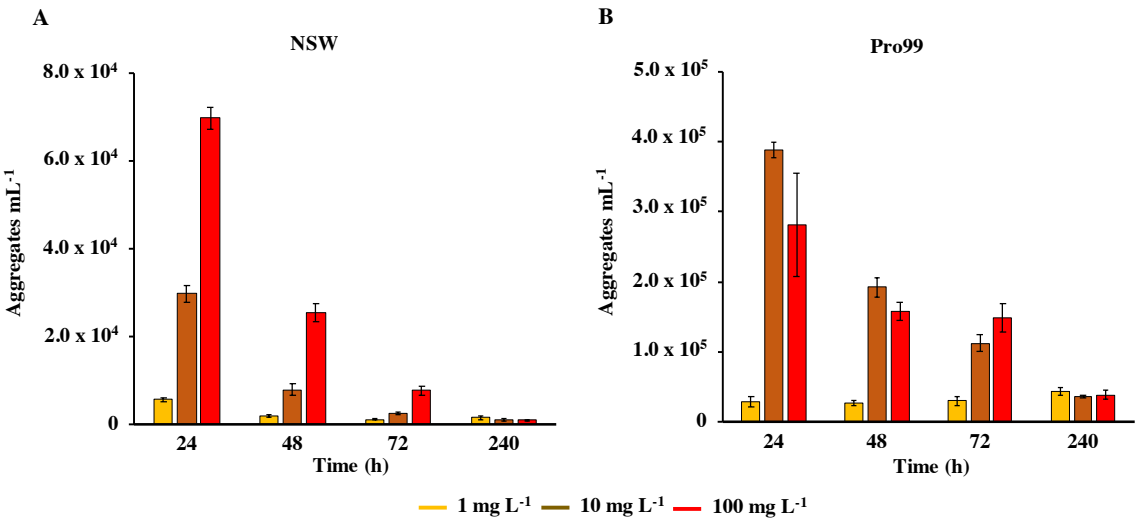

Figure 3.23. Estimated number of cyanobacterial-$nCeO_2$ aggregates as monitored during flow cytometric analysis of *Prochlorococcus sp.* MED4 cultures exposed to $nCeO_2$ in the mg L^{-1} range (1-100 mg L^{-1}). Data represents the mean of three culture replicates ± standard error (n=3). No such aggregates were observed during analysis of cultures exposed to lower concentrations (*i.e.,* 1-100 µg L^{-1}).

The estimated concentration of cyanobacterial-$nCeO_2$ aggregates in suspension appeared considerably higher in cell-dense cultures grown in Pro99 media compared to those grown in NSW, reaching peak average concentrations of $2.8x10^5$ and ~$7.0x10^4$ aggregates mL^{-1} respectively at the 24 h timepoint (Fig 3.23). This is likely due to the increased rate of encounter between nanoparticles and cyanobacteria under cell-dense conditions. In NSW, aggregate density appeared to follow a dose-wise trend, increasing with increased concentration, however this was not the case at the 240 h timepoint, where it is likely that aggregated material had precipitated out of the media and was therefore not present in the suspended fraction monitored by flow cytometry. In Pro99 media, this dose-wise trend was not observed, and highest values were recorded in the 10 mg L^{-1} treatment. Notably, aggregate density decreased the 24 and 48 h timepoints. This decrease is likely the result of rapid aggregation and precipitation of large, aggregated material due to increased density and, interestingly, at the last time point (*i.e.,* 240 h) the number of aggregates estimated at each concentration were in the same order of magnitude in both NSW and Pro99 media.

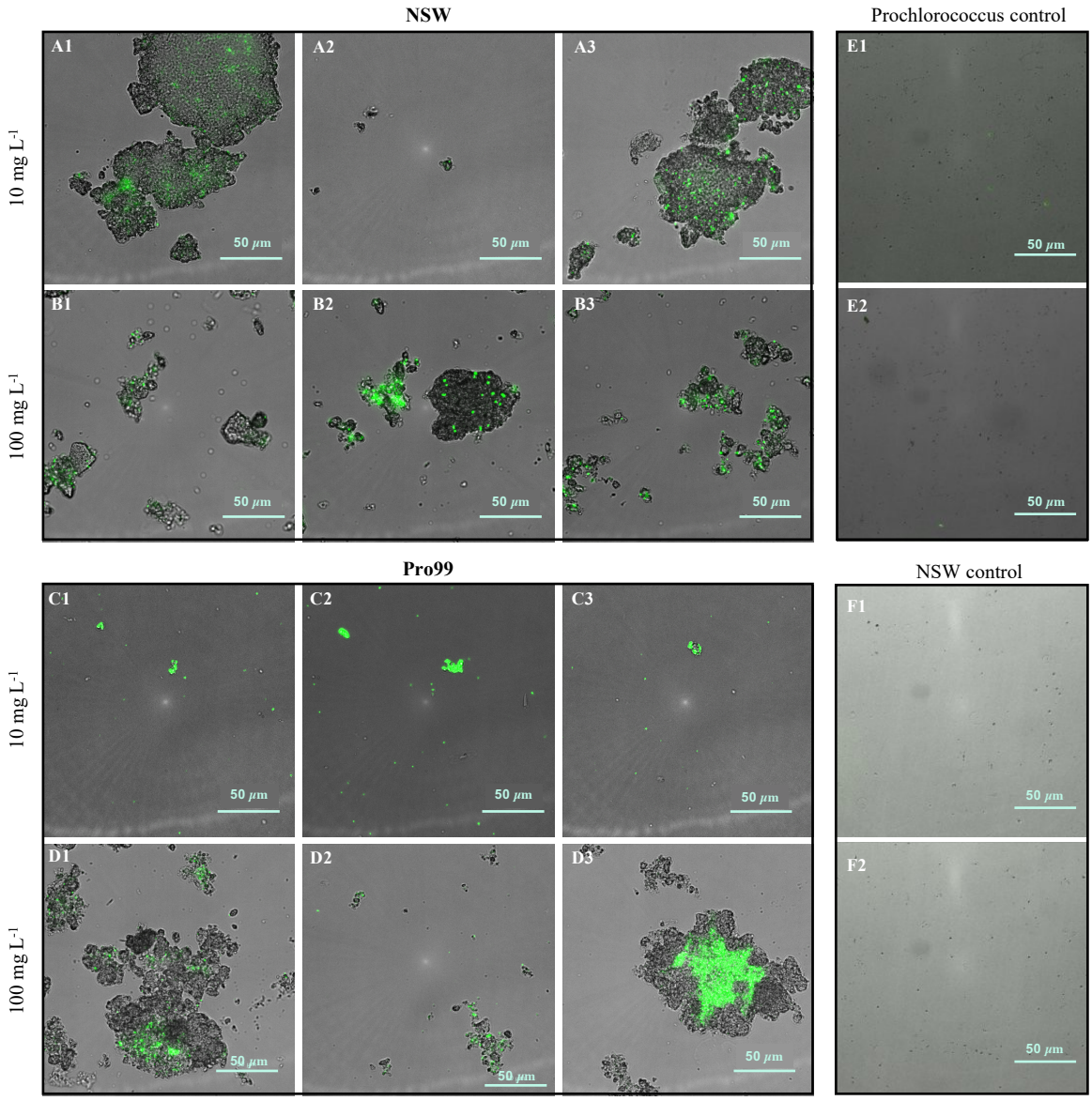

Figure 3.24. Hetero-aggregation of *Prochlorococcus sp.* MED4 (green) and $nCeO_2$ (10 and 100 mg L^{-1}) formed in natural oligotrophic seawater (Panels A and B) and Pro99 media (Panels C and D). Samples were stained with 1X SYBR Gold prior to imaging. Images were captured using fluorescent microscopy after under brightfield and GFP fluorescent and subsequently were merged. No such aggregates were visible in *Prochlorococcus* culture (E) or natural oligotrophic seawater (F) in the absence of nanoparticles.

The presence of cyanobacteria within precipitated aggregates of $nCeO_2$ was confirmed by carrying out fluorescent microscopy on precipitated material collected from the bottom of culture flasks that was subsequently stained with SYBR Gold (Fig 3.24). Here, *Prochlorococcus* was clearly visible within aggregates of $nCeO_2$ at concentrations of 10 and 100 mg L^{-1} in both NSW (Fig 3.24 A-B) and Pro99 media

(Fig 3.24 C-D) and reached sizes in the 10s-of-micron range. Some evidence of hetero-aggregation was observed within the 1 mg L^{-1} treatment; however, this was not apparent in cultures exposed to lower concentrations (1-100 µg L^{-1}**).** The hetero-aggregation between MO nanomaterials and phytoplankton has previously been reported in the literature,[98, 145, 146, 269, 270] and has been observed with $nCeO_2$,[98, 143] as well as during experiments with $nTiO_2$ described herein (section 3.1.3.4).

In previous research using the filamentous cyanobacterium, *Anabaena* CPB4337, positively charged $nCeO_2$ particles appeared to be attracted to the negatively charged cell walls of cyanobacteria.[98] The researchers proposed that toxicity may be induced by the direct contact of $nCeO_2$ to the cell wall; causing mechanical damage to the cell membrane, disrupting the exchange of nutrients and metabolites and exerting oxidative stress.[98] The same research group investigated the effects of $nCeO_2$ upon *P. subcapitata* in freshwater*,* observing damage to the cell membrane, and leakage of the cytoplasm.[98] Once again, this was believed to result from direct contact between nanoparticles and cells. Similar findings upon *P. subcapitata* have been recorded in other studies.[92] Hetero-aggregation between phytoplankton and MO NMs has also been proposed to cause shading effects which may reduce photosynthetic efficiency,[147] possibly causing the declines in photosynthetic output previously described.[143, 333]

It is concluded by Rodea-Palomares *et al.* (2010) that the cytotoxicity of $nCeO_2$ requires direct contact of particles to the cell wall or membrane. During this process it is likely that physical damage to cells will be caused, such as that described above, although additional study is required to confirm this. Despite reports of potential oxidative stress and disruption of photosynthetic processes during exposure to $nCeO_2$, it is suggested that the processes of entrapment and subsequent co-precipitation of cyanobacteria and $nCeO_2$ from the water column accounts for the temporary declines in *Prochlorococcus* presented herein (sections 3.2.3.2 and 3.2.3.3). The belief that physical effects are the key driver of the cyanobacterial decline presented, rather than oxidative stress, is supported by the fact that *Prochlorococcus* is highly susceptible to ROS and is sensitive to H_2O_2 concentrations as low as 200 nM.[240, 243] Hence, given that the viable free-living population recorded by flow cytometry is able to recover to

ambient cell densities in extended exposure, this suggests that ROS-mediated stress is likely not a feature of our work.

Over time the concentration of suspended $nCeO_2$ in *Prochlorococcus* cultures will display a continual decline as nanoparticles aggregate and undergo sedimentation, hence reducing their bioavailability and allowing the surviving cyanobacterial population to recover, as observed in *Prochlorococcus* populations grown in NSW (Fig 3.21 A1). It is important to note that in our work, uncoated $nCeO_2$ was utilised during experiments. The behaviour of these nanoparticles likely differs to those which are surface-modified, likely playing a key role in the effects recorded herein. It has been suggested that surface characteristics influence differences in toxicity by altering NM bioavailability.[97] For example, in contrast to the nanoparticles used in our work, Poly-(acrylic acid)-stabilised $nCeO_2$ appear well-dispersed in saline media, remaining biologically available to species occupying the water column, and hence enhancing toxicity towards these organisms.[97] However, findings vary and appear case-specific. Dextran-coated $nCeO_2$ have been recorded to exert negligible toxicity upon *E. coli*,[96] believed likely due to stabilization of the oxidative state of the nanoparticles by the polymer coating, as well as a reduction in contact between particles and cells.[96] Going forward it will be increasingly important to assess the surface characteristics of $nCeO_2$ entering the environment, such that greater insight into their likely fate and interaction with biota can be gained.

The occurrence of hetero-aggregation between nanoparticles and phytoplankton may increase the risk of bioaccumulation and transfer of particles to higher trophic levels by ingestion. Evidence of trophic transfer of $nCeO_2$ has previously been reported in a terrestrial plant model.[115] However, it must be noted that the widespread occurrence of hetero-aggregation between phytoplankton and nanoparticles recorded in laboratory investigation is likely driven at least partially by the relatively high concentrations examined and the closed-system nature of most experimental set-ups. As a result, such physical interactions between cells and nanoparticles are less likely in the natural environment at lower concentrations where nanoparticles appear more dilute and may alternatively interact with other particulate matter.

The recovery of *Prochlorococcus* recorded under environmentally relevant conditions in extended exposure and lack of adverse effect of concentrations <10 mg L^{-1} in NSW suggests that at current, the likely environmental risk of $nCeO_2$ exposure towards marine microbial species under natural conditions is low. The recovery of microbial populations in long-term exposure has previously been recorded during investigation with MO NMs,[99, 280, 298] often attributed to the aggregation behaviour of these NMs, leading to their reduced bioavailability over time,[99, 302] in accordance with DLS analysis and microscopic imaging described above. This evidence suggests that similarities between the impact of various MO NMs exist, allowing researchers to better understand their likely effect.

3.2.4 Conclusions

In this study new insight is provided on the effect of $nCeO_2$ upon marine microbial species using the ecologically significant marine cyanobacterium *Prochlorococcus sp.* MED4. To date, limited research has been carried out to assess the potential impact of this emerging contaminant upon marine microbial organisms, and hence the works presented herein address this gap in knowledge. It has been shown that despite evidence of short-term (<72 h) declines in cell density, $nCeO_2$ appears to exert little toxicity towards *Prochlorococcus* under natural conditions in the longer term, except at exceptionally high concentrations (*i.e.,* 100 mg L^{-1}). Cultures grown to higher cell densities in nutrient-rich media appear to suffer greater effects of exposure when incubations are extended to 240 h, believed due to the increased rate of encounter between cyanobacteria and nanoparticles. The occurrence of hetero-aggregation between $nCeO_2$ and *Prochlorococcus* is a key feature of exposure, in accordance with a number of studies examining the ecotoxicity of MO NMs, [98, 145, 146, 269, 270] driven by aggregation behaviour of $nCeO_2$ in saline media confirmed by DLS. Processes of entrapment and subsequent co-precipitation of nanoparticles and cyanobacteria is believed to account for the declines in cell number recorded. Over time, the concentration of suspended $nCeO_2$ is reduced, hence reducing the likelihood of interaction between nanoparticles and biota, allowing the remaining free-living cyanobacterial population to resume normal growth. However, it remains that the mechanism of cell decline observed in laboratory investigation is far less likely to

occur at the low $nCeO_2$ concentrations expected in the natural environment, where dilution effects likely limit the extent of both homo-aggregation and hetero-aggregation with phytoplankton, where nanoparticles may also interact with natural colloids or NOM. As such, in accordance with previous research,[13] it appears that the likely environmental risk of $nCeO_2$ towards marine microorganisms is low. One drawback from the works presented herein is the use of pristine research-grade nanomaterials. Such particles may not accurately represent those particles released into the environment. $nCeO_2$ is likely to undergo transformation upon its release into the environment, particularly $nCeO_2$ released from fuel *via* combustion.[69] Echoing the beliefs of Dale *et al.* (2017), future experimental work requires focus upon investigating the environmental impact of $nCeO_2$ and other MO NMs using materials that best represent those released into the environment.[9] It will be important to comprehensively characterise physicochemical properties as well as nanoparticle state in the environment. Here, synthetic approaches may be a useful tool to produce NMs which accurately match environmental particles. Efforts must also be directed towards accurately predicting the likely environmental concentration of $nCeO_2$, where marine transport may contribute substantially to the entry of nanoparticles into the ocean. In future studies, experiments conducted on whole communities may aid analysis of impacts upon ecological function and identify any taxonomic groups particularly susceptible to exposure.

3.3 Chapter Summary

In this chapter, the impact of MO NMs upon marine microorganisms has been evaluated using a range of materials that represent those commonly used in experimental research and by consumers. The ecologically significant cyanobacterium *Prochlorococcus sp.* MED4, previously understudied in the field of ecotoxicology, was found to suffer adverse effects of exposure to $nTiO_2$ and $nCeO_2$, dependent on specific exposure conditions. However, experiments revealed a remarkably similar impact of $nTiO_2$ and $nCeO_2$ upon marine microbial species, driven largely due to their similar behaviour upon entry into natural seawater, which has previously been noted.[63] As such, the works presented suggest that MO NMs may display a generalised behaviour in the marine environment, and hence common effect upon interaction with marine microbes, likely attributed to their propensity to aggregate in saline media. Additionally, effective protocols to extract and characterise nanoparticles from nano-product formulations have been presented, providing great scope for future work in the nano-ecotoxicological field, and enhancing environmental relevance of research.

Short-term exposure (<72 h) of *Prochlorococcus* to MO NMs at environmentally-relevant concentrations (μg L^{-1}) revealed significant declines in cell density under environmentally relevant conditions (ambient cell densities grown in oligotrophic NSW). Here, negative effects are recorded at considerably lower concentrations than EC_{50} values generated from studies upon diatom or green algae species (Table 3.1), suggesting marine cyanobacteria may be more susceptible to MO NMs than other phytoplankton in the natural environment, possibly due to their relatively small size. However, such negative responses were not observed in cultures grown at higher cell densities in nutrient-rich media during the short-term, perhaps due to a protective effect of larger cyanobacterial populations, as observed in earlier works with AgNPs (section 2.3.4). Experiments carried out with consumer $nTiO_2$ extracted from commercial products, displayed evidence of cell decline at concentrations 50-500 μg L^{-1}, however such effects were less severe than those recorded using research-grade $nTiO_2$. During this work, evidence of enhanced growth in the presence of extracted materials was also recorded, highlighting the variability in response of microorganisms to various nano-components. The use of extracted materials in future

work is recommended, and the methods presented in this thesis provide great scope for this purpose. Going forward it is increasingly important that researchers consider the impact of other components of nano-product formulations, which have been observed to exert both adverse and biostimulating effects, as well as the likely role of product matrixes in NM release. Related to this, increased works are needed to consider the transformation of NMs within the natural environment, and likely state of NMs which biota are likely to interact with.

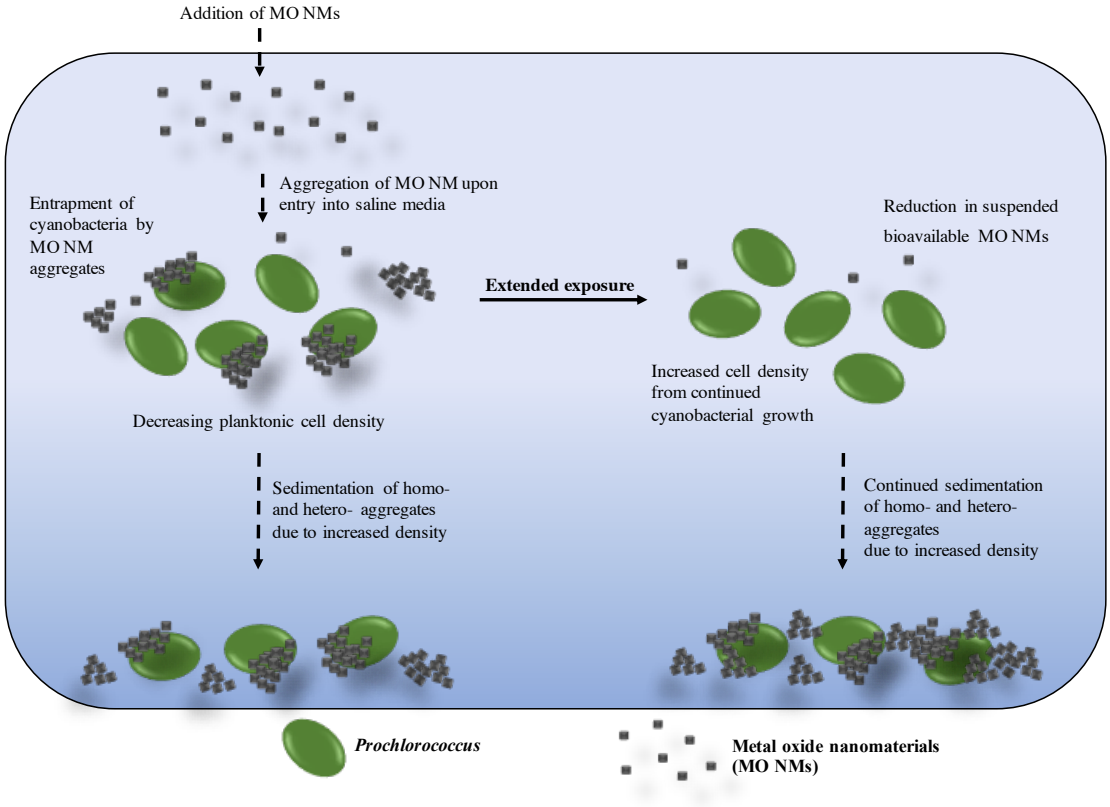

Figure 3.25. Graphical representation of the proposed mode of cell decline recorded in exposures of *Prochlorococcus* to metal oxide nanomaterials.

Upon extending incubations to examine the longer-term effects of exposure, the ability of *Prochlorococcus* to recover following the initial significant declines in cell density in response to MO NMs under natural conditions was revealed, except at extremely high concentrations (100 mg L^{-1}). This is in contrast to work with AgNPs, described in Chapter 2, which revealed such declines to be irreversible (section 2.3.5). Increasing test concentrations to supra-environmental levels highlighted the dynamic nature of MO NM toxicity, believed driven by the extensive aggregation behaviour of the MO NMs in natural seawater, confirmed using DLS. At the highest concentrations, aggregation caused the entrapment of cyanobacterial cells, leading to their removal

from the water column *via* sinking. This process is believed the key driver of cyanobacterial decline in the works presented in this chapter, supported by fluorescent microscopy and shotgun proteomic analysis of $nTiO_2$-treated cultures, which showed negligible molecular features of toxicity. The rapid aggregation and settlement of NMs is also thought to account for the recovery of populations in extended exposure as NM bioavailability is reduced (Fig 3.25). At higher cell densities, negative effects of entrapment were enhanced in both $nTiO_2$ and $nCeO_2$ exposures, likely due to an increased rate of encounter between cells of nanoparticles. It is likely that oxidative stress driven through the production of ROS at the cell surface following NP-attachment and physical damage caused to cell membranes also contribute to overall toxicity. However, this requires further research, where shotgun proteomic analysis of the entrapped fraction of cyanobacteria may provide insight. In future, investigation by SEM may also facilitate greater understanding of the hetero-aggregation process.

The evidence of adverse effects of MO NM exposure upon marine microbial organisms is a concern given their fundamental role in ecosystem functioning and contribution to major global biogeochemical cycles. However, it appears that the worst effects of exposure are only observed at concentrations far exceeding those predicted in the environment. It is likely that the closed-system nature of experimental work facilitates the physical interaction between cells and NMs at high concentrations, which will be less likely to occur in the natural environment. This alongside the fact that little impact was observed on natural communities exposed to $nTiO_2$ under environmental conditions, means that the likely environmental risk of MO NMs such as $nTiO_2$ and $nCeO_2$ appears low. The use of molecular techniques as done in this thesis, provides great scope for future research in the nano-ecotoxicological field, particularly with microbial species. It remains that exposure to concentrations close to predicted environmental values do reveal some adverse effect during the initial stages of exposure, and the overall effect of this temporary suppression in growth and decline in cell number upon ecosystem function requires further investigation to fully understand the impact of MO NMs on the wider marine community. Similarly, additional understanding of any subsequent impact of hetero-aggregation between phytoplankton and NMs, which may facilitate the transfer of NMs to higher trophic levels, is required.

Chapter 4

Testing the effects of novel cerium oxide nanoparticle surface coatings upon marine biofilm formation

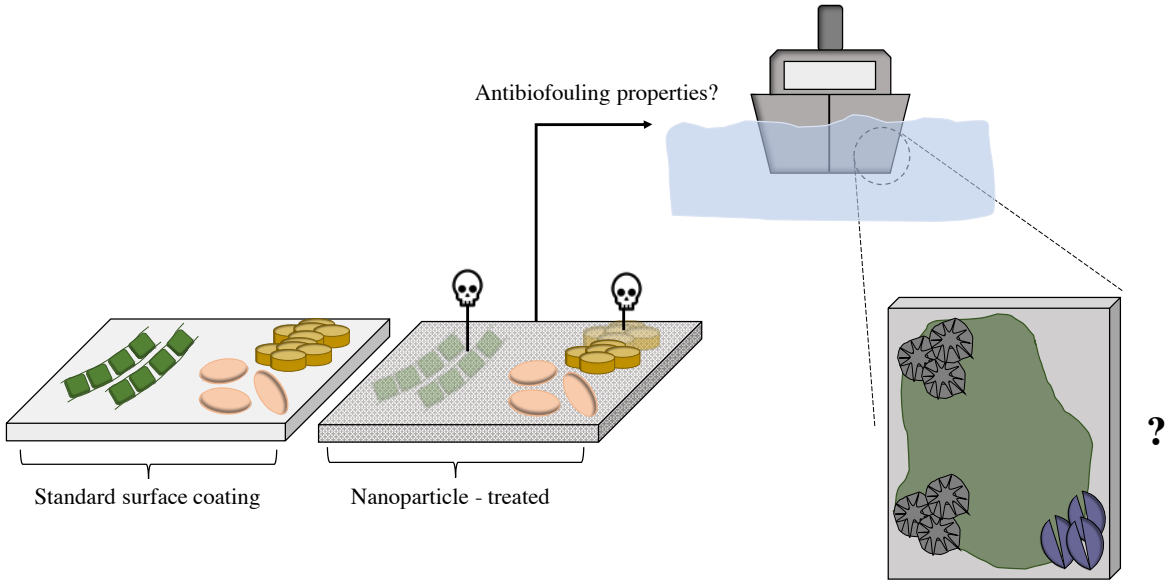

During this thesis, primarily the interaction between nanoparticles and planktonic microorganisms has been investigated. In this chapter, we move focus towards biofilm-forming communities and examine the potential impact of nanoparticles upon the growth and community structure of natural marine biofilms. To maximise environmental relevance, work was conducted in collaboration with Energenics Europe Ltd, a manufacturer of cerium oxide nanoparticles ($nCeO_2$). Herein, we incubated a range of novel $nCeO_2$ surface coatings in a recreational port representing appropriate field conditions for a period of 21 days, before assessing the impact of each upon marine biofilm formation and community structure using a novel approach comprising amplicon sequencing, nutrient analysis and advanced imaging.

4.1 Introduction

A biofilm is defined as an assemblage of microbial organisms that are 'surface-associated' and formed within a matrix comprised of extracellular polymeric substances (EPS).[334] The presence of such structures appear ubiquitous on submerged surfaces within the marine environment,[177, 335] and comprise the highest bacterial densities in the natural aquatic environment.[30, 336] These biological structures play key roles within natural ecosystems, contributing to both biogeochemical cycling and ecological functioning.[337]

Biofilm formation is a highly dynamic process dependent on a number of factors, including; season, location and predator-prey relationships.[338] Four key stages of a biofilm formation are presented by Dang and Lovell (2000);

1) Attachment of free-living bacteria to a substrate, forming an initial assemblage.
2) Increase in primary colonizing bacterial populations due to growth and reproduction, in turn modifying the surface characteristics of the substrate, facilitating secondary colonization.
3) A primary biofilm community is formed, due to interactions between the primary colonizing bacteria and other free-living bacteria within the local environment.
4) This continued interaction leads to the formation of a biofilm community through processes of competition and/or synergism between members inside and outside of the biofilm.[339]

Biofilm formation is a continual and highly dynamic process, and these complex structures provide cues to larger organisms, facilitating the settlement of marine invertebrate larvae, such as barnacles and mussels.[177, 335, 340] The specific surface characteristics of a particular substrate will influence colonisation by various taxa and the eventual community structure of biofilms that are formed; for example, previous research has revealed distinct structures of biofilm communities formed on acryl, glass and steel.[336]

In the marine environment, the formation of biofilms and associated recruitment of marine invertebrates can have a detrimental effect upon maritime industries, *e.g.,* shipping, aquaculture and oceanographic monitoring.[336, 338] Here, the formation of biofilms is referred to as marine biofouling, defined as the "undesirable accumulation of microorganisms, algae and animals on submerged structures in seawater".[341] In particular, biofouling exerts greatest impact upon the shipping industry, where ship's hulls represent 24% of all fouled man-made objects within the marine environment.[342] Primarily, the negative impact of biofouling upon shipping is reduced fuel efficiency, driven by increased drag and altered structure of the hull surface.[336, 343] For example, it is estimated that annual costs incurred by biofouling to the US naval fleet alone is up to $260 million.[338] With this in mind, and the additional pressures of anthropogenic climate change driven by use of fossil fuels, there is a great need to identify effective measures to reduce the impact of biofouling upon the shipping industry. Typically, antifouling paints have been used for this purpose.[344] Amara *et al*. (2018) list the most common biocidal agents utilized in antifouling paints as; Tributyltin (TBT), Chlorothalonil, Dichlofluanid, Sea-Nine 211, Diuron, Irgarol 1051 and Zinc Pyrithione.[345] Historically TBT-based paints were widely used; however, these were found to be highly toxic to marine wildlife and have since been widely replaced with copper-based paints.[346] Although to a lesser extent, these copper-based formulations remain toxic to marine biota.[345, 346] Despite environmental concerns, toxic antifouling coatings continue to be used globally.[347] As such, there is a requirement for the design of effective and 'ecologically-friendly' antifouling coatings that have the desired effect upon biofilm formation whilst mitigating toxicity towards other marine wildlife.[345]

More recently, NM-based antifouling surface coatings have been developed.[348-350] Copper nanoparticle (CuNP)- functionalised coatings have been shown to display antimicrobial properties similar to that of Cu-based biocidal coatings, whilst minimising the leaching of dissolved copper into the environment compared to traditional products.[348] Additionally, it is believed that NMs are more effectively fixed to surfaces compared to water soluble compounds, reducing the potential for leaching into the environment,[349] thus mitigating the negative effect of such agents on non-target species. Research suggests that NM-functionalised coatings can be effective against biofilm formation.[348-350] For example, biofilm formation on metal was

significantly reduced by the presence of a $nTiO_2$ coating added to prevent corrosion.[350] Likewise photocatalytic nZnO nanoparticles were effective at preventing biofilm growth on man-made surfaces, reducing growth by 20-40%.[349] As such, nanotechnology may prove useful in the development of 'environmentally friendly' antifouling agents.

Biofilms may interact with NMs in a number of ways, largely dependent on environmental factors such as salinity, pH and natural organic matter (NOM) content which will influence the fate and behaviour of NMs upon entry into the aquatic environment.[351-353] NMs may be internalised and accumulated within biofilms, particularly due to the increased sedimentation that occurs in the aquatic environment as observed in earlier work (see sections 3.1.3.5 and 3.2.3.1), and become a sink for aquatic NMs.[354, 355] The uptake and incorporation of NMs into the biofilm matrix has been recorded during experimentation.[356] In fact, retention of NMs by substrates such as quartz within aquatic media appears enhanced by the presence of a biofilm.[357-360] Under environmentally-relevant conditions, biofilms represent the major sink of NMs, for example of ~60% AuNPs retained by a FW mesocosm system, biofilms accumulated nanoparticles at their highest concentration.[354] A likely cause of retention of NMs by biofilms is due to electrostatic processes.[354, 359] Biofilms are largely formed of negatively charged monomers incorporated in the polysaccharides and proteins that make up the biofilm matrix,[361] which create a high affinity for positively charged NMs,[354] such as the AuNPs utilised in the study referred to above. However, such electrostatic interactions are dependent upon specific NM surface characteristics, and hence surface charge.

Upon entry into biofilms, NMs enter a 'heterogeneous microenvironment' that varies in local pH, nutrient content and oxygen availability, likely to influence their transport and transformation within and outside of the biofilm.[356, 362, 363] In experimental work with $nCeO_2$ adsorption of nanoparticles by the biofilm was observed, characterised by interaction of particles with microbial cell surfaces, spores and the EPS.[364] Here, it is believed that the structure of the biofilm allows for protected growth of microbes in the presence of NMs.[364] EPS is reported to readily bind to NMs and adsorb metal ions, thus likely acting as a protective barrier from NM exposure.[364-367] This mechanism has been observed under laboratory conditions following incubations with $nTiO_2$ and

AgNPs respectively.[154, 309] Despite the protective effect of the biofilm, NMs have been observed to enter individual cells within the biofilm community, varying in extent with organism type.[368] In the case of $nCeO_2$, NMs were more likely to enter bacterial cells compared to algal cells within periphytic biofilms.[368] Motility of NMs within the biofilm appears to be limited, which may lead to localised areas of toxicity.[356] Although accumulation of NMs at the biofilm surface is believed likely to reduce the toxicity incurred by deeper layers.[356]

Currently, information regarding the effects of NMs upon natural biofilm formation and community structure is limited, especially within the marine environment and in the long-term at sublethal concentrations.[309] Generally, biofilms are more tolerant to contaminants than planktonic populations, displaying up to 1000-times more resistance.[369] Despite this, negative impacts of NM exposure have been recorded; AgNPs have been found to adversely affect biofilm-forming bacteria by altering community succession of marine biofilms and driving changes in the relative abundance of major bacterial phyla.[30, 177, 370] Likewise, MO NMs such as $nTiO_2$ and $nCeO_2$ have been found to display antimicrobial effects when applied to aquatic biofilms, inducing effects such as the suppression of antioxidant activities.[350, 368] Variation in the response observed between varying community members has been recorded; following 21-d exposure to AgNPs relative abundance of Bacteroidetes, specifically Flavobacteria,[177] believed to be key colonising species was reduced,[371, 372] whereas the relative abundance of *Vibrionaceae* increased.[177] Similarly, differences in biofilm community response have been recorded in the presence of $nCeO_2$, $nTiO_2$ and nCuO.[309, 368, 373, 374] For example, Tang *et al*. (2018) observed firmicutes to decrease in relative abundance from 42% to 3%, whilst cyanobacteria increased approximately threefold in the same experiment.[368] In contrast, relative abundance of cyanobacteria was reduced by 69% in response to $nTiO_2$ (5 mg L^{-1}).[309] Thus, it is very likely various members of the biofilm community will respond differently to NM-treated surfaces. Alteration to the microbial consortia has the potential to cause impacts upon the functioning of the community. For example, exposure to $nCeO_2$ in the mg L^{-1} range compromised the phosphorous cycling activity of sludge biofilms inhabiting a batch reactor, reducing efficiency of phosphorous removal from 85-60%.[365] Similarly, incubation with $nTiO_2$ has induced negative effects on nutrient processing in freshwater biofilms.[309, 355] PICRUSt functional analysis and enzymatic assays

revealed alterations to carbon and nitrogen cycling in freshwater sediment biofilms exposed to nCuO (1 mg L^{-1}).[374] Such alterations to the functioning of biofilm communities may have knock-on effects upon other biota inhabiting aquatic environments.[355] Additionally, it has been suggested that the interaction between NMs and microbial species may induce indirect effects that may have adverse effects upon other species, for example the production of toxins.[373] Such an effect has been recorded in the harmful blooming algae, *Alexandrium tamarense*, which is observed to increase toxin production in the presence of $nTiO_2$.[272] Perhaps more notably, particularly in regards to the control of biofouling, the changes in biofilm community structure and presence of AgNPs led to decreased larval settlement of mussels by >30% compared to the untreated control.[177] Similar findings have been observed in exposure to $nTiO_2$.[180] Such findings highlight the dynamic nature of direct and indirect effects that may arise from NM exposure, as well as displaying the potential for NMs to act as an effective antifouling agent.

Nano-sized CeO_2 has previously been shown to display antimicrobial effects[98, 143, 151, 199, 368] and evidence for its adverse effect upon biofilms exists.[368] Whilst, in the previous chapter $nCeO_2$ (≤10 mg L^{-1}) exerted little impact on the marine cyanobacterium *Prochlorococcus* under natural conditions, when applied within a surface coating treatment, microorganisms will encounter a high localised concentration of relatively stable $nCeO_2$, where negative impacts are more likely. In comparison, bioavailability of $nCeO_2$ is reduced in planktonic cultures by processes of nanoparticle aggregation and sedimentation over time (see sections 3.2.3.1 and 3.2.3.4). The relatively low solubility and therefore slowed dissolution[98] of $nCeO_2$ means that it presents a strong candidate for use in antimicrobial surface coatings with a lowered environmental impact. In this chapter, the antifouling properties of novel surface coatings incorporating cerium oxide-based nanoparticles developed by Energenics Europe Ltd. was tested under relevant field conditions. A novel approach comprising of 16S/18S rRNA amplicon sequencing and total nutrient analysis was supported by advanced imaging techniques to provide new insight on the effects of MO NMs upon marine biofilm formation and community structure.

4.2 Materials and methods

4.2.1 Materials

Aluminium panels (AQ-2.36-5.51) were purchased from Q-Labs. The 60x140x0.32 mm panels were subsequently cut down to 8x30x0.32 mm on-site and washed with acetone before surface coatings were applied. NMs utilised in the study were synthesised and provided by Energenics Europe Ltd. Two cerium oxide- based nanoparticle formulations were used in this work; i) nano-sized $nCeO_2$ (NP1) and ii) copper-doped $nCeO_2$ with the composition of $Cu_{0.2}Ce_{1.8}O_2$ (NP2). Other nanoparticle characteristics are commercial protected by Energenics Europe Ltd. Surface-coatings were subsequently formulated and applied to aluminium strips by Energenics Europe Ltd. Here, two base surface coatings were used; chlorinated rubber paint to which NP1 only was added, and alkyd resin mixed with NP1 or NP2. For chlorinated rubber paint coatings, ARC-RITE Paint was purchased from an online retailer and mixed with NP1 dispersion to provide a final concentration of 1.9%. Subsequently, aluminium strips were dip-coated with either chlorinated paint only (no nanoparticles), acting as a control, or NP1-paint formulations and air-dried for 60 mins. For resin samples, Alkyd resin (Vilkyd 220W75) was mixed with aliphatic solvent D80 and NP1 or NP2 dispersions respectively, to provide a final concentration of 1.9% w/v. Alkyd resin controls, containing no nanoparticles, were prepared by mixing alkyd resin with Octa-soligen Cobalt 10 (as the drier for the alkyd resin) and alphatic solvent D80. Aluminium strips were dipped in alkyd resin formulations and air-dried for 10 mins. Subsequently, alkyd resin coatings were placed in a 60°C oven for 60 mins. Polyethylene piping used to construct the framework for experimentation was purchased from a local retailer and was constructed at the field site. Laboratory grade formaldehyde (33%) was purchased from Sigma Aldrich and used at a final concentration of 4%. Lysis buffer and DNeasy PowerBiofilm DNA extraction kit was purchased from Qiagen and used following the manufacturer's instructions.

4.2.2 Investigating the effects of novel $nCeO_2$ surface coatings upon marine biofilm formation.

a) Experimental set-up

Surface-coatings incorporating cerium oxide-based nanoparticles NP1 and NP2 were applied to bare aluminium strips and fixed to fishing line. A total of six surface coatings were tested, including three incorporating nanoparticles formulated by Energenics Europe Ltd. Treatments were compared to a bare aluminium control with no surface coating applied (see Table 4.1). Replicate strips of each treatment were fixed to a single length of fishing line and subsequently attached to a polyethylene framework at equal height in preparation for environmental exposure (Fig 4.1).

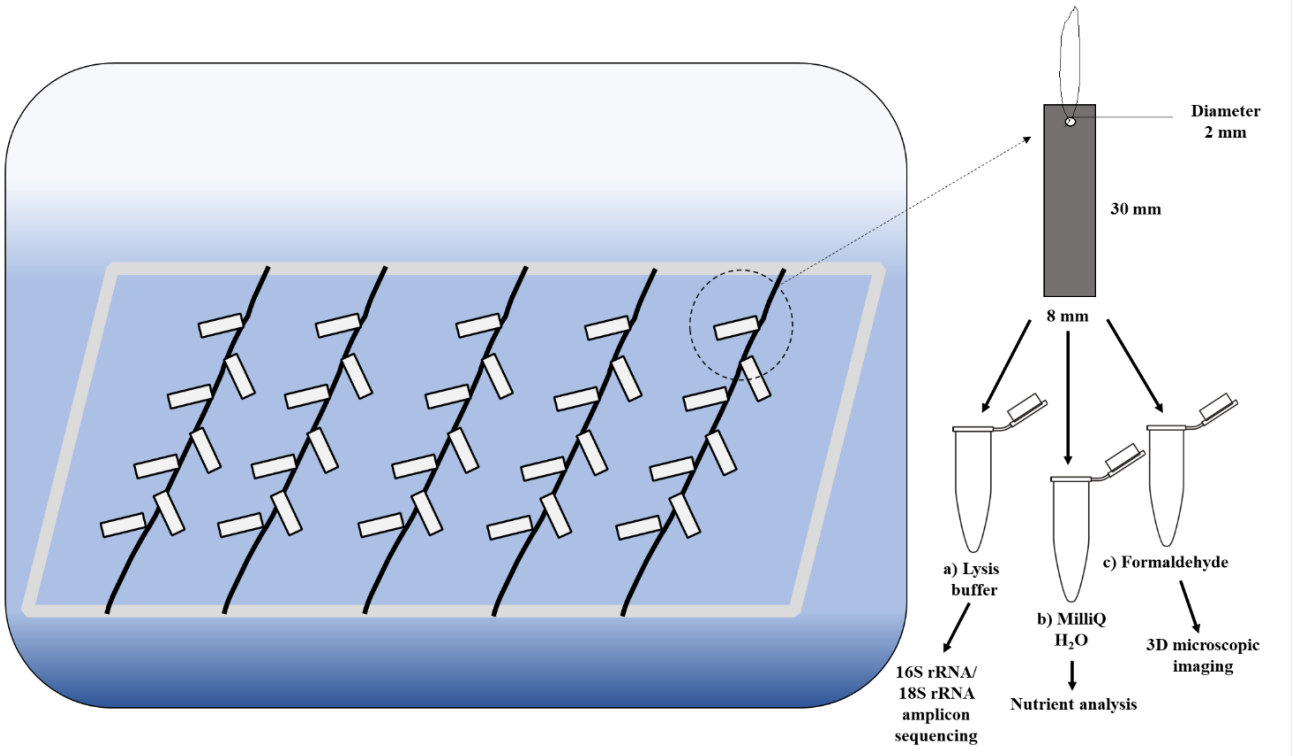

Figure 4.1. Experiment set-up utilised during fieldwork. Metal strips were attached to polyethylene frame and suspended in surface water for a period of 21 d. Following incubation, samples were removed from the framework and placed into eppendorfs containing; a) 1.5 mL lysis buffer to be used for 16S and 18S rRNA amplicon sequencing, b) 1.5 mL Milli-Q ultrapure water for nutrient analysis, or c) 1.5 mL formaldehyde (4%) to fix biofilm samples for 3D microscopic imaging.

A site representing a typical recreational port was selected in Badia de Palma, Mallorca, Spain (39.499964, 2.750736, Fig 4.2). This site is in constant use by recreational boat users and is therefore appropriate as a site for field testing of antifouling properties. Here at 0 h, the framework containing all samples was submerged in port surface water and secured in position by a bungie line to an adjacent boat. The exposure was carried out for 21 d during August 2018. Following exposure, the framework was removed from the water and the surface-coated aluminium strips were prepared for analysis by transferring samples and associated biofilm into 2 mL eppendorfs containing one of three media: A) 1.5 mL lysis buffer for subsequent DNA extraction; B) 1.5 mL Milli-Q ultrapure water to prepare samples for nutrient analysis; C) Formaldehyde (4%) to fix biofilms for imaging. Immediately after sample collection, those samples to be used for DNA extraction and nutrient analysis were stored at -20°C. All samples were transported back to the UK for analysis at the University of Warwick.

Figure 4.2. Location of field experiment; recreational port, Badia de Palma, Mallorca, Spain (39.499964, 2.750736). Images acquired using Google Maps™.

Table 4.1. Summary of treatments used during 21-day environmental exposure.

Treatment	Base Coat	NM Incorporated	Identifier	Replicates
1	None (Bare Aluminium)	None	Metal_C	Amplicon Sequencing (n=4) Nutrient Analysis (n=5) Imaging (n=2)
2	Chlorinated Paint	None	Paint_C	Amplicon Sequencing (n=3) Nutrient Analysis (n=4) Imaging (n=2)
3	Chlorinated Paint	$nCeO_2$ (NP1)	Paint_NP1	Amplicon Sequencing (n=5) Nutrient Analysis (n=5) Imaging (n=2)
4	Alkyd Resin	None	Resin_C	Amplicon Sequencing (n=5) Nutrient Analysis (n=5) Imaging (n=2)
6	Alkyd Resin	$nCeO_2$ (NP1)	Resin_NP1	Amplicon Sequencing (n=3) Imaging (n=2)
5	Alkyd Resin	Cu-doped $nCeO_2$ (NP2)	Resin_NP2	Amplicon Sequencing (n=5) Nutrient Analysis (n=5) Imaging (n=2)

b) 16S/18S rRNA amplicon sequencing

To investigate any alteration to the biofilm community formed in the presence of $nCeO_2$ surface coatings, amplicon sequencing of the 16S and 18S rRNA genes was carried out to provide a profile of bacterial and eukaryotic organisms present within each biofilm sample. DNA extraction was carried out using the DNeasy Power Biofilm extraction kit (Qiagen) according to the manufacturer's instructions, adding an additional bead beating procedure to ensure all biofilm material was well-lysed. Here, following one round of bead-beating a sterile blade was used to remove surface coatings containing the biofilm from each aluminium strip before the bead-beating procedure was carried out once more and the DNA extraction protocol continued. Quantities of DNA obtained from each sample were confirmed using a Qubit® HS DNA kit (Life Technologies Corporation) and extracted DNA samples stored at -20°C. Following DNA extraction, samples were prepared for amplicon sequencing as

described in section 3.1.2.9 in order to amplify the 16S rRNA v4-5 regions, and 18S rRNA v8-9 regions respectively.[283, 284] As previous, the Illumina MiSeq system with v3 reagent kit was used for sequencing, and data processing and downstream bioinformatics analysis was carried out as described in section 3.1.2.9 using MicrobiomeAnalyst software.[288, 289] An average of 7822 and 26744 reads for 16S and 18S rRNA datasets were obtained for analysis respectively. Three samples for 16S rRNA data, and one sample from 18S rRNA data which contained less than 1000 reads were removed from downstream analyses. Sequence files have been deposited in the NCBI Short Read Archive (SRA) database under Bioproject: PRJNA690566.

c) Nutrient analysis

To prepare samples for nutrient analysis, samples were left to defrost at room temperature for 30 mins. Subsequently, ~50 µg zirconia/silica beads (1 mm) were added to each sample and samples were homogenized for 30 s using a tissue homogenizer, to remove the biofilm and break up the surface coating. Three additional test controls consisting of Milli-Q ultrapure water were also processed to ensure the presence of beads did not alter results of nutrient analysis. This homogenisation process was subsequently repeated. Under sterile conditions the surface coating and associated biofilm was removed from the aluminium strip using a sterile laboratory blade and tweezers in a similar manner to that used in the DNA extraction process, described above. Aluminium strips were subsequently discarded. Samples were then homogenized as previous for a further two cycles to ensure maximal removal of the biofilm from the surface coating. To remove large pieces of debris and beads, samples were left to settle on ice for 20 mins. Subsequently, 1 mL of sample was carefully removed from the supernatant and diluted 25x in Milli-Q ultrapure water for analysis. All samples were then run on a Shimadzu TOC/TN Nutrient Analyzer under magnetic stirring to ensure samples were well mixed throughout the analysis. Five readings were taken from each sample for both Total Organic Carbon (TOC) and Total Nitrogen (TN), from which an average was taken. Milli-Q ultrapure water samples were sampled intermittently to provide regular washing and to ensure accuracy of readings.

d) Biofilm quantification by 3D imaging and COMSTAT analysis

Preparation of biofilm samples for imaging was carried out under darkness. First, metal strips and associated biofilms were removed from tubes containing 4% formaldehyde and washed three times in artificial seawater (ASW) for 15 mins. Subsequently, biofilms were stained with 1X SYBR Gold for 30 mins. Following this, washing was carried out three times as previous in ASW. Following washing, metal strips were carefully tapped onto absorbent paper to remove any residual water and one side of the metal strip was randomly selected and glued to a microscope slide. Subsequently, several drops of Antifade (ThermoFisher) were added across the exposed surface and a cover slip applied to the entire metal strip. Prepared slides were then dried horizontally for 48 h prior to imaging. To image the biofilms a Nikon Widefield Fluorescence Microscope was used with z-stack image capture, operated at 40x magnification. Images were taken under GFP fluorescence. Five z-stack images were captured across each biofilm, recording an image every 1 μm throughout the z-axis of the biofilm. Subsequently, COMSTAT2 analysis (http://www.comstat.dk/) was used to determine values for biofilm biomass, depth, and percentage area cover as previously described.[375, 376] Mean values for each parameter obtained from the five z-stack images were calculated for each sample respectively.

4.3 Results and Discussion

Novel surface coatings incorporating $nCeO_2$ (NP1) and copper-doped $nCeO_2$ (NP2) nanoparticles were applied to aluminium strips and submerged into natural seawater within a recreational port in Mallorca, Spain, in order to examine antifouling properties and impact upon marine biofilm formation under appropriate field-testing conditions. NP2 particles were doped with copper to enhance their antifouling effect, given the well-established antimicrobial nature of dissolved copper and copper-based nanoparticles.[279, 377] Two base surface coatings were examined, chlorinated rubber paint to which NP1 had been added, and alkyd resin treated with NP1 or NP2. Bare aluminium strips, and those treated with surface-coatings not containing the nanoparticles were also investigated, acting as controls for the experiment.

Natural marine biofilms were allowed to form over a period of 21 d, and upon visual observation well-established biofilms had grown on all samples. Through investigation of biofilm communities *via* amplicon sequencing, further evidence has been provided to show that surface characteristics of a particular substrate play a key role in determining the resultant biofilm community stucture.[336, 378, 379] However, the novel antifouling surface coatings incorporating nanoparticles appeared to have limited effect upon biofilm formation or their biodiversity compared to base coatings where the nanoparticles are absent (*i.e.,* chlorinated rubber paint and alkyd reason controls). Rather, biofilm communities established upon surface-coated surfaces appear distinct to those grown on bare aluminium, regardless of the presence of nanoparticles. Further analyses at lower taxonomic levels, in conjunction with analysis of the total nutrient content of biofilms, suggests that the presence of nanoparticles may act to drive subtle changes in the biofilm community, which upon increasing concentration may cause enhanced effects. Such data, provides preliminary data to inform on the design of novel 'ecologically-friendly' antimicrobial surface coatings, for which high demand exists,[338] and recommendations for future experimentation.

4.3.1 The impact of surface coating upon marine biofilm community dynamics

a) Bacterial diversity and community composition

The diversity of bacterial communities did not significantly differ between treatments in terms of both species' evenness and species richness (see Table 4.2). Unfortunately, due to removal of samples consisting of <1000 reads, only two replicates of the alkyd resin treated with NP1 treatment were available, and hence this treatment was removed from further analyses of the 16S rRNA dataset. Two-way T-tests comparing the species richness between bare aluminium controls and surface-coated samples, as well as between surface coating controls and those treated with nanoparticles revealed no statistical alteration for any measure of alpha diversity. Principle component analysis (PCA) based on Bray-curtis dissimilarity (Fig 4.3) displayed a distinct grouping of treatments, notably bare aluminium controls appeared to group away from all surface-coated samples regardless of the presence or absence of nanoparticles (PERMANOVA, $p<0.001$). However, little difference was apparent between

communities formed on respective paint and resin- coated surfaces in the presence or absence of NP1 or NP2.

Table 4.2. *Alpha* diversity of 21-day old marine biofilm bacterial communities.

			Species Richness		Species Evenness	
Sample	**n**	**ASVs**	**Chao 1**	**ACE**	**Shannon**	**Simpson**
Metal_C	4	1254.75 ± 314.07	1381.26 ± 253.84	1497.25 ± 238.74	5.68 ± 0.26	0.99
Paint_C	3	1312.33 ± 140.76	1258.29 ± 168.28	1336.37 ± 162.97	5.90 ± 0.17	0.99
Paint_NP1	5	1449.40 ± 186.68	1389.17 ± 192.94	1468.22 ± 180.64	5.79 ± 0.27	0.99
Resin_C	5	1288.40 ± 274.44	1267.46 ± 256.86	1355.43 ± 258.61	6.00 ± 0.19	0.99
Resin_NP2	5	1476.60 ± 340.99	1469.59 ± 333.45	1537.23 ± 326.72	5.89 ± 0.35	0.99

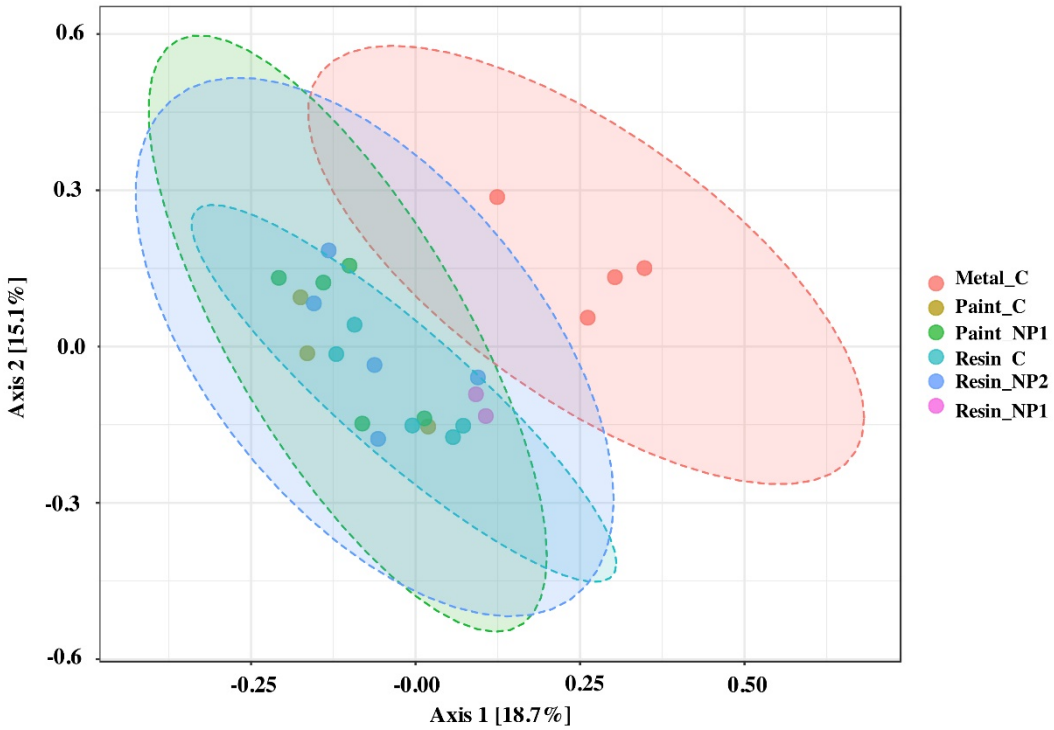

Figure 4.3. PCA plot of 16S rRNA data based on Bray Curtis dissimilarity PERMANOVA analysis: F-value: 2.2566, R-squared: 0.38531, p-value <0.001. Data points belonging to individual samples are coloured according to their respective treatment. Metal_C - Bare aluminium control (Red) n=4; Paint_C - Chlorinated rubber paint control (Gold) n=3; Paint_NP1 - Chlorinated rubber paint treated with $nCeO_2$ (Green) n=5; Resin_C – Alkyd resin control (Turquoise) n=5; Resin_NP2 – Alkyd resin treated with Cu-doped $nCeO_2$ (Blue) n=5; Resin_NP1 – Alkyd resin treated with $nCeO_2$ (Pink) n=2. Figures adapted from using MicrobiomeAnalyst output.

The relative abundance of respective bacterial phyla present in each treatment is presented in Figure 4.4. As can be seen, Proteobacteria, Bacteroidetes and Planctomycetes were most abundant, when combined these represented 84-92% of the bacterial community. Both Proteobacteria and Bacteroidetes have previously been recorded to dominate bacterial assemblages within biofilms formed in the Mediterranean.[380, 381] To examine changes in the relative abundance of phyla between treatments, two-way T-tests were carried out between treatments and the bare aluminium control, as well as between surface coating controls (*i.e.,* chlorinated rubber paint and alkyd resin with no nanoparticles) and respective nanoparticle-treatments. To further examine the impact of the addition of nanoparticles on biofilm community structure DeSeq2 differential abundance analysis was additionally used.[382]

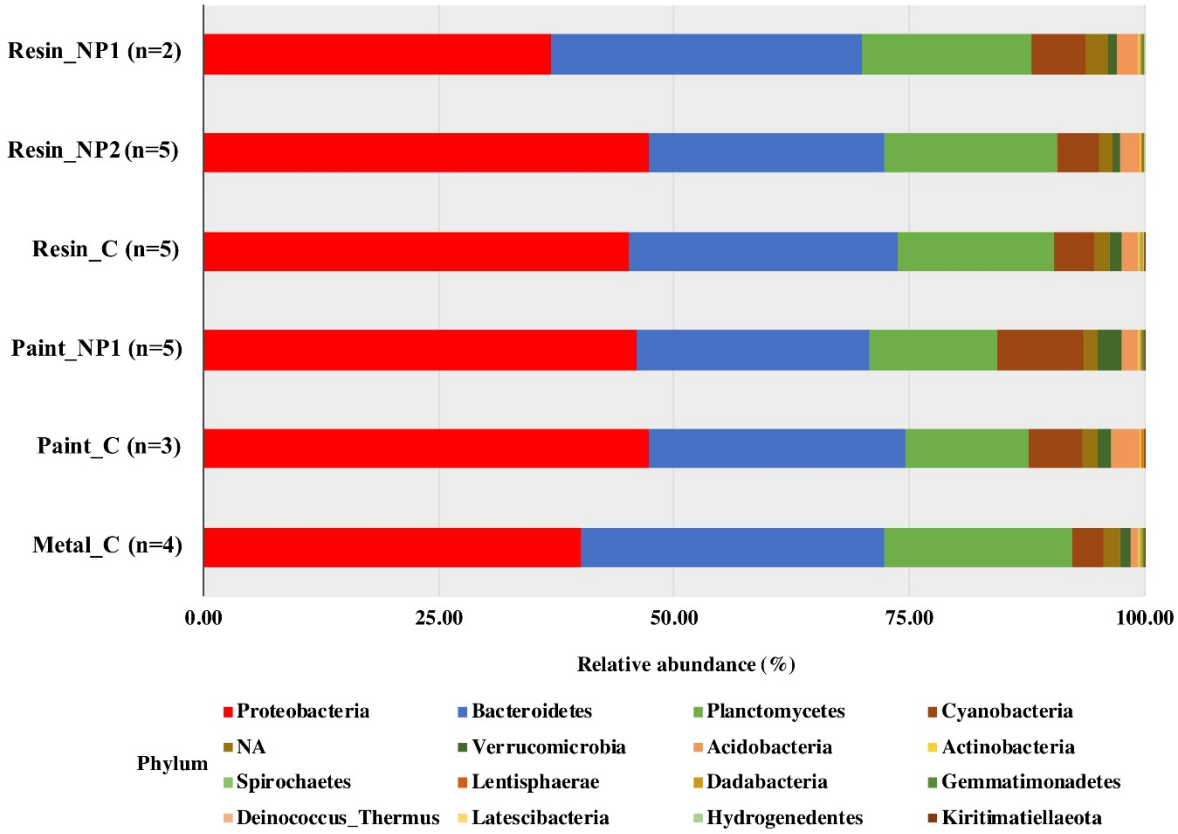

Figure 4.4. Relative abundance (%) of major phyla present in 16S rRNA samples grouped per treatment: Metal_C - Bare aluminium control (n=4); Paint_C - Chlorinated rubber paint control (n=3); Paint_NP1 - Chlorinated rubber paint treated with $nCeO_2$ (n=5); Resin_C – Alkyd resin control (n=5); Resin_NP2 – Alkyd resin treated with Cu-doped $nCeO_2$ (n=5); Resin_NP1 – Alkyd resin treated with functionalized $nCeO_2$ (n=2). Data is presented as the mean relative abundance for each phylum, respectively.

Primarily, significant alterations were identified between the bare aluminium control and surface-coated samples, irrespective of the presence of nanoparticles. Comparatively, little difference was seen upon comparison of bacterial communities formed on paint or resin surfaces in the presence or absence of nanoparticles. Most notably, significant decreases in the relative abundance of the abundant Bacteroidetes and Planctomycetes phyla were identified on all surface-coated samples compared to bare aluminium.

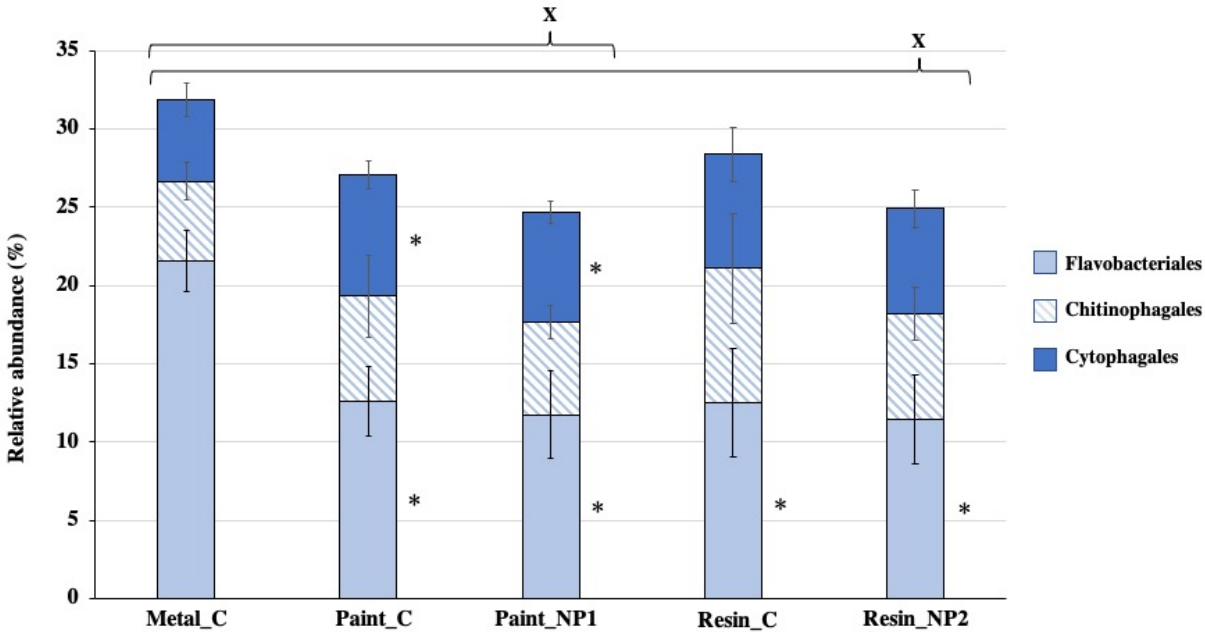

Figure 4.5. Relative Abundance (%) of major the Bacteroidetes orders; Flavobacteriales, Chitinophagales and Cytophagales, grouped per treatment: Metal_C - Bare aluminium control (n=4); Paint_C - Chlorinated rubber paint control (n=3); Paint_NP1 - Chlorinated rubber paint treated with $nCeO_2$ (n=5); Resin_C – Alkyd resin control (n=5); Resin_NP2 – Alkyd resin treated with Cu-doped $nCeO_2$ (n=5). Data is presented as the mean ± standard deviation. Crosses indicate significant differences in the relative abundance of the entire Bacteroidetes phylum between bare aluminium control and surface-coated samples (two-way T-test, $p \leq 0.05$). Stars indicate where relative abundance of each individual order differs significantly between bare aluminium control and surface-coated samples (two-way T-test, $p \leq 0.05$).

The Bacteroidetes phylum, which comprised approximately one third of the bacterial community in all treatments was on average reduced in surface-coated samples compared to the bare aluminium control respectively (Fig 4.5). Two-way T-tests revealed this decline to be significant only when nanoparticles were present ($p \leq 0.05$), indicating some effect of NP1 and NP2 upon the biofilm community formed upon

paint and resin treatments, respectively. Here, relative abundance of Bacteroidetes was reduced up to 8% compared to the bare aluminium control, declining to a similar extent in NP1 and NP2 treatments. The Bacteroidetes are believed highly adapted to surface living, but are thought to primarily contribute to secondary colonisation, feeding upon primary colonising species.[383] As such, a decline in the Bacteroidetes may not reduce overall biofouling of a surface as these are likely to be replaced by other secondary colonisers. Further analyses at lower taxonomic levels revealed that the decline in Bacteroidetes was largely driven by a decline in Flavobacteria (Fig 4.5), which were significantly reduced in all surface-coated samples, irrespective of the presence of nanoparticles, decreasing in relative abundance by ~10% compared to samples formed on bare aluminium (two-way T-test, $p \leq 0.05$). In contrast, the average relative abundance of the Chitinophagales and Cytophagales increased in respect to the bare aluminium control in all surface coatings, significant only for the Cytophagales present in chlorinated rubber paint samples treated with NP1 (two-way T-test, $p \leq 0.05$).

Flavobacteria are believed to be key to the functioning of marine biofilms and thrive when phytoplankton are abundant.[380, 384] These species are known to degrade a wide range of organic materials, playing an important role in nutrient cycling within the biofilm.[385] Previous network analysis of marine biofilm communities, carried out by Pollet *et al.* (2018), revealed that removal of Flavobacteria from a biofilm could cause a loss of connectivity between species and hence loss of other taxa.[380] As such, the decline in Flavobacteria due to the application of a surface coating, be that paint or resin-based, may act to compromise biofilm community development. Flavobacteria have previously been recorded to decrease in abundance within marine biofilms grown on PDMS in the presence of MO NMs.[180] Here, alterations in biofilm community composition were observed to significantly decrease the settlement of invertebrate larvae.[180] The decline in Flavobacteria was observed to be Family-specific, with the Flavobacteriaceae particularly affected (Fig 4.6A). The abundance of Flavobacteriaceae appears to drive the reduction in the Bacteroidetes phylum, displaying an approximate 20-30% decrease in relative abundance of total Bacteroidetes members on all surface-coated samples in respect to the bare aluminium control (two-way T-test, $p \leq 0.05$) (Fig 4.6B). In contrast the relative abundance of

Cryomorphaceae (Fig 4.6C), also a member of the Flavobacteriales, was significantly increased in surface-coated samples (two-way T-test, $p \leq 0.05$). The significant rise in Cytophagales observed in chlorinated rubber paint samples, described above, can be attributed to the respective 10-13% increase in relative abundance of Cyclobacteriaceae (Fig 4.6D) (two-way T-test, $p \leq 0.05$).

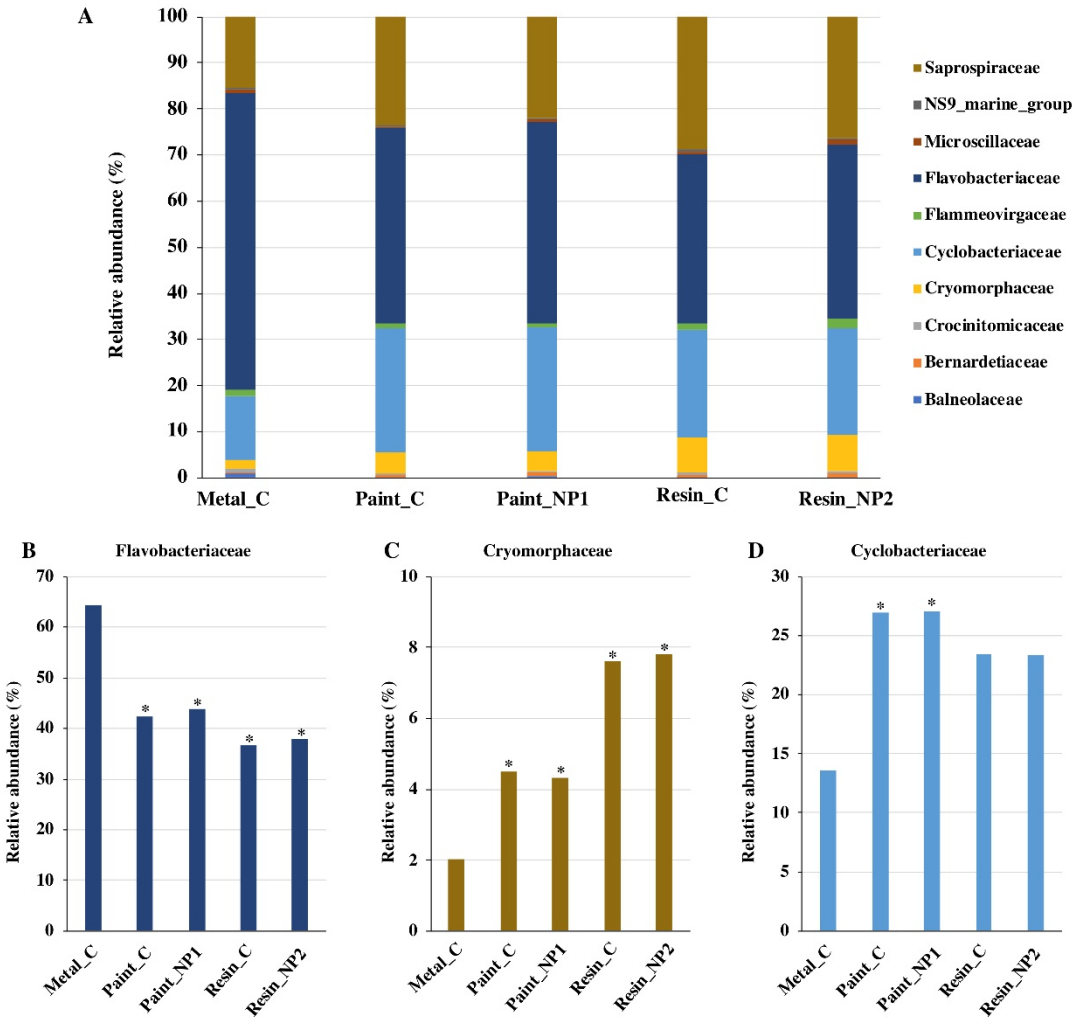

Figure 4.6. Relative abundance (%) of each respective Family within the Bacteroidetes phylum (A). Panels B-D display the respective relative abundance of the Flavobacteriacaea, Cryomorphaceae and Cyclobacteriaceae individually. Here, crosses indicate where two-way T-tests reveal a significant difference in the relative abundance of each Bacteroidete family between bare aluminium control and surface-coated samples ($p \leq 0.05$). Metal_C - Bare aluminium control (n=4); Paint_C - Chlorinated rubber paint control (n=3); Paint_NP1 - Chlorinated rubber paint treated with $nCeO_2$ (n=5); Resin_C – Alkyd resin control (n=5); Resin_NP2 – Alkyd resin treated with Cu-doped $nCeO_2$ (n=5).

The Planctomycetes were also recorded to be relatively less abundant within biofilm communities formed on surface coatings compared to bare aluminium (Fig 4.7). This distinctive bacterial group are believed to be well-adapted to substrate-associated living, and appear more abundant in biofilms than in planktonic environments.[386, 387] Often, Planctomycetes are associated with diatom or algal cells, where they are thought to have the potential to provide secondary metabolites to these phototrophic organisms.[388-390] Current limited data exists to accurately understand the ecological role of the Planctomycetes phylum,[386] however research suggests that some taxa have potentially significant roles in global carbon cycling and nitrogen cycling processes.[386, 387] As such, it is difficult to predict how their reduction in abundance is likely to affect the biofilm community. The Planctomycetes phylum made up ~13-20% of identified bacterial taxa across all samples and were reduced on average when a surface coating was applied, significant for all apart from alkyd resin treated with

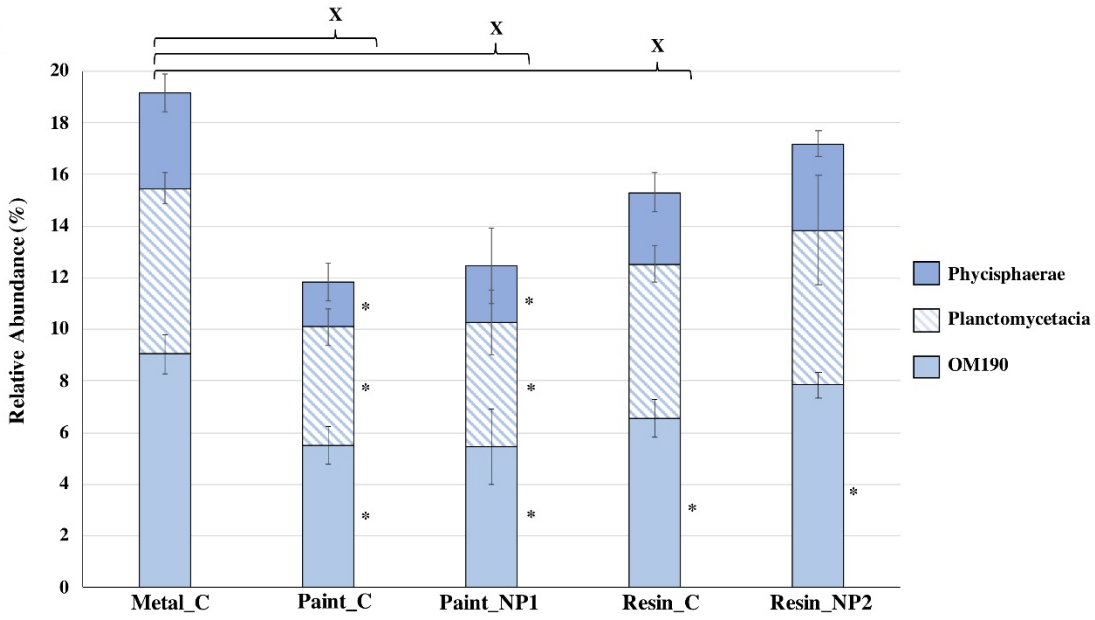

Figure 4.7. Relative Abundance (%) of the Planctomycete phylum, grouped by treatment and represented by the three major Classes: OM190, Planctomycetacia and Phycisphaerae respectively. Metal_C - Bare aluminium control (n=4); Paint_C - Chlorinated rubber paint control (n=3); Paint_NP1 - Chlorinated rubber paint treated with $nCeO_2$ (n=5); Resin_C – Alkyd resin control (n=5); Resin_NP2 – Alkyd resin treated with Cu-doped $nCeO_2$ (n=5). Data is presented as the mean ± standard deviation. Crosses indicate where two-way T-tests reveal a significant difference in the relative abundance of the Bacteroidetes phylum between bare aluminium control and surface-coated samples ($p \leq 0.05$). Stars indicate where relative abundance of each individual Class differs significantly between bare aluminium control and surface-coated samples ($p \leq 0.05$).

NP2 (two-way T-test, $p \leq 0.05$). Here, a decline in relative abundance of ~5-7% was observed, with effects more pronounced in paint compared to resin samples. As with the Bacteroidetes, this decline was again taxa-specific and varied with differing Planctomycete class (Fig 4.7). The OM190 class was significantly reduced in all surface-coated samples, irrespective of the addition of nanoparticles, compared to the bare aluminium control (two-way T-test, $p \leq 0.05$). The greatest decline in the OM190 class was observed in chlorinated rubber paint samples, where relative abundance decreased from 9.05% of total bacteria in the bare aluminium control to 5.51% in the paint control, and 5.47% in paint samples treated with NP1, respectively. The Planctomycetacia and Phycisphaerae were also significantly reduced in paint samples when NP1 was present or absent, compared to the bare aluminium control (two-way T-test, $p \leq 0.05$), however no effect was observed in resin treatments.

Also of note, cyanobacterial abundance displayed an approximately 3-fold increase in the chlorinated rubber paint treatment treated with NP1 compared to the bare aluminium control, increasing in relative abundance from 3.32% to 9.33% (two-way T-test, $p \leq 0.05$). The Acidobacteria were significantly more abundant in the chlorinated rubber paint control relative to bare aluminium, increasing in relative abundance from 0.83-3.11% (two-way T-test, $p \leq 0.05$). Overall, greater differences in bacterial community structure of biofilms caused by presence of a surface coating were apparent in chlorinated rubber paint samples compared to alkyd resin.

Upon comparing the bacterial communities formed upon surface coatings in the presence of nanoparticles in respect to surface coating controls (*i.e.,* paint and resin samples with no nanoparticles added), little variation was observed. For only one phylum, two-way T-tests revealed the relative abundance to vary significantly. In this case, the Spirochaetes phylum was reduced from 0.18% to 0.03% in alkyd resin samples in the presence of NP2 (two-way T-test, $p \leq 0.05$). As mentioned, to identify any subtle impacts of the addition of NP1 or NP2 in chlorinated rubber paint and alkyd resin treatments, pairwise comparisons of differential abundance were also assessed using DeSeq2 analysis.[382] This analysis identified a number of significant variations in abundance of various taxa present within chlorinated rubber paint samples and those treated with NP1. However, many of these were low abundant taxa (relative

abundance, <1%). Notable alterations include a reduction in the Caulobacterales in the presence of NP1 from 3.21% to 1.35% relative to the paint control (-1.54 log2FC) ($p \leq 0.05$). Interestingly, this decline was caused primarily by a decrease in relative abundance of the Hyphomonadaceae family, believed to be primary colonizing species which produce polysaccharide structures, enabling them to attach strongly to a substrate.[391] These organisms are particularly well-adapted to attach to smooth structures and have been recorded to colonize microplastics.[391] The significant reduction of this primary colonizing species upon the addition of NP1 in chlorinated rubber paint samples indicates some antibiofilm activity, which at higher concentrations may have implications for overall biofilm development if other similar taxa are affected. The Arenicelleles were also recorded to decline from 1.7% to 0.7% in the chlorinated rubber paint treatment when NP1 was present compared to the paint control (-1.18 log2FC) ($p \leq 0.05$). Whilst the Oceanospirillales and Opituales (Family - Puniceicoccaceae) both displayed a log2 fold-change of +2.06, increasing in relative abundance on average from 0.32-1.44% and 0.49-1.95%, respectively in chlorinated rubber paint samples when NP1 was added ($p \leq 0.05$). Additionally, the genera *Lentimonas,* belonging to the Verrucomicrobia, and the cyanobacteria *Symphothece*_PCC_700,2 were significantly increased in abundance 0.5% to 2.6% and 1.2% to 2.7% respectively, in the presence of NP1 within paint samples ($p \leq 0.05$). In contrast, DeSeq2 analysis identified little difference between alkyd resin treatments in the presence or absence of NP2. Hence whilst findings are limited, effects of nanoparticles upon the bacterial community appeared enhanced in chlorinated rubber paint treated with NP1 compared to alkyd resin NP2 formulations.

b) Eukaryotic diversity and community composition

The diversity of the eukaryotic community displayed greater variation between treatments than observed with bacterial samples (Table 4.3). On average the number of ASVs identified was higher in surface-coated treatments compared to the bare aluminium control, with the exception of the alkyd resin treated with NP1. However, two-way T-tests revealed that the number of ASVs did not significantly differ between surface-coated samples and the bare metal control, irrespective of the presence of nanoparticles NP1 or NP2, or between surface coating controls (*i.e.,* paint and resin samples in the absence of nanoparticles) and nanoparticle-treated groups. Based on

Table 4.3. *Alpha* diversity of 21-day old marine biofilm eukaryotic communities.
*Results presented as the mean value +/- standard deviation. (Yellow markers indicate where values significantly differ from the bare aluminium control; Orange markers indicate where nanoparticle-treated samples significantly vary from their respective control coating ($p<0.05$)).

			Species Richness		Species Evenness	
Sample	**n**	**ASVs**	**Chao 1**	**ACE**	**Shannon**	**Simpson**
Metal_C	4	265.75 ± 64.11	276.39 ± 66.24	284.80 ± 67.62	2.58 ± 0.29	0.78
Paint_C	4	325.75 ± 59.71	346.65 ± 64.74	284.80 ± 67.62	3.38 ± 0.33	0.92
Paint_NP1	5	353.40 ± 76.37	387.24 ± 70.20	358.54 ± 62.29	3.24 ± 0.23	0.86
Resin_C	5	313 ± 42.35	351.73 ± 52.31	396.66 ± 71.47	3.19 ± 0.18	0.88
Resin_NP1	3	225.67 ± 50.62	234.03 ± 50.24	243.14 ± 51.08	3.17 ± 0.06	0.90
Resin_NP2	5	329 ± 64.97	354.84 ± 65.15	360.07 ± 59.90	3.16 ± 0.18	0.89

Chao1 species richness, only the diversity of biofilms formed on chlorinated rubber paint samples treated with NP1 differed significantly from the bare aluminium control (two-way T-test, $p\leq0.05$). Species richness was found to significantly decrease in the alkyd resin treatment in the presence of NP1 compared to the alkyd resin control for both Chao 1 and ACE measures of diversity (two-way T-test, $p\leq0.05$). The species evenness of 18S rRNA data showed greater variation between surface coated samples and the bare aluminium control. Both Shannon and Simpson indices displayed significant increases in species evenness in all surface-coated samples (two-way T-test, $p\leq0.05$), irrespective of presence of $nCeO_2$, indicating greater diversity in species abundance. However, no significant differences in species evenness were identified upon comparing surface coating controls with NP1 or NP2 treatments. Principle component analysis based on Bray-Curtis dissimilarity and associated PERMANOVA analysis (Fig 4.8) revealed little difference between the eukaryotic communities belonging to various treatments.

The relative abundance of eukaryotic phyla present in biofilm samples for each treatment is presented in Figure 4.9. As with observations upon bacteria, variations in the abundance of eukaryotic members of the biofilm community were primarily observed between those grown on bare aluminium and surface-coated samples, irrespective of the presence of nanoparticles.

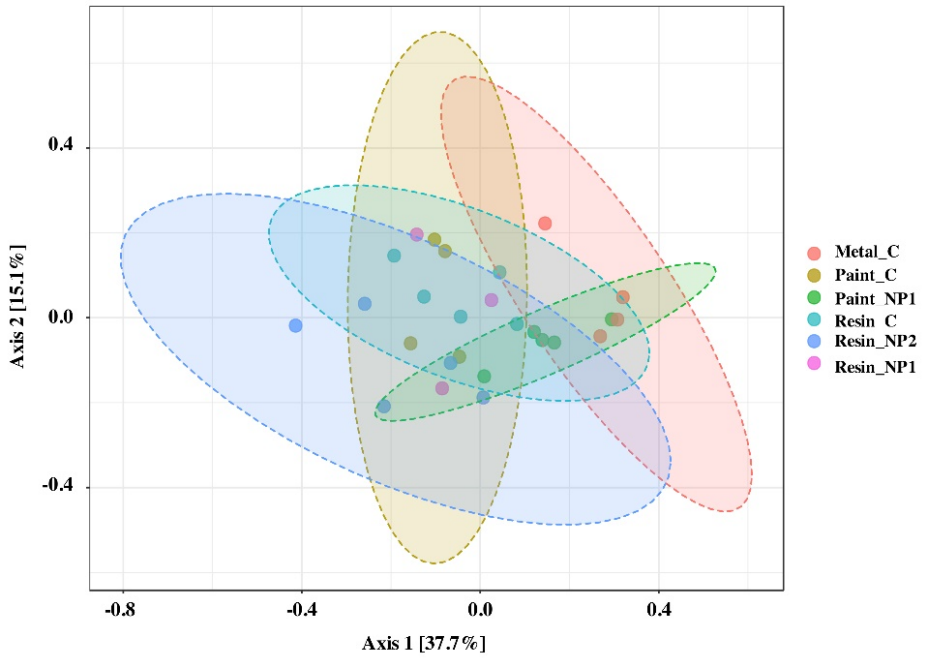

Figure 4.8. PCA plot of 18S rRNA data based on Bray Curtis dissimilarity PERMANOVA analysis: F-value: 3.6997, R-squared: 0.4805, p-value <0.001. Data points belonging to individual samples are coloured according to their respective treatment. Metal_C - Bare aluminium control (Red) n=4; Paint_C - Chlorinated rubber paint control (Gold) n=4; Paint_NP1 - Chlorinated rubber paint treated with $nCeO_2$ (Green) n=5; Resin_C – Alkyd resin control (Turquoise) n=5; Resin_NP2 – Alkyd resin treated with Cu-doped $nCeO_2$ (Blue) n=5; Resin_NP1 – Alkyd resin treated $nCeO_2$ (Pink) n=3. Figures adapted from MicrobiomeAnalyst output.

The eukaryotic assemblage of the 21 d old biofilms was dominated by the Ciliophora, which made-up 60-82% of eukaryotic taxa identified. This phylum represents the 'top predator' in microbial communities[392] and play a key role in energy transfer to higher trophic levels.[393-397] The Ciliophora usually become apparent within a biofilm once primary and secondary colonisation has been established,[398, 399] providing bacterial and eukaryotic prey.[400, 401] Hence, their abundance indicates that well-established biofilms had formed during the 21 d experiment. The abundance of specific Ciliophore taxa is shaped by the respective abundance of various prey, for which specific taxa are well-adapted to predate upon from both the water column and within the biofilm.[400, 401] In addition, Ciliophores are recorded to influence the extent of recruitment of various invertebrate larvae, hence impacting upon the resultant biofouling community established.[402] These features as well as the fact that Ciliophores exhibit a rapid response to environmental change, has led to the phylum being regularly used in water quality assessment,[403, 404] and hence their respective abundance in various surface

coating treatments may provide inside into antibiofilm properties. However, limited effects on the relative abundance of the Ciliophora phylum was recorded.

Across the dataset 3-11% of the community was not assigned to the phylum level during taxonomic assignment. Although measures of species evenness indicated that biofilm communities formed on bare aluminium surfaces displayed significantly lowered diversity, only low abundant phyla (relative abundance, <2%) were observed to vary significantly between bare aluminium and surface-coated samples.

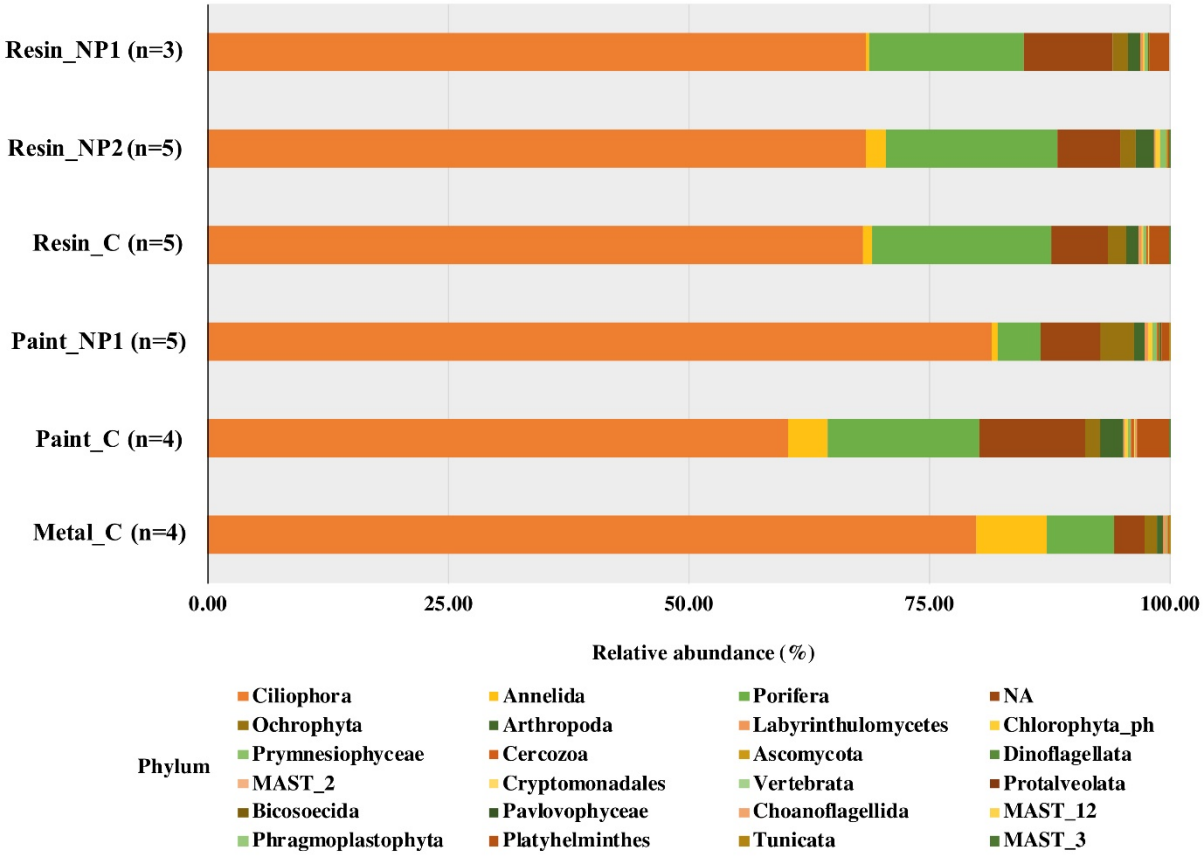

Figure 4.9. Relative abundance (%) of major phyla present in 18S rRNA samples grouped per treatment. Metal_C - Bare aluminium control (n=4); Paint_C - Chlorinated rubber paint control (n=4); Paint_NP1 - Chlorinated rubber paint treated with $nCeO_2$ (n=5); Resin_C – Alkyd resin control (n=5); Resin_NP2 – Alkyd resin treated with Cu-doped $nCeO_2$ (n=5); Resin_NP1 – Alkyd resin treated with $nCeO_2$ (n=3). Data is presented as the mean relative abundance for each phylum respectively.

Few significant differences in the relative abundance of eukaryotic phyla were identified upon comparing communities formed on chlorinated rubber paint or alkyd resin- coated samples in the presence or absence of nanoparticles. No statistically

significant variations were identified between relative abundance of various eukaryotic phyla within biofilms formed on samples belonging to the alkyd resin control and the alkyd resin NP1 treatment, when analysing data using two-way T-tests of relative abundance or DeSeq2 analysis, suggesting limited antifouling properties of NP1 nanoparticles within the alkyd resin matrix. Presence of NP2 in resin treatments was associated with a significant reduction in the relative abundance of the Platyhelminthes from 2.12% to 0.13% in respect to the alkyd resin control (two-way T-test, $p \leq 0.05$), representing a log2 fold change of -4.37 ($p \leq 0.05$). The Platyhelminthes are typically parasitic organisms which prey upon a variety of biota including ciliates, rotifers and amebae,[405] A reduction in parasitic taxa may act to enhance health of the biofilm, hence this effect may not benefit any antifouling impacts of the alkyd resin coating treated with NP2. The abundance of the Prymnesiophyceae was also found to differ significantly between the alkyd resin control and the alkyd resin NP2 treatment, increasing in abundance from 0.30% to 0.67% (two-way T-test, $p \leq 0.05$), representing a log2 fold change of +0.99 ($p \leq 0.05$). These phototrophic organisms comprise species including the coccolithophores and are often ecologically important taxa in coastal environments.[406] Some Prymnesiophyceae taxa are bloom-forming, including toxic bloom formation,[406] hence their increase in abundance is likely to not improve antifouling properties of the surface coating, however this phyla remains relatively low abundant (<1%). Results suggest a slight enhanced impact of NP2 compared to NP1 within the alkyd resin surface coating treatment upon biofilm community dynamics, perhaps attributed to the presence of copper within nanoparticles which may leach Cu^{2+} ions into the biofilm or surrounding waters. However, as reported, impacts upon individual taxa are varied so it is difficult to assess overall antifouling qualities of either nanoparticle type.

Three eukaryotic phyla were identified to be significantly altered by the addition of NP1 in chlorinated rubber paint treatments. Most notably the presence of the most abundant phylum, Ciliophora, was found to significantly increase in the presence of NP1 compared to the chlorinated rubber paint control by ~20% (two-way T-test, $p \leq 0.05$). In the longer-term, the increased abundance of Ciliophores in the presence of NP1, may act to alter the recruitment of invertebrate larvae as the biofilm matures, as described above, or act to reduce numbers of specific bacterial or algal species through

predation by the abundant ciliates. In addition, the relative abundance of the Ochrophyta was recorded to increase from 1.62% to 3.46% upon the addition of NP1 (two-way T-test, $p \leq 0.05$). This significant increase in Ochrophyta in was also recorded using DeSeq2 analysis ($p \leq 0.05$). The relative increase in abundance of phototrophic Ochrophyta taxa in the NP1 treatment, which includes groups such as the diatoms, provides a source of prey for higher trophic levels and may play a part in the increase in Ciliophora abundance also recorded. DeSeq2 analysis also identified the relatively abundant Porifera (Class: Demospongiae) to decrease in relative abundance from 16.04% in paint control samples, to 4.15% in the presence of NP1, representing a 1.83 log2 fold-decrease ($p \leq 0.05$). Additionally, the Sabellida order were found to decrease -9.81 (log2FC) from 3.34% to 0.01% in RA ($p \leq 0.05$).

The data obtained from 16S and 18S rRNA amplicon sequencing highlights the dynamic nature of the biofilm community upon interaction with varying substrates. Application of surface coatings onto bare aluminium caused a significant response in the biofilm community. Communities formed upon bare aluminium appeared distinct to other treatments, likely a result of specific properties of the bare metal surface. Previous works suggest that some colonisers are better able to adhere to coated substrates than bare metal.[407] Similarly, microbial attachment is believed reduced on metals compared to substrates with more hydrophobic and nonpolar properties.[334] An important distinguishing feature between bare aluminium and surface-coated surfaces may be the formation of the conditioning film on each respective coating. Here, organic or inorganic components of the paint and resin matrices may have provided conditions more beneficial for microbial growth,[334] thus driving the establishment of biofilm communities that varied from those on bare metal. It is also true that as a result of dissolution and oxidation, ionic aluminium species and alumina (Al_2O_3) may be released from bare aluminium following entry into seawater.[408] Aluminium oxide has been previously recorded to exert toxic effects upon marine biota such as phytoplankton,[409-411] and hence the presence of such ionic species may have played a role in the response observed upon bare metal presented herein. The oxidative release of ionic aluminium species is likely to also produce ROS. These toxic species are known to exert negative effects towards microbial species[210] and may also play a role in driving variation between bare metal communities and those grown on coated

surfaces. Further investigation is required to reveal the exact mechanisms by which the distinct communities recorded here were established on each substrate respectively.

4.3.2 The impact of surface coating upon total organic carbon and nitrogen content of marine biofilms

To provide greater understanding of the impact of surface coatings incorporating NP1 or NP2 upon marine biofilm formation and to support community analysis, the total organic carbon (TOC) and total nitrogen (TN) content of biofilms was recorded. Figure 4.9 displays the total organic carbon (TOC) and total nitrogen (TN) content of biofilms formed upon each surface coating investigated in this study. It must be noted that given the method of sample preparation and presence of coatings on treated samples, results may be altered by small portions of surface coating or zirconia/silica beads remaining in samples during analysis.

Two-way t-tests were carried out to identify any statistical variation between values obtained from bare aluminium control and surface-coated samples, as well as between surface coating controls (*i.e.,* chlorinated rubber paint and alkyd resin with no nanoparticles) and nanoparticle treatments. For all surface-coated samples, the TOC was higher than that of the bare aluminium control, statistically significant for all but chlorinated rubber paint samples treated with NP1 (two-way T-test, $p \leq 0.05$). TN was also on average higher in all treatments, although only statistically significant for the alkyd resin control (two-way T-test, $p \leq 0.05$). Given that increased extent of fouling will give rise to increased biological material, thus enhancing nutrient content, the higher TOC and TN content of biofilms suggests an increased extent of biofouling upon surface-coated samples compared to bare aluminium. Nutrient analysis appeared to reveal a subtle effect of the addition of cerium oxide-based nanoparticles upon marine biofilms. The presence of NP1 in chlorinated rubber paint samples, and NP2 in alkyd resin samples was recorded to reduce both the TOC and TN on average in comparison to respective surface coating controls, suggesting a slightly lowered extent of biofouling. This is most notable for TOC values which were recorded to decrease from 237.38 and 251.42 ppm to 167.56 and 193.90 ppm for chlorinated paint and alkyd

resin coatings in the presence of NP1 and NP2, respectively. This represented respective 29.1% and 22.9% decrease in average TOC in presence of NP1 and NP2, suggesting a slightly enhanced antibiofouling impact of NP1 within the paint matrix as compared to NP2 added to alkyd resin. However, T-tests did not identify these decreases to be statistically significant (p=0.08, chlorinated paint and p=0.07, alkyd resin respectively). It is possible that should concentrations of NP1 and NP2 added to surface coating formulations be increased, this effect would become more apparent, and such data provides scope for further development and testing. Despite the limitations described, this technique has great potential in the field of ecotoxicology focussing upon aquatic microbial organisms and offers a quick, high-throughput, automated sampling technique that can provide key data relevant to microbial growth and ecosystem functioning.

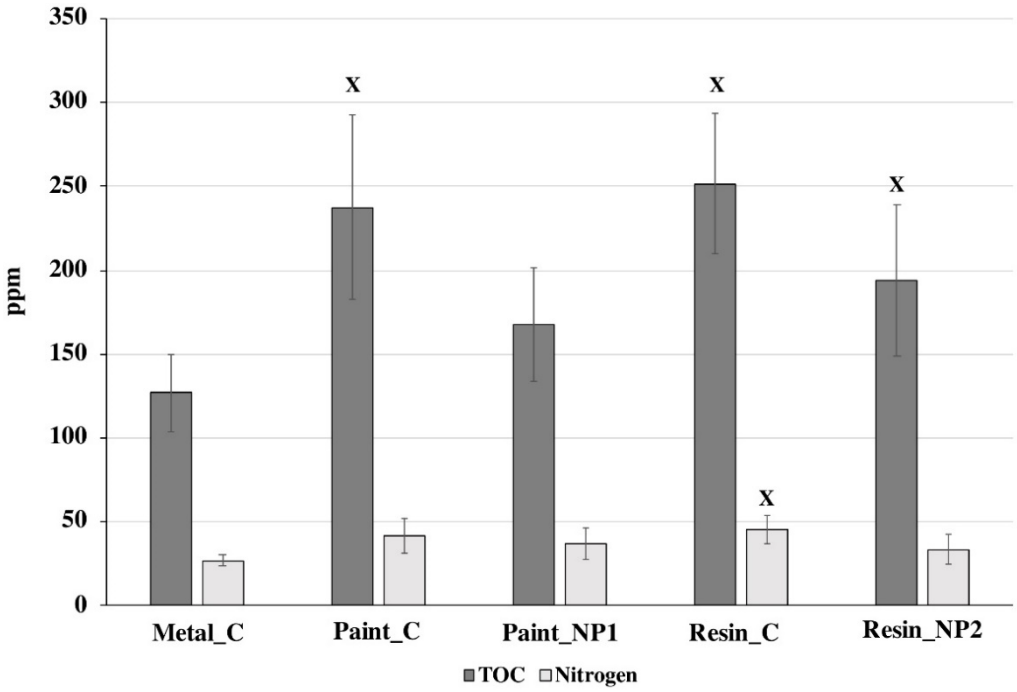

Figure 4.10. Total Organic Carbon (TOC) and Total Nitrogen (TN) content of marine biofilms formed upon aluminium strips with varying surface characteristics. Metal_C - Bare aluminium control (n=5); Paint_C - Chlorinated rubber paint control (n=4); Paint_NP1 - Chlorinated rubber paint treated with $nCeO_2$ (n=5); Resin_C – Alkyd resin control (n=5); Resin_NP2 – Alkyd resin treated with Cu-doped $nCeO_2$ (n=5). Data is provided as the mean ± standard deviation. Crosses indicate where the value differs significantly from the bare aluminium control (Metal_C) as identified by a two-way T-test ($p \leq 0.05$).

4.3.3 3D microscopic analysis of marine biofilms grown on $nCeO_2$ surface coatings.

To complement amplicon sequencing and nutrient analysis experiments, it was the aim to use microscopic techniques to quantify biofilm characteristics (*i.e.,* biomass, depth, percentage cover) using COMSTAT2 analysis, as has been done previously.[375, 412, 413] However, due to a number of limitations, it was not possible to acquire accurate and sufficient data using these methods. Here, biofilm depth, alongside warping and weathering of samples made image acquisition impossible on a number of samples due to the creation of an uneven surface, thus hindering the ability to focus the microscope. As such, data was only collected for a limited number of biofilm samples. Therefore, the results presented are displayed in support of other findings and for use in optimizing this sampling technique for future study. It was possible to perform COMSTAT2 analysis on 5 out of 12 samples, and a summary of the data obtained is presented in Table 4.4.

For the bare aluminium control 1 (Metal_C), and alkyd resin treated with NP1 (Resin_NP1) samples, only three z-stacks could be utilised for analysis; for all other samples five z-stacks were used. Measured parameters did not vary greatly between biofilms formed on surface coatings and bare aluminium. The average biofilm biomass was measured to range from 11.84 to 56.46 $\mu m^3/ \mu m^2$, with both values being recorded on bare aluminium samples. Taking into account all five samples analysed by the COMSTAT2 technique an average biomass of 32.04 $\mu m^3/ \mu m^2$ was observed. Similarly, upper and lower ranges of average biofilm thickness was observed in bare aluminium samples, ranging from 12.19 to 60.59 µm. Extent of biofilm area cover did not appear to vary greatly between individual samples, here an average area of 68.10±4.01% was recorded to be covered by biofilm. Representative microscopic images from within individual z-stacks and associated COMSTAT2 output for biofilm thickness are presented in Figures 4.11-4.15, for each sample respectively. Fluorescent microscopy revealed the high extent of biofouling on samples and the presence of the EPS matrix (Fig 4.16). EPS was observed to create a fluorescent signal during analysis, so disrupting image acquisition. However, as EPS is part of biofilm matrix, it is debatable whether this should be included or excluded from data and calculation of biofilm properties. Due to the fact that the COMSTAT2 programme utilised for

analysis is designed for bacterial samples, presence of eukaryotes, in particular larger organisms such as ciliates commonly observed in the study presented here, are also likely to have altered results. Despite these limitations, the use of such imaging techniques may provide useful information upon marine biofilm formation in future studies, particularly during early stages where biofilm depth is reduced, and bacteria dominate the assemblage. As such their incorporation into future experiments is recommended alongside complementary techniques.[414]

Table 4.4. Summary of data obtained from COMSTAT2 analysis of 21 d marine biofilms grown on varying surface coatings applied to aluminium strips.

Variable	Metal_C 1	Metal_C 2	Paint_C 1	Paint_C 2	Resin_NP1	Average
Biomass ($\mu m^3/\mu m^2$)	56.46 ± 6.57	11.84 ± 5.10	32.28 ± 17.86	25.33 ± 12.61	34.27 ± 15.68	**32.04 ± 16.24**
Max. Thickness (μm)	78.33 ± 12.06	16.60 ± 2.41	48.40 ± 22.01	35.20 ± 14.53	43.86 ± 24.27	**44.48 ± 22.50**
Average Thickness (μm)	60.59 ± 5.55	12.19 ± 4.65	36.71 ± 20.25	27.56 ± 13.60	36.53 ± 17.57	**34.71 ± 17.56**
Average % area cover	71.47 ± 3.81	65.49 ± 20.32	62.64 ± 10.42	68.84 ± 12.02	72.08 ± 8.52	**68.10 ± 4.01**

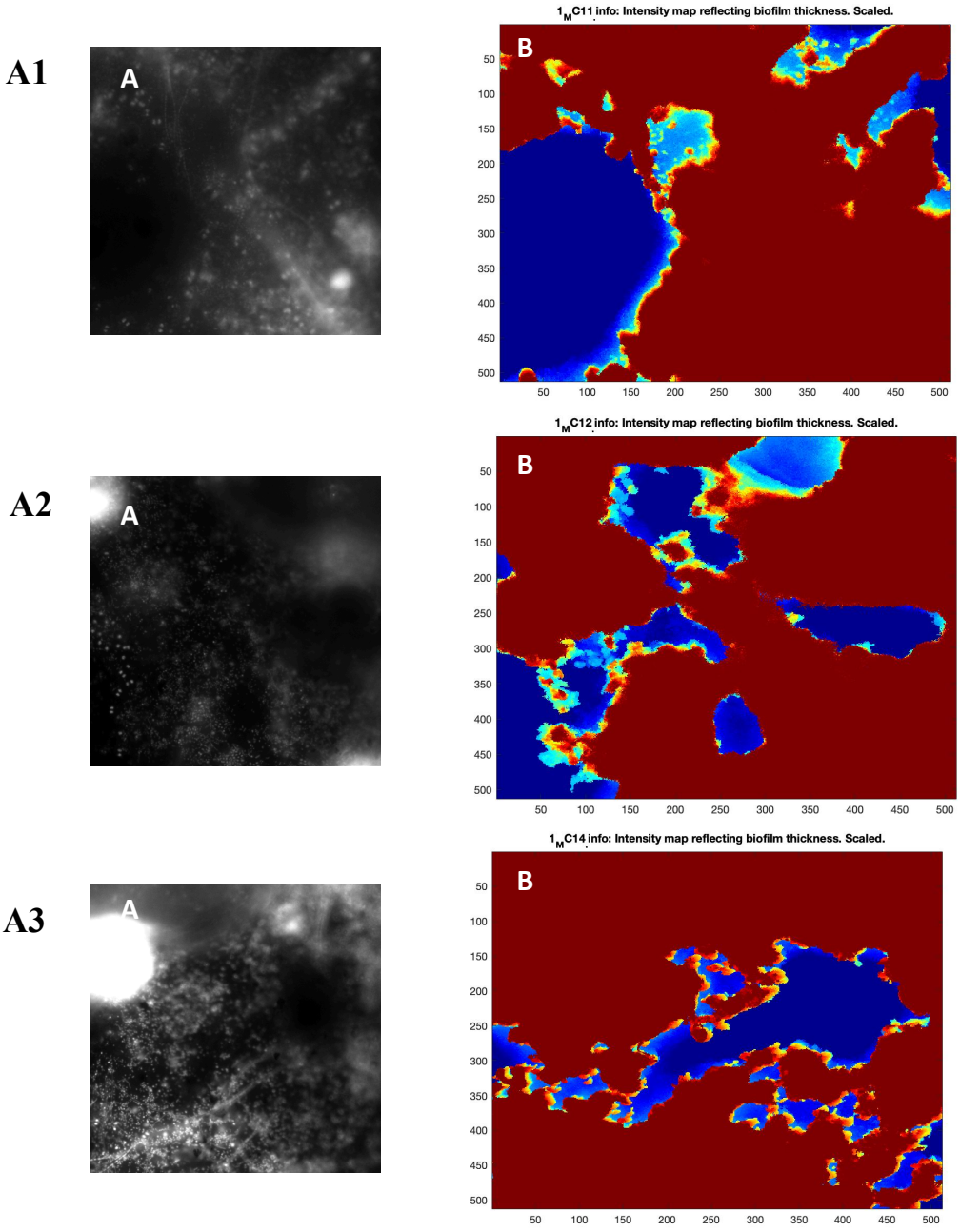

Figure 4.11. COMSTAT2 analysis of bare aluminium control 1 (Metal_C 1) z-stacks (n=3, A1-A3) In panel A, a respective .tif image obtained during fluorescent microscopy is presented, taken from the mid-point of the z-stack being analysed. Panel B displays the COMSTAT2 output for biofilm thickness where blue areas indicate areas of low biofilm thickness, and red areas represent those where biofilm thickness was highest.

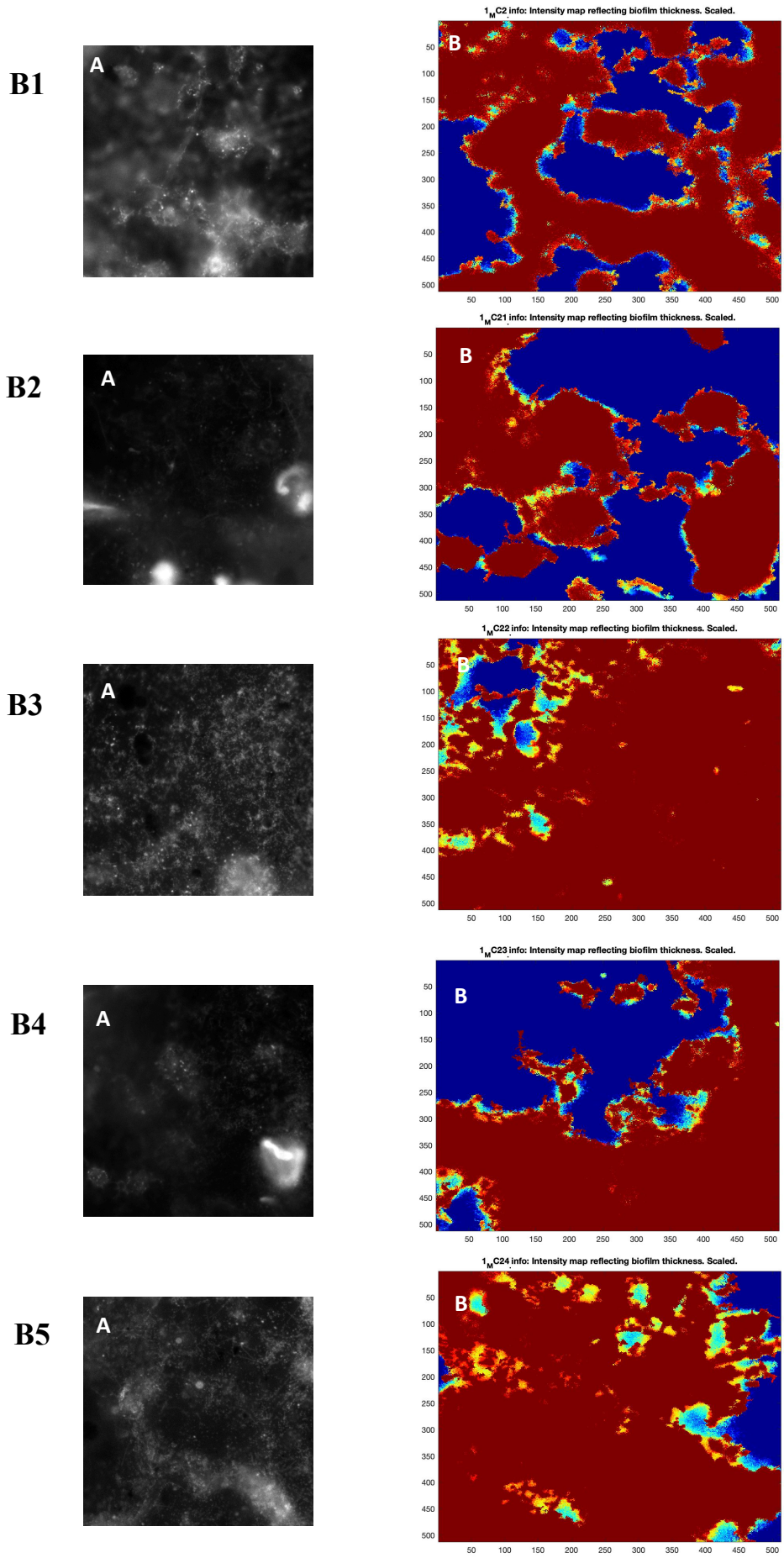

Figure 4.12. COMSTAT2 analysis of bare aluminium control 2 (Metal_C 2) z-stacks (n=5, B1-B5); In panel A, a respective .tif image obtained during fluorescent microscopy is presented, taken from the mid-point of the z-stack being analysed. Panel B displays the COMSTAT2 output for biofilm thickness where blue areas indicate areas of low biofilm thickness, and red areas represent those where biofilm thickness was highest.

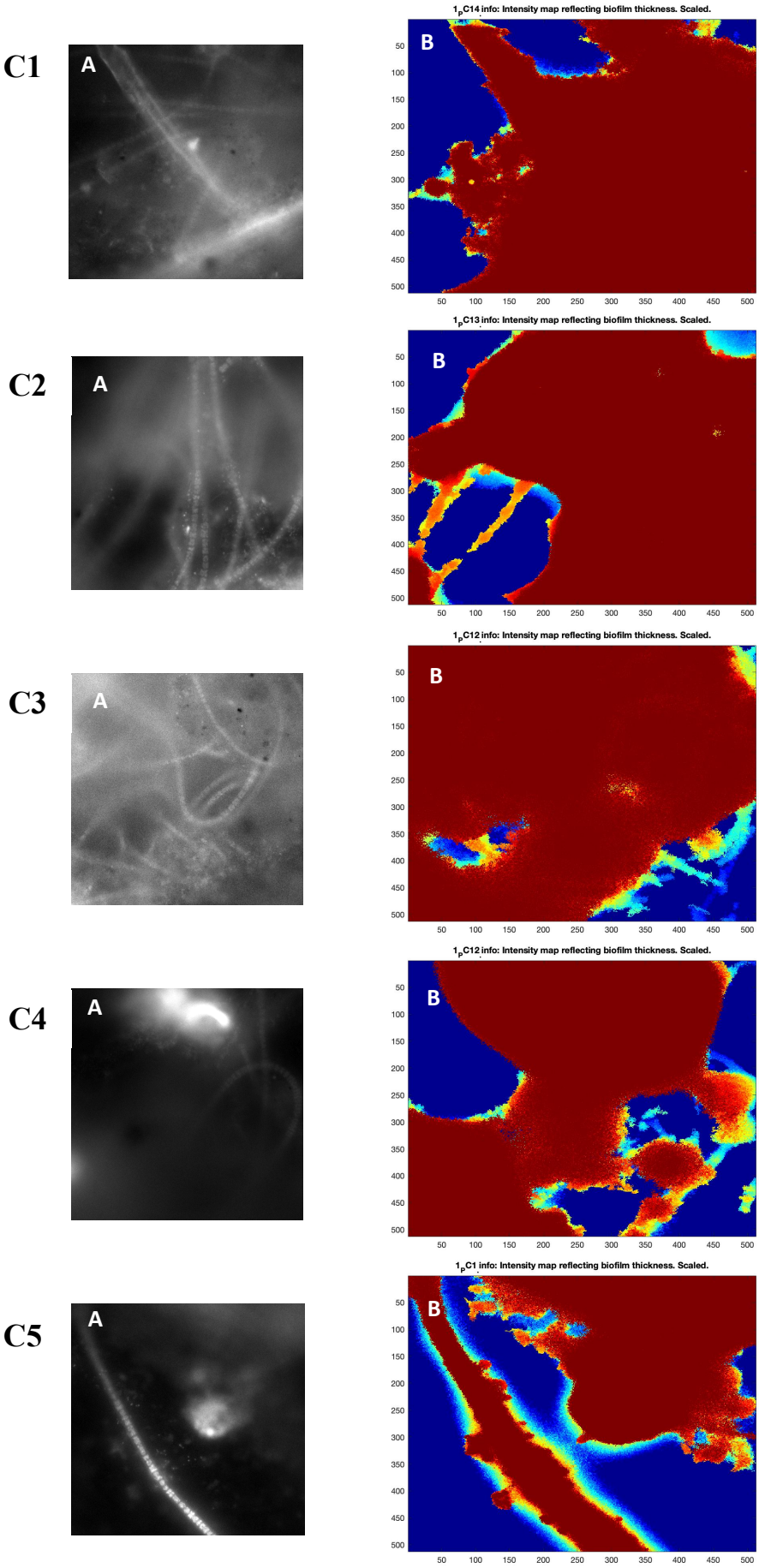

Figure 4.13. COMSTAT2 analysis of chlorinated rubber paint control 1 (Paint_C 1) z-stacks (n=5, C1-C5); In panel A, a respective .tif image obtained during fluorescent microscopy is presented, taken from the mid-point of the z-stack being analysed. Panel B displays the COMSTAT2 output for biofilm thickness where blue areas indicate areas of low biofilm thickness, and red areas represent those where biofilm thickness was highest.

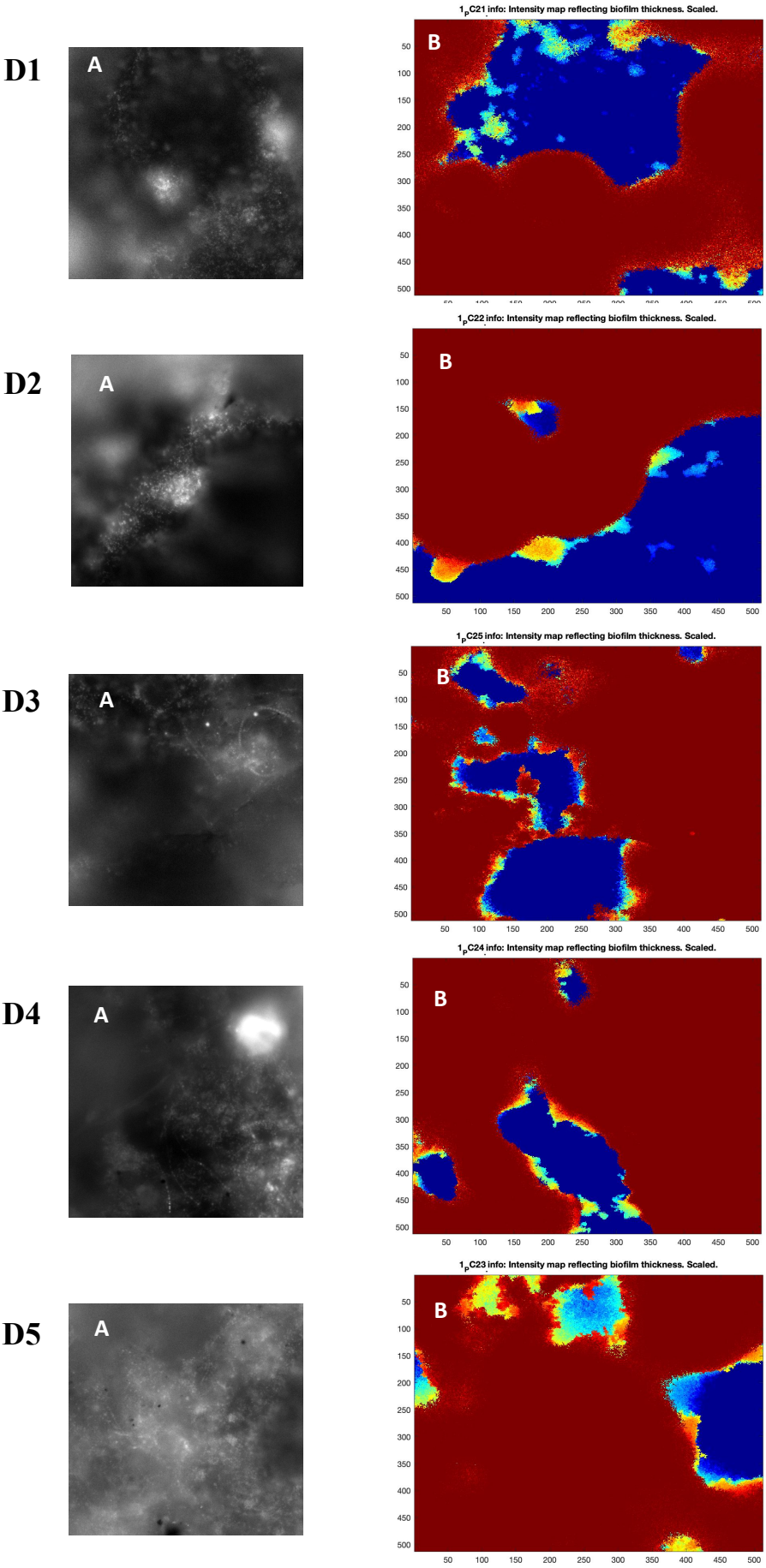

Figure 4.14. COMSTAT2 analysis of chlorinated rubber paint control 2 (Paint_C 2) z-stacks (n=5, D1-D5); In panel A, a respective .tif image obtained during fluorescent microscopy is presented, taken from the mid-point of the z-stack being analysed. Panel B displays the COMSTAT2 output for biofilm thickness where blue areas indicate areas of low biofilm thickness, and red areas represent those where biofilm thickness was highest.

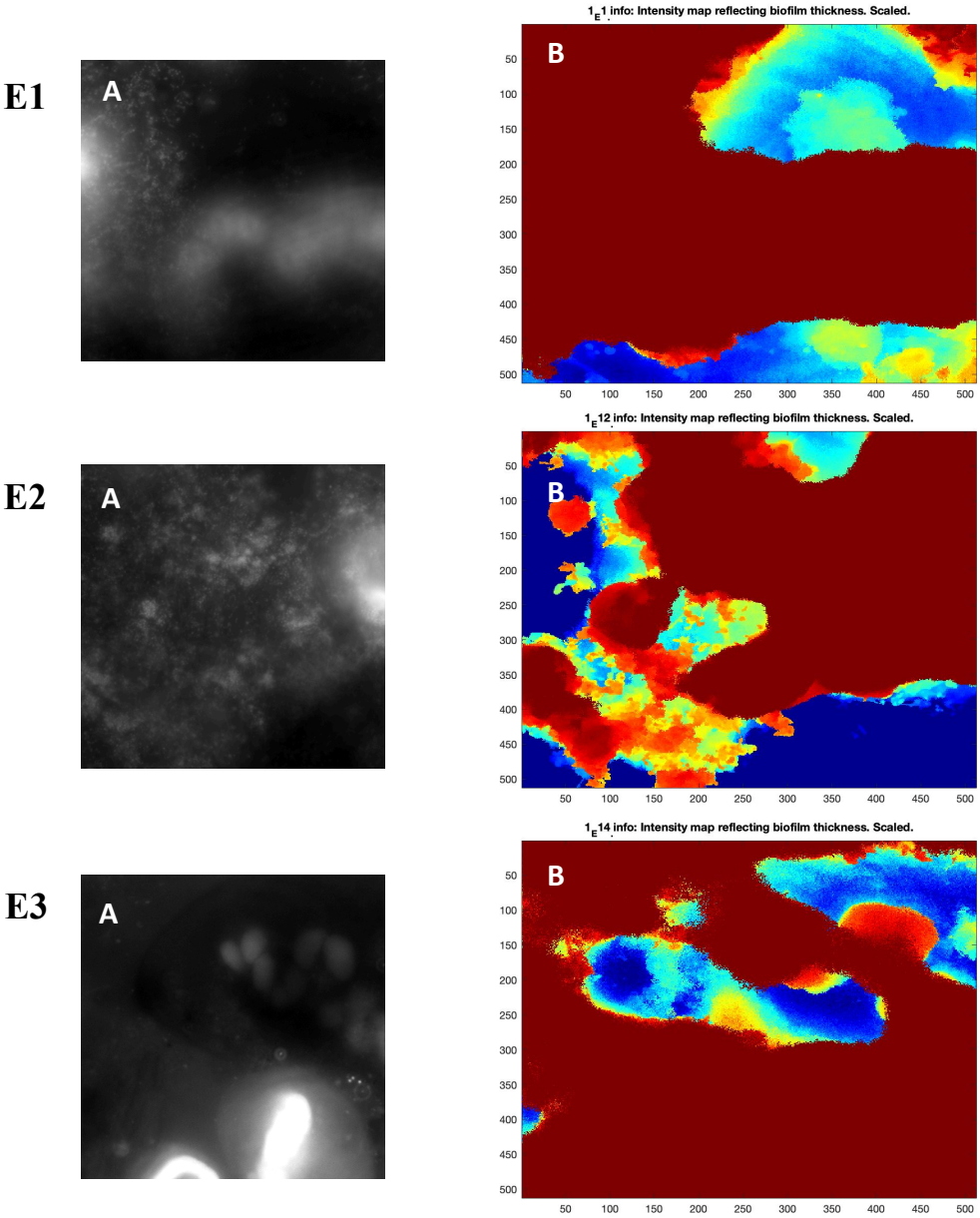

Figure 4.15. COMSTAT2 analysis of alkyd resin treated with NP1 (Resin_NP1) z-stacks (n=5, E1-E5); In panel A, a respective .tif image obtained during fluorescent microscopy is presented, taken from the mid-point of the z-stack being analysed. Panel B displays the COMSTAT2 output for biofilm thickness where blue areas indicate areas of low biofilm thickness, and red areas represent those where biofilm thickness was highest.

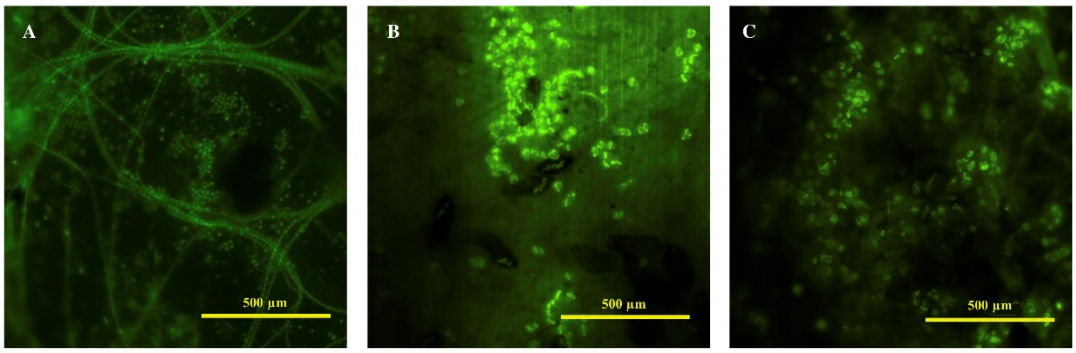

Figure 4.16. Example images of biofilm communities stained with 1X SYBR Gold obtained using fluorescent microscopy under GFP fluorescence (10x magnification); Images A and B were obtained from bare aluminium control samples; image C was obtained whilst imaging the alkyd resin control (no nanoparticles).

4.4 Chapter Summary

Marine biofouling remains an economical concern, and there is need for development of effective and "environmentally-friendly" antifouling surface coatings. In this study, chlorinated rubber paint and alkyd resin formulations were treated with cerium oxide-based nanoparticles and applied to bare aluminium, in order to examine their impact upon marine biofilm formation under natural conditions. Diverse biofilm communities were established on all surface coatings tested, irrespective of the addition of nanoparticles, as well as upon bare aluminium. However, community structure of biofilms grown on bare metal appeared distinct, likely due to the substrate-specific properties of the bare aluminium surface earlier discussed.

The addition of cerium oxide-based nanoparticles NP1 and NP2 to base surface coating formulations (*i.e.,* chlorinated rubber paint and alkyd resin without nanoparticles) had limited additional impact on community structure. However, a number of subtle taxa-specific responses were recorded. Typically, alterations between community structure of biofilms formed upon bare metal and surface coatings were more pronounced on chlorinated rubber paint treatments compared to alkyd resin, irrespective of the presence of nanoparticles. Due to the lack of direct comparison between NP1 and NP2 in analysis of 16S rRNA data because of exclusion of the alkyd resin NP1 treatment, it is difficult to compare the effectiveness of NP1 *versus* NP2, which was doped with copper. However, findings from 18S rRNA data

suggest an enhanced impact of NP2 on the structure of marine biofilm communities when included in alkyd resin formulations compared to NP1, likely due to the addition of copper which may leach into the biofilm or local environment. The addition of nanoparticles to surface coating formulations was observed to decrease average TOC and TN content of biofilms in respect to surface coatings without the nanoparticles, suggesting a reduced extent of biofouling and hence antifouling properties. It is possible that if concentrations of NP1 and NP2 were increased, this antifouling effect would be enhanced. In antifouling paints currently available, the active biocidal agent can be added at concentrations of up to 48% w/v,[415] in this study a concentration of 1.9% w/v was used, therefore it is feasible to suggest the surface coatings incorporating cerium oxide-based nanoparticles investigated herein would be more effective at the relatively high concentrations used in commercial products.

The taxa-specific response recorded during 16S and 18S rRNA analysis, highlights the great difficulty facing researchers in developing anti-biofilm substances that will have a wide and lasting effect upon communities, whilst not exerting a harmful response upon other wildlife. The wide ranging diversity of organisms that are able to effectively colonise surfaces and variation in attachment strategies exacerbates this issue.[338] By identifying taxa that appear more sensitive to a particular surface coating, it may be possible to gain useful insight into the possible mechanisms driving this response and apply this to produce more effective solutions in the future. For example, Flavobacteria recorded to significantly reduced by presence of a surface coating herein, appear a keystone species with marine biofilms, whose removal could compromise biofilm development. Alterations to the biofilm community may also impact upon invertebrate larval settlement, as observed by Yang *et al*. (2016) who reported that attachment of mussel larvae to biofilms was significantly lowered following both AgNP and $nTiO_2$ exposure.[177, 180] The colonisation of submerged surfaces in the aquatic environment occurs rapidly.[416, 417] Specific taxa such as the Rhodobacteriales are reported to be key primary colonisers, establishing the initial biofilm community.[417] Research suggests that due to succession and recruitment of secondary colonising bacterial species and eukaryotes, the biofilm community tends to converge over time so reducing variation between communities where initial colonisation was observed to vary.[418] Therefore, it is feasible to suggest that in early stages, biofilm community structure could have differed between the surface coating

treatments investigated during this study. Whilst the 21-d period utilised in this study allowed for the growth of well-established biofilm communities, a limitation of this sole timepoint is the inability to investigate initial stages of microbial colonisation and identify primary colonising species. Such information would allow for the specific targeting of antimicrobial agents towards those species which appear critical to the initial establishment of biofilm communities, and thus are key to biofouling. In future work assessing the effects of novel surface coatings, a range of timepoints spanning early and late succession stages will be beneficial. However, it remains that antifouling coatings must remain effective for relatively long periods, hence investigation over extended periods is still key. Despite the limitations discussed above, the approaches utilised in this study, offer a comprehensive investigation into biofilm properties and present great scope for future research.

Chapter 5

Nano-pollutants – Big impact?

5.1 Summary of findings

Through the works presented in this thesis, new evidence has been provided upon the impact of engineered NMs commonly utilized in commercial goods towards marine microbial organisms, including some of the first ecotoxicological assessment carried out upon the ecologically significant cyanobacterium *Prochlorococcus*. A comprehensive approach was used to understand ecotoxicity of common NMs under environmentally relevant conditions, before elucidating mechanistic features of exposure using a combination of NM characterisation, molecular techniques, and imaging to assess both organismal and community fitness, as well as cell-nanoparticle interactions. The development of novel experimental approaches provides scope and recommendations for future research in the field of nano-ecotoxicology.

In the first experimental chapter, the ecotoxicity of citrate-stabilised AgNPs was investigated. The global demand for AgNPs, and their inevitable release into the environment, is rapidly increasing. These NMs display antimicrobial properties and have previously been recorded to exert adverse effects upon marine phytoplankton. However, previous ecotoxicological research is often compromised by the use of non-ecologically relevant conditions, and hence the mechanisms of AgNP toxicity under environmental conditions remains unclear. Whilst *Prochlorococcus* represents the most abundant photosynthetic organism on Earth and contributes significantly to global primary productivity, little ecotoxicological research has been carried out on this cyanobacterium. To address this, *Prochlorococcus* was exposed to citrate-stabilised AgNPs, as well as silver in its ionic form, under simulated natural conditions. Both AgNPs and ionic silver were observed to reduce *Prochlorococcus* populations by over 90% at concentrations ≥10 μg L^{-1}, representing the upper limit of AgNP concentrations predicted in the environment (10 μg L^{-1}).[53] The extent of toxicity recorded between nanoparticle and ionic silver treatments was remarkedly similar,

recording significant cell declines of up to 95% and 96% in the presence of dissolved silver (Ag_2SO_4) and AgNPs, respectively. Since in dissolved silver treatments, bioavailable silver was in its ionic form, whereas this was not the case in AgNP treatments, this indicated the occurrence of a nanoparticle-specific effect, warranting further investigation. Longer-term assessment revealed significant declines to be a perturbation which was irreversible. The extent of toxicity was strongly dependent on cell density, and completely mitigated in more cell-dense cultures. To aid analysis the number of AgNPs applied per cell (NPs $cell^{-1}$) in each treatment was estimated, revealing a toxic threshold of 1000 NPs $cell^{-1}$ for the AgNPs used in this work. Hence, the calculation and reporting of the particle-to-cell ratio reveals that this parameter is effective for standardisation of experimental work and allows for direct comparison between studies where cell density may vary. Through use of quenching agents for superoxide and hydrogen peroxide, alongside incubations with ionic silver, it was revealed that AgNP toxicity likely arises from synergistic effects of toxic superoxide species generation and leaching of ionic silver. Subsequent shotgun proteomic analysis revealed that at toxic concentrations (5000 NPs $cell^{-1}$), approximately 20% of the cellular proteome of Prochlorococcus was significantly altered. Here, in accordance with the belief that SOx plays a key role in AgNP toxicity towards Prochlorococcus, the putative nickel-containing superoxide dismutase was significantly up-regulated in the presence of AgNPs in the cellular proteome.

Metal oxide NMs represent the highest produced nano-compounds worldwide, utilised for many purposes that may facilitate their entry into the natural aquatic environment (*e.g.,* fuels, sunscreens and cosmetic products). In the second experimental chapter of this thesis, the impact of common MO NMs ($nTiO_2$ and $nCeO_2$) upon model and natural marine microbial species was examined. Such materials have a clear pathway into the marine environment through the use of $nTiO_2$ in cosmetics products such as sunscreen which enter the marine environment directly, or indirectly through release into wastewater, and use of $nCeO_2$ as a fuel additive released by terrestrial and waterborne transport. Short term (<72 h) exposure revealed evidence of significant cell decline of the cyanobacterium *Prochlorococcus* in response to both $nTiO_2$ and $nCeO_2$ under environmentally relevant conditions (*i.e.,* oligotrophic NSW and μg L^{-1} NM concentrations). Following 72 h exposure, cell density of *Prochlorococcus* was reduced up to 70%. However, no evidence of such declines was observed following

72 h growth in cell-dense cultures grown in nutrient-rich Pro99 media as a result of such treatments. Protocols were established to extract nanoparticles from consumer nano-products, enabling the comparative toxicity of research-grade and consumer nanoparticles to be assessed. This work revealed evidence of significant declines of *Prochlorococcus* in response to such materials under natural conditions, however, these were lower in severity than those recorded in response to research-grade NMs under the same experimental conditions. Exposure of a natural community to such extracted products to an environmentally-relevant concentration (25 μg L^{-1}), revealed little impact of exposure upon natural marine microbial communities. Rather, effects are heightened when whole product formulations are introduced to microbial species, indicating a negative impact of other components of the product formulation, and hence highlighting the importance of considering the whole product matrix during work with consumer nanoproducts.

Interestingly, when MO NM exposures were extended to 240 h, a dynamic interaction between nanoparticles and microbial species was revealed. Under natural conditions, *Prochlorococcus* was observed to recover following initial significant cell decline in response to both $nTiO_2$ and $nCeO_2$, only experiencing negative impacts of exposure in response to supra-environmental concentrations (*i.e.,* 100 mg L^{-1}). This is unlike AgNP exposures, where declines of Prochlorococcus were irreversible. Hence, suggesting that the environmental risk of such NMs to marine microbial species under natural conditions is low. In contrast, cell-dense cultures which appeared more resilient in short-term exposure, appeared to suffer greater effects of MO NM treatments in the longer-term. Here, at concentrations relevant to the environment (*i.e.,* 10 and 100 μg L^{-1}) $nTiO_2$ was observed to significantly reduce cell density following 240 h. DLS was used to monitor the behaviour of $nTiO_2$ and $nCeO_2$ upon entry into NSW. This revealed a rapid and extensive aggregation of nanoparticles in saline media, which resulted in the sedimentation of aggregated material. Indeed, during extended exposure, deposited material was observable in culture flasks. Fluorescent microscopy was used to confirm that deposited material comprised of *Prochlorococcus* entrapped within aggregates of $nTiO_2$ or $nCeO_2$, which had subsequently been removed from the water column *via* sinking. The mechanism of cell entrapment through NM aggregation and subsequent co-precipitation is believed the key driver of cell decline observed in experimental work. It is possible that

significant cell declines observed in studies utilising high concentrations of MO NMs may well result from this process, where shading effects may also occur, compromising the photosynthetic activity of phototrophic organisms. This theory is supported by shotgun proteomic analysis, which revealed negligible impacts of $nTiO_2$ exposure upon the cellular or extracellular proteome of *Prochlorococcus*. Over time it is believed that through the processes of aggregation and sedimentation, the bioavailability of MO NMs such as $nTiO_2$ and $nCeO_2$ will be reduced. Therefore, we can predict that the risk of such materials to planktonic species will be reduced in the longer term, however these processes may facilitate the accumulation of NMs in benthic and sediment zones, where they may impact upon biota. The remarkably similar fate and impact of $nTiO_2$ and $nCeO_2$ recorded throughout this work, raises the possibility of a generalised behaviour of MO NMs in the marine environment, and hence provides useful information for evaluating their likely environmental risk.

In the final chapter, works were extended to investigate the impacts of nano-enabled products upon marine biofilm formation. Novel $nCeO_2$ antifouling surface coatings developed by an industrial collaborator were revealed to have little effect on biofilm formation or community structure. Noticeable differences were recorded between communities formed on bare metal compared to coated surfaces, in accordance with the literature outlining that specific surface characteristics determine colonisation. However, the presence of $nCeO_2$ within surface coatings had little impact upon the diversity or composition of marine biofilm communities. Whilst limited information on the likely impact of such nano-enabled surface coatings was gained, the experimental approach utilised provides scope for future ecotoxicological experimentation. By combining 16S and 18S rRNA amplicon sequencing with imaging and nutrient analysis, a comprehensive insight into effects upon biofilm formation and structure can be gained. Here, the incorporation of early timepoints will better facilitate the understanding of initial colonisation processes.

5.2 Evaluating the environmental risk of nanomaterials towards marine microorganisms.

Engineered NMs represent an emerging contaminant. It is believed approximately 0.4-7% of all manufactured NMs will enter the aquatic environment,[419] where the ocean

represents the eventual sink. It is well established and is strongly supported by works presented in this thesis that NM fate and behaviour in experimental media largely drives their interaction and effect upon biota. The propensity of engineered NMs to aggregate in saline media has been displayed repeatedly in both the works presented in this thesis and published literature. Both metal and MO NMs have been shown to aggregate immediately upon entry into natural seawater, with the latter doing so in a more extreme manner. Whilst AgNPs remain in the water column where they exert detrimental effects upon planktonic species such as the cyanobacteria studied herein, the action of MO NM aggregation results in an increase in density of particles and facilitates their transport through the water column towards deeper zones due to sedimentation. This action reduces the bioavailability of such materials to planktonic species as time increases, thus reducing their risk of exposure, as seen in the works examining the toxicity of $nTiO_2$ and $nCeO_2$ herein. However, if such processes are to occur in the natural environment, the bioavailability of NMs to marine sediment-dwelling and benthic species is likely to increase. Here, it is particularly important to increase research on the impact of exposure on sediment-dwelling and benthic microbes which have been little examined, as well as taxa occupying higher trophic levels such as filter-feeding organisms where bioaccumulation of NMs may occur.

Based on the works presented in this thesis, the environmental risk of engineered NMs towards planktonic marine microbial species appears low. Toxic impacts are restricted to concentrations at the upper limit of those predicted to occur in the environment and supra-environmental values. Natural communities appear little affected by NMs extracted from consumer products which are likely to enter the coastal environment, as well as whole nano-product formulations, at environmental concentrations. The adverse impact of NMs upon the model cyanobacterium, *Prochlorococcus* examined in our work, is largely dependent upon material type (*i.e.,* metal or metal-oxide) and their respective fate and behaviour in saline media, in accordance with previous research. However, given that significant impacts are only observed at relatively high concentrations, exceeding those predicted in the environment, it is unclear how the fate and behaviour of NMs at lower concentrations might influence their impact on biota in the natural environment. At lower concentration as NMs become more dilute, their likelihood of interaction with other natural particles and other NMs is reduced, and as such processes such as the entrapment of cells and subsequent co-precipitation

observed herein are less likely to occur in nature. Efforts must be directed towards establishing effective methods to comprehensively understand the fate and behaviour of NMs at these low concentrations.

Whilst NMs appear low risk at current environmental concentrations, such a conclusion may have been formed when discussing pollutants such as plastic debris many years ago, which has now developed into a global concern. Given that at supra-environmental concentrations, NMs are recorded to exert detrimental effects, we have an opportunity to take early action to monitor and control their entry into the environment and therefore prevent negative effects occurring in the future.

5.3 Research gaps and recommendations for future research

As a result of the works presented in this thesis, a number of recommendations for future research in the nano-ecotoxicological field have been generated. As mentioned above, a major focus of nano-ecotoxicological study must be directed towards establishing effective analytical techniques to accurately record engineered NM concentrations in the environment.[420] In addition, approaches which are able to comprehensively characterize the state of NMs in the environment (*i.e.,* aggregation, oxidative state, dissolution) will be beneficial. It is likely such an approach will require multiple techniques working in tandem, for example in a similar manner to the use of DLS alongside pyrolysis GC-MS to identify nanoplastics in the North Atlantic.[421]

Recently, there has been much discussion on the accuracy and environmental-relevance of media used in laboratory investigation, as well as methods to develop effective standardisation and comparison of studies completed by various researchers.[422] As part of a field-wide workshop, researchers proposed that a suite of laboratory prepared media should be used to simulate natural waters in future studies to provide enhanced consistency across the field.[422] The use of such recommendations will aid comparability between studies, thus improving our understanding in model systems. However, the great variation that exists between different natural environments, dependent upon dynamic processes such as biological activity, tidal processes and freshwater discharge means that countless test media could be used to represent environmental waters even within the same environmental zone (*i.e.* rivers,

lakes or oceans).[422] As such, whilst effective for standardisation, artificial media does not fully represent the complex nature of environmental systems.[73, 80] In future, by observing behaviour of NMs and carrying out laboratory experimentation in natural waters collected directly from the environment, key insight into their fate within a natural system can be obtained, whilst also providing data to compare against and validate work carried out in recommended laboratory-prepared media. Here, it will be important to comprehensively characterise natural waters to enhance their wider use by the nano-ecotoxicology community.

Given that it appears aggregation of NMs in the saline conditions of the marine environment is likely, albeit this will be influenced by NM concentration, a shift in focus of research to priority areas such as estuarine and coastal waters is required. Here, understanding the interaction between NMs and naturally occurring organic and particulate manner at environmental concentrations is key. It will be important to determine whether at lower concentrations, NMs remain in water column, or precipitate as observed in laboratory investigation. If the latter is to occur, the rate of sedimentation at environmental concentrations will be of great use in evaluating risk to planktonic species in particular. Hence, tracking the flux of NMs from water column to marine sediments and vice versa under representative conditions is key. Assuming NMs are transported to sediments, their impact upon sediment-dwelling organisms, and the potential for bioaccumulation through the food chain, should be addressed.

Going forward nano-ecotoxicological studies must move towards the use of NMs representative of those likely to enter the environment.[420, 423] The use of methods such as those presented in this thesis to extract NMs from product formulations provide scope to investigate the potential effects of exposure to a wide range of NMs utilized in nano-enabled products. Additionally, in this work the importance of considering whole product formulations of nano-enabled products is highlighted, which are likely to influence the outcome of exposure. Whilst such extracted materials better represent those NMs likely to enter the environment than pristine research-grade materials, they do not account for physicochemical transformations that may occur as NMs are used (*e.g.,* combusted), enter WWTPs, are released into aquatic environments, or after interaction with organic or particulate matter. We require greater understanding of release of NMs from product matrixes, and their state upon interaction with natural

particles and biota.[423] The impact of so-called end-product NMs and those 'aged' in the environment requires our focus as we determine the impact of such transformations on NM effect towards biota.[423] However given the vast variety of engineered NMs utilised, protocols will have to put in place to prioritize materials for research.[424] Here, the use of scoring schemes based on perceived hazards of various NMs may be required.[424]

Research has largely focused upon single-species exposure under traditional toxicity assessment. Results are largely case-specific and limited to model organisms, hence the development of high-throughput approaches are required to increase the output to examine an increased number of species-NM interactions.[425] Often cell-dense cultures are used, supplemented by nutrient-rich media, exposing microorganisms to NMs at cell numbers far higher than expected in the environment. In this thesis the influential role of subtle variations in cell density in altering outcome of ecotoxicity assessment is shown, and hence it is recommended that future research is carried out at ambient cell densities where any variation in cell density between experimental runs is accounted for by altering NM load. Use of omics approaches such as shotgun proteomics as used in this thesis provide great scope to examine the molecular response to NM exposure in a range of organisms. These methods provide great scope for future research across the field of ecotoxicology. The microbial community is dynamic, and its health relies on interspecies interactions and interaction with the natural environment. As such, to assess the risk of NMs in greater detail, community exposure is a great tool to identify any susceptible taxa, as well as to gain insight into likely impacts on community functioning at toxic and sub-lethal concentrations. To date, works in this area have mainly only been examined for AgNP exposure. Expanding this to investigate a range of NMs is required.

It is also important to consider that environmental changes are occurring in the ocean, such as sea temperature rise and ocean acidification.[426, 427] Recently, increased efforts are being placed into investigating what such changes might mean for NM toxicity. Increased water temperature appears to alter the manner by which biota interact with NMs, enhancing toxic responses such as disruption to photosynthetic processes.[428 135, 136] Therefore, as global seawater temperature rises populations inhabiting warmer waters may suffer greater adverse effects of NM exposure upon photosynthetic

processes at a greater rate than those in cooler waters. Similarly, Xia *et al*. (2018) found that ocean acidification increased the inhibitory effects of $nTiO_2$ growth of marine microalga. Under more acidic conditions particles did not aggregate as freely and remained more stable in suspension, thought to increase the internalisation of particles into cells, inducing oxidative stress.[306] Synergistic adverse effects of NM exposure and acidification have also been recorded in marine invertebrate species.[107, 429] In this era of environmental change it will be increasingly important to understand the interactions between anthropogenic contaminants and environmental changes.

A great number of anthropogenic pollutants enter the marine environment, and hence NMs are unlikely to be the sole contaminant that biota interact with, particularly in coastal regions.[430] NMs have been recorded to interact with a number of co-contaminants in the aquatic environment.[2, 105, 304, 311, 431-434] Materials such as $nTiO_2$ display high affinity for a number of metals and organic substances, enhancing toxicity of contaminants including TBT, PAHs and heavy metals in marine invertebrate species by increasing their bioavailability and facilitating their uptake.[2, 105, 304, 311, 431, 432] NMs have also been found to enhance the toxicity of other particulate material such as microplastics.[433, 435] For example, growth of the diatom *S. costatum* was inhibited by co-exposure to CuNPs and microplastic particles.[433] To further evaluate the likely impact of NMs in the natural marine environment, efforts should be made to investigate the likely synergistic effects of individual stressors upon wild species, as well as impacts upon the fate and behaviour of each respective contaminant which may be influenced by one another.[434]

References

1. Moore, M. N., Do nanoparticles present ecotoxicological risks for the health of the aquatic environment? *Environ Int* **2006,** *32* (8), 967-76.
2. Klaine, S. J.; Alvarez, P. J.; Batley, G. E.; Fernandes, T. F.; Handy, R. D.; Lyon, D. Y.; Mahendra, S.; McLaughlin, M. J.; Lead, J. R., Nanomaterials in the environment: behavior, fate, bioavailability, and effects. *Environ Toxicol Chem* **2008,** *27* (9), 1825-51.
3. Kim, H. A.; Choi, Y. J.; Kim, K. W.; Lee, B. T.; Ranville, J. F., Nanoparticles in the environment: stability and toxicity. *Rev Environ Health* **2012,** *27* (4), 175-9.
4. Esmaeillou, M.; Zarrini, G.; Ahangarzadeh Rezaee, M.; Shahbazi Mojarrad, J.; Bahadori, A., Vancomycin capped with silver nanoparticles as an antibacterial agent against Multi-Drug Resistance bacteria. *Adv Pharm Bull* **2017,** *7* (3), 479-483.
5. Jiang, Z. J.; Liu, C. Y.; Sun, L. W., Catalytic properties of silver nanoparticles supported on silica spheres. *J Phys Chem B* **2005,** *109* (5), 1730-5.
6. Park, S. H.; Seo, D. S.; Lee, J. K., Effect of lead-free frit on conductivity of nanoparticles-aided silver paste. *J Nanosci Nanotechnol* **2008,** *8* (10), 5331-6.
7. Galletti, A.; Seo, S.; Joo, S. H.; Su, C.; Blackwelder, P., Effects of titanium dioxide nanoparticles derived from consumer products on the marine diatom Thalassiosira pseudonana. *Environ Sci Pollut Res Int* **2016,** *23* (20), 21113-21122.
8. Jain, P. K.; Huang, X.; El-Sayed, I. H.; El-Sayed, M. A., Noble metals on the nanoscale: optical and photothermal properties and some applications in imaging, sensing, biology, and medicine. *Acc Chem Res* **2008,** *41* (12), 1578-86.
9. Vance, M. E.; Kuiken, T.; Vejerano, E. P.; McGinnis, S. P.; Hochella, M. F., Jr.; Rejeski, D.; Hull, M. S., Nanotechnology in the real world: Redeveloping the nanomaterial consumer products inventory. *Beilstein J Nanotechnol* **2015,** *6*, 1769-80.
10. Nanotechnologies, T. P. o. E., Consumer Products Inventory. 2020.
11. Whiteley, C. M.; Dalla Valle, M.; Jones, K. C.; Sweetman, A. J., Challenges in assessing release, exposure and fate of silver nanoparticles within the UK environment. *Environ Sci Process Impacts* **2013,** *15* (11), 2050-8.
12. McGillicuddy, E.; Murray, I.; Kavanagh, S.; Morrison, L.; Fogarty, A.; Cormican, M.; Dockery, P.; Prendergast, M.; Rowan, N.; Morris, D., Silver nanoparticles in the environment: Sources, detection and ecotoxicology. *Sci Total Environ* **2017,** *575*, 231-246.
13. Johnson, A. C.; Park, B., Predicting contamination by the fuel additive cerium oxide engineered nanoparticles within the United Kingdom and the associated risks. *Environ Toxicol Chem* **2012,** *31* (11), 2582-7.
14. Keller, A. A.; Wang, H.; Zhou, D.; Lenihan, H. S.; Cherr, G.; Cardinale, B. J.; Miller, R.; Ji, Z., Stability and aggregation of metal oxide nanoparticles in natural aqueous matrices. *Environ Sci Technol* **2010,** *44* (6), 1962-7.
15. Piccinno, F.; Gottschalk, F.; Seeger, S.; Nowack, B., Industrial production quantities and uses of ten engineered nanomaterials in Europe and the world. *J Nanopart Res* **2012,** *14* (1109), 1-11.
16. Future Markets, *Nanomaterials, The global market, Forecast from 2010 to 2025.*; **2015**.
17. Pulit-Prociak, J.; Banach, M., Silver nanoparticles – a material of the future…? *Open Chem.* **2016,** *14*, 76-91.

18. Krishna Priya, K.; Ramesh, M.; Saravanan, M.; Ponpandian, N., Ecological risk assessment of silicon dioxide nanoparticles in a freshwater fish Labeo rohita: Hematology, ionoregulation and gill Na(+)/K(+) ATPase activity. *Ecotoxicol Environ Saf* **2015,** *120*, 295-302.
19. Gottschalk, F.; Sonderer, T.; Scholz, R. W.; Nowack, B., Modeled environmental concentrations of engineered nanomaterials (TiO(2), ZnO, Ag, CNT, Fullerenes) for different regions. *Environ Sci Technol* **2009,** *43* (24), 9216-22.
20. Auffan, M.; Pedeutour, M.; Rose, J.; Masion, A.; Ziarelli, F.; Borschneck, D.; Chaneac, C.; Botta, C.; Chaurand, P.; Labille, J.; Bottero, J. Y., Structural degradation at the surface of a TiO(2)-based nanomaterial used in cosmetics. *Environ Sci Technol* **2010,** *44* (7), 2689-94.
21. Seshadri, R., Oxide nanoparticles. In *The chemistry of nanoparticles: synthesis, properties and applications.*, Rao, C. N. R.; Müller, A.; Cheetham, A. K., Eds. Wiley: Weinheim, 2004; pp 94-112.
22. Mirzaei, H.; Darroudi, m., Zinc oxide nanoparticles: Biological synthesis and biomedical applications. *Ceramics International* **2017,** *43* (1 Part B), 907-914.
23. Hassanpour, P.; Panahi, Y.; Ebrahimi-Kalan, A.; Akbarzadeh, A.; Davaran, S.; Nasibova, A. N.; Khalilov, R.; Kavetskyy, T., Biomedical applications of aluminium oxide nanoparticles. *Micro & Nano Letters* **2018,** *13* (9), 1227-1231.
24. Gbadamosi, A. O.; Junin, R.; Manan, M. A.; Agi, A.; Oseh, J. O.; Usman, J., Synergistic application of aluminium oxide nanoparticles and oilfield polyacrylamide for enhanced oil recovery. *Journal of Petroleum Science and Engineering* **2019,** *182*, 106345.
25. Paradise, M.; Goswami, T., Carbon nanotubes – Production and industrial applications. *Materials & Design* **2007,** *28* (5), 1477-1489.
26. Das, S.; Dowding, J. M.; Klump, K. E.; McGinnis, J. F.; Self, W.; Seal, S., Cerium oxide nanoparticles: applications and prospects in nanomedicine. *Nanomedicine (Lond)* **2013,** *8* (9), 1483-508.
27. Nyoka, M.; Choonara, Y. E.; Kumar, P.; Kondiah, P. P. D.; Pillay, V., Synthesis of cerium oxide nanoparticles using various methods: implications for biomedical applications. *Nanomaterials (Basel)* **2020,** *10* (2).
28. Merrifield, R. C.; Wang, Z. W.; Palmer, R. E.; Lead, J. R., Synthesis and characterization of polyvinylpyrrolidone coated cerium oxide nanoparticles. *Environ Sci Technol* **2013,** *47* (21), 12426-33.
29. Nadeem, M.; Khan, R.; Afridi, K.; Nadhman, A.; Ullah, S.; Faisal, S.; Mabood, Z. U.; Hano, C.; Abbasi, B. H., Green synthesis of cerium oxide nanoparticles (CeO2 NPs) and their antimicrobial applications: A review. *Int J Nanomedicine* **2020,** *15*, 5951-5961.
30. Fabrega, J.; Zhang, R.; Renshaw, J. C.; Liu, W. T.; Lead, J. R., Impact of silver nanoparticles on natural marine biofilm bacteria. *Chemosphere* **2011,** *85* (6), 961-6.
31. Yadav, B. C.; Kumar, R., Structure, properties and applications of fullerenes. *International Journal of Nanotechnology and Applications* **2008,** *2* (1), 15-24.
32. Teja, A. S.; Koh, P.-Y., Synthesis, properties, and applications of magnetic iron oxide nanoparticles. *Progress in Crystal Growth and Characterization of Materials* **2009,** *55* (1-2), 22-45.
33. Bagher, A. M., Quantum Dots Applications. *Sensors & Transducers* **2016,** *198* (3), 37-43.
34. Benn, T. M.; Westerhoff, P., Nanoparticle silver released into water from commercially available sock fabrics. *Environ Sci Technol* **2008,** *42* (11), 4133-9.

35. Geranio, L.; Heuberger, M.; Nowack, B., The behavior of silver nanotextiles during washing. *Environ Sci Technol* **2009,** *43* (21), 8113-8.
36. Fendall, L. S.; Sewell, M. A., Contributing to marine pollution by washing your face: microplastics in facial cleansers. *Mar Pollut Bull* **2009,** *58* (8), 1225-8.
37. Danovaro, R.; Bongiorni, L.; Corinaldesi, C.; Giovannelli, D.; Damiani, E.; Astolfi, P.; Greci, L.; Pusceddu, A., Sunscreens cause coral bleaching by promoting viral infections. *Environ Health Perspect* **2008,** *116* (4), 441-7.
38. Limbach, L. K.; Bereiter, R.; Muller, E.; Krebs, R.; Galli, R.; Stark, W. J., Removal of oxide nanoparticles in a model wastewater treatment plant: influence of agglomeration and surfactants on clearing efficiency. *Environ Sci Technol* **2008,** *42* (15), 5828-33.
39. Bauerlein, P. S.; Emke, E.; Tromp, P.; Hofman, J.; Carboni, A.; Schooneman, F.; de Voogt, P.; van Wezel, A. P., Is there evidence for man-made nanoparticles in the Dutch environment? *Sci Total Environ* **2017,** *576*, 273-283.
40. Khodakovskaya, M. V.; Kim, B. S.; Kim, J. N.; Alimohammadi, M.; Dervishi, E.; Mustafa, T.; Cernigla, C. E., Carbon nanotubes as plant growth regulators: effects on tomato growth, reproductive system, and soil microbial community. *Small* **2013,** *9* (1), 115-23.
41. Ahmed, F.; Rodrigues, D. F., Investigation of acute effects of graphene oxide on wastewater microbial community: a case study. *J Hazard Mater* **2013,** *256-257*, 33-9.
42. Doolette, C. L.; McLaughlin, M. J.; Kirby, J. K.; Batstone, D. J.; Harris, H. H.; Ge, H.; Cornelis, G., Transformation of PVP coated silver nanoparticles in a simulated wastewater treatment process and the effect on microbial communities. *Chem Cent J* **2013,** *7*, 46.
43. Yang, Y.; Chen, Q.; Wall, J. D.; Hu, Z., Potential nanosilver impact on anaerobic digestion at moderate silver concentrations. *Water Res* **2012,** *46* (4), 1176-84.
44. Chen, Y.; Wang, D.; Zhu, X.; Zheng, X.; Feng, L., Long-term effects of copper nanoparticles on wastewater biological nutrient removal and N2O generation in the activated sludge process. *Environ Sci Technol* **2012,** *46* (22), 12452-8.
45. European Environment Agency, Council Directive (91/271/EEC). 1991.
46. US Environmental Protection Agency, Ocean Dumping Ban Act of 1988.
47. Johnson, A. C.; Bowes, M. J.; Crossley, A.; Jarvie, H. P.; Jurkschat, K.; Jurgens, M. D.; Lawlor, A. J.; Park, B.; Rowland, P.; Spurgeon, D.; Svendsen, C.; Thompson, I. P.; Barnes, R. J.; Williams, R. J.; Xu, N., An assessment of the fate, behaviour and environmental risk associated with sunscreen TiO(2) nanoparticles in UK field scenarios. *Sci Total Environ* **2011,** *409* (13), 2503-10.
48. Blaser, S. A.; Scheringer, M.; Macleod, M.; Hungerbuhler, K., Estimation of cumulative aquatic exposure and risk due to silver: contribution of nano-functionalized plastics and textiles. *Sci Total Environ* **2008,** *390* (2-3), 396-409.
49. Tungittiplakorn, W.; Lion, L. W.; Cohen, C.; Kim, J. Y., Engineered polymeric nanoparticles for soil remediation. *Environ Sci Technol* **2004,** *38* (5), 1605-10.
50. Bessa da Silva, M.; Abrantes, N.; Nogueira, V.; Goncalves, F.; Pereira, R., TiO2 nanoparticles for the remediation of eutrophic shallow freshwater systems: Efficiency and impacts on aquatic biota under a microcosm experiment. *Aquat Toxicol* **2016,** *178*, 58-71.
51. Domingos, R. F.; Baalousha, M. A.; Ju-Nam, Y.; Reid, M. M.; Tufenkji, N.; Lead, J. R.; Leppard, G. G.; Wilkinson, K. J., Characterizing manufactured

nanoparticles in the environment: multimethod determination of particle sizes. *Environ Sci Technol* **2009,** *43* (19), 7277-84.
52. Praetorius, A.; Scheringer, M.; Hungerbuhler, K., Development of environmental fate models for engineered nanoparticles--a case study of TiO2 nanoparticles in the Rhine River. *Environ Sci Technol* **2012,** *46* (12), 6705-13.
53. Maurer-Jones, M. A.; Gunsolus, I. L.; Murphy, C. J.; Haynes, C. L., Toxicity of engineered nanoparticles in the environment. *Anal Chem* **2013,** *85* (6), 3036-49.
54. Graca, B.; Zgrundo, A.; Zakrzewska, D.; Rzodkiewicz, M.; Karczewski, J., Origin and fate of nanoparticles in marine water - Preliminary results. *Chemosphere* **2018,** *206*, 359-368.
55. von der Kammer, F.; Ferguson, P. L.; Holden, P. A.; Masion, A.; Rogers, K. R.; Klaine, S. J.; Koelmans, A. A.; Horne, N.; Unrine, J. M., Analysis of engineered nanomaterials in complex matrices (environment and biota): General considerations and conceptual case studies. *Environ Toxicol Chem* **2011,** *31* (1), 32-49.
56. Chekli, L.; Zhao, Y. X.; Tijing, L. D.; Phuntsho, S.; Donner, E.; Lombi, E.; Gao, B. Y.; Shon, H. K., Aggregation behaviour of engineered nanoparticles in natural waters: characterising aggregate structure using on-line laser light scattering. *J Hazard Mater* **2015,** *284*, 190-200.
57. Xu, F., Review of analytical studies on TiO2 nanoparticles and particle aggregation, coagulation, flocculation, sedimentation, stabilization. *Chemosphere* **2018,** *212*, 662-677.
58. Clavier, A.; Praetorius, A.; Stoll, S., Determination of nanoparticle heteroaggregation attachment efficiencies and rates in presence of natural organic matter monomers. Monte Carlo modelling. *Sci Total Environ* **2019,** *650* (Pt 1), 530-540.
59. Stebounova, L. V.; Guio, E.; Grassian, V. H., Silver nanoparticles in simulated biological media: a study of aggregation, sedimentation, and dissolution. *J Nanopart Res* **2011,** *13*, 233-244.
60. Gallego-Urrea, J. A.; Tuoriniemi, J.; Hassellov, M., Applications of particle-tracking analysis to the determination of size distributions and concentrations of nanoparticles in environmental, biological and food samples. *TrAC Trends in Analytical Chemistry* **2011,** *30* (3), 473-483.
61. Monikh, F. A.; Praetorius, A.; Schmid, A.; Kozin, P.; Meisterjahn, B.; Makarova, E.; Hofmann, T.; von der Kammer, F., Scientific rationale for the development of an OECD test guideline on engineered nanomaterial stability. *NanoImpact* **2018,** *11*, 42-50.
62. Antonio, D. C.; Cascio, C.; Jaksic, Z.; Jurasin, D.; Lyons, D. M.; Nogueira, A. J.; Rossi, F.; Calzolai, L., Assessing silver nanoparticles behaviour in artificial seawater by mean of AF4 and spICP-MS. *Mar Environ Res* **2015,** *111*, 162-9.
63. Markus, A. A.; Parsons, J. R.; Roex, E. W.; de Voogt, P.; Laane, R. W., Modeling aggregation and sedimentation of nanoparticles in the aquatic environment. *Sci Total Environ* **2015,** *506-507*, 323-9.
64. Koelmans, A. A.; Quik, J. T.; Velzeboer, I., Lake retention of manufactured nanoparticles. *Environ Pollut* **2015,** *196*, 171-5.
65. Quik, J. T.; van De Meent, D.; Koelmans, A. A., Simplifying modeling of nanoparticle aggregation-sedimentation behavior in environmental systems: a theoretical analysis. *Water Res* **2014,** *62*, 193-201.
66. Williams, R. J.; Harrison, S.; Keller, V.; Kuensen, J.; Lofts, S.; Praetorius, A.; Svendsen, C.; Vermeulen, L. C.; van Wijnen, J., Models for assessing engineered

nanomaterial fate and behaviour in the aquatic environment. *Current Opinion in Environmental Sustainability* **2019,** *36*, 105-115.
67. Quik, J. T.; Velzeboer, I.; Wouterse, M.; Koelmans, A. A.; van de Meent, D., Heteroaggregation and sedimentation rates for nanomaterials in natural waters. *Water Res* **2014,** *48*, 269-79.
68. Markus, A. A.; Parsons, J. R.; Roex, E. W. M.; de Voogt, P.; Laane, R., Modelling the release, transport and fate of engineered nanoparticles in the aquatic environment - A review. *Rev Environ Contam Toxicol* **2017,** *243*, 53-87.
69. Dale, J. G.; Cox, S. S.; Vance, M. E.; Marr, L. C.; Hochella, M. F., Jr., Transformation of cerium oxide nanoparticles from a diesel fuel additive during combustion in a diesel engine. *Environ Sci Technol* **2017,** *51* (4), 1973-1980.
70. Collin, B.; Auffan, M.; Johnson, A. C.; Kaur, I.; Keller, A. A.; Lazareva, A.; Lead, J. R.; Ma, X.; Merrifield, R. C.; Svendsen, C., Environmental release, fate and ecotoxicological effects of manufac- tured ceria nanomaterials. *Environ. Sci.: Nano* **2014,** *1* (6), 533-548.
71. Nowack, B., The behavior and effects of nanoparticles in the environment. *Environ Pollut* **2009,** *157* (4), 1063-4.
72. Romer, I.; White, T. A.; Baalousha, M.; Chipman, K.; Viant, M. R.; Lead, J. R., Aggregation and dispersion of silver nanoparticles in exposure media for aquatic toxicity tests. *J Chromatogr A* **2011,** *1218* (27), 4226-33.
73. Van Koetsem, F.; Verstraete, S.; Van der Meeren, P.; Du Laing, G., Stability of engineered nanomaterials in complex aqueous matrices: Settling behaviour of CeO2 nanoparticles in natural surface waters. *Environ Res* **2015,** *142*, 207-14.
74. Angel, B. M.; Batley, G. E.; Jarolimek, C. V.; Rogers, N. J., The impact of size on the fate and toxicity of nanoparticulate silver in aquatic systems. *Chemosphere* **2013,** *93* (2), 359-65.
75. Ellis, L. A.; Valsami-Jones, E.; Lead, J. R.; Baalousha, M., Impact of surface coating and environmental conditions on the fate and transport of silver nanoparticles in the aquatic environment. *Sci Total Environ* **2016,** *568*, 95-106.
76. Guzman, M.; Dille, J.; Godet, S., Synthesis and antibacterial activity of silver nanoparticles against gram-positive and gram-negative bacteria. *Nanomedicine* **2012,** *8* (1), 37-45.
77. Sendra, M.; Yeste, M. P.; Gatica, J. M.; Moreno-Garrido, I.; Blasco, J., Direct and indirect effects of silver nanoparticles on freshwater and marine microalgae (Chlamydomonas reinhardtii and Phaeodactylum tricornutum). *Chemosphere* **2017,** *179*, 279-289.
78. Miao, A. J.; Zhang, X. Y.; Luo, Z.; Chen, C. S.; Chin, W. C.; Santschi, P. H.; Quigg, A., Zinc oxide-engineered nanoparticles: dissolution and toxicity to marine phytoplankton. *Environ Toxicol Chem* **2010,** *29* (12), 2814-22.
79. Li, Y.; Zhang, W.; Niu, J.; Chen, Y., Surface-coating-dependent dissolution, aggregation, and reactive oxygen species (ROS) generation of silver nanoparticles under different irradiation conditions. *Environ Sci Technol* **2013,** *47* (18), 10293-301.
80. Nasser, F.; Constantinou, J.; Lynch, I., Nanomaterials in the Environment Acquire an "Eco-Corona" Impacting their Toxicity to Daphnia Magna-a Call for Updating Toxicity Testing Policies. *Proteomics* **2019**, e1800412.
81. Foroozandeh, P.; Aziz, A. A., Merging worlds of nanomaterials and biological environment: factors governing protein corona formation on nanoparticles and its biological consequences. *Nanoscale Res Lett* **2015,** *10*, 221.

82. Neikov, O. D.; Yefimov, N. A., Handbook of Non-Ferrous Metal Powders (Second Edition). Frantsevich Institute for Problems of Materials Science (IPMS), Kiev, Ukraine, 2019; Vol. 2, p 36.
83. Berman, S. S.; McLaren, J. W.; Willie, S. N., Simultaneous determination of five trace metals in seawater by Inductively Coupled Plasma Atomic Emission Spectrometry with ultrasonic nebulization. *Anal. Chem.* **1980,** *52*, 488-492.
84. Malvern *Zetasizer NANO series: Performance, Simplicity, Versatility*; Malvern Instruments Limited: Accessed 2021.
85. Velzeboer, I.; Quik, J. T.; van de Meent, D.; Koelmans, A. A., Rapid settling of nanoparticles due to heteroaggregation with suspended sediment. *Environ Toxicol Chem* **2014,** *33* (8), 1766-73.
86. Topuz, E.; Traber, J.; Sigg, L.; Talinli, I., Agglomeration of Ag and TiO2 nanoparticles in surface and wastewater: Role of calcium ions and of organic carbon fractions. *Environ Pollut* **2015,** *204*, 313-23.
87. Bae, S.; Hwang, Y. S.; Lee, Y. J.; Lee, S. K., Effects of water chemistry on aggregation and soil adsorption of silver nanoparticles. . *Environmental health and toxicology* **2013,** *28*, e2013006.
88. Xu, H.; Jiang, H., Effects of cyanobacterial extracellular polymeric substances on the stability of ZnO nanoparticles in eutrophic shallow lakes. *Environ Pollut* **2015,** *197*, 231-239.
89. Noventa, S.; Rowe, D.; Galloway, T., Mitigating effect of organic matter on the in vivo toxicity of metal oxide nanoparticles in the marine environment. *Environ. Sci.: Nano* **2018,** *5*, 1764-1777.
90. Bone, A. J.; Matson, C. W.; Colman, B. P.; Yang, X.; Meyer, J. N.; Di Giulio, R. T., Silver nanoparticle toxicity to Atlantic killifish (Fundulus heteroclitus) and Caenorhabditis elegans: a comparison of mesocosm, microcosm, and conventional laboratory studies. *Environ Toxicol Chem* **2015,** *34* (2), 275-82.
91. Arnold, M. C.; Badireddy, A. R.; Wiesner, M. R.; Di Giulio, R. T.; Meyer, J. N., Cerium oxide nanoparticles are more toxic than equimolar bulk cerium oxide in Caenorhabditis elegans. *Arch Environ Contam Toxicol* **2013,** *65* (2), 224-33.
92. Rogers, N. J.; Franklin, N. M.; Apte, S. C.; Batley, G. E.; Angel, B.; Lead, J. R.; Baalousha, M., Physico-chemical behaviour and algal toxicity of nanoparticulate CeO2 in freshwater. *Environ. Chem.* **2010,** *7*, 50-60.
93. Ivask, A.; Kurvet, I.; Kasemets, K.; Blinova, I.; Aruoja, V.; Suppi, S.; Vija, H.; Kakinen, A.; Titma, T.; Heinlaan, M.; Visnapuu, M.; Koller, D.; Kisand, V.; Kahru, A., Size-dependent toxicity of silver nanoparticles to bacteria, yeast, algae, crustaceans and mammalian cells in vitro. *PLoS One* **2014,** *9* (7), e102108.
94. Dai, L.; Banta, G. T.; Selck, H.; Forbes, V. E., Influence of copper oxide nanoparticle form and shape on toxicity and bioaccumulation in the deposit feeder, Capitella teleta. *Mar Environ Res* **2015,** *111*, 99-106.
95. Clement, L.; Hurel, C.; Marmier, N., Toxicity of TiO(2) nanoparticles to cladocerans, algae, rotifers and plants - effects of size and crystalline structure. *Chemosphere* **2013,** *90* (3), 1083-90.
96. Shah, V.; Shah, S.; Shah, H.; Rispoli, F. J.; McDonnell, K. T.; Workeneh, S.; Karakoti, A.; Kumar, A.; Seal, S., Antibacterial activity of polymer coated cerium oxide nanoparticles. *PLoS One* **2012,** *7* (10), e47827.
97. Booth, A.; Storseth, T.; Altin, D.; Fornara, A.; Ahniyaz, A.; Jungnickel, H.; Laux, P.; Luch, A.; Sorensen, L., Freshwater dispersion stability of PAA-stabilised cerium oxide nanoparticles and toxicity towards Pseudokirchneriella subcapitata. *Sci Total Environ* **2015,** *505*, 596-605.

98. Rodea-Palomares, I.; Boltes, K.; Fernández-Piñas, F.; Leganés, F.; García-Calvo, E.; Santiago, J.; Rosal, R., Physicochemical characterization and ecotoxicological assessment of CeO2 nanoparticles using two aquatic microorganisms. *Toxicol Sci* **2010,** *119* (1), 135-145.
99. Hazeem, L. J.; Bououdina, M.; Rashdan, S.; Brunet, L.; Slomianny, C.; Boukherroub, R., Cumulative effect of zinc oxide and titanium oxide nanoparticles on growth and chlorophyll a content of Picochlorum sp. *Environ Sci Pollut Res Int* **2016,** *23* (3), 2821-30.
100. Jurasin, D. D.; Curlin, M.; Capjak, I.; Crnkovic, T.; Lovric, M.; Babic, M.; Horak, D.; Vinkovic Vrcek, I.; Gajovic, S., Surface coating affects behavior of metallic nanoparticles in a biological environment. *Beilstein J Nanotechnol* **2016,** *7*, 246-62.
101. Cong, Y.; Jin, F.; Wang, J.; Mu, J., The embryotoxicity of ZnO nanoparticles to marine medaka, Oryzias melastigma. *Aquat Toxicol* **2017,** *185*, 11-18.
102. Wang, J.; Wang, W. X., Low bioavailability of silver nanoparticles presents trophic toxicity to marine medaka (Oryzias melastigma). *Environ Sci Technol* **2014,** *48* (14), 8152-61.
103. Wong, S. W.; Leung, P. T.; Djurisic, A. B.; Leung, K. M., Toxicities of nano zinc oxide to five marine organisms: influences of aggregate size and ion solubility. *Anal Bioanal Chem* **2010,** *396* (2), 609-18.
104. Wang, Z.; Yin, L.; Zhao, J.; Xing, B., Trophic transfer and accumulation of TiO2 nanoparticles from clamworm (Perinereis aibuhitensis) to juvenile turbot (Scophthalmus maximus) along a marine benthic food chain. *Water Res* **2016,** *95*, 250-9.
105. Lu, J.; Tian, S.; Lv, X.; Chen, Z.; Chen, B.; Zhu, X.; Cai, Z., TiO2 nanoparticles in the marine environment: Impact on the toxicity of phenanthrene and Cd(2+) to marine zooplankton Artemia salina. *Sci Total Environ* **2018,** *615*, 375-380.
106. Hanna, S. K.; Miller, R. J.; Lenihan, H. S., Accumulation and Toxicity of Copper Oxide Engineered Nanoparticles in a Marine Mussel. *Nanomaterials (Basel)* **2014,** *4* (3), 535-547.
107. Huang, X.; Liu, Z.; Xie, Z.; Dupont, S.; Huang, W.; Wu, F.; Kong, H.; Liu, L.; Sui, Y.; Lin, D.; Lu, W.; Hu, M.; Wang, Y., Oxidative stress induced by titanium dioxide nanoparticles increases under seawater acidification in the thick shell mussel Mytilus coruscus. *Mar Environ Res* **2018,** *137*, 49-59.
108. Jimeno-Romero, A.; Bilbao, E.; Izagirre, U.; Cajaraville, M. P.; Marigomez, I.; Soto, M., Digestive cell lysosomes as main targets for Ag accumulation and toxicity in marine mussels, Mytilus galloprovincialis, exposed to maltose-stabilised Ag nanoparticles of different sizes. *Nanotoxicology* **2017,** *11* (2), 168-183.
109. Huang, J.; Cheng, J.; Yi, J., Impact of silver nanoparticles on marine diatom Skeletonema costatum. *J Appl Toxicol* **2016,** *36* (10), 1343-54.
110. Yung, M. M.; Wong, S. W.; Kwok, K. W.; Liu, F. Z.; Leung, Y. H.; Chan, W. T.; Li, X. Y.; Djurisic, A. B.; Leung, K. M., Salinity-dependent toxicities of zinc oxide nanoparticles to the marine diatom Thalassiosira pseudonana. *Aquat Toxicol* **2015,** *165*, 31-40.
111. Wang, H.; Ho, K. T.; Scheckel, K. G.; Wu, F.; Cantwell, M. G.; Katz, D. R.; Horowitz, D. B.; Boothman, W. S.; Burgess, R. M., Toxicity, bioaccumulation, and biotransformation of silver nanoparticles in marine organisms. *Environ Sci Technol* **2014,** *48* (23), 13711-7.

112. Pavagadhi, S.; Sathishkumar, M.; Balasubramanian, R., Uptake of Ag and TiO2 nanoparticles by zebrafish embryos in the presence of other contaminants in the aquatic environment. *Water Res* **2014,** *55*, 280-91.
113. Montes, M. O.; Hanna, S. K.; Lenihan, H. S.; Keller, A. A., Uptake, accumulation, and biotransformation of metal oxide nanoparticles by a marine suspension-feeder. *J Hazard Mater* **2012,** *225-226*, 139-45.
114. Cole, M.; Lindeque, P.; Fileman, E.; Clark, J.; Lewis, C.; Halsband, C.; Galloway, T. S., Microplastics Alter the Properties and Sinking Rates of Zooplankton Faecal Pellets. *Environ Sci Technol* **2016,** *60* (6), 3239-3246.
115. Hawthorne, J.; De la Torre Roche, R.; Xing, B.; Newman, L. A.; Ma, X.; Majumdar, S.; Gardea-Torresdey, J.; White, J. C., Particle-size dependent accumulation and trophic transfer of cerium oxide through a terrestrial food chain. *Environ Sci Technol* **2014,** *48* (22), 13102-9.
116. Vignardi, C. P.; Hasue, F. M.; Sartorio, P. V.; Cardoso, C. M.; Machado, A. S.; Passos, M. J.; Santos, T. C.; Nucci, J. M.; Hewer, T. L.; Watanabe, I. S.; Gomes, V.; Phan, N. V., Genotoxicity, potential cytotoxicity and cell uptake of titanium dioxide nanoparticles in the marine fish Trachinotus carolinus (Linnaeus, 1766). *Aquat Toxicol* **2015,** *158*, 218-29.
117. Nigro, M.; Bernardeschi, M.; Costagliola, D.; Della Torre, C.; Frenzilli, G.; Guidi, P.; Lucchesi, P.; Mottola, F.; Santonastaso, M.; Scarcelli, V.; Monaci, F.; Corsi, I.; Stingo, V.; Rocco, L., n-TiO2 and CdCl2 co-exposure to titanium dioxide nanoparticles and cadmium: Genomic, DNA and chromosomal damage evaluation in the marine fish European sea bass (Dicentrarchus labrax). *Aquat Toxicol* **2015,** *168*, 72-7.
118. Rocco, L.; Santonastaso, M.; Nigro, M.; Mottola, F.; Costagliola, D.; Bernardeschi, M.; Guidi, P.; Lucchesi, P.; Scarcelli, V.; Corsi, I.; Stingo, V.; Frenzilli, G., Genomic and chromosomal damage in the marine mussel Mytilus galloprovincialis: Effects of the combined exposure to titanium dioxide nanoparticles and cadmium chloride. *Mar Environ Res* **2015,** *111*, 144-8.
119. Garcia, C. P.; Burchardt, A. D.; Carvalho, R. N.; Gilliland, D.; Antonio, D. C.; Rossi, F.; Lettieri, T., Detection of silver nanoparticles inside marine diatom Thalassiosira pseudonana by electron microscopy and focused ion beam. *PLoS One* **2014,** *9* (5), e96078.
120. Falugi, C.; Aluigi, M. G.; Chiantore, M. C.; Privitera, D.; Ramoino, P.; Gatti, M. A.; Fabrizi, A.; Pinsino, A.; Matranga, V., Toxicity of metal oxide nanoparticles in immune cells of the sea urchin. *Mar Environ Res* **2012,** *76*, 114-21.
121. Garaud, M.; Trapp, J.; Devin, S.; Cossu-Leguille, C.; Pain-Devin, S.; Felten, V.; Giamberini, L., Multibiomarker assessment of cerium dioxide nanoparticle (nCeO2) sublethal effects on two freshwater invertebrates, Dreissena polymorpha and Gammarus roeseli. *Aquat Toxicol* **2015,** *158*, 63-74.
122. Sa-Pereira, P.; Diniz, M. S.; Moita, L.; Pinheiro, T.; Mendonca, E.; Paixao, S. M.; Picado, A., Protein profiling as early detection biomarkers for TiO2 nanoparticle toxicity in Daphnia magna. *Ecotoxicology* **2018,** *27* (4), 430-439.
123. Hook, S. E.; Fisher, N. S., Sublethal effects of silver in zooplankton: importance of exposure pathways and implications for toxicity testing. *Environ Toxicol Chem* **2001,** *20* (3), 568-74.
124. Buffet, P. E.; Tankoua, O. F.; Pan, J. F.; Berhanu, D.; Herrenknecht, C.; Poirier, L.; Amiard-Triquet, C.; Amiard, J. C.; Berard, J. B.; Risso, C.; Guibbolini, M.; Romeo, M.; Reip, P.; Valsami-Jones, E.; Mouneyrac, C., Behavioural and

biochemical responses of two marine invertebrates Scrobicularia plana and Hediste diversicolor to copper oxide nanoparticles. *Chemosphere* **2011,** *84* (1), 166-74.
125. Gambardella, C.; Costa, E.; Piazza, V.; Fabbrocini, A.; Magi, E.; Faimali, M.; Garaventa, F., Effect of silver nanoparticles on marine organisms belonging to different trophic levels. *Mar Environ Res* **2015,** *111*, 41-9.
126. Garcia-Alonso, J.; Rodriguez-Sanchez, N.; Misra, S. K.; Valsami-Jones, E.; Croteau, M. N.; Luoma, S. N.; Rainbow, P. S., Toxicity and accumulation of silver nanoparticles during development of the marine polychaete Platynereis dumerilii. *Sci Total Environ* **2014,** *476-477*, 688-95.
127. Chan, C. Y.; Chiu, J. M., Chronic Effects of Coated Silver Nanoparticles on Marine Invertebrate Larvae: A Proof of Concept Study. *PLoS One* **2015,** *10* (7), e0132457.
128. Xia, B.; Zhu, L.; Han, Q.; Sun, X.; Chen, B.; Qu, K., Effects of TiO2 nanoparticles at predicted environmental relevant concentration on the marine scallop Chlamys farreri: An integrated biomarker approach. *Environ Toxicol Pharmacol* **2017,** *50*, 128-135.
129. Boyles, M. S.; Ranninger, C.; Reischl, R.; Rurik, M.; Tessadri, R.; Kohlbacher, O.; Duschl, A.; Huber, C. G., Copper oxide nanoparticle toxicity profiling using untargeted metabolomics. *Part Fibre Toxicol* **2016,** *13* (1), 49.
130. Poirier, I.; Pallud, M.; Kuhn, L.; Hammann, P.; Demortiere, A.; Jamali, A.; Chicher, J.; Caplat, C.; Gallon, R. K.; Bertrand, M., Toxicological effects of CdSe nanocrystals on the marine diatom Phaeodactylum tricornutum: The first mass spectrometry-based proteomic approach. *Ecotoxicol Environ Saf* **2018,** *152*, 78-90.
131. Field, C. B.; Behrenfeld, M. J.; Randerson, J. T.; Falkowski, P., Primary production of the biosphere: integrating terrestrial and oceanic components. *Science* **1998,** *281* (5374), 237-40.
132. Miller, R. J.; Lenihan, H. S.; Muller, E. B.; Tseng, N.; Hanna, S. K.; Keller, A. A., Impacts of metal oxide nanoparticles on marine phytoplankton. *Environ Sci Technol* **2010,** *44* (19), 7329-34.
133. Flombaum, P.; Gallegos, J. L.; Gordillo, R. A.; Rincon, J.; Zabala, L. L.; Jiao, N.; Karl, D. M.; Li, W. K.; Lomas, M. W.; Veneziano, D.; Vera, C. S.; Vrugt, J. A.; Martiny, A. C., Present and future global distributions of the marine Cyanobacteria Prochlorococcus and Synechococcus. *Proc Natl Acad Sci U S A* **2013,** *110* (24), 9824-9.
134. Grgacic, E. V.; Anderson, D. A., Virus-like particles: passport to immune recognition. *Methods* **2006,** *40* (1), 60-5.
135. Oukarroum, A.; Bras, S.; Perreault, F.; Popovic, R., Inhibitory effects of silver nanoparticles in two green algae, Chlorella vulgaris and Dunaliella tertiolecta. *Ecotoxicol Environ Saf* **2012,** *78*, 80-5.
136. Oukarroum, A.; Polchtchikov, S.; Perreault, F.; Popovic, R., Temperature influence on silver nanoparticles inhibitory effect on photosystem II photochemistry in two green algae, Chlorella vulgaris and Dunaliella tertiolecta. *Environ Sci Pollut Res Int* **2012,** *19* (5), 1755-62.
137. Castro-Bugallo, A.; Gonzalez-Fernandez, A.; Guisande, C.; Barreiro, A., Comparative responses to metal oxide nanoparticles in marine phytoplankton. *Arch Environ Contam Toxicol* **2014,** *67* (4), 483-93.
138. Demir, V.; Ates, M.; Arslan, Z.; Camas, M.; Celik, F.; Bogatu, C.; Can, S. S., Influence of Alpha and Gamma-Iron Oxide Nanoparticles on Marine Microalgae Species. *Bull Environ Contam Toxicol* **2015,** *95* (6), 752-7.

139. He, D.; Dorantes-Aranda, J. J.; Waite, T. D., Silver nanoparticle-algae interactions: oxidative dissolution, reactive oxygen species generation and synergistic toxic effects. *Environ Sci Technol* **2012,** *46* (16), 8731-8.
140. Sendra, M.; Sanchez-Quiles, D.; Blasco, J.; Moreno-Garrido, I.; Lubian, L. M.; Perez-Garcia, S.; Tovar-Sanchez, A., Effects of TiO2 nanoparticles and sunscreens on coastal marine microalgae: Ultraviolet radiation is key variable for toxicity assessment. *Environ Int* **2017,** *98*, 62-68.
141. Burchardt, A. D.; Carvalho, R. N.; Valente, A.; Nativo, P.; Gilliland, D.; Garcia, C. P.; Passarella, R.; Pedroni, V.; Rossi, F.; Lettieri, T., Effects of silver nanoparticles in diatom Thalassiosira pseudonana and cyanobacterium Synechococcus sp. *Environ Sci Technol* **2012,** *46* (20), 11336-44.
142. Aravantinou, A. F.; Tsarpali, V.; Dailianis, S.; Manariotis, I. D., Effect of cultivation media on the toxicity of ZnO nanoparticles to freshwater and marine microalgae. *Ecotoxicol Environ Saf* **2015,** *114*, 109-16.
143. Deng, X. Y.; Cheng, J.; Hu, X. L.; Wang, L.; Li, D.; Gao, K., Biological effects of TiO2 and CeO2 nanoparticles on the growth, photosynthetic activity, and cellular components of a marine diatom Phaeodactylum tricornutum. *Sci Total Environ* **2017,** *575*, 87-96.
144. Mu, D.; Yu, X.; Xu, Z.; Du, Z.; Chen, G., Physiological and transcriptomic analyses reveal mechanistic insight into the adaption of marine Bacillus subtilis C01 to alumina nanoparticles. *Sci Rep* **2016,** *6*, 29953.
145. Wang, Y.; Zhu, X.; Lao, Y.; Lv, X.; Tao, Y.; Huang, B.; Wang, J.; Zhou, J.; Cai, Z., TiO2 nanoparticles in the marine environment: Physical effects responsible for the toxicity on algae Phaeodactylum tricornutum. *Sci Total Environ* **2016,** *565*, 818-826.
146. Morelli, E.; Gabellieri, E.; Bonomini, A.; Tognotti, D.; Grassi, G.; Corsi, I., TiO2 nanoparticles in seawater: Aggregation and interactions with the green alga Dunaliella tertiolecta. *Ecotoxicol Environ Saf* **2018,** *148*, 184-193.
147. Hu, J.; Wang, J.; Liu, S.; Zhang, Z.; Zhang, H.; Cai, X.; Pan, J.; Liu, J., Effect of TiO2 nanoparticle aggregation on marine microalgae Isochrysis galbana. *J Environ Sci (China)* **2018,** *66*, 208-215.
148. Chen, X.; Zhang, C.; Tan, L.; Wang, J., Toxicity of Co nanoparticles on three species of marine microalgae. *Environ Pollut* **2018,** *236*, 454-461.
149. Hwang, E. T.; Lee, J. H.; Chae, Y. J.; Kim, Y. S.; Kim, B. C.; Sang, B. I.; Gu, M. B., Analysis of the toxic mode of action of silver nanoparticles using stress-specific bioluminescent bacteria. *Small* **2008,** *4* (6), 746-50.
150. Choi, O.; Hu, Z., Size dependent and reactive oxygen species related nanosilver toxicity to nitrifying bacteria. *Environ Sci Technol* **2008,** *42* (12), 4583-8.
151. Pulido-Reyes, G.; Rodea-Palomares, I.; Das, S.; Sakthivel, T. S.; Leganes, F.; Rosal, R.; Seal, S.; Fernandez-Pinas, F., Untangling the biological effects of cerium oxide nanoparticles: the role of surface valence states. *Sci Rep* **2015,** *5*, 15613.
152. Bielmyer, G. K.; Grosell, M.; Brixti, K. V., Toxicity of silver, zinc, copper, and nickel to the copepod Acartia tonsa exposed via a phytoplankton diet. *Environ Sci Technol* **2006,** *40* (6), 2063-8.
153. Bielmyer-Fraser, G. K.; Jarvis, T. A.; Lenihan, H. S.; Miller, R. J., Cellular partitioning of nanoparticulate versus dissolved metals in marine phytoplankton. *Environ Sci Technol* **2014,** *48* (22), 13443-50.
154. Zhou, K.; Hu, Y.; Zhang, L.; Yang, K.; Lin, D., The role of exopolymeric substances in the bioaccumulation and toxicity of Ag nanoparticles to algae. *Sci Rep* **2016,** *6*, 32998.

155. Planchon, M.; Jittawuttipoka, T.; Cassier-Chauvat, C.; Guyot, F.; Gelabert, A.; Benedetti, M. F.; Chauvat, F.; Spalla, O., Exopolysaccharides protect Synechocystis against the deleterious effects of titanium dioxide nanoparticles in natural and artificial waters. *J Colloid Interface Sci* **2013,** *405*, 35-43.
156. Mohanty, A.; Wu, Y.; Cao, B., Impacts of engineered nanomaterials on microbial community structure and function in natural and engineered ecosystems. *Appl Microbiol Biotechnol* **2014,** *98* (20), 8457-68.
157. Jin, L.; Son, Y.; DeForest, J. L.; Kang, Y. J.; Kim, W.; Chung, H., Single-walled carbon nanotubes alter soil microbial community composition. *Sci Total Environ* **2014,** *466-467*, 533-8.
158. Jin, L.; Son, Y.; Yoon, T. K.; Kang, Y. J.; Kim, W.; Chung, H., High concentrations of single-walled carbon nanotubes lower soil enzyme activity and microbial biomass. *Ecotoxicol Environ Saf* **2013,** *88*, 9-15.
159. Chung, H.; Son, Y.; Yoon, T. K.; Kim, S.; Kim, W., The effect of multi-walled carbon nanotubes on soil microbial activity. *Ecotoxicol Environ Saf* **2011,** *74* (4), 569-75.
160. Masrahi, A.; VandeVoort, A. R.; Arai, Y., Effects of silver nanoparticle on soil-nitrification processes. *Arch Environ Contam Toxicol* **2014,** *66* (4), 504-13.
161. Pawlett, M.; Ritz, K.; Dorey, R. A.; Rocks, S.; Ramsden, J.; Harris, J. A., The impact of zero-valent iron nanoparticles upon soil microbial communities is context dependent. *Environ Sci Pollut Res Int* **2013,** *20* (2), 1041-9.
162. Ge, Y.; Schimel, J. P.; Holden, P. A., Evidence for negative effects of TiO2 and ZnO nanoparticles on soil bacterial communities. *Environ Sci Technol* **2011,** *45* (4), 1659-64.
163. Nogueira, V.; Lopes, I.; Rocha-Santos, T.; Santos, A. L.; Rasteiro, G. M.; Antunes, F.; Goncalves, F.; Soares, A. M.; Cunha, A.; Almeida, A.; Gomes, N. C.; Pereira, R., Impact of organic and inorganic nanomaterials in the soil microbial community structure. *Sci Total Environ* **2012,** *424*, 344-50.
164. Bradford, A.; Handy, R. D.; Readman, J. W.; Atfield, A.; Muhling, M., Impact of silver nanoparticle contamination on the genetic diversity of natural bacterial assemblages in estuarine sediments. *Environ Sci Technol* **2009,** *43* (12), 4530-6.
165. Luo, Z.; Chen, Z.; Qiu, Z.; Li, Y.; Laing, G. D.; Liu, A.; Yan, C., Gold and silver nanoparticle effects on ammonia-oxidizing bacteria cultures under ammoxidation. *Chemosphere* **2015,** *120*, 737-42.
166. Kang, S.; Mauter, M. S.; Elimelech, M., Microbial cytotoxicity of carbon-based nanomaterials: implications for river water and wastewater effluent. *Environ Sci Technol* **2009,** *43* (7), 2648-53.
167. Das, P.; Williams, C. J.; Fulthorpe, R. R.; Hoque, M. E.; Metcalfe, C. D.; Xenopoulos, M. A., Changes in bacterial community structure after exposure to silver nanoparticles in natural waters. *Environ Sci Technol* **2012,** *46* (16), 9120-8.
168. Binh, C. T.; Tong, T.; Gaillard, J. F.; Gray, K. A.; Kelly, J. J., Acute effects of TiO2 nanomaterials on the viability and taxonomic composition of aquatic bacterial communities assessed via high-throughput screening and next generation sequencing. *PLoS One* **2014,** *9* (8), e106280.
169. Tong, Z.; Bischoff, M.; Nies, L.; Applegate, B.; Turco, R. F., Impact of fullerene (C60) on a soil microbial community. *Environ Sci Technol* **2007,** *41* (8), 2985-91.
170. Nyberg, L.; Turco, R. F.; Nies, L., Assessing the impact of nanomaterials on anaerobic microbial communities. *Environ Sci Technol* **2008,** *42* (6), 1938-43.

171. Shrestha, B.; Acosta-Martinez, V.; Cox, S. B.; Green, M. J.; Li, S.; Canas-Carrell, J. E., An evaluation of the impact of multiwalled carbon nanotubes on soil microbial community structure and functioning. *J Hazard Mater* **2013,** *261*, 188-97.
172. Sheng, Z.; Liu, Y., Effects of silver nanoparticles on wastewater biofilms. *Water Res* **2011,** *45* (18), 6039-50.
173. Baptista, M. S.; Miller, R. J.; Halewood, E. R.; Hanna, S. K.; Almeida, C. M.; Vasconcelos, V. M.; Keller, A. A.; Lenihan, H. S., Impacts of silver nanoparticles on a natural estuarine plankton community. *Environ Sci Technol* **2015,** *49* (21), 12968-74.
174. Doiron, K.; Pelletier, E.; Lemarchand, K., Impact of polymer-coated silver nanoparticles on marine microbial communities: a microcosm study. *Aquat Toxicol* **2012,** *124-125*, 22-7.
175. Tsiola, A.; Pitta, P.; Callol, A. J.; Kagiorgi, M.; Kalantzi, I.; Mylona, K.; Santi, I.; Toncelli, C.; Pergantis, S.; Tsapakis, M., The impact of silver nanoparticles on marine plankton dynamics: Dependence on coating, size and concentration. *Sci Total Environ* **2017,** *601-602*, 1838-1848.
176. Tsiola, A.; Toncelli, C.; Fodelianakis, S.; Michoud, G.; Bucheli, T. D.; Gavriilidou, A.; Kagiorgi, M.; Kalantzi, I.; Knauer, K.; Kotoulas, G.; Mylona, K.; Papadopoulou, E.; Psarra, S.; Santi, I.; Tsapakis, M.; Daffonchio, D.; Pergantis, S. A.; Pittab, P., Low-dose addition of silver nanoparticles stresses marine plankton communities. *Environ. Sci.: Nano* **2018**.
177. Yang, J. L.; Li, Y. F.; Liang, X.; Guo, X. P.; Ding, D. W.; Zhang, D.; Zhou, S.; Bao, W. Y.; Bellou, N.; Dobretsov, S., Silver Nanoparticles Impact Biofilm Communities and Mussel Settlement. *Sci Rep* **2016,** *6*, 37406.
178. Battin, T. J.; Kammer, F. V.; Weilhartner, A.; Ottofuelling, S.; Hofmann, T., Nanostructured TiO2: transport behavior and effects on aquatic microbial communities under environmental conditions. *Environ Sci Technol* **2009,** *43* (21), 8098-104.
179. Zheng, X.; Chen, Y.; Wu, R., Long-term effects of titanium dioxide nanoparticles on nitrogen and phosphorus removal from wastewater and bacterial community shift in activated sludge. *Environ Sci Technol* **2011,** *45* (17), 7284-90.
180. Yang, J. L.; Li, Y. F.; Guo, X. P.; Liang, X.; Xu, Y. F.; Ding, D. W.; Bao, W. Y.; Dobretsov, S., The effect of carbon nanotubes and titanium dioxide incorporated in PDMS on biofilm community composition and subsequent mussel plantigrade settlement. *Biofouling* **2016,** *32* (7), 763-77.
181. Sun, X.; Sheng, Z.; Liu, Y., Effects of silver nanoparticles on microbial community structure in activated sludge. *Sci Total Environ* **2013,** *443*, 828-35.
182. Zhu, Y.; Liu, X.; Hu, Y.; Wang, R.; Chen, M.; Wu, J.; Wang, Y.; Kang, S.; Sun, Y.; Zhu, M., Behavior, remediation effect and toxicity of nanomaterials in water environments. *Environ Res* **2019,** *174*, 54-60.
183. Kalantzi, I.; Mylona, K.; Toncelli, C.; Bucheli, T. D.; Knauer, K.; Pergantis, S. A.; Pitta, P.; Tsiola, A.; Tsapakis, M., Ecotoxicity of silver nanoparticles on plankton organisms: a review. *J Nanopart Res* **2019,** *21* (65), 1-26.
184. Stauber, R. H.; Siemer, S.; Becker, S.; Ding, G. B.; Strieth, S.; Knauer, S. K., Small Meets Smaller: Effects of Nanomaterials on Microbial Biology, Pathology, and Ecology. *ACS Nano* **2018,** *12* (7), 6351-6359.
185. Sintubin, L.; Verstraete, W.; Boon, N., Biologically produced nanosilver: current state and future perspectives. *Biotechnol Bioeng* **2012,** *109* (10), 2422-36.

186. Fabrega, J.; Luoma, S. N.; Tyler, C. R.; Galloway, T. S.; Lead, J. R., Silver nanoparticles: behaviour and effects in the aquatic environment. *Environ Int* **2011,** *37* (2), 517-31.
187. Furberg, A.; Arvidsson, R.; Molander, S., *Very small flows? Review of the societal metabolism of nanomaterials*. Nova Science Publisher, Inc: Hauppauge, New York, 2016; Vol. 15.
188. Syafiuddin, A.; Salmiati; Salim, M. R.; Kueh, A. B. H.; Hadibarata, T.; Nur, H., A review of silver nanoparticles: Research trends, global consumption, synthesis, properties, and future challenges. *Journal of the Chinese Chemical Society* **2017,** *64* (7), 732-756.
189. Liu, J.; Sonshine, D. A.; Shervani, S.; Hurt, R. H., Controlled release of biologically active silver from nanosilver surfaces. *ACS Nano* **2010,** *4* (11), 6903-13.
190. Pillai, Z. S.; Kamat, P. V. J., What factors control the size and shape of silver nanoparticles in the citrate ion reduction method? *Phys. Chem. B* **2003,** *108* (3), 945-951.
191. Damm, C.; Munstedt, H., Kinetic aspects of the silver ion release from antimicrobial polyamide/silver nanocomposites. . *Appl. Phys. A: Mater. Sci. Process.* **2008,** *91* (3), 479-486.
192. Tolaymat, T. M.; El Badawy, A. M.; Genaidy, A.; Scheckel, K. G.; Luxton, T. P.; Suidan, M., An evidence-based environmental perspective of manufactured silver nanoparticle in syntheses and applications: A systematic review and critical appraisal of peer-reviewed scientific papers. *Sci. Total Environ.* **2010,** *408* (5), 999-1006.
193. Zhang, W.; Yao, Y.; Sullivan, N.; Chen, Y., Modeling the primary size effects of citrate-coated silver nanoparticles on their ion release kinetics. *Environ Sci Technol* **2011,** *45* (10), 4422-8.
194. Kaegi, R.; Sinnet, B.; Zuleeg, S.; Hagendorfer, H.; Mueller, E.; Vonbank, R.; Boller, M.; Burkhardt, M., Release of silver nanoparticles from outdoor facades. *Environ Pollut* **2010,** *158* (9), 2900-5.
195. Holden, P. A.; Klaessig, F.; Turco, R. F.; Priester, J. H.; Rico, C. M.; Avila-Arias, H.; Mortimer, M.; Pacpaco, K.; Gardea-Torresdey, J. L., Evaluation of exposure concentrations used in assessing manufactured nanomaterial environmental hazards: are they relevant? *Environ Sci Technol* **2014,** *48* (18), 10541-51.
196. Butz, S. V.; Pinckney, J. L.; Apte, S. C.; Lead, J. R., Uptake and impact of silver nanoparticles on the growth of an estuarine T dinoflagellate, Prorocentrum minimum. *NanoImpact* **2019,** *15* (100181).
197. Pham, T.-L., Toxicity of silver nanoparticles to tropical microalgae Scenedesmus acuminatus, Chaetoceros gracilis and crustacean Daphnia lumholtzi. *Turk. J. Fish.& Aquat. Sci.* **2018,** *19* (12), 1009-1016.
198. Pham, T.-L., Effect of silver nanoparticles on tropical freshwater and marine microalgae. *Hindawi Journal of Chemistry* **2019,** *2019*, 1-7.
199. Sendra, M.; Blasco, J.; Araujo, C. V. M., Is the cell wall of marine phytoplankton a protective barrier or a T nanoparticle interaction site? Toxicological responses of Chlorella autotrophica and Dunaliella salina to Ag and CeO2 nanoparticles. *Ecological Indicators* **2018,** *95*, 1053-1067.
200. Hazeem, L. J.; Kuku, G.; Dewailly, E.; Slomianny, C.; Barras, A.; Hamdi, A.; Boukherroub, R.; Culha, M.; Bououdina, M., Toxicity effect of silver nanoparticles on photosynthetic pigment content, growth, ROS production and ultrastructural changes of microalgae Chlorella vulgaris. *Nanomaterials (Basel)* **2019,** *9* (7).

201. Jin, X.; Li, M.; Wang, J.; Marambio-Jones, C.; Peng, F.; Huang, X.; Damoiseaux, R.; Hoek, E. M., High-throughput screening of silver nanoparticle stability and bacterial inactivation in aquatic media: influence of specific ions. *Environ Sci Technol* **2010,** *44* (19), 7321-8.
202. Scanlan, D. J.; Ostrowski, M.; Mazard, S.; Dufresne, A.; Garczarek, L.; Hess, W. R.; Post, A. F.; Hagemann, M.; Paulsen, I.; Partensky, F., Ecological genomics of marine picocyanobacteria. *Microbiol Mol Biol Rev* **2009,** *73* (2), 249-99.
203. Bagby, S. C.; Chisholm, S. W., Response of Prochlorococcus to varying CO2:O2 ratios. *ISME J* **2015,** *9* (10), 2232-45.
204. Dong, X.; Ji, X.; Jing, J.; Li, M.; Li, J.; Yang, W., Synthesis of triangular silver nanoprisms by stepwise reduction of sodium Bborohydride and Trisodium Citrate. *J. Phys. Chem.* **2010,** *114*, 2070-2074.
205. Moore, L. R.; Post, A. F.; Rocap, G.; Chisholm, S. W., Utilization of different nitrogen sources by the marine cyanobacteria Prochlorococcus and Synechococcus. *Limnology and Oceanography* **2002,** *47* (4), 989-996.
206. Tyler, R. H.; Boyer, T. P.; Minami, T.; Zweng, M. M.; Reagan, J. R., Electrical conductivity of the global ocean. *Earth Planets Space* **2017,** *69*, 156.
207. Mella-Flores, D.; Mazard, S.; Humily, F.; Partensky, F.; Mahe, F.; Bariat, L.; Courties, C.; Marie, D.; Ras, J.; Mauriac, R.; Jeanthon, C.; Mahdi Bendif, E.; Ostrowski, M.; Scanlan, D. J.; Garczarek, L., Is the distribution of Prochlorococcus and Synechococcus ecotypes in the Mediterranean Sea affected by global warming? *Biogeosciences* **2011,** *8*, 2785-2804.
208. Nemati, F.; Dubernet, C.; Colin de Verdiere, A.; Poupon, M. F.; Treupel-Acar, L.; Puisieux, F.; Couvreur, P., Some parameters influencing cytotoxicity of free doxorubicin and doxorubicin-loaded nanoparticles in sensitive and multidrug resistant leucemic murine cells: incubation time, number of nanoparticles per cell. *Intemational Journal of Pharmaceutics* **1994,** *102*, 55-62.
209. Metzler, D. M.; Li, M.; Erdem, A.; Huang, C. P., Responses of algae to photocatalytic nano-TiO2 particles with an emphasis on the effect of particle size. *Chemical Engineering Journal* **2011,** *170*, 538-546.
210. Zinser, E. R., The microbial contribution to reactive oxygen species dynamics in marine ecosystems. *Environ Microbiol Rep* **2018,** *10* (4), 412-427.
211. Christie-Oleza, J. A.; Armengaud, J., In-depth analysis of exoproteomes from marine bacteria by shotgun liquid chromatography-tandem mass spectrometry: the Ruegeria pomeroyi DSS-3 case-study. *Mar Drugs* **2010,** *8* (8), 2223-39.
212. Zadjelovic, V.; Chhun, A.; Quareshy, M.; Silvano, E.; Hernandez-Fernaud, J. R.; Aguilo-Ferretjans, M. M.; Bosch, R.; Dorador, C.; Gibson, M. I.; Christie-Oleza, J. A., Beyond oil degradation: enzymatic potential of Alcanivorax to degrade natural and synthetic polyesters. *Environ Microbiol* **2020,** *22* (4), 1356-1369.
213. Shevchenko, A.; Tomas, H.; Havlis, J.; Olsen, J. V.; Mann, M., In-gel digestion for mass spectrometric characterization of proteins and proteomes. *Nat Protoc* **2006,** *1* (6), 2856-60.
214. Christie-Oleza, J. A.; Scanlan, D. J.; Armengaud, J., "You produce while I clean up", a strategy revealed by exoproteomics during Synechococcus-Roseobacter interactions. *Proteomics* **2015,** *15* (20), 3454-62.
215. Perez-Riverol, Y.; Csordas, A.; Bai, J.; Bernal-Llinares, M.; Hewapathirana, S.; Kundu, D. J.; Inuganti, A.; Griss, J.; Mayer, G.; Eisenacher, M.; Perez, E.; Uszkoreit, J.; Pfeuffer, J.; Sachsenberg, T.; Yilmaz, S.; Tiwary, S.; Cox, J.; Audain, E.; Walzer, M.; Jarnuczak, A. F.; Ternent, T.; Brazma, A.; Vizcaino, J. A., The

PRIDE database and related tools and resources in 2019: improving support for quantification data. *Nucleic Acids Res* **2019,** *47* (D1), D442-D450.
216. Cox, J.; Mann, M., MaxQuant enables high peptide identification rates, individualized p.p.b.-range mass accuracies and proteome-wide protein quantification. *Nat Biotechnol* **2008,** *26* (12), 1367-72.
217. Tyanova, S.; Temu, T.; Sinitcyn, P.; Carlson, A.; Hein, M. Y.; Geiger, T.; Mann, M.; Cox, J., The Perseus computational platform for comprehensive analysis of (prote)omics data. *Nat Methods* **2016,** *13* (9), 731-40.
218. Kaur, A.; Hernandez-Fernaud, J. R.; Aguilo-Ferretjans, M. D. M.; Wellington, E. M.; Christie-Oleza, J. A., 100 Days of marine Synechococcus-Ruegeria pomeroyi interaction: A detailed analysis of the exoproteome. *Environ Microbiol* **2018,** *20* (2), 785-799.
219. Xiu, Z. M.; Zhang, Q. B.; Puppala, H. L.; Colvin, V. L.; Alvarez, P. J., Negligible particle-specific antibacterial activity of silver nanoparticles. *Nano Lett* **2012,** *12* (8), 4271-5.
220. Dobias, J.; Bernier-Latmani, R., Silver release from silver nanoparticles in natural waters. *Environ Sci Technol* **2013,** *47* (9), 4140-6.
221. Liu, J.; Hurt, R. H., Ion release kinetics and particle persistence in aqueous nano-silver colloids. *Environ Sci Technol* **2010,** *44* (6), 2169-75.
222. Ratte, H.-T., Bioaccumulation and toxicity of silver compounds: A review. *Environmental Toxicology and Chemistry* **1999,** *18* (1), 89-108.
223. Morris, J. J.; Lenski, R. E.; Zinser, E. R., The black queen hypothesis: evolution of dependencies through adaptive gene loss. *MBio* **2012,** *3* (2).
224. Ma, L.; Calfee, B. C.; Morris, J. J.; Johnson, Z. I.; Zinser, E. R., Degradation of hydrogen peroxide at the ocean's surface: the influence of the microbial community on the realized thermal niche of Prochlorococcus. *ISME J* **2017**.
225. Guo, H.; Zhang, Z.; Xing, B.; Mukherjee, A.; Musante, C.; White, J. C.; He, L., Analysis of silver nanoparticles in antimicrobial products using surface-enhanced raman spectroscopy (SERS). *Environ. Sci. Technol.* **2015,** *49* (7), 4317–4324.
226. Levard, C.; Hotze, E. M.; Lowry, G. V.; Brown, G. E., Jr., Environmental transformations of silver nanoparticles: impact on stability and toxicity. *Environ Sci Technol* **2012,** *46* (13), 6900-14.
227. Bertrand, C.; Zalouk-Vergnoux, A.; Giamberini, L.; Poirier, L.; Devin, S.; Labille, J.; Perrein-Ettajani, H.; Pagnout, C.; Chatel, A.; Levard, C.; Auffan, M.; Mouneyrac, C., The influence of salinity on the fate and behavior of silver standardized nanomaterial and toxicity effects in the estuarine bivalve Scrobicularia plana. *Environ Toxicol Chem* **2016,** *35* (10), 2550-2561.
228. Stuart, E. J.; Rees, N. V.; Cullen, J. T.; Compton, R. G., Direct electrochemical detection and sizing of silver nanoparticles in seawater media. *Nanoscale* **2013,** *5* (1), 174-7.
229. Furtado, L. M.; Norman, B. C.; Xenopoulos, M. A.; Frost, P. C.; Metcalfe, C. D.; Hintelmann, H., Environmental fate of silver nanoparticles in boreal lake ecosystems. *Environ Sci Technol* **2015,** *49* (14), 8441-50.
230. Gottschalk, F.; Sun, T.; Nowack, B., Environmental concentrations of engineered nanomaterials: review of modeling and analytical studies. *Environ Pollut* **2013,** *181*, 287-300.
231. Thio, B. J.; Montes, M. O.; Mahmoud, M. A.; Lee, D. W.; Zhou, D.; Keller, A. A., Mobility of capped silver nanoparticles under environmentally relevant conditions. *Environ Sci Technol* **2012,** *46* (13), 6985-91.

232. Kittler, S.; Greulich, C.; Diendorf, J.; Koller, M.; Epple, M., Toxicity of silver nanoparticles increases during storage because of slow dissolution under release of silver ions. *Chem. Mater.* **2010,** *22*, 4548 - 4554.
233. Loza, K.; Diendorf, J.; Sengstock, C.; Ruiz-Gonzalez, L.; Gonzalez-Calbet, J. M.; Vallet-Regi, M.; Koller, M.; Epple, M., The dissolution and biological effects of silver nanoparticles in biological media. *J. Mater. Chem. B* **2014,** *2*, 1634 -1643.
234. Graf, C.; Nordmeyer, D.; Sengstock, C.; Ahlberg, S.; Diendorf, J.; Raabe, J.; Epple, M.; Koller, M.; Lademann, J.; Vogt, A.; Rancan, F.; Ruhl, E., Shape-dependent dissolution and cellular uptake of silver nanoparticles. *Langmuir* **2018,** *34* (4), 1506-1519.
235. Ma, R.; Levard, C.; Marinakos, S. M.; Cheng, Y.; Liu, J.; Michel, F. M.; Brown, G. E.; Lowry, G. V., Size-controlled dissolution of organic-coated silver nanoparticles. *Environ Sci Technol* **2012,** *46* (2), 752-9.
236. Christie-Oleza, J. A.; Sousoni, D.; Lloyd, M.; Armengaud, J.; Scanlan, D. J., Nutrient recycling facilitates long-term stability of marine microbial phototroph-heterotroph interactions. *Nat Microbiol* **2017,** *2*, 17100.
237. Roth-Rosenberg, D.; Aharonovich, D.; Luzzatto-Knaan, T.; Vogts, A.; Zoccarato, L.; Eigemann, F.; Nago, N.; Grossart, H.-P.; Voss, M.; Sher, D., Prochlorococcus rely on microbial interactions rather than on chlorotic resting stages to survive long-term nutrient starvation. *bioRxiv* **2020**.
238. Unciti-Broceta, J. D.; Cano-Cortes, V.; Altea-Manzano, P.; Pernagallo, S.; Diaz-Mochon, J. J.; Sanchez-Martin, R. M., Number of nanoparticles per cell through a spectrophotometric method - a key parameter to assess nanoparticle-based cellular assays. *Sci Rep* **2015,** *5*, 10091.
239. Vadrucci, M. R.; Sabetta, L.; Fiocca, A.; Mazziotti, C.; Silvestri, C.; Cabrini, M.; Guardiani, B.; Konjka, E.; Evangelopoulos, A.; Koutsoubas, D.; Basset, A., Statistical evaluation of differences in phytoplankton richness and abundance as constrained by environmental drivers in transitional waters of the Mediterranean basin. *Aquatic Conservation: Marine and Freshwater Ecosystems* **2008,** *18* (51), S88-S104.
240. Zinser, E. R., Cross-protection from hydrogen peroxide by helper microbes: the impacts on the cyanobacterium Prochlorococcus and other beneficiaries in marine communities. *Environ Microbiol Rep* **2018,** *10* (4), 399-411.
241. Regelsberger, G.; Jakopitsch, C.; Plasser, L.; Schwaiger, H.; Furtmüller, P. G.; Peschek, G. A.; Zámocký, M.; Obinger, C., Occurrence and biochemistry of hydroperoxidases in oxygenic phototrophic prokaryotes (cyanobacteria). *Plant Physiol. Biochem.* **2002,** *40*, 479-490.
242. Eitinger, T., In vivo production of active nickel superoxide dismutase from Prochlorococcus marinus MIT9313 is dependent on its cognate peptidase. *J Bacteriol* **2004,** *186* (22), 7821-5.
243. Morris, J. J.; Johnson, Z. I.; Szul, M. J.; Keller, M.; Zinser, E. R., Dependence of the cyanobacterium Prochlorococcus on hydrogen peroxide scavenging microbes for growth at the ocean's surface. *PLoS One* **2011,** *6* (2), e16805.
244. Rose, A. L., The influence of extracellular superoxide on iron redox chemistry and bioavailability to aquatic microorganisms. *Front Microbiol* **2012,** *3*, 124.
245. Planchon, M.; Leger, T.; Spalla, O.; Huber, G.; Ferrari, R., Metabolomic and proteomic investigations of impacts of titanium dioxide nanoparticles on Escherichia coli. *PLoS One* **2017,** *12* (6), e0178437.

246. Los, D. A.; Zorina, A.; Sinetova, M.; Kryazhov, S.; Mironov, K.; Zinchenko, V. V., Stress sensors and signal transducers in cyanobacteria. *Sensors (Basel)* **2010,** *10* (3), 2386-415.
247. Babele, P. K., Zinc oxide nanoparticles impose metabolic toxicity by de-regulating proteome and metabolome in Saccharomyces cerevisiae. *Toxicology Reports* **2019**, 64-73.
248. Li, W. R.; Xie, X. B.; Shi, Q. S.; Duan, S. S.; Ouyang, Y. S.; Chen, Y. B., Antibacterial effect of silver nanoparticles on Staphylococcus aureus. *Biometals* **2011,** *24* (1), 135-41.
249. Soni, D.; Bafana, A.; Gandhi, D.; Sivanesan, S.; Pandey, R. A., Stress response of Pseudomonas species to silver nanoparticles at the molecular level. *Environ Toxicol Chem* **2014,** *33* (9), 2126-32.
250. McQuillan, J. S.; Shaw, A. M., Differential gene regulation in the Ag nanoparticle and Ag(+)-induced silver stress response in Escherichia coli: a full transcriptomic profile. *Nanotoxicology* **2014,** *8 Suppl 1*, 177-84.
251. Zeller, T.; Klug, G., Thioredoxins in bacteria: functions in oxidative stress response and regulation of thioredoxin genes. *Naturwissenschaften* **2006,** *93* (6), 259-66.
252. Lemaire, S.; Keryer, E.; Stein, M.; Schepens, I. I.; Issakidis-Bourguet, E.; C, G. r.-H.; Miginiac-Maslow, M.; Jacquot, J. P., Heavy-metal regulation of thioredoxin gene expression in chlamydomonas reinhardtii. *Plant Physiol* **1999,** *120* (3), 773-8.
253. Ross, S. J.; Findlay, V. J.; Malakasi, P.; Morgan, B. A., Thioredoxin peroxidase is required for the transcriptional response to oxidative stress in budding yeast. *Mol Biol Cell* **2000,** *11* (8), 2631-42.
254. Vuilleumier, S., Bacterial glutathione S-transferases: what are they good for? *J Bacteriol* **1997,** *179* (5), 1431-41.
255. Tamburro, A.; Allocati, N.; Masulli, M.; Rotilio, D.; Di Ilio, C.; Favaloro, B., Bacterial peptide methionine sulphoxide reductase: co-induction with glutathione S-transferase during chemical stress conditions. *Biochem J* **2001,** *360* (Pt 3), 675-81.
256. Tarrago, L.; Laugier, E.; Rey, P., Protein-repairing methionine sulfoxide reductases in photosynthetic organisms: gene organization, reduction mechanisms, and physiological roles. *Mol Plant* **2009,** *2* (2), 202-17.
257. Hansen, J. M.; Zhang, H.; Jones, D. P., Differential oxidation of thioredoxin-1, thioredoxin-2, and glutathione by metal ions. *Free Radic Biol Med* **2006,** *40* (1), 138-45.
258. Sowell, S. M.; Norbeck, A. D.; Lipton, M. S.; Nicora, C. D.; Callister, S. J.; Smith, R. D.; Barofsky, D. F.; Giovannoni, S. J., Proteomic analysis of stationary phase in the marine bacterium "Candidatus Pelagibacter ubique". *Appl Environ Microbiol* **2008,** *74* (13), 4091-100.
259. Menard, A.; Drobne, D.; Jemec, A., Ecotoxicity of nanosized TiO2. Review of in vivo data. *Environ Pollut* **2011,** *159* (3), 677-84.
260. Chen, X.; Selloni, A., Introduction: titanium dioxide (TiO2) nanomaterials. *Chem Rev* **2014,** *114* (19), 9281-2.
261. Hanaor, D. A. H.; Sorrell, C. C., Review of the anatase to rutile phase transformation. *J. Mater. Sci.* **2011,** *46*, 855-874.
262. Foltete, A. S.; Masfaraud, J. F.; Bigorgne, E.; Nahmani, J.; Chaurand, P.; Botta, C.; Labille, J.; Rose, J.; Ferard, J. F.; Cotelle, S., Environmental impact of sunscreen nanomaterials: ecotoxicity and genotoxicity of altered TiO2 nanocomposites on Vicia faba. *Environ Pollut* **2011,** *159* (10), 2515-22.

263. Dransfield, G. P., Inorganic Sunscreens. *Radiation Protection Dosimetry* **2000,** *91* (1-3), 271-273.
264. Schiavo, S.; Oliviero, M.; Philippe, A.; Manzo, S., Nanoparticles based sunscreens provoke adverse effects on marine microalgae Dunaliella tertiolecta. *Environ Sci Nano* **2018,** *5*, 3011-3022.
265. Philippe, A.; Kosik, J.; Welle, A.; Guigner, J.-M.; Clemens, O.; Schaumann, G. E., Extraction and characterization methods for titanium dioxide nanoparticles from commercialized sunscreens. *Environ Sci Nano* **2018,** *5*, 191-202.
266. Gondikas, A.; von der Kammer, F.; Kaegi, R.; Borovinskaya, O.; Neubauer, E.; Navratilova, J.; Praetorius, A.; Cornelis, G.; Hofmann, T., Where is the nano? Analytical approaches for the detection and quantification of TiO2 engineered nanoparticles in surface waters. *Environ Sci Nano* **2018,** *5*, 313-326.
267. Tovar-Sanchez, A.; Sanchez-Quiles, D.; Basterretxea, G.; Benede, J. L.; Chisvert, A.; Salvador, A.; Moreno-Garrido, I.; Blasco, J., Sunscreen products as emerging pollutants to coastal waters. *PLoS One* **2013,** *8* (6), e65451.
268. Miller, R. J.; Bennett, S.; Keller, A. A.; Pease, S.; Lenihan, H. S., TiO2 nanoparticles are phototoxic to marine phytoplankton. *PLoS One* **2012,** *7* (1), e30321.
269. Xia, B.; Chen, B.; Sun, X.; Qu, K.; Ma, F.; Du, M., Interaction of TiO2 nanoparticles with the marine microalga Nitzschia closterium: growth inhibition, oxidative stress and internalization. *Sci Total Environ* **2015,** *508*, 525-33.
270. Manzo, S.; Buono, S.; Rametta, G.; Miglietta, M.; Schiavo, S.; Di Francia, G., The diverse toxic effect of SiO(2) and TiO(2) nanoparticles toward the marine microalgae Dunaliella tertiolecta. *Environ Sci Pollut Res Int* **2015,** *22* (20), 15941-51.
271. Xia, B.; Sui, Q.; Sun, X.; Han, Q.; Chen, B.; Zhu, L.; Qu, K., Ocean acidification increases the toxic effects of TiO2 nanoparticles on the marine microalga Chlorella vulgaris. *J Hazard Mater* **2018,** *346*, 1-9.
272. Li, M.; Chen, D.; Liu, Y.; Chuang, C. Y.; Kong, F.; Harrison, P. J.; Zhu, X.; Jiang, Y., Exposure of engineered nanoparticles to Alexandrium tamarense (Dinophyceae): Healthy impacts of nanoparticles via toxin-producing dinoflagellate. *Science of the Total Environment* **2018,** *610-611*, 356-366.
273. Thiagarajan, V.; Ramasubbu, S.; Natarajan, C.; Mukherjee, A., Differential sensitivity of marine algae Dunaliella salina and Chlorella sp. to P25 TiO2 NPs. *Environ Sci Pollut Res Int* **2019,** *26* (21), 21394-21403.
274. Fu, L.; Hamzeh, M.; Dodard, S.; Zhao, Y. H.; Sunahara, G. I., Effects of TiO2 nanoparticles on ROS production and growth inhibition using freshwater green algae pre-exposed to UV irradiation. *Environ Toxicol Pharmacol* **2015,** *39* (3), 1074-80.
275. Campos, B.; Rivetti, C.; Rosenkranz, P.; Navas, J. M.; Barata, C., Effects of nanoparticles of TiO2 on food depletion and life-history responses of Daphnia magna. *Aquatic Toxicology* **2013**, 174-183.
276. Sendra, M.; Yeste, M. P.; Gatica, J. M.; Moreno-Garrido, I.; Blasco, J., Homoagglomeration and heteroagglomeration of TiO2, in nanoparticle and bulk form, onto freshwater and marine microalgae. *Sci Total Environ* **2017,** *592*, 403-411.
277. Farner, J. M.; Cheong, R. S.; Mahe, E.; Anand, H.; Tufenkji, N., Comparing TiO2 nanoparticle formulations: stability and photoreactivity are key factors in acute toxicity to Daphnia magna. *Environ Sci Nano* **2019**.
278. Manzo, S.; Miglietta, M. L.; Rametta, G.; Buono, S.; Di Francia, G., Toxic effects of ZnO nanoparticles towards marine algae Dunaliella tertiolecta. *Sci Total Environ* **2013,** *445-446*, 371-6.

279. Fazelian, N.; Movafeghi, A.; Yousefzadi, M.; Rahimzadeh, M., Cytotoxic impacts of CuO nanoparticles on the marine microalga Nannochloropsis oculata. *Environ Sci Pollut Res Int* **2019,** *26* (17), 17499-17511.
280. Li, M.; Jiang, Y.; Chuang, C. Y.; Zhou, J.; Zhu, X.; Chen, D., Recovery of Alexandrium tamarense under chronic exposure of TiO2 nanoparticles and possible mechanisms. *Aquat Toxicol* **2019,** *208*, 98-108.
281. Dedman, C. J.; Newson, G. C.; Davies, G.-L.; Christie-Oleza, J. A., Mechanisms of silver nanoparticle toxicity on the marine cyanobacterium Prochlorococcus under environmentally-relevant conditions. *Sci Total Environ* **2020,** *141229*.
282. Wright, R. J.; Gibson, M. I.; Christie-Oleza, J. A., Understanding microbial community dynamics to improve optimal microbiome selection. *Microbiome* **2019,** *7* (1), 85.
283. Parada, A. E.; Needham, D. M.; Fuhrman, J. A., Every base matters: assessing small subunit rRNA primers for marine microbiomes with mock communities, time series and global field samples. *Environ Microbiol* **2016,** *18* (5), 1403-14.
284. Bradley, I. M.; Pinto, A. J.; Guest, J. S., Design and Evaluation of Illumina MiSeq-Compatible, 18S rRNA Gene-Specific Primers for Improved Characterization of Mixed Phototrophic Communities. *Appl Environ Microbiol* **2016,** *82* (19), 5878-91.
285. Callahan, B. J.; McMurdie, P. J.; Rosen, M. J.; Han, A. W.; Johnson, A. J.; Holmes, S. P., DADA2: High-resolution sample inference from Illumina amplicon data. *Nat Methods* **2016,** *13* (7), 581-3.
286. Callahan, B. J.; Sankaran, K.; Fukuyama, J. A.; McMurdie, P. J.; Holmes, S. P., Bioconductor Workflow for Microbiome Data Analysis: from raw reads to community analyses. *F1000Res* **2016,** *5*, 1492.
287. Hugerth, L. W.; Andersson, A. F., Analysing microbial community composition through amplicon sequencing: from sampling to hypothesis testing. *Front Microbiol* **2017,** *8*, 1561.
288. Chong, J.; Liu, P.; Zhou, G.; Xia, J., Using MicrobiomeAnalyst for comprehensive statistical, functional, and meta-analysis of microbiome data. *Nat Protoc* **2020,** *15* (3), 799-821.
289. Dhariwal, A.; Chong, J.; Habib, S.; King, I. L.; Agellon, L. B.; Xia, J., MicrobiomeAnalyst: a web-based tool for comprehensive statistical, visual and meta-analysis of microbiome data. *Nucleic Acids Res* **2017,** *45* (W1), W180-W188.
290. Liao, Y.; Que, W.; Jia, Q.; He, Y.; Zhang, J.; Zhong, P., Controllable synthesis of brookite/anatase/rutile TiO2 nanocomposites and single-crystalline rutilenanorods array. *J. Mater. Chem.* **2012,** *22*, 7937-7944.
291. Li, J.-G.; Ishigaki, T.; Sun, X., Anatase, Brookite, and Rutile Nanocrystals via Redox Reactions under Mild Hydrothermal Conditions: Phase-Selective Synthesis and Physicochemical Properties. *J. Phys. Chem. C* **2007,** *111* (13), 4969-4976.
292. Chen, X.; Zhu, Y.; Yang, K.; Zhu, L.; Lin, D., Nanoparticle TiO2 size and rutile content impact bioconcentration and biomagnification from algae to daphnia. *Environ Pollut* **2019,** *247*, 421-430.
293. Al-Kattan, A.; Wichser, A.; Zuin, S.; Arroyo, Y.; Golanski, L.; Ulrich, A.; Nowack, B., Behavior of TiO(2) released from Nano-TiO(2)-containing paint and comparison to pristine Nano-TiO(2). *Environ Sci Technol* **2014,** *48* (12), 6710-8.
294. Moore, L. R.; Coe, A.; Saito, M. A.; Sullivan, M. B.; Lindell, D.; Frois-Moniz, K.; Waterbury, J.; Chisholm, S. W., Culturing the marine cyanobacterium Prochlorococcus. *Limnol. Oceanogr.: Methods* **2007,** *5* (10), 353–362.

295. Tetu, S. G.; Sarker, I.; Schrameyer, V.; Pickford, R.; Elbourne, L. D. H.; Moore, L. R.; Paulsen, I. T., Plastic leachates impair growth and oxygen production in Prochlorococcus, the ocean's most abundant photosynthetic bacteria. *Commun Biol* **2019,** *2*, 184.
296. Giraldo, A.; Montes, R.; Rodil, R.; Quintana, J. B.; Vidal-Linan, L.; Beiras, R., Ecotoxicological evaluation of the uv filters ethylhexyl dimethyl p-aminobenzoic acid and octocrylene using marine organisms Isochrysis galbana, Mytilus galloprovincialis and Paracentrotus lividus. *Arch Environ Contam Toxicol* **2017,** *72* (4), 606-611.
297. Tovar-Sanchez, A.; Sanchez-Quiles, D.; Rodriguez-Romero, A., Massive coastal tourism influx to the Mediterranean Sea: The environmental risk of sunscreens. *Sci Total Environ* **2019,** *656*, 316-321.
298. Mitchell, S. L.; Hudson-Smith, N. V.; Cahill, M. S.; Reynolds, B. N.; Frand, S. D.; Green, C. M.; Wang, C.; Feng, Z. V.; Haynes, C. L.; Carlson, E. E., Chronic exposure to complex metal oxide nanoparticles elicits rapid resistance in Shewanella oneidensis MR-1. *Chem Sci* **2019**.
299. Aruoja, V.; Dubourguier, H. C.; Kasemets, K.; Kahru, A., Toxicity of nanoparticles of CuO, ZnO and TiO2 to microalgae Pseudokirchneriella subcapitata. *Sci Total Environ* **2009,** *407* (4), 1461-8.
300. Chiu, M. H.; Khan, Z. A.; Garcia, S. G.; Le, A. D.; Kagiri, A.; Ramos, J.; Tsai, S. M.; Drobenaire, H. W.; Santschi, P. H.; Quigg, A.; Chin, W. C., Effect of Engineered Nanoparticles on Exopolymeric Substances Release from Marine Phytoplankton. *Nanoscale Res Lett* **2017,** *12* (1), 620.
301. Zheng, S.; Zhou, Q.; Chen, C.; Yang, F.; Cai, Z.; Li, D.; Geng, Q.; Feng, Y.; Wang, H., Role of extracellular polymeric substances on the behavior and toxicity of silver nanoparticles and ions to green algae Chlorella vulgaris. *Sci Total Environ* **2019,** *660*, 1182-1190.
302. Thiagarajan, V.; M, P.; S, A.; R, S.; N, C.; G, K. S.; Mukherjee, A., Diminishing bioavailability and toxicity of P25 TiO2 NPs during continuous exposure to marine algae Chlorella sp. *Chemosphere* **2019,** *233*, 363-372.
303. Pereira, S. B.; Mota, R.; Vieira, C. P.; Vieira, J.; Tamagnini, P., Phylum-wide analysis of genes/proteins related to the last steps of assembly and export of extracellular polymeric substances (EPS) in cyanobacteria. *Sci Rep* **2015,** *5*, 14835.
304. Zhu, X.; Zhou, J.; Cai, Z., TiO2 nanoparticles in the marine environment: impact on the toxicity of tributyltin to abalone (Haliotis diversicolor supertexta) embryos. *Environ Sci Technol* **2011,** *45* (8), 3753-8.
305. Tantra, R.; Jing, S.; Pichaimuthu, S. K.; Walker, N.; Noble, J.; Hackley, V. A., Dispersion stability of nanoparticles in ecotoxicological investigations: the need for adequate measurement tools. *J Nanopart Res* **2011,** *13*, 3765-3780.
306. Xia, T.; Kovochich, M.; Liong, M.; Madler, L.; Gilbert, B.; Shi, H.; Yeh, J. I.; Zink, J. I.; Nel, A. E., Comparison of the mechanism of toxicity of zinc oxide and cerium oxide nanoparticles based on dissolution and oxidative stress properties. *ACS Nano* **2008,** *2* (10), 2121-34.
307. Wu, D.; Yang, S.; Du, W.; Yin, Y.; Zhang, J.; Guo, H., Effects of titanium dioxide nanoparticles on Microcystis aeruginosa and microcystins production and release. *J Hazard Mater* **2019,** *377*, 1-7.
308. Dasari, T. P.; Pathakoti, K.; Hwang, H. M., Determination of the mechanism of photoinduced toxicity of selected metal oxide nanoparticles (ZnO, CuO, Co3O4 and TiO2) to E. coli bacteria. *J Environ Sci (China)* **2013,** *25* (5), 882-8.

309. Hou, J.; Li, T.; Miao, L.; You, G.; Xu, Y.; Liu, S., Effects of titanium dioxide nanoparticles on algal and bacterial communities in periphytic biofilms. *Environ Pollut* **2019,** *251*, 407-414.
310. Kuwabara, J. S.; Davis, J. A.; Chang, C. C. Y., Algal growth response to particle-bound orthophosphate and zinc. *Limnol Oceanogr* **1986,** *31*, 503-511.
311. Fan, W.; Cui, M.; Liu, H.; Wang, C.; Shi, Z.; Tan, C.; Yang, X., Nano-TiO2 enhances the toxicity of copper in natural water to Daphnia magna. *Environ Pollut* **2011,** *159* (3), 729-34.
312. Liu, X.; Wang, J.; Huang, Y.-W.; Kong, T., Algae (Raphidocelis) reduce combined toxicity of nano-TiO2 and lead on C. dubia. *Sci Total Environ* **2019,** *686*, 246-253.
313. Singh, K. R. B.; Nayak, V.; Sarkar, T.; Singh, R. P., Cerium oxide nanoparticles: properties, biosynthesis and biomedical application. *RSC Adv* **2020,** *10*, 27194.
314. European Commission*, Commission Staff Working Paper: Types and Uses of Nanomaterials, Including Safety Aspects.* 2012.
315. Hallquist, A. M.; Fridell, E.; Westerlund, J.; Hallquist, M., Onboard measurements of nanoparticles from a SCR-equipped marine diesel engine. *Environ Sci Technol* **2013,** *47* (2), 773-80.
316. Somasundaram, D.; Elango, A.; Karthikeyan, S., Combustion and emission analysis of fishing - boat diesel engine running on diesel-ethanol-biodiesel-ceria-alumina nano blends. *Indian Journal of Geo Marine Sciences* **2017,** *46* (8), 1704-1709.
317. Somasundaram, D.; Elango, A.; Karthikeyan, S., Estimation of carbon credits of fishing boat diesel engine running ondiesel-ethanol-bio-diesel blends with nano alumina doped ceria-zirconia. *Materials Today: Proceedings* **2020**.
318. E, J.; Zhang, Z.; Chen, J.; Pham, M.; Zhao, X.; Peng, Q.; Zhang, B.; Yin, Z., Performance and emission evaluation of a marine diesel engine fueled by water biodiesel-diesel emulsion blends with a fuel additive of a cerium oxide nanoparticle. *Energy Conversion and Management* **2018,** *169*, 194-205.
319. Hu, Z. Y.; Haneklaus, S.; Sparovek, G.; Schnug, E., Rare earth elements in soils. *Commun Soil Sci Plant Anal* **2006,** *37*, 1381-1420.
320. Charron, A.; Harrison, R. M., Fine (PM2.5) and coarse (PM2.5-10) particulate matter on a heavily trafficked London highway: sources and processes. *Environ Sci Technol* **2005,** *39* (20), 7768-76.
321. Neil, C. W.; Wu, X.; Kim, D.; Jung, H.; Zhu, Y.; Ray, J. R.; Jun, Y.-S., Arsenite oxyanions affect CeO2 nanoparticle dissolution and colloidal stability. *Environ Sci Nano* **2021,** *8*, 233-244.
322. Lucas, A.; Dupont, C.; Tai, V.; Largier, J.; Palenik, B.; Franks, P., The green ribbon: multiscale physical control of phytoplankton productivity and community structure over a narrow continental shelf. *Limnol. Oceanogr.* **2011,** *56* (2), 611-626.
323. Sendra, M.; Yeste, P. M.; Moreno-Garrido, I.; Gatica, J. M.; Blasco, J., CeO2 NPs, toxic or protective to phytoplankton? Charge of nanoparticles and cell wall as factors which cause changes in cell complexity. *Sci Total Environ* **2017,** *590-591*, 304-315.
324. Calvache-Munoz, J.; Prado, F. A.; Rodriguez-Paez, J. E., Cerium oxide nanoparticles: Synthesis, characterization and tentative mechanism of particle formation. *Colloids and Surfaces A: Physicochemical and Engineering Aspects* **2017,** *529*, 146-159.

325. Fronzi, M.; Soon, A.; Dolley, B.; Traversa, E.; C., S., Stability and morphology of cerium oxide surfaces in an oxidizing environment: A first-principles investigation. *The Journal of Chemical Physics* **2009,** *131* (10), 104701.
326. Afrooz, A. R. M. N.; Hussain, S. M.; Saleh, N. B., Aggregate size and structure determina- tion of nanomaterials in physiological media: importance of dynamic evolution. *J. Nanopart. Res.* **2014,** *16* (2771).
327. Petosa, A. R.; Jaisi, D. P.; Quevedo, I. R.; Elimelech, M.; Tufenkji, N., Aggregation and deposition of engineered nanomaterials in aquatic environments: role of physicochemical interactions. *Environ Sci Technol* **2010,** *44* (17), 6532-49.
328. Handy, R. D.; van den Brink, N.; Chappell, M.; Muhling, M.; Behra, R.; Dusinska, M.; Simpson, P.; Ahtiainen, J.; Jha, A. N.; Seiter, J.; Bednar, A.; Kennedy, A.; Fernandes, T. F.; Riediker, M., Practical considerations for conducting ecotoxicity test methods with manufactured nanomaterials: what have we learnt so far? *Ecotoxicology* **2012,** *21* (4), 933-72.
329. Ottofuelling, S.; Von der Kammer, F.; Hofmann, T., Commercial titanium dioxide nanoparticles in both natural and synthetic water: comprehensive multidimensional testing and prediction of aggregation behavior. *Environ Sci Technol* **2011,** *45* (23), 10045-52.
330. Lowry, G. V.; Gregory, K. B.; Apte, S. C.; Lead, J. R., Transformations of nanomaterials in the environment. *Environ Sci Technol* **2012,** *46* (13), 6893-9.
331. Quik, J. T.; Lynch, I.; Van Hoecke, K.; Miermans, C. J.; De Schamphelaere, K. A.; Janssen, C. R.; Dawson, K. A.; Stuart, M. A.; Van De Meent, D., Effect of natural organic matter on cerium dioxide nanoparticles settling in model fresh water. *Chemosphere* **2010,** *81* (6), 711-5.
332. Mattson, M. P., Hormesis defined. *Ageing Res Rev* **2008,** *7* (1), 1-7.
333. Taylor, N. S.; Merrifield, R.; Williams, T. D.; Chipman, J. K.; Lead, J. R.; Viant, M. R., Molecular toxicity of cerium oxide nanoparticles to the freshwater alga Chlamydomonas reinhardtii is associated with supra-environmental exposure concentrations. *Nanotoxicology* **2016,** *10* (1), 32-41.
334. Donlan, R. M., Biofilms: Microbial Life on Surfaces. *Emerging Infectious Diseases* **2002,** *8* (9), 881-890.
335. Dobretsov, S.; Abed, R. M.; Teplitski, M., Mini-review: Inhibition of biofouling by marine microorganisms. *Biofouling* **2013,** *29* (4), 423-41.
336. Lee, J. W.; Nam, J. H.; Kim, Y. H.; Lee, K. H.; Lee, D. H., Bacterial communities in the initial stage of marine biofilm formation on artificial surfaces. *J Microbiol* **2008,** *46* (2), 174-82.
337. Flemming, H. C.; Wingender, J.; Szewzyk, U.; Steinberg, P.; Rice, S. A.; Kjelleberg, S., Biofilms: an emergent form of bacterial life. *Nat Rev Microbiol* **2016,** *14* (9), 563-75.
338. Callow, J. A.; Callow, M. E., Trends in the development of environmentally friendly fouling-resistant marine coatings. *Nat Commun* **2011,** *2*, 244.
339. Dang, H.; Lovell, C. R., Bacterial primary colonization and early succession on surfaces in marine waters as determined by amplified rRNA gene restriction analysis and sequence analysis of 16S rRNA genes. *Appl Environ Microbiol* **2000,** *66* (2), 467-75.
340. Hadfield, M. G., Biofilms and marine invertebrate larvae: what bacteria produce that larvae use to choose settlement sites. *Ann Rev Mar Sci* **2011,** *3*, 453-70.
341. Fay, F.; Carteau, D.; Linossier, I.; Vallee-Rehel, K., Evaluation of anti-microfouling activity of marine paints by microscopical techniques. *Progress in Organic Coatings* **2011,** *72*, 579-585.

342. Railkin, A. I., *Marine Biofouling Colonization Processes and Defenses*. CRC Press LLC: 2004.
343. Schultz, M. P.; Bendick, J. A.; Holm, E. R.; Hertel, W. M., Economic impact of biofouling on a naval surface ship. *Biofouling* **2011,** *27* (1), 87-98.
344. Chambers, L. D.; Stokes, K. R.; Walsh, F. C.; Wood, R. J. K., Modern approaches to marine antifouling coatings. *Surface & Coatings Technology* **2006,** *201*, 3642-3652.
345. Amara, I.; Miled, W.; Slama, R. B.; Ladhari, N., Antifouling processes and toxicity effects of antifouling paints on marine environment. A review. *Environ Toxicol Pharmacol* **2018,** *57*, 115-130.
346. Melander, C.; Moeller, P. D.; Ballard, T. E.; Richards, J. J.; Huigens, R. W., 3rd; Cavanagh, J., Evaluation of dihydrooroidin as an antifouling additive in marine paint. *Int Biodeterior Biodegradation* **2009,** *63* (4), 529-532.
347. Chen, C.-L.; Maki, J. S.; Rittschof, D.; Teo, S. L.-M., Early marine bacterial biofilm on a copper-based antifouling paint. *International Biodeterioration & Biodegradation* **2013,** *83*, 71-76.
348. Anyaogu, K. C.; Fedorov, A. V.; Neckers, D. C., Synthesis, characterization, and antifouling potential of functionalized copper nanoparticles. *Langmuir* **2008,** *24* (8), 4340-6.
349. Gladis, F.; Eggert, A.; Karsten, U.; Schumann, R., Prevention of biofilm growth on man-made surfaces: evaluation of antialgal activity of two biocides and photocatalytic nanoparticles. *Biofouling* **2010,** *26* (1), 89-101.
350. Babakhani, F. A.; Mehrabadi, A. R.; Lens, P. N. L.; Sadatian, M., Prevention of biofilm formation in water and wastewater installations by application of TiO2 nano particles coating. *Desalin. Water Treat.* **2011,** *28*, 83-87.
351. Wirth, S. M.; Lowry, G. V.; Tilton, R. D., Natural organic matter alters biofilm tolerance to silver nanoparticles and dissolved silver. *Environ Sci Technol* **2012,** *46* (22), 12687-96.
352. Miao, L.; Wang, C.; Hou, J.; Wang, P.; Ao, Y.; Dai, S.; Lv, B., Effects of pH and natural organic matter (NOM) on the adsorptive removal of CuO nanoparticles by periphyton. *Environ Sci Pollut Res Int* **2015,** *22* (10), 7696-704.
353. Miao, L. Z.; Wang, C.; Hou, J.; Wang, P. F.; Qian, J.; Dai, S. S., Kinetics and Equilibrium Biosorption of Nano-ZnO Particles on Periphytic Biofilm under Different Environmental Conditions. *Journal of Environmental Informatics* **2014,** *23* (2), 1-9.
354. Ferry, J. L.; Craig, P.; Hexel, C.; Sisco, P.; Frey, R.; Pennington, P. L.; Fulton, M. H.; Scott, I. G.; Decho, A. W.; Kashiwada, S.; Murphy, C. J.; Shaw, T. J., Transfer of gold nanoparticles from the water column to the estuarine food web. *Nat Nanotechnol* **2009,** *4* (7), 441-4.
355. Schug, H.; Isaacson, C. W.; Sigg, L.; Ammann, A. A.; Schirmer, K., Effect of TiO2 nanoparticles and UV radiation on extracellular enzyme activity of intact heterotrophic biofilms. *Environ Sci Technol* **2014,** *48* (19), 11620-8.
356. Peulen, T. O.; Wilkinson, K. J., Diffusion of nanoparticles in a biofilm. *Environ Sci Technol* **2011,** *45* (8), 3367-73.
357. Tong, M.; Ding, J.; Shen, Y.; Zhu, P., Influence of biofilm on the transport of fullerene (C60) nanoparticles in porous media. *Water Res* **2010,** *44* (4), 1094-103.
358. Jiang, X.; Wang, X.; Tong, M.; Kim, H., Initial transport and retention behaviors of ZnO nanoparticles in quartz sand porous media coated with Escherichia coli biofilm. *Environ Pollut* **2013,** *174*, 38-49.

359. Mitzel, M. R.; Sand, S.; Whalen, J. K.; Tufenkji, N., Hydrophobicity of biofilm coatings influences the transport dynamics of polystyrene nanoparticles in biofilm-coated sand. *Water Res* **2016,** *92*, 113-20.
360. Lerner, R. N.; Lu, Q.; Zeng, H.; Liu, Y., The effects of biofilm on the transport of stabilized zerovalent iron nanoparticles in saturated porous media. *Water Res* **2012,** *46* (4), 975-85.
361. Decho, A. W., Microbial exopolymer secretions in ocean environments: their role(s) in food webs and marine processes. *Oceanogr. Mar. Biol. Ann. Rev* **1990,** *28*, 73-153.
362. Flemming, H. C.; Wingender, J., Relevance of microbial extracellular polymeric substances (EPSs)--Part II: Technical aspects. *Water Sci Technol* **2001,** *43* (6), 9-16.
363. Strathmann, M.; Leon-Morales, F.; Flemming, H. C., *In Influence of biofilms on colloid mobility in the subsurface*. Springer: Berlin, 2007.
364. Jing, H.; Mezgebe, B.; Aly Hassan, A.; Sahle-Demessie, E.; Sorial, G. A.; Bennett-Stamper, C., Experimental and modeling studies of sorption of ceria nanoparticle on microbial biofilms. *Bioresour Technol* **2014,** *161*, 109-17.
365. Xu, Y.; Wang, C.; Hou, J.; Wang, P.; You, G.; Miao, L.; Lv, B.; Yang, Y., Effects of cerium oxide nanoparticles on the species and distribution of phosphorus in enhanced phosphorus removal sequencing batch biofilm reactor. *Bioresour Technol* **2017,** *227*, 393-397.
366. Guibaud, G.; van Hullebusch, E.; Bordas, F., Lead and cadmium biosorption by extracellular polymeric substances (EPS) extracted from activated sludges: pH-sorption edge tests and mathematical equilibrium modelling. *Chemosphere* **2006,** *64* (11), 1955-62.
367. Guibaud, G.; van Hullebusch, E.; Bordas, F.; d'Abzac, P.; Joussein, E., Sorption of Cd(II) and Pb(II) by exopolymeric substances (EPS) extracted from activated sludges and pure bacterial strains: modeling of the metal/ligand ratio effect and role of the mineral fraction. *Bioresour Technol* **2009,** *100* (12), 2959-68.
368. Tang, J.; Zhu, N.; Zhu, Y.; Zamir, S. M.; Wu, Y., Sustainable pollutant removal by periphytic biofilm via microbial composition shifts induced by uneven distribution of CeO2 nanoparticles. *Bioresour Technol* **2018,** *248* (Pt B), 75-81.
369. Mah, T. F.; O'Toole, G. A., Mechanisms of biofilm resistance to antimicrobial agents. *Trends Microbiol* **2001,** *9* (1), 34-9.
370. Inbakandan, D.; Kumar, C.; Abraham, L. S.; Kirubagaran, R.; Venkatesan, R.; Khan, S. A., Silver nanoparticles with anti microfouling effect: a study against marine biofilm forming bacteria. *Colloids Surf B Biointerfaces* **2013,** *111*, 636-43.
371. Kirchman, D. L., The ecology of Cytophaga-Flavobacteria in aquatic environments. *FEMS Microbiol Ecol* **2002,** *39* (2), 91-100.
372. Newton, R. J.; Jones, S. E.; Eiler, A.; McMahon, K. D.; Bertilsson, S., A guide to the natural history of freshwater lake bacteria. *Microbiol Mol Biol Rev* **2011,** *75* (1), 14-49.
373. Bour, A.; Mouchet, F.; Verneuil, L.; Evariste, L.; Silvestre, J.; Pinelli, E.; Gauthier, L., Toxicity of CeO2 nanoparticles at different trophic levels--effects on diatoms, chironomids and amphibians. *Chemosphere* **2015,** *120*, 230-6.
374. Miao, L.; Wang, P.; Hou, J.; Yao, Y.; Liu, Z.; Liu, S., Low concentrations of copper oxide nanoparticles alter microbial community structure and function of sediment biofilms. *Sci Total Environ* **2019,** *653*, 705-713.

375. Heydorn, A.; Nielsen, A. T.; Hentzer, M.; Sternberg, C.; Givskov, M.; Ersboll, B. K.; Molin, S., Quantification of biofilm structures by the novel computer program COMSTAT. *Microbiology (Reading)* **2000,** *146 (Pt 10)*, 2395-2407.
376. Vorregaard, M. Comstat2 - a modern 3D image analysis environment for biofilms. Technical University of Denmark, Kongens Lyngby, 2008.
377. Yebra, D. M.; Kiil, S.; Dam-Johansen, K., Antifouling technology-past, present and future steps towards efficient and environmentally friendly antifouling coatings. *Progress in Organic Coatings* **2004,** *50*, 75-104.
378. Muthukumar, T.; Aravinthan, A.; Lakshmi, K.; Venkatesan, R.; Vedaprakash, L.; Doble, M., Fouling and stability of polymers and composites in marine environment. *International Biodeterioration & Biodegradation* **2011,** *65*, 276-284.
379. Muthukrishnan, T.; Al Khaburi, M.; Abed, R. M. M., Fouling microbial communities on plastics compared with wood and steel: are they substrate- or location-specific? *Microb Ecol* **2019,** *78* (2), 361-374.
380. Pollet, T.; Berdjeb, L.; Garnier, C.; Durrieu, G.; Le Poupon, C.; Misson, B.; Jean-Francois, B., Prokaryotic community successions and interactions in marine biofilms: the key role of Flavobacteriia. *FEMS Microbiol Ecol* **2018,** *94* (6).
381. Briand, J. F.; Barani, A.; Garnier, C.; Rehel, K.; Urvois, F.; LePoupon, C.; Bouchez, A.; Debroas, D.; Bressy, C., Spatio-Temporal Variations of Marine Biofilm Communities Colonizing Artificial Substrata Including Antifouling Coatings in Contrasted French Coastal Environments. *Microb Ecol* **2017,** *74* (3), 585-598.
382. Love, M. I.; Huber, W.; Anders, S., Moderated estimation of fold change and dispersion for RNA-seq data with DESeq2. *Genome Biol* **2014,** *15* (12), 550.
383. Dang, H.; Lovell, C. R., Microbial Surface Colonization and Biofilm Development in Marine Environments. *Microbiol Mol Biol Rev* **2016,** *80* (1), 91-138.
384. Buchan, A.; LeCleir, G. R.; Gulvik, C. A.; Gonzalez, J. M., Master recyclers: features and functions of bacteria associated with phytoplankton blooms. *Nat Rev Microbiol* **2014,** *12* (10), 686-98.
385. Williams, T. J.; Wilkins, D.; Long, E.; Evans, F.; DeMaere, M. Z.; Raftery, M. J.; Cavicchioli, R., The role of planktonic Flavobacteria in processing algal organic matter in coastal East Antarctica revealed using metagenomics and metaproteomics. *Environ Microbiol* **2013,** *15* (5), 1302-17.
386. Bengtsson, M. M.; Ovreas, L., Planctomycetes dominate biofilms on surfaces of the kelp Laminaria hyperborea. *BMC Microbiol* **2010,** *10*, 261.
387. Fuerst, J. A.; Sagulenko, E., Beyond the bacterium: planctomycetes challenge our concepts of microbial structure and function. *Nat Rev Microbiol* **2011,** *9* (6), 403-13.
388. Morris, R. M.; Longnecker, K.; Giovannoni, S. J., Pirellula and OM43 are among the dominant lineages identified in an Oregon coast diatom bloom. *Environ Microbiol* **2006,** *8* (8), 1361-70.
389. Musat, N.; Werner, U.; Knittel, K.; Kolb, S.; Dodenhof, T.; van Beusekom, J. E.; de Beer, D.; Dubilier, N.; Amann, R., Microbial community structure of sandy intertidal sediments in the North Sea, Sylt-Romo Basin, Wadden Sea. *Syst Appl Microbiol* **2006,** *29* (4), 333-48.
390. Lage, O. M.; Bondoso, J., Planctomycetes diversity associated with macroalgae. *FEMS Microbiol Ecol* **2011,** *78* (2), 366-75.
391. Oberbeckmann, S.; Kreikemeyer, B.; Labrenz, M., Environmental factors support the formation of specific bacterial assemblages on microplastics. *Front Microbiol* **2017,** *8*, 2709.

392. Lynn, D. H., *Ciliophora*. John Wiley & Sons, Ltd: 2012.
393. Finlay, B. J.; Esteban, G. F., Freshwater protozoa: biodiversity and ecological function. *Biodivers. Conserv.* **1998,** *7*, 1163–1186.
394. Norf, H.; Arndt, H.; Weitere, M., Responses of biofilm-dwelling ciliate communities to planktonic and benthic resource enrichment. *Microb Ecol* **2009,** *57* (4), 687-700.
395. Sikder, M. N. A.; Abdullah Al, M.; Hu, G.; Xu, H., Colonization dynamics of periphytic ciliates at different water depths in coastal waters of the Yellow Sea, northern China. . *J. Mar. Biol. Assoc. U.K.* **2019,** *99*, 1065–1073.
396. Sikder, M. N. A.; Abdullah Al, M.; Xu, G.; Hu, G.; Xu, H., Spatial variations in trophic-functional patterns of periphytic ciliates and indications to water quality in coastal waters of the Yellow Sea. *Environ Sci Pollut Res Int* **2019,** *26* (3), 2592-2602.
397. Sikder, M. N. A.; Bai, X.; Warren, A.; Xu, H., An approach to determining homogeneity in taxonomic breadth of periphytic ciliate communities in colonization surveys for bioassessment. *Ecol. Indic.* **2019,** *107*, 105671.
398. Franco, C.; Esteban, G.; Tellez, C., Colonization and succession of ciliated protozoa associated with submerged leaves in a river. *Limnologica* **1998,** *28*, 275–283.
399. Railkin, A. I., Heterotrophic flagellates on artificial substrates in the White Sea. . *Cytology* **1995,** *37*, 951–957.
400. Pratt, J.; Cairns, J., J., Functional groups in the Protozoa: roles in differing ecosystems. *J. Protozool.* **1985,** *32*, 415-423.
401. Fernandez-Leborans, G., Relative importance of protozoan functional roups in three marine sublittoral areas. *J. Mar. Biol. Assoc. U.K.* **2001,** *81*, 735-750.
402. Shimeta, J.; Cutajar, J.; Watson, M. G.; Vlamis, T., Influences of biofilm-associated ciliates on the settlement of marine invertebrate larvae. *Marine Ecology Progress Series* **2012,** *449*, 1-12.
403. Cairns, J., J.; Lanza, G. R.; Parker, B. C., Pollution related to structural and functional changes in aquatic communities with emphasis on freshwater algae and protozoa. *Proc. Acad. Natl. Sci. Phila.* **1972,** *124*, 79–127.
404. Xu, H.; Zhang, W.; Jiang, Y.; Yang, E. J., Use of biofilm-dwelling ciliate communities to determine environmental quality status of coastal waters. *Sci. Total Environ.* **2014,** *470-471*, 511-518.
405. Noreña, C.; Damborenea, C.; Brusa, F., *Phylum Platyhelminthes*. Fourth Edition ed.; Academic Press: 2015.
406. Eikrem, W.; Medlin, L. K.; Henderiks, J.; Rokitta, S.; Rost, B.; Probert, I.; Throndsen, J.; Edvardsen, B., Haptophyta. In *Handbook of the Protists.*, al., A. J. e., Ed. Springer, Cham.: 2017; pp 1-61.
407. Smirnova, T. A.; Didenko, L. V.; Azizbekyan, R. R.; Romanova, Y. M., Structural and functional characteristics of bacterial biofilms. *Microbiology* **2010,** *49* (4), 413-423.
408. Kloppel, H.; Fliedner, A.; Kordel, W., Behaviour and ecotoxicology of aluminium in soil and water--review of the scientific literature. *Chemosphere* **1997,** *35* (1-2), 353-63.
409. Xie, J.; Bai, X.; Lavoie, M.; Lu, H.; Fan, X.; Pan, X.; Fu, Z.; Qian, H., Analysis of the Proteome of the Marine Diatom Phaeodactylum tricornutum Exposed to Aluminum Providing Insights into Aluminum Toxicity Mechanisms. *Environ Sci Technol* **2015,** *49* (18), 11182-90.
410. Harford, A. J.; Hogan, A. C.; Tsang, J. J.; Parry, D. L.; Negri, A. P.; Adams, M. S.; Stauber, J. L.; van Dam, R. A., Effects of alumina refinery wastewater and

signature metal constituents at the upper thermal tolerance of: 1. The tropical diatom Nitzschia closterium. *Mar Pollut Bull* **2011,** *62* (3), 466-73.
411. Golding, L. A.; Angel, B. M.; Batley, G. E.; Apte, S. C.; Krassoi, R.; Doyle, C. J., Derivation of a water quality guideline for aluminium in marine waters. *Environ Toxicol Chem* **2015,** *34* (1), 141-51.
412. Guillonneau, R.; Baraquet, C.; Bazire, A.; Molmeret, M., Multispecies biofilm development of marine bacteria implies complex relationships through competition and synergy and modification of matrix components. *Front Microbiol* **2018,** *9*, 1960.
413. He, X.; Liu, Y.; Bai, X.; Yuan, C.; Li, H., Alginate/albumin in incubation solution mediates the adhesion and biofilm formation of typical marine bacteria and algae. *Biochemical Engineering Journal* **2018,** *139*, 25-32.
414. Wright, R. J.; Erni-Cassola, G.; Zadjelovic, V.; Latva, M.; Christie-Oleza, J. A., Marine plastic debris – a new surface for microbial colonization. *Environ Sci Technol* **2020**.
415. Adeleye, A. S.; Oranu, E. A.; Tao, M.; Keller, A. A., Release and detection of nanosized copper from a commercial antifouling paint. *Water Res* **2016,** *102*, 374-382.
416. Costerton, J. W.; Lewandowski, Z.; Caldwell, D. E.; Korber, D. R.; Lappin-Scott, H. M., Microbial biofilms. *Annu Rev Microbiol* **1995,** *49*, 711-45.
417. Dang, H.; Li, T.; Chen, M.; Huang, G., Cross-ocean distribution of Rhodobacterales bacteria as primary surface colonizers in temperate coastal marine waters. *Appl Environ Microbiol* **2008,** *74* (1), 52-60.
418. Jones, P. R.; Cottrell, M. T.; Kirchman, D. L.; Dexter, S. C., Bacterial community structure of biofilms on artificial surfaces in an estuary. *Microb Ecol* **2007,** *53* (1), 153-62.
419. Keller, A.; McFerran, S.; Lazareva, A.; Suh, S., Global life cycle releases of engineered nanomaterials. *J Nanopart Res* **2013,** *15* (1692).
420. Ren, C.; Hu, X.; Zhou, Q., Influence of environmental factors on nanotoxicity and knowledge gaps thereof. *NanoImpact* **2016,** *2*, 82-92.
421. Ter Halle, A.; Jeanneau, L.; Martignac, M.; Jarde, E.; Pedrono, B.; Brach, L.; Gigault, J., Nanoplastic in the north atlantic subtropical gyre. *Environ Sci Technol* **2017,** *51* (23), 13689-13697.
422. Geitner, N. K.; Ogilvie Hendren, C.; Cornelis, G.; Kaegi, R.; Lead, J. R.; Lowry, G. V.; Lynch, I.; Nowack, B.; Petersen, E.; Bernhardt, E.; Brown, S.; Chen, W.; de Garidel-Thoron, C.; Hanson, J.; Harper, S.; Jones, K.; von der Kammer, F.; Kennedy, A.; Kidd, J.; Matson, C.; Metcalfe, C. D.; Pedersen, J.; Peijnenburg, W. J. G. M.; Quik, J. T. K.; Rodrigues, S. M.; Rose, J.; Sayre, P.; Simonin, M.; Svendsen, C.; Tanguay, R.; Tefenkji, N.; van Teunenbroek, T.; Thies, G.; Tian, Y.; Rice, J.; Turner, A.; Liu, J.; Unrine, J.; Vance, M.; White, J. C.; Wiesner, M. R., Harmonizing across environmental nanomaterial testing media for increased comparability of nanomaterial datasets. *Environmental Science: Nano* **2020,** *7* (1), 13-36.
423. Svendsen, C.; Walker, L. A.; Matzke, M.; Lahive, E.; Harrison, S.; Crossley, A.; Park, B.; Lofts, S.; Lynch, I.; Vazquez-Campos, S.; Kaegi, R.; Gogos, A.; Asbach, C.; Cornelis, G.; von der Kammer, F.; van den Brink, N. W.; Mays, C.; Spurgeon, D. J., Key principles and operational practices for improved nanotechnology environmental exposure assessment. *Nat Nanotechnol* **2020,** *15* (9), 731-742.

424. Kuhnel, D.; Nickel, C.; Hellack, B.; van der Zalm, E.; Kussatz, C.; Herrchen, M.; Meisterjahn, B.; Hund-Rinke, K., Closing gaps for environmental risk screening of engineered nanomaterials. *NanoImpact* **2019,** *15*, 100173.
425. Miller, R. J.; Muller, E. B.; Cole, B.; Martin, T.; Nisbet, R.; Bielmyer-Fraser, G. K.; Jarvis, T. A.; Keller, A. A.; Cherr, G.; Lenihan, H. S., Photosynthetic efficiency predicts toxic effects of metal nanomaterials in phytoplankton. *Aquat Toxicol* **2017,** *183*, 85-93.
426. Doney, S. C.; Fabry, V. J.; Feely, R. A.; Kleypas, J. A., Ocean acidification: the other CO2 problem. *Ann Rev Mar Sci* **2009,** *1*, 169-92.
427. Levitus, S.; Antonov, J.; Boyer, T., Warming of the world ocean, 1955–2003. *Geophys. Res. Lett.* **2005,** *32* (2), L02604.
428. Ferreira, P.; Fonte, E.; Soares, M. E.; Carvalho, F.; Guilhermino, L., Effects of multi-stressors on juveniles of the marine fish Pomatoschistus microps: Gold nanoparticles, microplastics and temperature. *Aquat Toxicol* **2016,** *170*, 89-103.
429. Kong, H.; Wu, F.; Jiang, X.; Wang, T.; Hu, M.; Chen, J.; Huang, W.; Bao, Y.; Wang, Y., Nano-TiO2 impairs digestive enzyme activities of marine mussels under ocean acidification. *Chemosphere* **2019,** *237*, 124561.
430. Singh, N.; Bhagat, J.; Tiwari, E.; Khandelwal, N.; Darbha, G. K.; Shyama, S. K., Metal oxide nanoparticles and polycyclic aromatic hydrocarbons alter nanoplastic's stability and toxicity to zebrafish. *J Hazard Mater* **2021,** *407*, 124382.
431. Tian, S.; Zhang, Y.; Song, C.; Zhu, X.; Xing, B., Titanium dioxide nanoparticles as carrier facilitate bioaccumulation of phenanthrene in marine bivalve, ark shell (Scapharca subcrenata). *Environ Pollut* **2014,** *192*, 59-64.
432. Tian, S.; Zhang, Y.; Song, C.; Zhu, X.; Xing, B., Bioaccumulation and biotransformation of polybrominated diphenyl ethers in the marine bivalve (Scapharca subcrenata): influence of titanium dioxide nanoparticles. *Mar Pollut Bull* **2015,** *90* (1-2), 48-53.
433. Zhu, X.; Zhao, W.; Chen, X.; Zhao, T.; Tan, L.; Wang, J., Growth inhibition of the microalgae Skeletonema costatum under copper nanoparticles with microplastic exposure. *Mar Environ Res* **2020,** *158*, 105005.
434. Li, P.; Zou, X.; Wang, X.; Su, M.; Chen, C.; Sun, X.; Zhang, H., A preliminary study of the interactions between microplastics and citrate-coated silver nanoparticles in aquatic environments. *J Hazard Mater* **2020,** *385*, 121601.
435. Pacheco, A.; Martins, A.; Guilhermino, L., Toxicological interactions induced by chronic exposure to gold nanoparticles and microplastics mixtures in Daphnia magna. *Sci Total Environ* **2018,** *628-629*, 474-483.
436. Quast, C.; Pruesse, E.; Yilmaz, P.; Gerken, J.; Schweer, T.; Yarza, P.; Peplies, J.; Glockner, F. O., The SILVA ribosomal RNA gene database project: improved data processing and web-based tools. *Nucleic Acids Res* **2013,** *41*, D590-6.

Appendix 1

Supporting Information

A1.1 Chapter 2 Supplementary Information

A1.1.1. Proteomics analysis of *Prochlorococcus sp.* MED4 exposed to AgNPs: Supporting data.

Data tables supporting shotgun proteomic analysis of *Prochlorococcus sp.* MED4 exposed to AgNPs are provided on the pages below.

A full list of proteins, and associated function, identified during shotgun proteomic analyses presented in this thesis are provided in the electronic supplementary data tables 1-10.

Table A1.1. Lowest 20 q-value proteins as identified in the cellular-proteome during Proteomics experiment 1 (~250 NPs cell^{-1}) (***p≤0.05; *p≤0.1).

Protein	Function	UP/Down-regulated	RA% Control	RA% AgNPs	q-value	Significance
Putative glycosyl transferase, group 1	Other/Undefined	DOWN	0.0076	0.0057	0.0413	***
Tyrosine binding protein	Basic cellular processes	DOWN	0.0875	0.0679	0.0496	***
Indole-3-glycerol phosphate synthase	Central Metabolism	DOWN	0.0113	0.0085	0.0531	*
DNA gyrase subunit A	Other/Undefined	DOWN	0.0014	0.0011	0.062	*
Putative ATP-dependent Clp protease, Hsp 100, ATP-binding subunit ClpB	Basic cellular processes	DOWN	0.0137	0.0099	0.062	*
50S ribosomal protein L28	Basic cellular processes	UP	0.1081	0.1542	0.0827	*
Carbamoyl-phosphate synthase large chain	Central Metabolism	DOWN	0.0132	0.0107	0.124	
Photosystem I iron-sulfur center	Photosynthesis	UP	0.398	0.8408	0.132	
ATP-dependent Clp protease, Hsp 100, ATP-binding subunit ClpB	Basic cellular processes	DOWN	0.1485	0.1382	0.1347	
Zeta-carotene desaturase	Photosynthesis	DOWN	0.0139	0.011	0.1382	
Possible uncharacterized restriction enzyme, interrupted-C	Other/Undefined	DOWN	0.0131	0.0104	0.152	
50S ribosomal protein L18	Basic cellular processes	UP	0.06	0.0848	0.1631	
Circadian clock protein kinase KaiC	Other/Undefined	DOWN	0.0585	0.0474	0.167	
Aminotransferase	Central Metabolism	DOWN	0.156	0.1496	0.1679	
Riboflavin biosynthesis protein RibD	Central Metabolism	DOWN	0.0154	0.0126	0.1689	
Photosystem I protein PsaD	Photosynthesis	UP	0.9589	1.3693	0.1708	
Glycosyl transferase, family 2	Other/Undefined	DOWN	0.0272	0.0213	0.171	
33 kDa chaperonin	Basic cellular processes	DOWN	0.0034	0.0024	0.1716	
RNA polymerase sigma factor	Basic cellular processes	DOWN	0.0497	0.04	0.1727	
Uncharacterized protein	Other/Undefined	UP	0.0691	0.0723	0.1746	

Table A1.2. Lowest 20 q-value proteins as identified in the exo-proteome during Proteomics experiment 1 (~250 NPs cell^{-1})

Protein	Function	UP/Down-regulated	RA% Control	RA% AgNPs	q-value
Magnesium transporter MgtE	Membrane Transport	DOWN	0.017	0.007	0.202
Putative cell division inhibitor	Other	DOWN	0.006	0.002	0.206
Putative sulfate transporter	Membrane Transport	DOWN	0.009	0.004	0.207
Chaperone protein DnaK	Basic Cellular Processes	DOWN	0.009	0.006	0.208
Elongation factor P	Other	UP	0.083	0.099	0.212
Putative chaperon-like protein for quinone binding in photosystem II	Photosynthesis	DOWN	0.021	0.013	0.215
Transaldolase	Central Metabolism	UP	0.013	0.021	0.215
Alanine--tRNA ligase	Basic Cellular Processes	DOWN	0.058	0.043	0.215
ATP-dependent zinc metalloprotease FtsH	Basic Cellular Processes	DOWN	0.048	0.024	0.216
Protein translocase subunit SecA	Membrane Transport	DOWN	0.171	0.116	0.216
Aspartate kinase	Basic Cellular Processes	UP	0.01	0.011	0.217
Guanylate kinase	Energy Production and Conversion	UP	0.061	0.072	0.219
D-3-phosphoglycerate dehydrogenase	Central Metabolism	UP	0.136	0.15	0.22
Transaldolase	Central Metabolism	UP	0.271	0.336	0.221
Putative ATP-dependent Clp protease, Hsp 100, ATP-binding subunit ClpB	Basic Cellular Processes	DOWN	0.013	0.009	0.221
Possible cAMP phosphodiesterases class-II	Central Metabolism	UP	0.113	0.145	0.221
2-isopropylmalate synthase	Central Metabolism	DOWN	0.033	0.025	0.222
Adenylyl-sulfate kinase	Inorganic Nutrient Processing	UP	0.064	0.078	0.224
DNA topoisomerase 1	Basic Cellular Processes	DOWN	0.041	0.03	0.227
Chaperone protein HtpG	Basic Cellular Processes	DOWN	0.431	0.341	0.227

Table A1.3. Lowest 20 q-value proteins as identified in the cellular-proteome during Proteomics experiment 2A (~750 NPs cell^{-1})

Protein	Function	UP/Down-regulated	RA% Control	RA% AgNPs	q-value
50S ribosomal protein L5	Basic Cellular Processes	DOWN	0.154	0.142	0.233
30S ribosomal protein S5	Basic Cellular Processes	DOWN	0.543	0.487	0.237
Possible Major surface glycoprotein	Basic Cellular Processes	DOWN	0.136	0.105	0.278
NDP-hexose 3,4-dehydratase	Central Metabolism	DOWN	0.072	0.059	0.282
30S ribosomal protein S2	Basic Cellular Processes	DOWN	0.274	0.249	0.29
Cell division protein FtsZ	Basic Cellular Processes	UP	0.981	1.136	0.295
Photosystem II reaction center protein I	Photosynthesis	DOWN	0.836	0.618	0.298
Putative sulfate transporter	Membrane Transport	DOWN	0.013	0.01	0.303
Adenosylhomocysteinase	Central Metabolism	UP	0.029	0.036	0.304
Chromosome partition protein Smc	Basic Cellular Processes	DOWN	0.007	0.006	0.309
50S ribosomal protein L7/L12	Basic Cellular Processes	UP	0.224	0.279	0.31
50S ribosomal protein L4	Basic Cellular Processes	DOWN	0.176	0.156	0.315
GMP synthase	Central Metabolism	DOWN	0.024	0.003	0.316
50S ribosomal protein L22	Basic Cellular Processes	DOWN	0.131	0.083	0.333
30S ribosomal protein S1-like protein A	Basic Cellular Processes	UP	0.454	0.559	0.339
Acetyl-coenzyme A carboxylase carboxyl transferase subunit beta	Central Metabolism	DOWN	0.031	0.027	0.341
Sulfolipid (UDP-sulfoquinovose) biosynthesis protein	Central Metabolism	DOWN	0.045	0.038	0.342
Replicative DNA helicase	Basic Cellular Processes	UP	0.02	0.024	0.349
Mg-protoporphyrin IX chelatase	Photosynthesis	DOWN	0.016	0.014	0.358
ATP synthase gamma chain	Energy Production and Conversion	DOWN	0.172	0.143	0.374

Table A1.4. Lowest 20 q-value proteins as identified in the cellular-proteome during Proteomics experiment 2B (~1500 NPs cell^{-1})

Protein	Function	UP/Down-regulated	RA% Control	RA% AgNPs	q-value
30S ribosomal protein S4	Basic Cellular Processes	DOWN	0.418	0.324	0.103
Histidine--tRNA ligase	Basic Cellular Processes	DOWN	0.041	0.033	0.107
3-oxoacyl-[acyl-carrier protein] reductase	Central Metabolism	DOWN	0.013	0.006	0.149
Putative iron ABC transporter, substrate binding protein	Membrane Transport	DOWN	0.443	0.341	0.152
30S ribosomal protein S5	Basic Cellular Processes	DOWN	0.543	0.473	0.154
DNA-directed RNA polymerase subunit alpha	Basic Cellular Processes	DOWN	0.516	0.424	0.158
Dihydrolipoamide acetyltransferase component of pyruvate dehydrogenase complex	Central Metabolism	UP	0.212	0.237	0.159
30S ribosomal protein S7	Basic Cellular Processes	DOWN	0.822	0.641	0.16
ABC transporter, membrane component	Membrane Transport	DOWN	0.026	0.02	0.16
50S ribosomal protein L22	Basic Cellular Processes	DOWN	0.131	0.076	0.162
Cell division protein FtsZ	Basic Cellular Processes	UP	0.981	1.158	0.164
NDP-hexose 3,4-dehydratase	Central Metabolism	DOWN	0.072	0.057	0.173
50S ribosomal protein L4	Basic Cellular Processes	DOWN	0.176	0.129	0.179
Phosphate-binding protein	Membrane Transport	DOWN	1.179	0.983	0.189
Threonine synthase	Central Metabolism	DOWN	0.339	0.292	0.19
Glyceraldehyde-3-phosphate dehydrogenase	Central Metabolism	DOWN	1.495	1.269	0.19
dCTP deaminase	Central Metabolism	DOWN	0.041	0.029	0.194
Putative sulfate transporter	Membrane Transport	DOWN	0.013	0.009	0.196
Branched-chain-amino-acid aminotransferase	Basic Cellular Processes	DOWN	0.036	0.027	0.197
Transcription termination/antitermination protein NusG	Basic Cellular Processes	DOWN	0.946	0.767	0.2

Table A1.5. Lowest 20 q-value proteins as identified in the exo-proteome during Proteomics experiment 2A (~750 NPs cell^{-1})

Protein	Function	UP/Down-regulated	RA% Control	RA% AgNPs	q-value
ATP-dependent protease La (LON) domain	Basic Cellular Processes	DOWN	0.043	0.05	0.2335
Carboxysome shell protein CsoS2	Carbon fixation	UP	1.387	1.517	0.2568
Bifunctional protein HldE	Other	DOWN	0.011	0.005	0.2853
Protein translocase subunit SecA	Membrane Transport	UP	0.189	0.194	0.2973
Elongation factor Ts	Other	UP	0.125	0.136	0.3026
Putative ATP-dependent Clp protease, Hsp 100, ATP-binding subunit ClpB	Basic Cellular Processes	DOWN	0.023	0.005	0.321
Putative potassium channel, VIC family	Membrane Transport	DOWN	0.017	0.015	0.3229
50S ribosomal protein L13	Basic Cellular Processes	UP	0.031	0.052	0.3258
Glucose-1-phosphate denylyltransferase	Central Metabolism	DOWN	0.444	0.368	0.3304
Uncharacterized protein	Uncharacterized	-	-	0.082	0.3306
Aminotransferase	Central Metabolism	UP	0.036	0.04	0.3307
Uncharacterized protein	Uncharacterized	-	-	0.145	0.3432
DNA topoisomerase 1	Basic Cellular Processes	UP	0.076	0.079	0.3513
60 kDa chaperonin 2	Basic Cellular Processes	DOWN	5.4	3.959	0.3604
Pyruvate kinase	Central Metabolism	UP	0.092	0.104	0.3632
ATP synthase subunit beta	Energy Production and Conversion	DOWN	0.39	0.291	0.3767
Dehydrogenase E1 component beta subunit	Central Metabolism	DOWN	0.2	0.154	0.3783
Cysteine synthase	Central Metabolism	UP	0.932	0.971	0.38
Uncharacterized protein	Uncharacterized	-	-	0.47	0.3948
Chaperone protein DnaK	Basic Cellular Processes	UP	0.039	1.1	0.4127

Table A1.6. Lowest 20 q-value proteins as identified in the exo-proteome during Proteomics experiment 2B (~1500 NPs cell^{-1}); ***p≤0.05; *p≤0.1

Protein	Function	UP/Down-regulated	RA% Control	RA% AgNPs	q-value	Significance
30S ribosomal protein S7	Basic Cellular Processes	UP	0.289	0.173	0	***
30S ribosomal protein S21	Basic Cellular Processes	DOWN	0.22	0.079	0.028	***
S1 RNA binding domain:Ribonuclease E and G	Basic Cellular Processes	DOWN	0.019	0.003	0.037	***
30S ribosomal protein S12	Basic Cellular Processes	DOWN	0.358	0.278	0.039	***
30S ribosomal protein S8	Basic Cellular Processes	DOWN	0.458	0.394	0.044	***
Transketolase	Carbon Fixation	DOWN	0.394	0.717	0.051	*
50S ribosomal protein L19	Basic Cellular Processes	DOWN	0.069	0.056	0.056	*
Protein GrpE	Other	DOWN	0.143	0.067	0.062	*
Uncharacterized protein	Uncharacterized	UP	0.914	0.415	0.088	*
50S ribosomal protein L24	Basic Cellular Processes	DOWN	0.128	0.076	0.098	*
Possible Major surface glycoprotein	Membrane Transport	DOWN	0.124	0.066	0.114	
Uncharacterized protein	Uncharacterized	UP	0.408	0.206	0.124	
3-oxoacyl-[acyl-carrier protein] reductase	Central Metabolism	DOWN	0.017	0.022	0.133	
Glutamine--fructose-6-phosphate aminotransferase	Central Metabolism	DOWN	0.058	0.05	0.141	
50S ribosomal protein L18	Basic Cellular Processes	DOWN	0.554	0.329	0.152	
30S ribosomal protein S3	Basic Cellular Processes	DOWN	0.054	0.044	0.159	
Photosystem I reaction center subunit IV	Photosynthesis	UP	0.998	0.884	0.16	
Chaperone protein HtpG	Basic Cellular Processes	DOWN	0.239	0.304	0.169	
DNA-directed RNA polymerase subunit beta	Basic Cellular Processes	DOWN	0.967	1.284	0.18	
ATP-dependent Clp protease ATP-binding subunit ClpX	Basic Cellular Processes	DOWN	0.163	0.127	0.19	

Table A1.7. Significant proteins in AgNP treatment

Protein	Annotation	Function	RA% Control	RA% AgNPs	Log2 Fold Change	q-value
Q7UZK2	50S ribosomal protein L35	Basic cellular processes	0.005	0.020	1.999	0.103
Q7V3P9	UDP-N-acetylenolpyruvoylglucosamine reductase	Basic cellular processes	0.001	0.002	1.839	0.107
Q7TU99	50S ribosomal protein L33	Basic cellular processes	0.030	0.064	1.264	0.149
Q7V1H0	50S ribosomal protein L28	Basic cellular processes	0.041	0.071	0.949	0.152
Q7V384	50S ribosomal protein L7/L12	Basic cellular processes	0.171	0.271	0.816	0.154
Q7UZV1	50S ribosomal protein L22	Basic cellular processes	0.026	0.041	0.804	0.158
Q7V3A1	Endoribonuclease YbeY	Basic cellular processes	0.001	0.002	0.777	0.159
Q7V3C4	Bacterial regulatory protein, LuxR family	Basic cellular processes	0.029	0.043	0.712	0.16
Q7UZK1	50S ribosomal protein L20	Basic cellular processes	0.026	0.038	0.700	0.16
Q7UZW1	50S ribosomal protein L15	Basic cellular processes	0.074	0.107	0.681	0.162
Q7V1K4	Putative tRNA (cytidine(34)-2'-O)-methyltransferase	Basic cellular processes	0.002	0.003	0.662	0.164
Q7TU67	30S ribosomal protein S14	Basic cellular processes	0.057	0.080	0.651	0.173
Q7UZV3	50S ribosomal protein L16	Basic cellular processes	0.074	0.102	0.617	0.179
Q7V1P0	Ribosomal silencing factor RsfS	Basic cellular processes	0.007	0.009	0.611	0.189
Q7TU65	30S ribosomal protein S16	Basic cellular processes	0.147	0.201	0.603	0.19
Q7UZU9	50S ribosomal protein L23	Basic cellular processes	0.092	0.126	0.598	0.19
Q7V0C3	Circadian clock protein KaiB	Basic cellular processes	0.045	0.061	0.579	0.194
Q7TU29	50S ribosomal protein L14	Basic cellular processes	0.117	0.156	0.577	0.196
Q7V0G6	Peptidyl-prolyl cis-trans isomerase	Basic cellular processes	0.026	0.035	0.563	0.197
Q7V382	50S ribosomal protein L1	Basic cellular processes	0.143	0.186	0.526	0.2

Table A1.7. Significant proteins in AgNP treatment

Protein	Annotation	Function	RA% Control	RA% AgNPs	Log2 Fold Change	q-value
Q7UZY4	30S ribosomal protein S12	Basic cellular processes	0.055	0.071	0.508	0.029
Q7UZY5	30S ribosomal protein S7	Basic cellular processes	0.179	0.229	0.505	0.028
Q7UZV6	50S ribosomal protein L5	Basic cellular processes	0.086	0.110	0.505	0.036
Q7V383	50S ribosomal protein L10	Basic cellular processes	0.094	0.120	0.505	0.031
Q7TU27	30S ribosomal protein	Basic cellular processes	0.063	0.079	0.486	0.030
Q7V0A5	UDP-N-acetylmuramoylalanine--D-glutamate ligase	Basic cellular processes	0.001	0.002	0.485	0.019
Q7TU43	10 kDa chaperonin	Basic cellular processes	0.989	1.219	0.458	0.043
Q7V3K7	Peptide deformylase	Basic cellular processes	0.013	0.015	0.450	0.029
Q7UZW4	30S ribosomal protein S13	Basic cellular processes	0.109	0.134	0.449	0.029
Q7V1V0	30S ribosomal protein S2	Basic cellular processes	0.136	0.165	0.435	0.000
Q7V2S2	Cell division protein SepF	Basic cellular processes	0.040	0.049	0.431	0.044
Q7TU24	Translation initiation factor IF-3	Basic cellular processes	0.064	0.074	0.364	0.029
Q7TU53	Possible Helix-turn-helix protein, copG family	Basic cellular processes	0.028	0.032	0.352	0.038
Q7UZV4	50S ribosomal protein L29	Basic cellular processes	0.071	0.080	0.325	0.011
Q7UZW7	50S ribosomal protein L17	Basic cellular processes	0.105	0.119	0.325	0.033
Q7V1F2	SAM (And some other nucleotide) binding motif:Generic methyl-transferase	Basic cellular processes	0.012	0.014	0.324	0.022
Q7UZV5	50S ribosomal protein L24	Basic cellular processes	0.052	0.059	0.322	0.031
Q7UZW0	30S ribosomal protein S5	Basic cellular processes	0.170	0.190	0.316	0.018
Q7V381	50S ribosomal protein L11	Basic cellular processes	0.147	0.165	0.315	0.021
Q7V2R1	30S ribosomal protein S4	Basic cellular processes	0.107	0.120	0.312	0.028

Table A1.7. Significant proteins in AgNP treatment

Protein	Annotation	Function	RA% Control	RA% AgNPs	Log2 Fold Change	q-value
Q7TUG0	Queuine tRNA-ribosyltransferase	Basic cellular processes	0.008	0.009	0.288	0.030
Q7UZW8	50S ribosomal protein L13	Basic cellular processes	0.117	0.128	0.283	0.039
Q7TU44	60 kDa chaperonin 2	Basic cellular processes	6.232	6.815	0.279	0.025
Q7V2K6	tRNA N6-adenosine threonylcarbamoyltransferase	Basic cellular processes	0.005	0.006	0.271	0.037
Q7V3P5	Elongation factor P	Basic cellular processes	0.052	0.057	0.271	0.030
Q7UZM3	Possible transcriptional regulator	Basic cellular processes	0.035	0.038	0.267	0.029
Q7UZV8	50S ribosomal protein L6	Basic cellular processes	0.169	0.184	0.264	0.029
Q7UZW6	DNA-directed RNA polymerase subunit alpha	Basic cellular processes	0.415	0.448	0.259	0.024
Q7TUB2	Possible Major surface glycoprotein	Basic cellular processes	0.183	0.196	0.250	0.043
Q7UZJ1	50S ribosomal protein L9	Basic cellular processes	0.141	0.152	0.249	0.038
Q7TUC9	Possible Helix-turn-helix domain of resolvase	Basic cellular processes	0.058	0.063	0.247	0.033
Q7UZU7	50S ribosomal protein L3	Basic cellular processes	0.077	0.082	0.238	0.033
Q7UZN9	Two-component response regulator	Basic cellular processes	0.127	0.135	0.233	0.039
Q7TU61	Cell division protein FtsZ	Basic cellular processes	1.092	1.144	0.215	0.028
Q7UZW9	30S ribosomal protein S9	Basic cellular processes	0.029	0.030	0.199	0.028
Q7V0F6	D-alanine--D-alanine ligase	Basic cellular processes	0.013	0.013	0.186	0.047
Q7V305	Putative gluconeogenesis factor	Basic cellular processes	0.019	0.020	0.176	0.036
Q7UZY8	30S ribosomal protein S10	Basic cellular processes	0.128	0.130	0.173	0.039
Q7V0H2	Signal recognition particle protein	Basic cellular processes	0.104	0.105	0.166	0.033
Q7UZN6	Rod shape determining protein	Basic cellular processes	0.279	0.282	0.162	0.027

Table A1.7. Significant proteins in AgNP treatment

Protein	Annotation	Function	RA% Control	RA% AgNPs	Log2 Fold Change	q-value
Q7UZN6	Rod shape determining protein	Basic cellular processes	0.279	0.282	0.162	0.027
Q7V3E3	DNA repair protein RadA	Basic cellular processes	0.015	0.015	0.159	0.030
Q7V0Y1	Two-component response regulator	Basic cellular processes	0.265	0.266	0.159	0.047
Q7UZJ0	Replicative DNA helicase	Basic cellular processes	0.032	0.032	0.155	0.047
Q7TUH5	Putative Rubisco transcriptional regulator	Basic cellular processes	0.134	0.131	0.121	0.042
Q7V106	ClpC	Basic cellular processes	0.240	0.235	0.116	0.009
Q7V2M3	60 kDa chaperonin 1	Basic cellular processes	1.460	1.420	0.109	0.030
Q7V228	Peptide chain release factor 3	Basic cellular processes	0.051	0.049	0.077	0.033
Q7V1K0	Methionine--tRNA ligase	Basic cellular processes	0.291	0.246	-0.091	0.029
Q7V0C4	Circadian clock protein kinase KaiC	Basic cellular processes	0.151	0.126	-0.120	0.031
Q7V3R4	DNA topoisomerase (ATP-hydrolyzing)	Basic cellular processes	0.025	0.020	-0.136	0.029
Q7UZM4	DNA gyrase subunit B	Basic cellular processes	0.132	0.106	-0.163	0.028
Q7V1D0	Glutamyl-tRNA(Gln) amidotransferase subunit A	Basic cellular processes	0.122	0.098	-0.170	0.036
Q7V0T8	Glycine--tRNA ligase alpha subunit	Basic cellular processes	0.074	0.057	-0.209	0.028
Q7V0R3	Ribosomal RNA small subunit methyltransferase I	Basic cellular processes	0.019	0.015	-0.229	0.028
Q7V3Q3	Chaperone protein DnaJ	Basic cellular processes	0.092	0.069	-0.260	0.029
Q7V0W1	Cysteine--tRNA ligase	Basic cellular processes	0.018	0.013	-0.261	0.039
Q7V309	NUDIX hydrolase	Basic cellular processes	0.072	0.053	-0.291	0.027
Q7V3R7	DNA polymerase III subunit beta	Basic cellular processes	0.292	0.211	-0.320	0.033
Q7TUG3	Global nitrogen regulatory protein, CRP family	Basic cellular processes	0.009	0.006	-0.414	0.041

Table A1.7. Significant proteins in AgNP treatment

Protein	Annotation	Function	RA% Control	RA% AgNPs	Log2 Fold Change	q-value
Q7TUF7	tRNA nucleotidyltransferase/poly(A) polymerase	Basic cellular processes	0.010	0.006	-0.439	0.028
Q7V156	Ferric uptake regulator family	Basic cellular processes	0.007	0.004	-0.449	0.033
Q7V2D1	Carbon dioxide-concentrating mechanism protein CcmK	Carbon fixation	2.196	2.980	0.595	0.029
Q7V2D0	Ribulose bisphosphate carboxylase large chain	Carbon fixation	1.426	1.771	0.457	0.050
Q7V003	Ribose-5-phosphate isomerase A	Carbon fixation	0.137	0.081	-0.614	0.019
Q7UZT0	Phosphoenolpyruvate carboxylase	Carbon fixation	0.110	0.093	-0.098	0.047
Q7V1V7	Insulinase family (Peptidase family M16)	Central Metabolism	0.000	0.002	2.133	0.000
Q7V3A8	Probable O-succinylbenzoic acid--CoA ligase (OSB-CoA synthetase)	Central Metabolism	0.005	0.008	0.862	0.029
Q7V2I5	Putative pterin-4-alpha-carbinolamine dehydratase	Central Metabolism	0.077	0.119	0.794	0.032
Q7V308	Possible 2-amino-4-hydroxy-6-hydroxymethyldihydropteridine pyrophosphokinase	Central Metabolism	0.010	0.014	0.752	0.039
Q7TUG4	dCTP deaminase	Central Metabolism	0.050	0.069	0.607	0.000
Q7V254	Putative lycopene epsilon cyclase	Central Metabolism	0.006	0.008	0.598	0.033
Q7V3C6	Putative sugar-phosphate nucleotidyl transferase	Central Metabolism	0.008	0.011	0.582	0.032
Q7V1F4	Serine:pyruvate/alanine:glyoxylate aminotransferase	Central Metabolism	0.005	0.006	0.544	0.030
Q7V200	Short-chain dehydrogenase/reductase (SDR) superfamily	Central Metabolism	0.022	0.028	0.490	0.027
Q7V2M1	2-C-methyl-D-erythritol 4-phosphate cytidylyltransferase	Central Metabolism	0.015	0.018	0.457	0.029
Q7V3B5	N5-carboxyaminoimidazole ribonucleotide mutase	Central Metabolism	0.038	0.046	0.435	0.043
Q7V0D2	Lipid-A-disaccharide synthase	Central Metabolism	0.004	0.005	0.420	0.017
Q7V271	2-phosphosulfolactate phosphatase	Central Metabolism	0.024	0.028	0.405	0.029
Q7UZZ7	Dolichyl-phosphate-mannose-protein mannosyltransferase	Central Metabolism	0.001	0.001	0.397	0.048

Table A1.7. Significant proteins in AgNP treatment

Protein	Annotation	Function	RA% Control	RA% AgNPs	Log2 Fold Change	q-value
Q7V1Z9	Glutamine amidotransferase class-I	Central Metabolism	0.003	0.003	0.385	0.022
Q7V3A7	Putative O-succinylbenzoate synthase	Central Metabolism	0.003	0.004	0.365	0.030
Q7V215	4-hydroxy-3-methylbut-2-en-1-yl diphosphate synthase (ferredoxin)	Central Metabolism	0.023	0.026	0.347	0.048
Q7V1E4	Pyruvate dehydrogenase E1 beta subunit	Central Metabolism	0.051	0.058	0.334	0.040
Q7V320	Orotate phosphoribosyltransferase	Central Metabolism	0.138	0.155	0.321	0.013
Q7V153	Cobalamin synthesis protein/P47K	Central Metabolism	0.163	0.182	0.310	0.042
Q7V3E0	3-oxoacyl-[acyl-carrier-protein] synthase 3	Central Metabolism	0.023	0.026	0.302	0.028
Q7V1D4	Possible cAMP phosphodiesterases class-II	Central Metabolism	0.074	0.082	0.285	0.030
Q7UZZ6	Glycosyl transferase, family 2	Central Metabolism	0.010	0.011	0.277	0.043
Q7V0N5	Glycosyl transferase, group 1	Central Metabolism	0.003	0.003	0.275	0.037
Q7V288	Putative glucokinase	Central Metabolism	0.005	0.006	0.270	0.029
Q7V1H9	N-acetyl-gamma-glutamyl-phosphate reductase	Central Metabolism	0.020	0.022	0.267	0.029
Q7V0I3	Thiamine-phosphate synthase	Central Metabolism	0.012	0.013	0.264	0.038
Q7V1G6	1-deoxy-D-xylulose-5-phosphate synthase	Central Metabolism	0.098	0.106	0.261	0.028
Q7UZT5	ATP:corrinoid adenosyltransferase BtuR/CobO/CobP	Central Metabolism	0.007	0.008	0.260	0.009
Q7V1N1	4-hydroxy-tetrahydrodipicolinate reductase	Central Metabolism	0.106	0.115	0.257	0.030
Q7V3D2	Phytoene desaturase	Central Metabolism	0.122	0.131	0.252	0.047
Q7V364	Chorismate synthase	Central Metabolism	0.109	0.117	0.251	0.038
Q7V1R9	3-isopropylmalate dehydrogenase	Central Metabolism	0.026	0.028	0.246	0.000
Q7V2E5	Putative short-chain dehydrogenase	Central Metabolism	0.024	0.026	0.245	0.038

Table A1.7. Significant proteins in AgNP treatment

Protein	Annotation	Function	RA% Control	RA% AgNPs	Log2 Fold Change	q-value
Q7TU15	Threonine synthase	Central Metabolism	0.136	0.145	0.243	0.047
Q7TUC8	Tryptophan synthase alpha chain	Central Metabolism	0.037	0.039	0.237	0.038
Q7TUF4	Carboxyl-terminal processing proteinase	Central Metabolism	0.082	0.086	0.223	0.039
Q7V217	Aminotransferase	Central Metabolism	0.117	0.122	0.211	0.008
Q7V3C0	Citrate synthase	Central Metabolism	0.221	0.230	0.206	0.028
Q7V3L5	Acetyl-CoA carboxylase, biotin carboxylase subunit	Central Metabolism	0.070	0.073	0.204	0.030
Q7V024	Fumarate hydratase class II	Central Metabolism	0.057	0.059	0.204	0.018
Q7V2E9	Creatininase	Central Metabolism	0.048	0.050	0.195	0.035
Q7V299	1,4-alpha-glucan branching enzyme GlgB	Central Metabolism	0.051	0.051	0.170	0.029
Q7V397	Aminotransferase	Central Metabolism	0.031	0.031	0.144	0.029
Q7V111	Ribose-phosphate pyrophosphokinase	Central Metabolism	0.059	0.059	0.141	0.031
Q7UZN3	Adenosylhomocysteinase	Central Metabolism	0.154	0.152	0.128	0.036
Q7V1G1	Pyruvate kinase	Central Metabolism	0.222	0.219	0.125	0.028
Q7V3E1	Phosphate acyltransferase	Central Metabolism	0.061	0.059	0.100	0.030
Q7V0L3	Possible methyltransferase	Central Metabolism	0.064	0.061	0.099	0.034
Q7V2D2	HAM1 family protein	Central Metabolism	0.026	0.022	-0.083	0.032
Q7V352	Isoleucine--tRNA ligase	Central Metabolism	0.045	0.038	-0.094	0.047
Q7V0X9	Putative carotenoid isomerase	Central Metabolism	0.036	0.030	-0.112	0.049
Q7V108	Orn/Lys/Arg decarboxylases family 1	Central Metabolism	0.026	0.021	-0.143	0.047
Q7V267	Acetyl-coenzyme A synthetase	Central Metabolism	0.118	0.096	-0.143	0.029

Table A1.7. Significant proteins in AgNP treatment

Protein	Annotation	Function	RA% Control	RA% AgNPs	Log2 Fold Change	q-value
Q7V0J5	UDP-glucose 6-dehydrogenase	Central Metabolism	0.121	0.099	-0.147	0.030
Q7V2A0	Uroporphyrinogen decarboxylase	Central Metabolism	0.142	0.114	-0.160	0.039
Q7TUD1	Acetylglutamate kinase	Central Metabolism	0.119	0.096	-0.169	0.012
Q7V1U6	Glycine--tRNA ligase beta subunit	Central Metabolism	0.051	0.040	-0.191	0.025
Q7V3M9	Biosynthetic arginine decarboxylase	Central Metabolism	0.025	0.020	-0.205	0.038
Q7V2H0	Proline--tRNA ligase	Central Metabolism	0.079	0.062	-0.208	0.034
Q7V1H8	Riboflavin biosynthesis protein RibBA	Central Metabolism	0.091	0.071	-0.212	0.030
Q7V3J9	Phosphoglucomutase	Central Metabolism	0.098	0.076	-0.227	0.031
Q7V2K3	Glutamate--tRNA ligase	Central Metabolism	0.027	0.021	-0.228	0.030
Q7V116	Glucose-6-phosphate 1-dehydrogenase	Central Metabolism	0.089	0.068	-0.234	0.033
Q7TU35	Prephenate dehydratase	Central Metabolism	0.015	0.011	-0.236	0.029
Q7TUH0	Tryptophan synthase beta chain	Central Metabolism	0.063	0.048	-0.240	0.032
Q7V2F4	Acetolactate synthase	Central Metabolism	0.123	0.093	-0.246	0.044
Q7UZX4	Glycosyl transferase, family 2	Central Metabolism	0.018	0.014	-0.253	0.037
Q7V2Z6	S-methyl-5'-thioadenosine phosphorylase	Central Metabolism	0.039	0.029	-0.254	0.047
Q7V3N7	GMP synthase [glutamine-hydrolyzing]	Central Metabolism	0.148	0.111	-0.262	0.016
Q7V0E4	Putative isoamylase	Central Metabolism	0.022	0.016	-0.273	0.028
Q7V0I4	Riboflavin biosynthesis protein	Central Metabolism	0.017	0.013	-0.280	0.040
Q7V3R5	Phosphoribosylformylglycinamidine synthase subunit PurL	Central Metabolism	0.063	0.047	-0.291	0.029
Q7V0K2	Putative glycosyl transferase, family 2	Central Metabolism	0.011	0.008	-0.311	0.028

Table A1.7. Significant proteins in AgNP treatment

Protein	Annotation	Function	RA% Control	RA% AgNPs	Log2 Fold Change	q-value
Q7UZQ7	Alpha-1,4 glucan phosphorylase	Central Metabolism	0.057	0.041	-0.331	0.011
Q7V135	Homoserine dehydrogenase	Central Metabolism	0.046	0.032	-0.354	0.024
Q7V1F6	Pyridoxal-dependent decarboxylase family protein	Central Metabolism	0.011	0.007	-0.358	0.032
Q7V0Q3	CDP-glucose 4,6-dehydratase	Central Metabolism	0.030	0.020	-0.464	0.030
Q7V1H2	Inositol-1-monophosphatase	Central Metabolism	0.017	0.010	-0.564	0.047
Q7V324	Adenosylcobinamide-GDP ribazoletransferase	Central Metabolism	0.003	0.001	-1.248	0.029
Q7TU69	Possible Trehalase	Energy production and conversion	0.001	0.003	1.235	0.041
Q7UZU6	NAD(P)H-quinone oxidoreductase subunit N	Energy production and conversion	0.019	0.025	0.567	0.030
Q7TUH2	Putative NADH Dehydrogenase (Complex I) subunit (Chain 6)	Energy production and conversion	0.013	0.017	0.480	0.047
Q7V035	ATP synthase subunit b	Energy production and conversion	0.051	0.061	0.401	0.039
Q7V3B0	NAD(P)H-quinone oxidoreductase subunit H	Energy production and conversion	0.044	0.051	0.370	0.041
Q7V038	ATP synthase gamma chain	Energy production and conversion	0.097	0.102	0.215	0.030
Q7V049	ATP synthase subunit beta	Energy production and conversion	0.664	0.648	0.114	0.033
Q7V2Q2	Probable malate:quinone oxidoreductase	Energy production and conversion	0.016	0.013	-0.176	0.033
Q7UZW3	Adenylate kinase	Energy production and conversion	0.035	0.018	-0.823	0.000
Q7V0H3	PhoH-like phosphate starvation-inducible protein	Inorganic nutrient processing	0.020	0.022	0.321	0.029
Q7V025	Nitrogen regulatory protein P-II	Inorganic nutrient processing	0.241	0.238	0.130	0.000
Q7TU42	ATP synthase epsilon chain	Membrane transport	0.009	0.024	1.655	0.010
Q7V1A9	Putative urea ABC transporter, substrate binding protein	Membrane transport	0.297	0.331	0.307	0.033
Q7V0T9	Putative iron ABC transporter, substrate binding protein	Membrane transport	6.839	7.450	0.273	0.030

Table A1.7. Significant proteins in AgNP treatment

Protein	Annotation	Function	RA% Control	RA% AgNPs	Log2 Fold Change	q-value
Q7V371	Putative sulfate transporter	Membrane transport	0.042	0.044	0.207	0.030
Q7V3J0	Putative potassium channel, VIC family	Membrane transport	0.137	0.143	0.207	0.010
Q7V1N6	ABC transporter, possibly multidrug efflux	Membrane transport	0.037	0.037	0.164	0.028
Q7V1G0	Possible ABC transporter	Membrane transport	0.024	0.023	0.122	0.029
Q7V0S4	Signal peptide peptidase SppA (Protease IV)	Membrane transport	0.290	0.283	0.111	0.012
Q7V244	Putative sulfate transporter	Membrane transport	0.013	0.010	-0.280	0.028
Q7V393	ABC transporter, ATP binding component, possibly for oligopeptides	Membrane transport	0.004	0.003	-0.351	0.034
Q7V2K4	Putative Na+/H+ antiporter, CPA1 family	Membrane transport	0.003	0.002	-0.546	0.029
Q7V379	Protein translocase subunit SecE	Membrane transport	0.069	0.040	-0.623	0.031
Q7TU84	Possible Integrin alpha cytoplasmic region	Other	0.013	0.022	1.004	0.049
Q7TUE9	Possible Spectrin repeat	Other	0.011	0.015	0.611	0.030
Q7V3F1	UPF0367 protein PMM0124	Other	0.166	0.216	0.537	0.043
Q7TU52	Possible Heat-labile enterotoxin alpha chain	Other	0.004	0.005	0.500	0.000
Q7V3B3	Two-component response regulator	Other	0.214	0.245	0.339	0.023
Q7V1W1	Protein Thf1	Other	0.043	0.048	0.321	0.030
Q7V0Q4	Possible nucleoside-diphosphate-sugar epimerase	Other	0.025	0.025	0.195	0.036
Q7V0N7	Putative nucleoside-diphosphate sugar epimerase	Other	0.078	0.061	-0.209	0.046
Q7V243	FAD linked oxidase, N-terminal	Other	0.003	0.002	-0.260	0.028
Q7V2U6	Type-1 copper (Blue) domain	Other	0.006	0.004	-0.402	0.009
Q7V2U7	Possible DsrE-like protein	Other	0.029	0.019	-0.455	0.032

Table A1.7. Significant proteins in AgNP treatment

Protein	Annotation	Function	RA% Control	RA% AgNPs	Log2 Fold Change	q-value
Q7V0G5	Putative nickel-containing superoxide dismutase (NISOD)	Oxidative stress	0.184	0.250	0.592	0.033
Q7V126	Thioredoxin	Oxidative stress	0.319	0.405	0.498	0.008
Q7V366	Glutathione S-transferase C terminus	Oxidative stress	0.005	0.006	0.375	0.039
Q7V0D3	Peptide methionine sulfoxide reductase MsrA	Oxidative stress	0.007	0.008	0.280	0.010
Q7V1K9	Thioredoxin peroxidase	Oxidative stress	1.086	0.772	-0.344	0.029
Q7V2A2	Plastocyanin	Photosynthesis	0.027	0.044	0.858	0.012
Q7V2Z8	Photosystem II reaction center protein L	Photosynthesis	0.013	0.020	0.815	0.009
Q7V303	NAD(P)H-quinone oxidoreductase subunit K	Photosynthesis	0.012	0.018	0.707	0.009
Q7V2L4	Cytochrome b6-f complex iron-sulfur subunit	Photosynthesis	0.010	0.014	0.653	0.043
Q7V3E4	Photosystem I assembly protein Ycf3	Photosynthesis	0.003	0.005	0.594	0.030
Q7V0U6	Photosystem I assembly protein Ycf4	Photosynthesis	0.039	0.052	0.558	0.013
Q7V2D6	Light-independent protochlorophyllide reductase subunit B	Photosynthesis	0.004	0.005	0.523	0.016
Q7V1U5	Aromatic-ring hydroxylase (Flavoprotein monooxygenase)	Photosynthesis	0.106	0.130	0.436	0.009
Q7V115	Ferredoxin-NADP oxidoreductase (FNR)	Photosynthesis	0.398	0.462	0.364	0.031
Q7UZS7	Photosystem I protein PsaD	Photosynthesis	0.262	0.301	0.351	0.009
Q9RC08	Photosystem I P700 chlorophyll a apoprotein A1	Photosynthesis	0.097	0.109	0.330	0.029
Q7TUF5	Photosystem II reaction center protein M	Photosynthesis	0.019	0.019	0.194	0.041
Q7V1N2	Protoporphyrin IX magnesium chelatase, subunit chlH	Photosynthesis	0.024	0.024	0.174	0.028
Q7V1T7	Glutamyl-tRNA reductase	Photosynthesis	0.037	0.036	0.133	0.047
Q7V072	Uncharacterized protein	Uncharacterized	0.002	0.060	5.024	0.000

Table A1.7. Significant proteins in AgNP treatment

Protein	Annotation	Function	RA% Control	RA% AgNPs	Log2 Fold Change	q-value
Q7UZT7	Uncharacterized protein	Uncharacterized	0.017	0.091	2.506	0.010
Q7V2Z1	Uncharacterized protein	Uncharacterized	0.022	0.058	1.620	0.039
Q7V0D5	Uncharacterized protein	Uncharacterized	0.001	0.002	1.482	0.012
A8WI63	Uncharacterized protein	Uncharacterized	0.737	1.713	1.365	0.000
Q7V353	Uncharacterized protein	Uncharacterized	0.001	0.003	1.213	0.046
Q7V012	Uncharacterized protein	Uncharacterized	0.003	0.006	1.176	0.049
Q7V1S8	Uncharacterized protein	Uncharacterized	0.005	0.010	1.047	0.008
Q7UZP1	Uncharacterized protein	Uncharacterized	0.017	0.028	0.900	0.011
Q7V2T7	Uncharacterized protein	Uncharacterized	0.038	0.061	0.816	0.018
Q7V3H6	Uncharacterized protein	Uncharacterized	0.001	0.002	0.806	0.039
Q7V0S9	Uncharacterized protein	Uncharacterized	0.004	0.007	0.794	0.043
Q7V1A4	Uncharacterized protein	Uncharacterized	0.010	0.015	0.749	0.010
Q7V2D4	Conserved hypothetical	Uncharacterized	0.039	0.058	0.702	0.027
Q7V2T5	Uncharacterized protein	Uncharacterized	0.025	0.036	0.673	0.046
Q7V0D6	Uncharacterized protein	Uncharacterized	0.008	0.011	0.635	0.047
Q7V0M0	Uncharacterized protein	Uncharacterized	0.026	0.037	0.629	0.010
Q7V2B5	Uncharacterized protein	Uncharacterized	0.002	0.003	0.573	0.037
Q7V2I9	Uncharacterized protein	Uncharacterized	0.017	0.022	0.483	0.030
Q7V078	Uncharacterized protein	Uncharacterized	0.009	0.011	0.463	0.047
Q7V1D2	Uncharacterized protein	Uncharacterized	0.012	0.015	0.459	0.013

Table A1.7. Significant proteins in AgNP treatment

Protein	Annotation	Function	RA% Control	RA% AgNPs	Log2 Fold Change	q-value
Q7V0F5	Uncharacterized protein	Uncharacterized	0.021	0.027	0.454	0.046
Q7V0R9	Uncharacterized protein	Uncharacterized	0.077	0.092	0.408	0.035
Q7V2K2	Uncharacterized protein	Uncharacterized	0.048	0.057	0.398	0.029
Q7V1I5	Uncharacterized protein	Uncharacterized	0.018	0.020	0.335	0.032
Q7V0Y8	Uncharacterized protein	Uncharacterized	0.079	0.089	0.325	0.000
Q7V2I4	Uncharacterized protein	Uncharacterized	0.011	0.012	0.312	0.036
Q7V321	Uncharacterized protein	Uncharacterized	0.048	0.054	0.311	0.032
Q7V0R1	Uncharacterized protein	Uncharacterized	0.010	0.011	0.304	0.023
Q7V1N9	Uncharacterized protein	Uncharacterized	0.044	0.049	0.288	0.030
Q7V3R3	Uncharacterized protein	Uncharacterized	0.002	0.002	0.274	0.038
Q7V210	Uncharacterized protein	Uncharacterized	0.012	0.013	0.273	0.009
Q7V227	Uncharacterized protein	Uncharacterized	0.007	0.007	0.264	0.047
Q7V3D0	Uncharacterized protein	Uncharacterized	0.008	0.008	0.230	0.030
Q7V120	Uncharacterized protein	Uncharacterized	0.007	0.007	0.212	0.022
Q7V3B9	Uncharacterized protein	Uncharacterized	0.003	0.003	0.211	0.035
Q7V318	Uncharacterized protein	Uncharacterized	0.005	0.005	0.210	0.039
Q7V2R6	Uncharacterized protein	Uncharacterized	0.174	0.177	0.176	0.028
Q7V1L3	Uncharacterized protein	Uncharacterized	0.006	0.004	-0.175	0.033
Q7V0N1	Uncharacterized protein	Uncharacterized	0.062	0.049	-0.181	0.028
Q7V0S2	Uncharacterized protein	Uncharacterized	0.084	0.066	-0.188	0.043

Table A1.7. Significant proteins in AgNP treatment

Protein	Annotation	Function	RA% Control	RA% AgNPs	Log2 Fold Change	q-value
Q7V2J0	Uncharacterized protein	Uncharacterized	0.036	0.029	-0.199	0.048
Q7V1M0	Uncharacterized protein	Uncharacterized	0.120	0.092	-0.235	0.038
Q7V373	Uncharacterized protein	Uncharacterized	0.024	0.018	-0.277	0.032
Q7V1R0	Uncharacterized protein	Uncharacterized	0.023	0.017	-0.286	0.028
Q7V246	Uncharacterized protein	Uncharacterized	0.096	0.071	-0.289	0.039
Q7V319	Uncharacterized protein	Uncharacterized	0.006	0.004	-0.295	0.047
Q7V298	Uncharacterized protein	Uncharacterized	0.011	0.008	-0.300	0.033
Q7V0U0	Uncharacterized protein	Uncharacterized	0.017	0.012	-0.315	0.027
Q7V139	Uncharacterized protein	Uncharacterized	0.006	0.005	-0.345	0.027
Q7V0P4	Uncharacterized protein	Uncharacterized	0.021	0.014	-0.377	0.029
Q7V1T0	Conserved hypothetical	Uncharacterized	0.043	0.025	-0.637	0.042
Q7V176	Uncharacterized protein	Uncharacterized	0.456	0.209	-0.974	0.033
Q7UZT8	Uncharacterized protein	Uncharacterized	0.001	0.000	-1.630	0.032
Q7UZF9	Uncharacterized protein	Uncharacterized	0.014	0.003	-1.940	0.032

Table A1.8. BLAST search results for significant uncharacterised proteins

Protein	Description	Per. Ident (%)	Accession	Function
Q7UZF9	DUF3134 domain-containing protein [Prochlorococcus marinus]	100.00%	WP_011133335.1	NA
Q7UZT8	phosphotransferase [Prochlorococcus marinus]	100.00%	WP_011133195.1	Central Metabolism
Q7V176	Cell division protein FtsK [Prochlorococcus marinus str. EQPAC1]	99.10%	KGF88848.1	Basic cellular processes
Q7V1T0	membrane protein [Prochlorococcus marinus]	100.00%	WP_011132409.1	NA
Q7V0P4	SAM-dependent methyltransferase-like [Prochlorococcus marinus str. LG]	55.79%	KGG14241.1	Central Metabolism
Q7V139	alpha/beta hydrolase [Prochlorococcus marinus]	100.00%	WP_011132680.1	NA
Q7V0U0	hypothetical protein [Prochlorococcus marinus]	100.00%	WP_011132796.1	NA
Q7V298	CocE/NonD family hydrolase [Prochlorococcus marinus]	100.00%	WP_011132219.1	Central Metabolism
Q7V319	Folate-dependent protein for Fe/S cluster synthesis/repair in oxidative stress [Prochlorococcus marinus str. EQPAC1]	100.00%	KGF86417.1	NA
Q7V246	hypothetical protein [Prochlorococcus marinus]	100.00%	WP_011132275.1	NA
Q7V1R0	DUF3685 domain-containing protein [Prochlorococcus marinus]	100.00%	WP_011132429.1	NA
Q7V373	nitrogen regulatory protein P-II [Prochlorococcus marinus]	94.62%	WP_032514600.1	Basic cellular processes
Q7V1M0	DUF2996 domain-containing protein [Prochlorococcus marinus]	100.00%	WP_011132479.1	NA
Q7V0N1	hypothetical protein [Prochlorococcus marinus]	100.00%	WP_011132859.1	NA
Q7V1L3	DUF565 domain-containing protein [Prochlorococcus marinus]	100.00%	WP_011132486.1	NA
Q7V041	DUF3326 domain-containing protein [Prochlorococcus marinus]	100.00%	WP_011133076.1	NA
Q7V2A1	NAD(P)-dependent oxidoreductase [Prochlorococcus marinus]	100.00%	WP_011132216.1	NA
Q7V2R6	hypothetical protein [Prochlorococcus marinus]	100.00%	WP_011132039.1	NA
Q7V318	DNA repair enzyme [Prochlorococcus marinus str. EQPAC1]	100.00%	KGF86416.1	Basic cellular processes
Q7V3B9	hypothetical protein [Prochlorococcus marinus]	100.00%	WP_011131801.1	NA

Table A1.8. BLAST search results for significant uncharacterised proteins

Protein	Description	Per. Ident (%)	Accession	Function
Q7V120	HDIG domain-containing protein [Prochlorococcus marinus]	100.00%	WP_011132701.1	NA
Q7V3D0	DUF3172 domain-containing protein [Prochlorococcus marinus]	100.00%	WP_011131785.1	NA
Q7V227	hypothetical protein [Prochlorococcus marinus]	100.00%	WP_011132298.1	NA
Q7V210	SAM-dependent methyltransferase [Prochlorococcus marinus]	100.00%	WP_011132315.1	Central Metabolism
Q7V3R3	tetratricopeptide repeat protein [Prochlorococcus marinus]	100.00%	WP_011131644.1	NA
Q7V1N9	DUF3318 domain-containing protein [Prochlorococcus marinus]	100.00%	WP_011132458.1	NA
Q7V0R1	hypothetical protein [Prochlorococcus marinus]	100.00%	WP_011132829.1	NA
Q7V321	HlyC/CorC family transporter [Prochlorococcus marinus]	100.00%	WP_011131911.1	Membrane Transport
Q7V2I4	secondary thiamine-phosphate synthase enzyme [Prochlorococcus sp. MED105]	98.14%	MAK08367.1	Central Metabolism
Q7V0Y8	DUF2488 family protein [Prochlorococcus marinus]	100.00%	WP_011132739.1	NA
Q7V1I5	DUF1995 family protein [Prochlorococcus marinus]	100.00%	WP_011132519.1	NA
Q7V2K2	Hypothetical protein P9211_04751 [Prochlorococcus marinus str. MIT 9211]	100.00%	ABX08406.1	NA
Q7V0R9	PH domain-containing protein [Prochlorococcus marinus]	100.00%	WP_011132819.1	NA
Q7V0F5	hypothetical protein [Prochlorococcus marinus]	100.00%	WP_011132941.1	NA
Q7V1D2	DUF3464 family protein [Prochlorococcus marinus]	100.00%	WP_011132577.1	NA
Q7V078	ferredoxin-NADP reductase [Prochlorococcus sp. MED-G72]	67.16%	RCL49643.1	Photosynthesis
Q7V2I9	nickel pincer cofactor biosynthesis protein LarC [Prochlorococcus marinus]	100.00%	WP_011132122.1	Central Metabolism
Q7V2B5	glutathione S-transferase family protein [Prochlorococcus marinus]	100.00%	WP_011132200.1	Oxidative stress
Q7V0M0	transketolase [Prochlorococcus marinus]	100.00%	WP_011132870.1	Carbon Fixation
Q7V0D6	DUF1825 family protein [Prochlorococcus marinus]	100.00%	WP_011132964.1	NA

Table A1.8. BLAST search results for significant uncharacterised proteins

Protein	Description	Per. Ident (%)	Accession	Function
Q7V2T5	DUF3303 domain-containing protein [Prochlorococcus marinus]	100.00%	WP_011132016.1	NA
Q7V1A4	DUF2862 domain-containing protein [Prochlorococcus marinus]	100.00%	WP_011132608.1	NA
Q7V0S9	hypothetical protein [Prochlorococcus marinus]	100.00%	WP_011132808.1	NA
Q7V3H6	DUF3120 domain-containing protein [Prochlorococcus marinus]	100.00%	WP_011131737.1	NA
Q7V2T7	hypothetical protein [Prochlorococcus marinus]	100.00%	WP_011132014.1	NA
Q7UZP1	hypothetical protein [Prochlorococcus marinus]	100.00%	WP_011133244.1	NA
Q7V1S8	pentapeptide repeat-containing protein [Prochlorococcus marinus]	100.00%	WP_011132411.1	NA
Q7V012	DUF2997 domain-containing protein [Prochlorococcus marinus]	100.00%	WP_011133107.1	Photosynthesis
Q7V353	hypothetical protein [Prochlorococcus marinus]	100.00%	WP_011131875.1	NA
A8WI63	hypothetical protein [Prochlorococcus marinus]	100.00%	WP_011132965.1	NA
Q7V0D5	Conserved hypothetical protein [Prochlorococcus marinus subsp. pastoris str. CCMP1986]	100.00%	CAP16350.1	NA
Q7V2Z1	hypothetical protein [Prochlorococcus marinus]	100.00%	WP_011131944.1	NA
Q7UZT7	putative membrane protein [Prochlorococcus marinus str. P0903-H212]	72.73%	AJW30875.1	NA

A1.2 Chapter 3 Supplementary Information

A1.2.1. Investigating the effect of consumer $nTiO_2$ upon natural marine communities: Additional Information

a) Library Preparation

The 16S rRNA gene v4-5 regions (515F-Y and 926R primers) and 18S rRNA gene v8-9 regions (V8F and 1510R primers) were amplified using the Q5® Hot Start High-Fidelity 2X Master Mix (New England Biolabs® inc.). PCR conditions were as follows; 16S rRNA: 98°C (30 s), 25 cycles of: 98°C (10 s), 50°C (15 s), 72°C (20 s), 72°C (5 min), and cool to 4°C; 18S rRNA: 98°C (3 min), 25 cycles of: 98°C (20 s), 65°C (15 s), 72°C (15 s), and cool to 4°C. Following PCR, Ampliclean magnetic beads (Nimagen) were used to purify the PCR product. Normalisation was carried out using a SequelPrep® Normalisation Plate Kit (ThermoFisher Scientific). NEBNext Library Quant Kit for Illumina (New England Biolabs, UK) was used to pool and quantify the 16S rRNA and 18S rRNA libraries before diluting to 4 nM. Subsequently, 0.2N NaOH was used to denature the libraries and the MiSeq Reagent Kit v3 (600 cycles; Illumina) was used for amplicon sequencing following the manufacturer's instructions for a library of 14 pM, using phiX (2%) and an internal reference. Amplicon sequencing was carried out on an Illumina MiSeq and reads subsequently demultiplexed using BaseSpace (Illumina).

b) DADA2 Analysis

The DADA2 pipeline (version 1.8.0) was used to analyse data obtained from sequencing.[285, 286] This pipeline was chosen due to its enhanced resolution upon taxonomic assignment compared to other methods.[287] The output from the DADA2 pipeline are referred to as amplicon sequencing variants (ASVs). Here, the SILVA reference database (v132) was used in order to classify ASVs.[436] Prior to downstream analysis, mammalia, chloroplasts, and mitochondria were removed from both the bacterial (16S rRNA) and eukaryotic (18S rRNA) datasets, as well as removing any eukaryotes from the 16S rRNA data and any bacteria or archaea from the 18S rRNA data. On average, 16S rRNA and 18S rRNA data contained an average of 11263 and

28699 reads per sample respectively. Any samples that contained less than 1000 reads were removed from downstream analyses.

c) Analysis of 16S rRNA and 18S rRNA data using MicrobiomeAnalyst

16S rRNA and 18S rRNA datasets were analysed using the web-based tool MicrobiomeAnalyst.[288, 289] This tool was selected based on its ease-of-use and effectiveness to gain quick insight into possible alterations in alpha- and beta- diversity of microbiome data. Briefly, ASV data was uploaded to the MicrobiomeAnalyst platform and filtered as follows; for low count ASVs, those with less than 2 counts or in the lowest 10% prevalence were removed, as well as those in the lowest 10% based on interquartile range. This resulted in a total of 1316 ASVs being taken forward for analysis in the 16S rRNA dataset, and 1480 ASVs in the 18S rRNA dataset respectively. No rarefication was applied as read counts did not vary substantially between samples in either the 16S or 18S rRNA datasets. Total sum scaling was performed on data and no transformation was applied. Subsequently, various measures of alpha diversity were calculated to assess differences in species richness and evenness between treatments. Relative abundance of major bacterial (16S rRNA dataset) and eukaryotic (18S rRNA dataset) phyla were then calculated and bar charts produced to visualise this data. To assess any statistically significant differences between communities belonging to individual treatments, PCoA was carried out (PERMANOVA based on Bray-Curtis dissimilarity) were used to assess differences in the 16S rRNA and 18S rRNA datasets respectively. Figures for both relative abundance and PCoA plots were downloaded and utilised to present data. Relative abundance values were utilised for subsequent statistical analysis via two-way T-tests between control and treated samples and a variety of taxonomic levels.

A1.2.2 TEM of $nTiO_2$ extracted from consumer products utilised in experimental work: Additional images.

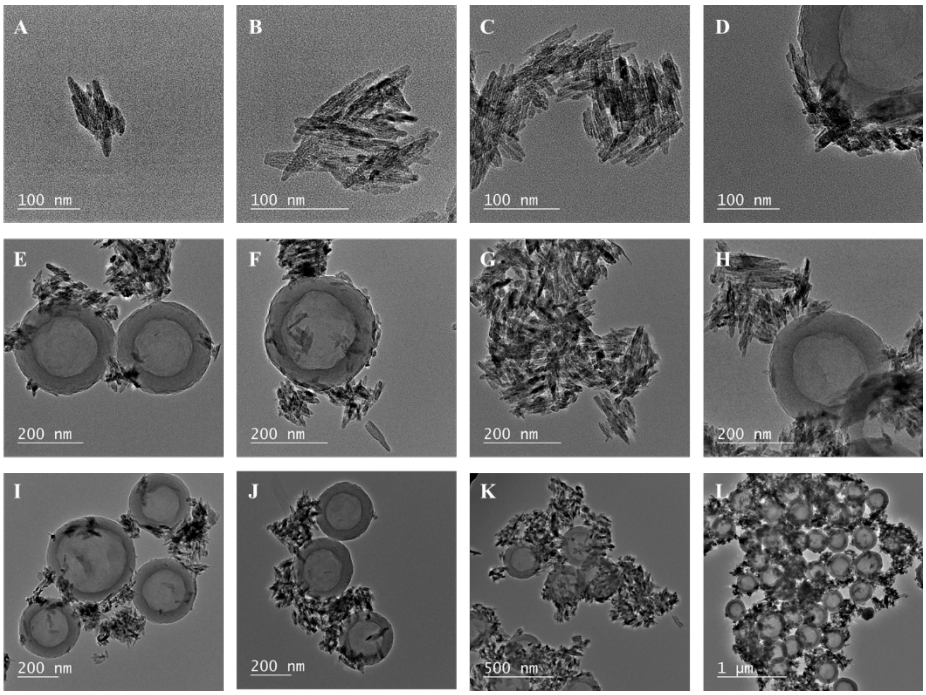

Figure A1.1. TEM imaging of particles extracted from Skinceuticals sunscreen.

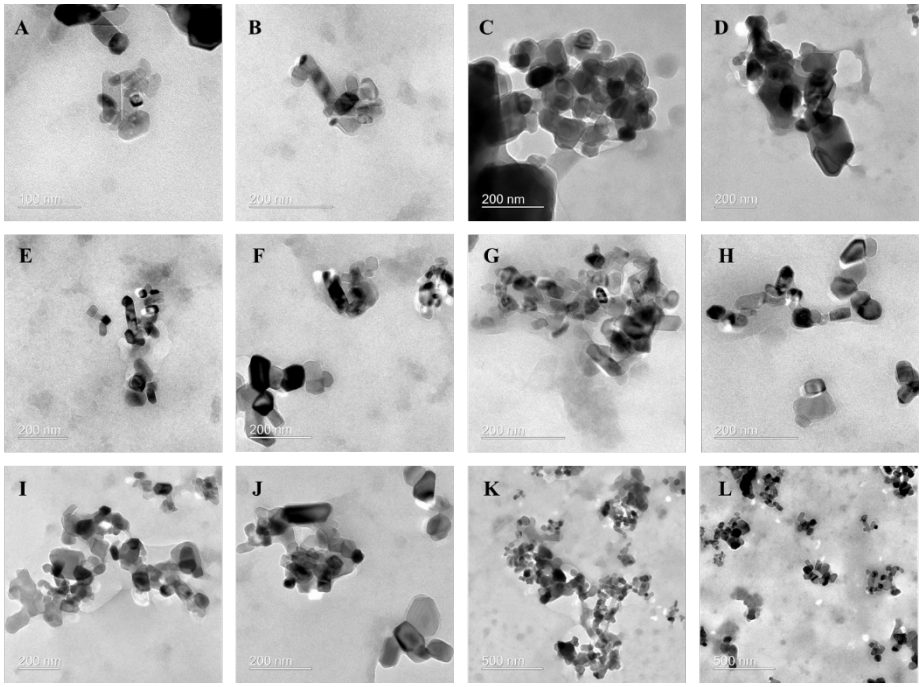

Figure A1.2. TEM imaging of particles extracted from Boots Soltan sunscreen.

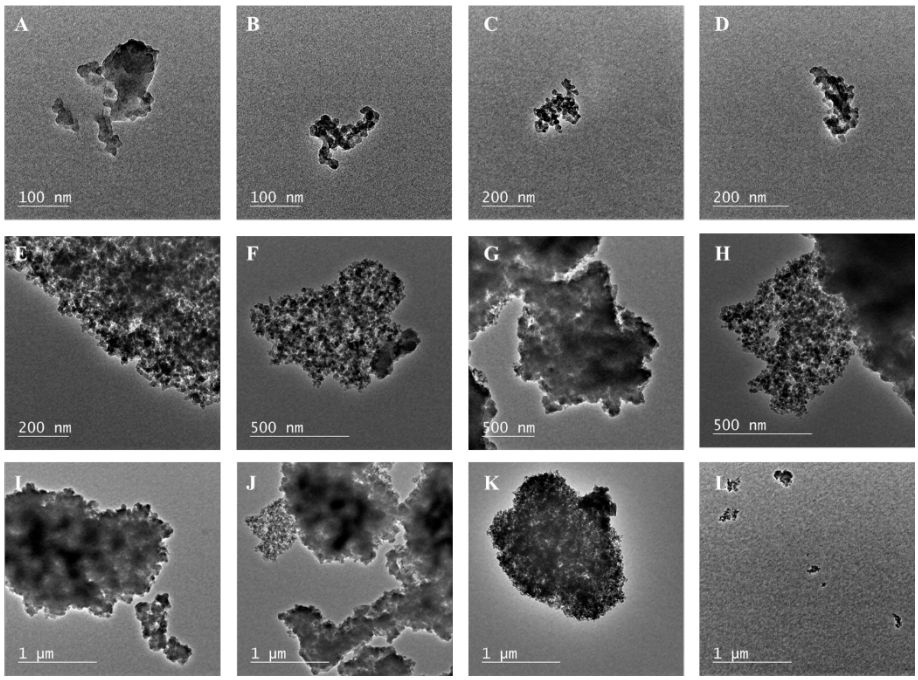

Figure A1.3. TEM imaging of particles extracted from Body Shop Foundation.

Appendix 2

Published Works

The published articles derived from the works carried out during this thesis are appended below: